UNIVERSIDAD COMPLUTENSE DE MADRID
FACULTAD DE CIENCIAS BIOLÓGICAS
Departamento de Bioquímica y Biología Molecular

TESIS DOCTORAL

Proteína del surfactante SP-D en el contexto pulmonar: oligomerización, actividad biológica y papel protector en la homeostasis pulmonar

Surfactant protein SP-D in the lung context : oligomerization, biological activity and protective role in lung homeostasis

MEMORIA PARA OPTAR AL GRADO DE DOCTOR

PRESENTADA POR

Raquel Arroyo Rodríguez

Directores

Jesús Pérez Gil
Mercedes Echaide Torreguitar

Madrid
Ed. electrónica 2019

UNIVERSIDAD COMPLUTENSE DE MADRID

FACULTAD DE CIENCIAS BIOLÓGICAS

Departamento de Bioquímica y Biología Molecular

PROTEÍNA DEL SURFACTANTE SP-D EN EL CONTEXTO PULMONAR: OLIGOMERIZACIÓN, ACTIVIDAD BIOLÓGICA Y PAPEL PROTECTOR EN LA HOMEOSTASIS PULMONAR

SURFACTANT PROTEIN SP-D IN THE LUNG CONTEXT: OLIGOMERIZATION, BIOLOGICAL ACTIVITY AND PROTECTIVE ROLE IN LUNG HOMEOSTASIS

MEMORIA PARA OPTAR AL GRADO DE DOCTOR

PRESENTADA POR

RAQUEL ARROYO RODRÍGUEZ

DIRECTORES

JESÚS PÉREZ GIL

MERCEDES ECHAIDE TORREGUITAR

MADRID, 2018

The research included in this Thesis has been conducted in the Department of Biochemistry and Molecular Biology of Complutense University of Madrid under the supervision of Prof. Jesús Pérez Gil, Ph.D. and Mercedes Echaide Torreguitar, Ph.D. Part of the experimental work was performed in collaboration with Jan Rosenbaum, Ph.D. from Airway Therapeutics LLC. (Cincinnati, OH, USA); Prof. Fernando Moreno Herrero, Ph.D. from "Centro Nacional de Biotecnología (CNB-CSIC)" (Madrid, Spain); Prof. Paul Kingma, MD, Ph.D. from Cincinnati Children's Hospital Medical Center (CCHMC) (Cincinnati, OH, USA); Prof. Nades Palaniyar, Ph.D. from SickKids Hospital (Toronto, ON, Canada); Prof. Alberto Galindo, MD from the Gynecology and Obstetrics Department of "Hospital 12 de Octubre" (Madrid, Spain); Robert Wilmanowski, Ph.D. from Glycotope GmbH (Berlin, Germany). Funding for short-term stays was provided by the Spanish Ministry of Education, Culture and Sport (EST16/00922).

The financial support to complete this Thesis was provided by the Spanish Ministry of Education, Culture and Sport (FPU14/03398) and research grants from Spanish Ministry of Economy and Competitiveness (BIO2012-30733, BIO2015-67930-R) and the Regional Government of Madrid (S2013/MIT-2807).

ACKNOWLEDGEMENTS
AGRADECIMIENTOS

A mis directores de tesis, Jesús y Mercedes.
A mis compañeros del grupo BIOMIL.
A Fernando Moreno y su grupo, por acogerme con los brazos abiertos.
A Paul Kingma y Nades Palaniyar por permitirme trabajar unos meses es sus laboratorios.
A mi familia y amigos.

TABLE OF CONTENTS

LIST OF ABBREVIATIONS

4-AP: 4-aminophenazone
ABCA3: ATP-binding cassette transporter A3
AF: amniotic fluid
AFM: atomic force microscopy
AM: amplitude modulation
ARDS: acute respiratory distress syndrome
ATII: alveolar type II cells
BAL: bronchoalveolar lavage
BALF: bronchoalveolar lavage fluid
BCA: bicinchoninic acid
CBS: captive bubble surfactometer
CHE: cholesterol esterase
CHO: Chinese hamster ovary
CHOD: cholesterol oxidase
CitH3: citrullinated histone 3
COPD: chronic obstructive pulmonary disease
CRD: carbohydrate recognition domain
DPPC: dipalmitoylphosphatidylcholine
Dyn: dynamic cycles
ER: endoplasmic reticulum
FBS: fetal bovine serum
GA: glutaraldehyde
GlcNAc: N-Acetyl-glucosamine
GM-CSF: granulocyte-macrophage colony stimulating factor
HRP: horseradish peroxidase
IA: initial adsorption
KO: knock out
LA: large aggregates
LAL: Limulus Amebocyte Lysate
LB: lamellar body
LPS: lipopolysaccharide
LS: lung surfactant
MAS: meconium aspiration syndrome
MW: molecular weight
NETs: neutrophil extracellular traps
NOX: NADPH oxidase
OE: organic extract
PAGE: polyacrylamide gel electrophoresis
PAP: pulmonary alveolar proteinosis
PC: phosphatidyl choline
PEA: post expansion adsorption
PG: phosphatidylglycerol
PI: phosphatidylinositol
PL: phospholipids
pNA: p-nitroaniline
POD: peroxidase
RER: rough endoplasmic reticulum
ROS: reactive oxygen species
RPM: revolutions per minute
SA: small aggregates
SDS: sodium dodecyl sulfate
SEC: size exclusion chromatography
SP-A: surfactant protein A
SP-B: surfactant protein B
SP-C: surfactant protein C
SP-D: surfactant protein D
TBS: tris buffered saline (150 mM NaCl, 50 mM Tris (pH 7))
TEM: transmission electron microscopy
TM: tubular myelin
WT: wild type

SUMMARY

Lungs are branched organs that in their terminal ends contain alveoli, small chambers where a large surface is exposed to the external environment and the gas exchange takes place. At this level, the first barrier to prevent the entry of pathogens through the respiratory pathway is a lipid-protein complex called lung surfactant (LS). This complex coats the air-liquid interface and it is essential to allow alveoli to compress and expand to carry out an effortless breathing while preventing alveolar collapse. This last function is referred as the biophysical function of lung surfactant, where phospholipids (PL), especially saturated PL, and surfactant hydrophobic proteins (SP-B and SP-C) are crucial. In a combined action and to protect the lungs from pathogens invasion, surfactant also contains two collectin proteins, SP-A and SP-D, which work as pattern recognition molecules that help to fight against invading microorganisms and to modulate the immune response triggered in lungs upon infection.

Surfactant protein SP-D has been found in the alveolar airspaces and other locations in the human body. In addition, it has been also detected and obtained from amniotic fluid near term pregnancy. The 43 kDa monomer of SP-D is formed by a cysteine rich N-terminal domain, a long collagen region, a neck domain with a coiled-coil α-helical conformation, and a carbohydrate recognition domain (CRD), characteristic of C-type lectins. SP-D is N-glycosylated in an asparagine (Asn^{70}) at the collagen domain. Three monomers associate into trimers through the folding of collagen regions, guided by the neck domains and stabilized by disulfide bonds within the N-terminal domains. Furthermore, association of trimers forms cruciform structures, dodecamers, and even larger oligomers with a variable number of trimeric arms, called “fuzzy balls” or “asterisk-like” structures. However, the interactions involved in protein oligomerization from trimers to large oligomers remain unknown to be characterized.

SP-D participates in the host defense of lungs. It recognizes certain ligands, mainly carbohydrate structures present at the surface of invading microbes. Pathogen recognition triggers binding, aggregation, opsonization and stimulation of host cells to initiate clearance of these potential pathogens. In addition, it regulates the innate immune response in the lungs, stimulating pro- or anti-inflammatory pathways. Moreover, it is involved in lung surfactant homeostasis, regulating phospholipid pool sizes and their accumulation into the alveolar space. Many studies have been performed to figure out which domains of SP-D are essential for the different protein functions. Moreover, the activity of the different oligomeric forms has been also studied, although not all of them have been individually isolated and evaluated in the different assays. Data have pointed to large oligomers as the most active structures.

Taking into account this evidence, the main objective of this Thesis has been to characterize SP-D oligomeric forms, the interactions that drive the oligomerization pathway and the possible distinct activity of those oligomers, using human SP-D and a full-length recombinant version of the protein. In addition, the protective role of SP-D on lung homeostasis and breathing compliance has been addressed under inflammatory conditions. The specific objectives have been:

- Characterization and quantification of SP-D oligomeric forms and study of the interactions that govern the oligomerization pathway, using a recombinant human rhSP-D
- Isolation and evaluation of the activity and function of the different recombinant human rhSP-D oligomers, especially to aggregate and bind to bacteria.
- Structural and functional characterization of human SP-D from two different sources: amniotic fluid and BAL from proteinosis patients.
- Investigation of the possible modulatory role of SP-D in LPS-induced NETosis and its protective role to protect lung surfactant from NETs inhibition.

The results have shown that SP-D is assembled into trimers, hexamers, dodecamers and fuzzy balls, being the first time that hexamers are described as a defined oligomeric form of the protein. We have proposed that hexamers are necessary intermediate states between trimers and dodecamers or fuzzy balls. It has been found that non-covalent interactions govern this oligomerization process from trimers to higher order oligomers (hexamers, dodecamers and fuzzy balls), especially between N-terminal and the beginning of the collagen domains. A bright protrusion has been found in AFM images, which coincides with the N-glycosylation site in the collagen domain of SP-D. Glycosylation could interfere with protein oligomerization. Moreover, dodecamers and fuzzy balls are the most abundant oligomeric forms in rhSP-D and hSP-D, respectively, being this quantitative distribution sensitive to external conditions, such as pH.

The isolation of trimers, hexamers and fuzzy balls have allowed us to study and compare them with respect to protein functions that depend on the CRD domains. Results have shown that fuzzy balls are the most active oligomeric form to aggregate and bind to *E. coli*. Moreover, although the affinity of binding of trimers and hexamers to bacteria was similar, trimers did not aggregate bacteria, while hexamers did.

The structural and functional analysis of human SP-D obtained from two sources, amniotic fluid and proteinosis, have revealed that hSP-D from the disease condition was assembled mainly as fuzzy balls, whereas in hSP-D from amniotic fluid, fuzzy balls were also the major structure, but very closely followed by dodecamers. Moreover, the oligomeric forms observed in hSP-D were the same as in rhSP-D, and the quantitative distribution found in hSP-D from amniotic fluid was similar to the one in rhSP-D. Results of functional assays of these two hSP-D preparations were consistent with previous results, showing that hSP-D from proteinosis is more active than the protein from amniotic fluid, probably due to the distribution of the oligomeric forms found in both cases.

Last, we have seen that SP-D can modulate NETosis, one of the mechanism of neutrophils to fight against pathogens. In addition, it has been found that an excess of NETs may be harmful for the biophysical activity of lung surfactant and, that SP-D protects lung surfactant from NETs inactivation.

In summary, in this PhD Thesis the structure and oligomerization process of SP-D have been studied. It has been observed that it is assembled as trimers, hexamers, dodecamers and fuzzy balls, being the two last ones the most abundant oligomers. The oligomerization process is mainly governed by non-covalent interactions and sensitive to environmental conditions. Fuzzy balls have been found to be the most active structure, at least in terms of bacteria aggregation and binding. Last, SP-D has shown a protective role in surfactant inactivation by NETs and a modulatory effect in LPS induce NETosis, a process implicated in the immune defense of the lungs.

RESUMEN

Los pulmones son órganos ramificados cuyas ramificaciones terminan en los alvéolos. En los sacos alveolares, una gran superficie expuesta al medio externo, es donde tiene lugar el intercambio de gases que constituye la base de la respiración. A este nivel, un complejo lípido-proteico, el surfactante pulmonar (SP), constituye la primera barrera para prevenir la entrada de patógenos al organismo a través de las vías respiratorias. El surfactante pulmonar recubre y se extiende a lo largo de la interfase aire-líquido en los alvéolos, permitiéndoles expandirse y contraerse durante la entrada y salida de aire, sin colapsar y sin un gran esfuerzo por parte de los músculos respiratorios. Esto es lo que se considera la función biofísica del surfactante pulmonar. Para llevar a cabo esta función en su composición son esenciales los fosfolípidos, especialmente aquellos con cadenas saturadas, y las proteínas hidrofóbicas (SP-B y SP-C). Por otro lado, para proteger al organismo de la invasión de patógenos, el surfactante pulmonar también contiene entre sus componentes dos proteínas de la familia de las colectinas, SP-A y SP-D, que actúan como moléculas de reconocimiento de patrones. Estas colectinas luchan contra la invasión de microorganismos y modulan la respuesta inmune desencadenada en los pulmones cuando hay una infección.

La proteína del surfactante SP-D se encuentra en los espacios alveolares, así como en otras localizaciones del organismo. Además, ha sido detectada en líquido amniótico y purificada del mismo procedente de embarazos a término. El monómero de la SP-D (43 kDa) está formado por un dominio N-terminal, rico en cisteínas, seguido de un dominio colagénico largo, que continúa con un dominio conector con una conformación de hélice superenrollada y acaba con el dominio de reconocimiento de carbohidratos ("CRD", del inglés), característico de las colectinas tipo C. La SP-D se encuentra N-glicosilada en una asparagina (Asn^{70}) localizada en el dominio colágeno. Tres monómeros se unen dando lugar a trímeros a través del plegamiento y formación de una triple hélice de colágeno, con participación de los dominios conectores. Los trímeros son estabilizados por puentes disulfuro entre las cisteínas en los dominios N-terminales. La unión de trímeros da lugar a dodecámeros, estructuras con forma de cruz, y a oligómeros más grandes, con un número variable de trímeros, llamados "fuzzy balls" o estructuras tipo asterisco. Sin embargo, hasta la fecha se desconocen el tipo de interacciones implicadas en la oligomerización desde trímeros hasta los oligómeros grandes.

La SP-D participa en la defensa inmune de los pulmones del hospedador. Reconoce ciertos ligandos, principalmente estructuras de tipo carbohidrato presentes en la superficie de los microorganismos invasores. El reconocimiento de patógenos desencadena su unión, agregación, opsonización y estimulación de

células del hospedador para llevar a cabo la eliminación de esos potenciales patógenos. Además, la SP-D regula la respuesta inmune innata en los pulmones, estimulando rutas pro- y anti-inflamatorias. Por otro lado, la proteína está implicada en la homeostasis del surfactante pulmonar, regulando el tamaño de las estructuras de reserva del mismo y su acumulación en la subfase alveolar. Muchos estudios se han llevado a cabo para encontrar qué dominios de la SP-D son esenciales para las diferentes funciones descritas. También se ha estudiado la actividad de las diferentes formas oligoméricas de la proteína, aunque no todas ellas han sido aisladas individualmente y evaluadas en los diferentes ensayos funcionales. Los datos obtenidos señalan a los oligómeros grandes (fuzzy balls) como las estructuras más activas de la proteína.

Teniendo en consideración toda esta información, el principal objetivo de esta Tesis ha sido caracterizar las diferentes formas oligoméricas de la SP-D, así como el tipo de interacciones que participan en la ruta de oligomerización y la posible distinta actividad de estos oligómeros. Para ello se han empleado dos preparaciones de SP-D humanas y una forma recombinante de la SP-D humana (rhSP-D) que contiene la estructura completa. Además, se ha estudiado el papel protector de la SP-D en la homeostasis pulmonar sobre la función biofísica del surfactante pulmonar en condiciones de inflamación pulmonar. Los objetivos específicos han sido:

- Caracterización y cuantificación de las formas oligoméricas de la SP-D y estudio de la naturaleza de las interacciones implicadas en el ensamblado de las mismas, usando para ello una proteína recombinante humana (rhSP-D).
- Aislamiento y evaluación de la actividad y función de los diferentes oligómeros de la proteína recombinante rhSP-D, especialmente en términos de agregación y unión a bacterias.
- Caracterización estructural y funcional de dos preparaciones de SP-D humana de diferente origen: líquido amniótico y lavado bronco-alveolar de pacientes con proteinosis.
- Investigación del posible papel modulador de la SP-D sobre la NETosis inducida por LPS y su papel protector en la inhibición del surfactante pulmonar por la presencia de NETs.

Los resultados obtenidos han mostrado que la SP-D se ensambla en trímeros, hexámeros, dodecámeros y oligómeros grandes (fuzzy balls), siendo ésta la primera vez que los hexámeros son descritos como una forma oligomérica definida de la proteína. Se ha propuesto que los hexámeros son estados intermedios necesarios

entre los trímeros y dodecámeros o fuzzy balls. Se ha visto que las interacciones no covalentes dirigen el proceso de oligomerización desde trímeros a formas superiores (hexámeros, dodecámeros y fuzzy balls), teniendo lugar entre los dominios N-terminal y la zona cercana a éstos de los dominios colágeno. En las imágenes de AFM, se ha observado un punto brillante en el dominio colágeno, que corresponde con el sitio de N-glicosilación de la proteína y podría tener implicación en el proceso de oligomerización. Además, se ha visto que los dodecámeros y los fuzzy balls son las estructuras más abundantes en rhSP-D y hSP-D, respectivamente, siendo esta distribución cuantitativa sensible a las condiciones del medio en el cuál se encuentra la proteína, por ejemplo, el pH.

El aislamiento de trímeros, hexámeros y fuzzy balls ha permitido estudiar y comparar la actividad de estas diferentes estructuras, en funciones de la proteína que dependen del dominio CRD. En ensayos de agregación y unión a *E. coli*, los fuzzy balls han sido los oligómeros más activos. Además, se ha visto que la afinidad de unión de trímeros y hexámeros a bacterias es similar, pero los trímeros no inducen agregación de bacterias, mientras que los hexámeros sí lo hacen.

El análisis estructural y funcional de la SP-D humana procedente de dos fuentes diferentes, líquido amniótico y proteinosis, ha revelado que la hSP-D procedente de la condición patológica presenta principalmente fuzzy balls, mientras que en la hSP-D de líquido amniótico, los fuzzy balls fueron también la estructura mayoritaria, pero con una proporción muy parecida de dodecámeros. Los oligómeros observados en la hSP-D fueron los mismos que en rhSP-D, y la distribución cuantitativa en la hSP-D purificada de líquido amniótico fue muy similar a la de la proteína recombinante (rhSP-D). Los resultados de los ensayos funcionales de las dos SP-D humanas concordaron con resultados previos, siendo la hSP-D de proteinosis más activa que la proteína de líquido amniótico, probablemente debido a la distribución de las formas oligoméricas observadas en cada caso, siendo el porcentaje de fuzzy balls mucho mayor en el caso de la proteína de proteinosis.

Por último, se ha visto que la SP-D puede modular la NETosis, que es uno de los mecanismos que poseen los neutrófilos para luchar contra patógenos invasores. Además, se ha visto que un exceso de NETs puede ser dañino para la actividad biofísica del surfactante pulmonar y, que la SP-D protege al mismo de la inactivación por NETs.

En resumen, en la presente Tesis se ha estudiado la estructura y el proceso de oligomerización de la SP-D. Se ha visto que está ensamblada como trímeros, hexámeros, dodecámeros y fuzzy balls, siendo los dos últimos los oligómeros más

abundantes. El proceso de oligomerización de la proteína está mediado por interacciones no covalentes principalmente y es sensible a las condiciones del medio externo en el cuál se encuentra. Los fuzzy balls han demostrado ser la estructura más activa, al menos en términos de agregación y unión a bacteria. Por último, la SP-D ha mostrado un papel protector en la inactivación del surfactante producida por NETs, como consecuencia de la NETosis inducida por LPS, un proceso implicado en la defensa inmune del pulmón.

INTRODUCTION

LUNG DEVELOPMENT

The respiratory system is developed in the fetus during gestation and the firsts years of life until total enlargement and maturation. The respiratory tree is formed by the trachea and the lungs. Lungs contain a branched network formed by bronchi, bronchioles and alveoli, where the exchange of gases takes place during breathing. There are five histological stages along fetal lung development, from the first stages until final maturation: i) embryonic (4-7 weeks), ii) pseudoglandular (7-17 weeks), iii) canicular (16-25 weeks), iv) saccular stage (24-38 weeks), v) alveolar stage (just before birth - first few years of life) (Maeda et al., 2007, Mullassery and Smith, 2015). During the two first stages, two lung buds are developed and branched accompanied with vasculogenesis. In the canicular stage, the air-blood barrier appears between the cells that cover the pulmonary epithelium and the blood vessels, the bronchial tree is expanded, and late in that period, cells in the epithelium start to differentiate into Type I and II cells (Herriges and Morrisey, 2014, Mullassery and Smith, 2015). In the saccular stage, the formation of alveolar sacs starts as well as the synthesis of lung surfactant (LS) (around 26 weeks) by differentiated Type II cells. Secretion of lung surfactant begins around week 30, which will be crucial at birth time to open the airway spaces and fill them with air, without alveolar collapse allowing the baby to start breathing (Maeda et al., 2007, Mullassery and Smith, 2015). Last, alveolar stage comprises high alveolarization, where at the end, Type I cells will cover 90-95% of the pulmonary epithelium, whereas type II cells will cover only 5-10% although they account for 60% of total cells in the alveolar epithelium (George and Hook, 1984, Fehrenbach, 2001).

Interestingly, during lung development in the period close to term pregnancy, lung surfactant has been found as part of amniotic fluid (Lemke et al., 2017). This could be explained due to breathing movements of the fetal lungs, which contain lung surfactant from around week 30 and contribute to the efflux of lung fluids into the amniotic fluid (Underwood et al., 2005). Moreover, cells in the innermost fetal membranes that surround the amniotic cavity, have been shown to produce and secrete components similar to lung surfactant (Lemke et al., 2017).

LUNG SURFACTANT

In lungs, a lipid-protein complex called lung surfactant (LS) lines the extensive respiratory air-liquid interface (Pattle, 1955, Clements, 1957). This complex is essential as a first defense barrier to protect lungs from pathogen invasion and to allow lungs to compress and expand without alveolar collapse during breathing (Avery and Mead, 1959, Perez-Gil and Weaver, 2010, Parra and Perez-Gil, 2015).

♦ **Composition**

Lung surfactant is composed by around 90% lipids and 10% proteins by mass (Johansson and Curstedt, 1997, Perez-Gil, 2008).

Regarding lipids, phospholipids (PL) are the major component (~80%), including zwitterionic phosphatidylcholines (PC) (60-70%), and anionic PLs like phosphatidylglycerol (PG) and phosphatidylinositol (PI) that together account for around 8-15 % by mass (Figure 1). Neutral lipids, such as cholesterol constitute 8-10% by mass. It is remarkable and important for LS biophysical function, the high proportion of saturated dipalmitoyl phosphatidylcholine (DPPC), in the order of 40% of total LS mass in mammals (Goerke, 1998, Parra and Perez-Gil, 2015).

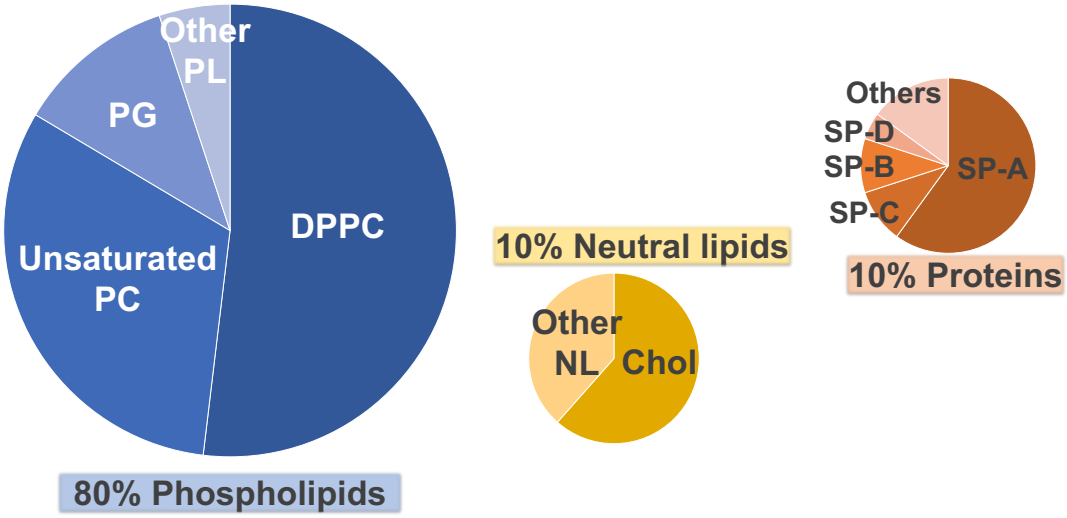

Figure 1: Composition of lung surfactant. Lung surfactant is composed by 80% phospholipids, 10% neutral lipids and 10% proteins, including specific surfactant-associated proteins. Each chart represents the relative distribution, considering the total 100% of the species in that group.

Four specific surfactant proteins have been described: SP-A, B, C and D. They can be classified in 2 groups: i) the hydrophilic collectin proteins SP-A (~6% by mass) and SP-D (<0.5%), and ii) the hydrophobic proteins SP-B (~1%) and SP-C (~1%) (Figure 1) (Weaver and Whitsett, 1991, Johansson and Curstedt, 1997). Collectin proteins will be described later in a separate section.

Surfactant proteins B and C (SP-B, C) are small cationic peptides, with a high hydrophobic character. SP-B contains 7 cysteines in its amino acids sequence and can be found as a covalent homodimer (17.4 kDa), in a parallel and superficial arrangement between LS lipid membranes (Figure 2) (Johansson et al., 1991, Vandenbussche et al., 1992, Cruz et al., 1998, Perez-Gil, 2008). Further studies have suggested a supramolecular organization of the protein in the form of ring-like structures composed by 5-6 homodimers (Olmeda et al., 2015). The absence of SP-B is life-threatening; inactivation of the expression of the SP-B gene leads to a lethal

respiratory failure at birth (Clark et al., 1995, Nogee, 2004). SP-C is the smallest surfactant protein (4.2 kDa), which is found as a monomer, mainly with an α-helical structure except for its unstructured N-terminal region, where two cysteines are found palmitoylated (Johansson et al., 1994). SP-C adopts a transmembrane orientation in LS membranes (Figure 2) (Perez-Gil, 2008, Roldan et al., 2015). Inactivation of the expression of the SP-C gene is not lethal, although it leads to severe respiratory pathologies at long-term (Glasser et al., 2001, Glasser et al., 2003, Nogee, 2004).

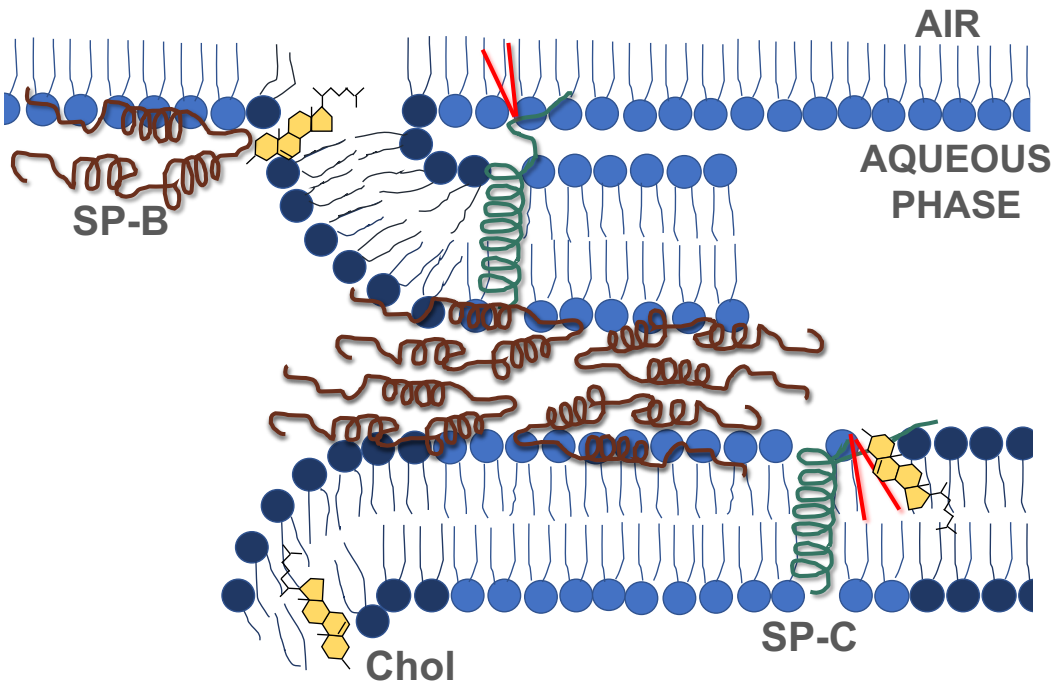

Figure 2: Membrane-associated surfactant proteins SP-B and SP-C and their interaction with phospholipids layers. Adapted from (Echaide et al., 2017), based on accepted models (Johansson et al., 1994, Cruz et al., 1998, Roldan et al., 2015).

- **Synthesis, secretion and homeostasis**

LS lipids and hydrophobic proteins are synthesized in the endoplasmic reticulum (ER) of type II cells (ATII). Then, they are transported and incorporated into concentric multilayered packed membranous structures, called lamellar bodies (LB). The transport of lipids takes place through the ATP-binding cassette transporter A3 (ABCA3) (Ban et al., 2007, Cheong et al., 2007) while hydrophobic proteins are transferred by multi-vesicular bodies. Hydrophilic proteins, SP-A and SP-D, are also synthetized in the ER in type II cells, but they are further modified in the Golgi apparatus and then, secreted to the aqueous sub-phase by a different pathway than hydrophobic proteins (Olmeda et al., 2017). Once surfactant complexes are secreted in the form of lamellar bodies, it has been shown that these highly dense surfactant packages unravel to form a lattice structure called tubular myelin (TM)

(Figure 3). SP-A, SP-B and calcium ions orchestrate this process. TM functions in the lung are not fully understood, although it has been proposed that it is involved in antimicrobial actions (McCormack and Whitsett, 2002, Perez-Gil, 2008). Finally, lung surfactant complexes are adsorbed into the air-liquid interface and spread along it to form a surface-active film (Figure 3). This process is energetically unfavorable because the transfer of lipids implies the transient exposure of acyl lipid chains to the aqueous environment, which makes it slow and inefficient. This problem is solved by the action of the hydrophobic proteins, which are involved in transferring PLs to the air-liquid interface, overcoming the energetic impediment and, allowing this process to happen very fast, within seconds (Walters et al., 2000, Lopez-Rodriguez and Perez-Gil, 2014). Besides, it has been described the existence of stack multilayered membranes, constituting surfactant reservoirs associated to the interfacial film, where again, hydrophobic proteins have a key role facilitating the adsorption of stored phospholipids into the interface, also with the participation of SP-A (Schurch et al., 1998, Parra and Perez-Gil, 2015, Lopez-Rodriguez et al., 2016).

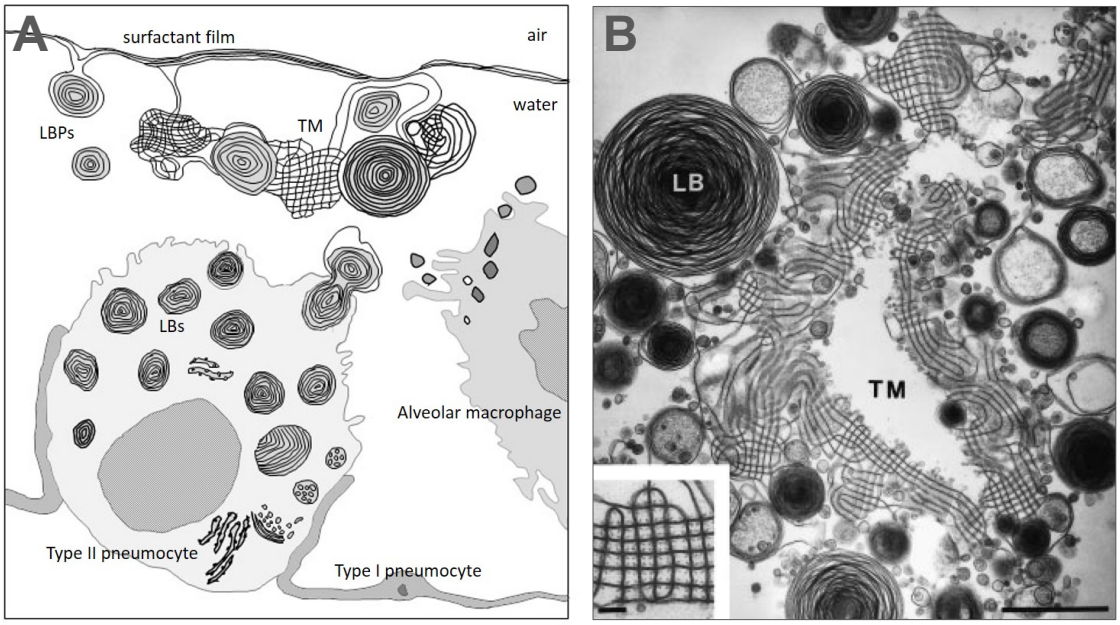

Figure 3: Synthesis and secretion of surfactant complexes by ATII cells, as lamellar bodies, and unraveling in the alveolar aqueous phase. ***A***, surfactant is synthesized in type II pneumocytes (ATII) and packed into lamellar bodies (LB) that are secreted to the alveolar aqueous sub-phase. Some of secreted LBs unpack to form tubular myelin (TM) and lung surfactant complexes are further adsorbed to the air-liquid interface. Taken from (Olmeda et al., 2017). ***B***, surfactant complexes in the alveolar sub-phase, where lamellar bodies (LB) and tubular myelin (TM) can be observed; the scale bar represents 1 μm (*right*). *Left bottom*, inset with a magnification of tubular myelin; scale bar = 0.1 μm. Taken from (Goerke, 1998).

During breathing, after several compression-expansion cycles, surfactant complexes adsorbed at the interface are converted into less active lipid-protein

complexes (Gunther et al., 1999). This "used" material is released from the interface as small aggregates that will be further cleared by ATII cells and alveolar macrophages (Olmeda et al., 2017). It has been described that 65% of the material is recycled by ATII cells, while 20% is cleared by macrophages (Rider et al., 1992), and 15% is lost by diffusion towards the upper airways via the mucociliary escalator (Pettenazzo et al., 1988). SP-A promotes the uptake of surfactant by ATII cells, where small aggregates are internalized via clathrin-coated vesicles (Bates, 2010). SP-C and SP-D are also involved in surfactant uptake by ATII cells, especially through the conversion of surfactant large aggregates (LA) to small aggregates (SA) (Ikegami et al., 2005, Roldan et al., 2016). It has been shown that SP-D has a lytic activity in large surfactant aggregates to generate small aggregates that will be preferentially internalized by ATII cells (Ikegami et al., 2009). Mice lacking SP-D accumulate increased surfactant pools that cannot be properly metabolized, where foamy macrophages are also found (Korfhagen et al., 1998). However, up to now the mechanism by which SP-D participates in the regulation of surfactant pool is not totally understood. Clearance and catabolism of surfactant by macrophages is essential to avoid intra-alveolar accumulation of lipids and proteins. In this pathway, the granulocyte-macrophage colony stimulating factor (GM-CSF) plays a key role (Ikegami et al., 2001), whose absence leads to pulmonary alveolar proteinosis (PAP), a disease characterized by accumulation of surfactant in the alveoli (Trapnell and Whitsett, 2002, Borie et al., 2011). Last, part of the lipids that are detached from the interface will undergo degradation by the action of phospholipases, mainly PLA2, which are found at the airway epithelium, alveolar macrophages and emigrating leukocytes, such as neutrophils (Hite et al., 2012).

There is an important crosstalk between the pathways of surfactant synthesis *de novo* and recycling, which are closely regulated and compensated to produce functional surfactant complexes according to the needs and avoiding overaccumulation in the alveoli.

- **Function**

Lung surfactant accomplishes two main functions in the lungs. First, a biophysical function involved in the gas exchange process in the alveoli, which takes place because the air comes in and goes out as a consequence of lung compression and expansion cycles during breathing (Perez-Gil, 2008). Secondly, an immune function; the respiratory area is one of the largest surfaces exposed to the outer environment in the body, being LS the first barrier against the entry of pathogens (Han and Mallampalli, 2015).

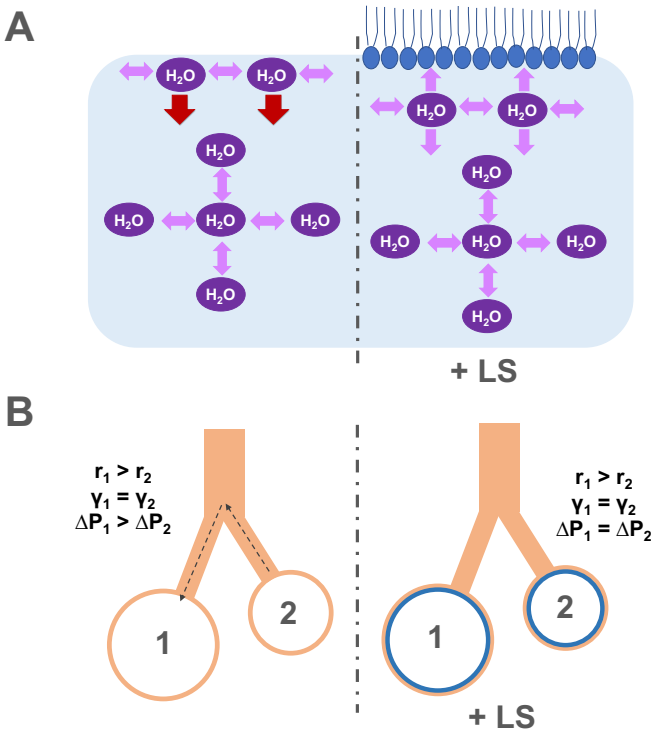

Figure 4: *A*, schematic representation of the surface tension forces experienced by water molecules inside a solution and at the interface in the absence (*left*) or presence (*right*) of lung surfactant (LS). ***B***, interpretation of Young-Laplace law applied to alveoli that are considered as spherical structures in the absence (*left*) or presence (*right*) of LS.

Two different substances become in contact at the alveolar sacs: the aqueous fluid lining the epithelium and air. Inside the alveoli, the volume occupied by air is increased during inspiration, while it is reduced during expiration and this needs to happen without collapse (closing) of the alveolar sacs (Hills, 1999, Orgeig et al., 2007). There is an essential concept at this point: the surface tension. Surface tension (γ) is the energy required to increment the surface of a fluid per area or length unit. In the lung context, it means that the water molecules at the air-liquid interface experience a net attractive force towards the bulk of the fluid, while in the water molecules submerged deep into the solution, those forces are compensated by the surrounding water molecules (Figure 4A). During inspiration, alveolar units are completely opened and filled with a high volume of air, the area of liquid exposed to air inside the alveolus increases, generating high surface tension forces. Therefore, a high amount of energy will be required to counteract those forces, which lately means that the lung muscles and diaphragm will have to make a huge effort to open the alveoli. Besides, during expiration, there is another critical situation where the air volume inside the alveoli is reduced, and that needs to happen without alveolar collapse. In other words, a small air chamber needs to persist surrounded by liquid inside the alveoli, holding the high surface pressure to keep the alveoli opened. The forces acting during this last situation can be explained by the Young-Laplace law ($\Delta P = 2\gamma / r$). Pressure forces are originated by the surface tension of the liquid molecules lining the inner surface of a curved

structure. Considering the alveoli as spherical interconnected structures, lateral interactions between water molecules at the interface exert a net force towards the center of the sphere that translates in pressure, which is inversely correlated with the radius of the sphere. Thus, during compression (expiration), if two alveoli of different sizes are interconnected at a given surface tension, the smallest one (smaller radius) would sustain a higher pressure and it would collapse into the bigger one (Figure 4B, left). This would implicate a gradual collapse of alveoli in lungs which would end in respiratory failure (Hills, 1999, Parmigiani and Solari, 2003, Lopez-Rodriguez and Perez-Gil, 2014).

However, the presence of a surface-active agent at the air-liquid interface would prevent those situations: increased unsustainable surface tensions and alveolar collapse. This is what, lung surfactant, with its particular phospholipid composition and the presence of hydrophobic proteins, does (Perez-Gil, 2008).

To overcome these situations and accomplish an effortless respiration, lung surfactant needs to fulfil three biophysical properties (Parra and Perez-Gil, 2015):

i) Rapid adsorption to the air-liquid interface to reach the equilibrium surface tension. Phospholipids contained in lung surfactant are amphipathic molecules that can be orientated with their polar groups towards the liquid side and their acyl chains orientated to the air side, when they are transferred to an air-liquid interface. When the interface is saturated with PL, the air-water surface tension (70mN/m) drops down to the equilibrium surface tension (22-25 mN/m). This process occurs very fast, within seconds, due to the presence of the proteins SP-B and SP-C that help to overcome the energetic barrier (Lopez-Rodriguez and Perez-Gil, 2014). The speed at which this adsorption step occurs is critical, for example, in babies opening their lungs and filling them with air for the first time when they are born.

ii) Maximal surface tension reduction and film stability. During lung compression (Figure 5, top), the interfacial area in the alveolus decreases, which means that the surfactant monolayer has to be compressed and reach very low surface tensions, close to zero, in order to sustain this high-pressure status. The "squeeze out" model has been proposed to explain this situation. During compression, the surfactant film at the air-liquid interface is enriched in DPPC, due to the exclusion of unsaturated phospholipids and neutral lipids towards multilayered complexes at the aqueous sub-phase (Bangham et al., 1979, Perez-Gil and Keough, 1998). DPPC molecules can be tightly packed due to their saturated acyl chains, which allows surfactant to compress and reach the minimal surface tensions ~ 0 mN/m. Hydrophobic proteins participate in this transference of lipids (Schurch et al., 2010).

iii) Effective film re-spreading. During inspiration, the alveolar units are reopened again. The interfacial area increases and it needs to be replenished with new PLs coming from the reservoirs (Figure 5, bottom). Those reservoirs are multilayered surfactant membranes connected by hydrophobic proteins SP-B and SP-C, which again make possible the rapid transfer of lipids from the reservoirs to the interface to keep the equilibrium surface tension (Keating et al., 2012).

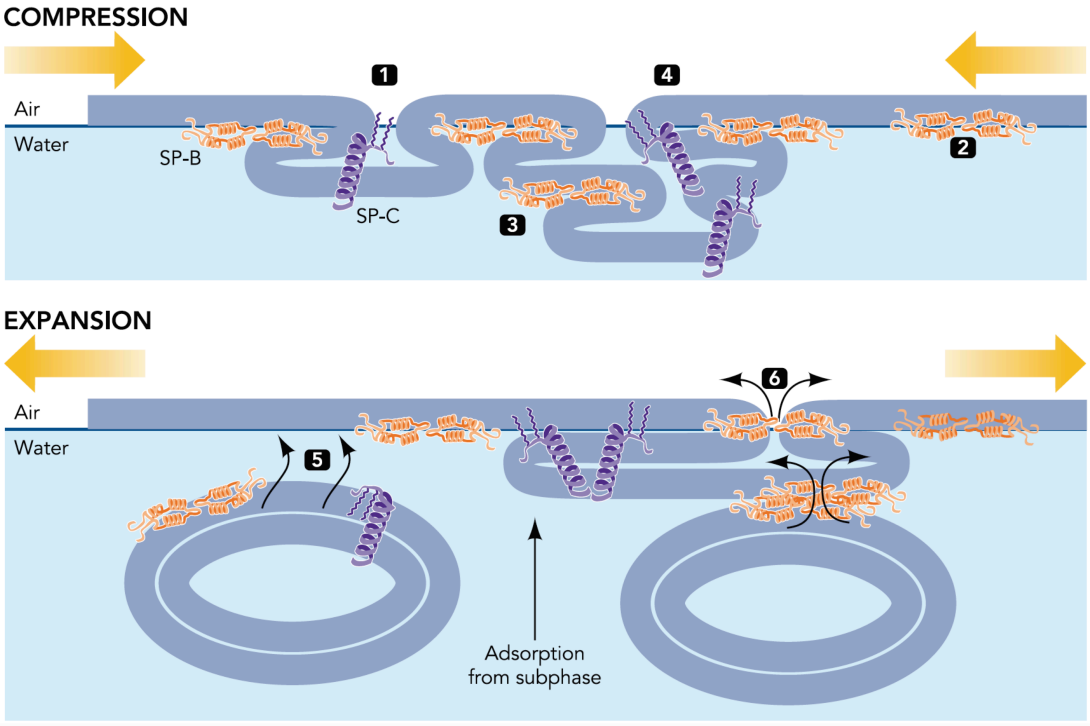

Figure 5: Surfactant dynamics during respiratory compression-expansion cycling. During expiration (*top*) SP-B and SP-C promote refinement of the surfactant surface film (***1***). SP-B stabilizes the film (***2***) and promotes membrane-membrane contacts (***3***) leading to the formation of multimembrane structures. SP-C might facilitate association of excluded surfactant structures with the interface, anchoring by its palmitic chains (***4***). During inspiration (*bottom*), SP-B and SP-C seem to promote insertion (***5***) and re-spreading (***6***) of phospholipids back to the air-liquid interface. Taken from (Perez-Gil and Weaver, 2010).

LUNG COLLECTINS AND THE INNATE IMMUNE DEFENSE OF THE LUNGS

There is a second major challenge at the air-liquid border in the alveoli: the potential invasion by inhaled microorganisms. The huge surface exposed to the air by lungs – in the order of 70 m^2 (Brown, 1957) – supposes a major opportunity for pathogens to enter in the body through this "door". Lung surfactant acts as a first barrier against those insults and it is equipped with hydrophilic proteins, SP-A and SP-D, to fight against invading pathogens. These surfactant hydrophilic proteins belong to the collectin family, particularly they are C-type calcium-dependent

lectins, which work as pattern recognition molecules. They collaborate in the first line of defense of the lungs through their ability to recognize a broad spectrum of pathogens *de novo*, resulting in agglutination and enhanced clearance of microorganisms (Sano and Kuroki, 2005, Kingma and Whitsett, 2006, Haczku, 2008, Ariki et al., 2012).

- **Collectin family**

Nine collectin proteins have been described up to date: mannose binding lectin (MBL), surfactant proteins A and D (SP-A, SP-D), collectin liver 1 (CL-L1), collectin placenta 1 (CL-P1), collectin kidney 1 (CL-K1), conglutinin and collectins of 43 kDa and 46 kDa (CL-43 and CL-46). The last three are not found in humans, but only in the *Bovidae* family (Holmskov, 2000, van de Wetering et al., 2004, Howard et al., 2018). They can be expressed and found in many organs, but in general terms, MBL, CL-L1, conglutinin, CL-43 and CL-46 are found in liver and circulation; SP-A and SP-D in lungs and non-pulmonary mucosas such as tears, amniotic epithelium, mesenteric cells, etc; CL-K1 in kidneys and CL-P1 in placenta and other tissues (Howard et al., 2018).

Collectin family members have four common structural determinants (Figure 6): an N-terminal region that is rich in cysteines, a collagen domain whose length varies among the family members, a neck region with a helical coiled-coil structure and, a carbohydrate recognition domain (CRD), the proper lectin domain. Three monomers associate into trimers through the folding of the collagen domains and with the participation of the neck region, which is finally stabilized by disulfide bonds within the N-terminal regions (Hakansson and Reid, 2000). Some of the family members can form higher order oligomers, such as dodecamers with cruciform-like shape in the case of SP-D or conglutinin, or for example octadecamers with bouquet-like shape, in the case of SP-A and MBL (Holmskov, 2000).

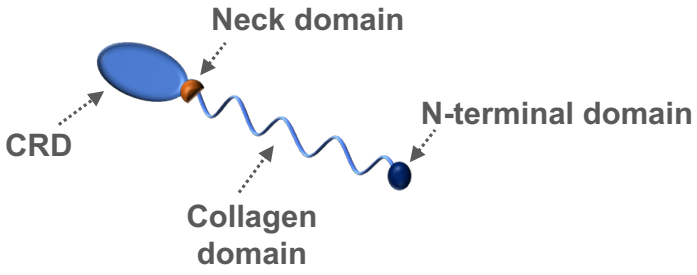

Figure 6: Structural domains in collectin proteins. Taking as an example the SP-D monomer, it contains the N-terminal domain, followed by a long collagen domain, whose length changes among the different collectins. The collagen domain is continued by the neck domain that presents a coiled-coil structure, and finally a globular region at the C-terminal end, which constitutes the carbohydrate recognition domain (CRD).

Collectins are pattern recognition molecules that recognize carbohydrate structures or lipid moieties attached to the surface of microbes. The minimal ligand recognition unit appears to be the trimeric carbohydrate recognition domain. The presence of calcium ions in the calcium binding sites within the CRD is essential, because it allows this region to adopt a specific conformation that permits to establish interactions with the hydroxyl groups contained in the carbohydrate structures, which are decorating the surface of pathogens (Hakansson and Reid, 2000, Seaton et al., 2010). Binding to pathogens may result in microbial clearance through aggregation, agglutination, inhibition of microbial growth, opsonization and activation of phagocytosis. Moreover, MBL can also induce complement activation. Last, collectins may also modulate inflammatory and allergic responses, affect apoptotic cell clearance and modulate the adaptive immune system (Holmskov, 2000, van de Wetering et al., 2004, Howard et al., 2018).

- **Surfactant protein A (SP-A)**

Surfactant protein A can be found as two isoforms in humans: SP-A1 and SP-A2 (Floros et al., 2009). Its principal location is the lung, but it can be also found in other parts of the body, for example in the gastrointestinal and renal system (Vieira et al., 2017). One of the key differences between both protein isoforms is the amino acid in position 85, a cysteine in SP-A1 and an arginine in SP-A2, which affects protein oligomerization and somehow protein surfactant-related activities (Wang et al., 2007). Three 35 kDa monomers with the characteristic collectin structure associate intro trimers of 105 kDa (Figure 7, left). It has been proposed that each trimer consists of two SP-A1 molecules and one SP-A2 molecule (Voss et al., 1991, Wang et al., 2004). In native human SP-A purified from bronchoalveolar lavage, structures composed of up to 6 trimeric units have been observed, octadecamers (~650 kDa) with a bouquet-like shape (Palaniyar et al., 2001).

SP-A recognizes and binds carbohydrates on the surface of microbes, and surfactant phospholipids, preferentially DPPC, by its CRD domains in the presence of calcium (Palaniyar et al., 2001). Carbohydrate binding preference has been determined by in vitro solid phase-binding assays using adsorbed mannan, and resulted to be: N-acetylmannosamine > L-fucose > maltose > glucose > mannose, with no inhibition observed by galactose, N-acetylglucosamine or N-acetylgalactosamine (Haczku, 2008).

Generation of recombinant versions of SP-A1 and SP-A2, as well as humanized mice encoding each protein, have been performed to study the structural and functional differences between these two variants. SP-A1 has been

shown to form higher order oligomers and to carry out a more important role in the biophysical activity of lung surfactant, whereas, SP-A2 is assembled into less oligomerized structures and it could be more implicated in innate immune functions, based on the published literature (Wang et al., 2004, Wang et al., 2007, Sanchez-Barbero et al., 2007, Lopez-Rodriguez et al., 2016).

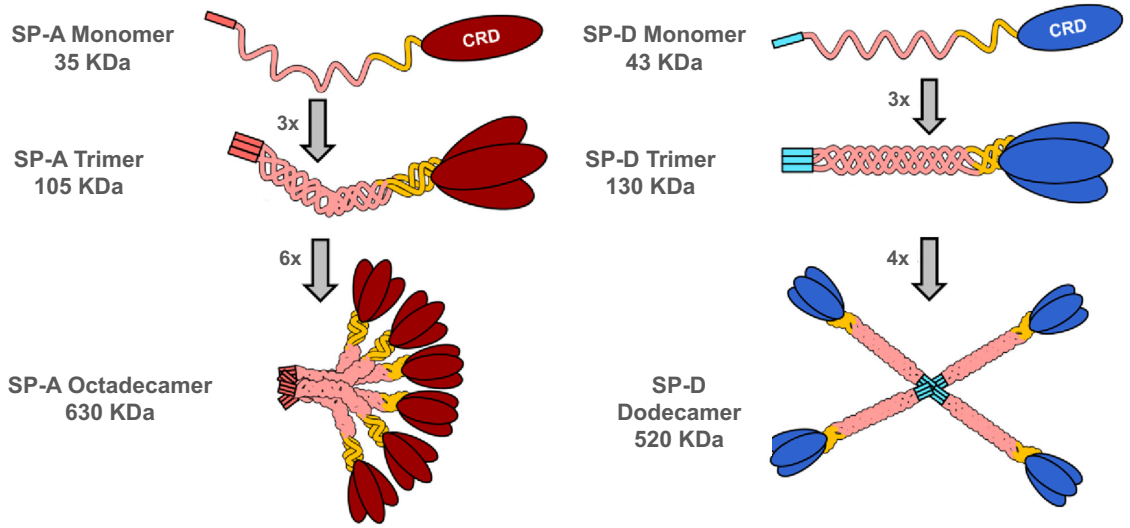

Figure 7: Structure and oligomeric forms of surfactant proteins SP-A and SP-D. In both cases, three monomers with the typical collectin structure associate into trimers. **SP-A** (*left*), the association of 6 trimers originates octadecamers with a bouquet-like conformation. **SP-D** (*right*), the association of 4 trimers forms a dodecamer. Adapted from (Vieira et al., 2017).

SP-A host defense functions include interactions with monocytes and macrophages to mediate chemotaxis and phagocytosis and interactions with microbes to facilitate their clearance: i) bacteria, for example *Staphylococcus aureus* and *Mycobacterium tuberculosis*, ii) virus, like respiratory syncytial virus, and iii) fungi, such as *Pneumocystis carinii* (Kishore et al., 2006, Haczku, 2008). Moreover, it also participates in allergen clearance and modulation of the allergic response (Wang et al., 1998).

- **Surfactant protein SP-D**

In 1985, Phelps and Taeusch designated a class D of surfactant proteins that contained uncharacterized basic proteins of 40-45 kDa (Phelps and Taeusch, 1985). In 1988, Persson and colleagues identified a collagenous glycoprotein of 43 kDa, which was synthesized by rat type II pneumocytes, and it was called CP4 (Persson et al., 1988). One year later, CP4 was purified from bronchoalveolar lavage of rats as part of lung surfactant and it was characterized biochemically. It was proposed to be designated and named as surfactant protein SP-D (Persson et al., 1989), according to the accepted nomenclature for surfactant-associated

proteins (Possmayer, 1988). Since 1989, many structural and functional studies have been carried out to elucidate the structure and function of SP-D.

1. Structure

SP-D encloses the four characteristic structural domains of collectin proteins: N-terminal domain, collagen domain, neck domain and carbohydrate recognition domain (CRD). The structure of the protein is described for human SP-D (Figure 8), which contains 355 amino acids (375 considering the signal peptide added at the N-terminal end). SP-D has been observed as a mixture of oligomeric forms: trimers, which are formed by the association of 3 monomers, dodecamers (4 trimers) and large oligomers (≥ 6 trimers), so-called fuzzy balls (Crouch, 1998, Crouch, 2000, Kishore et al., 2006).

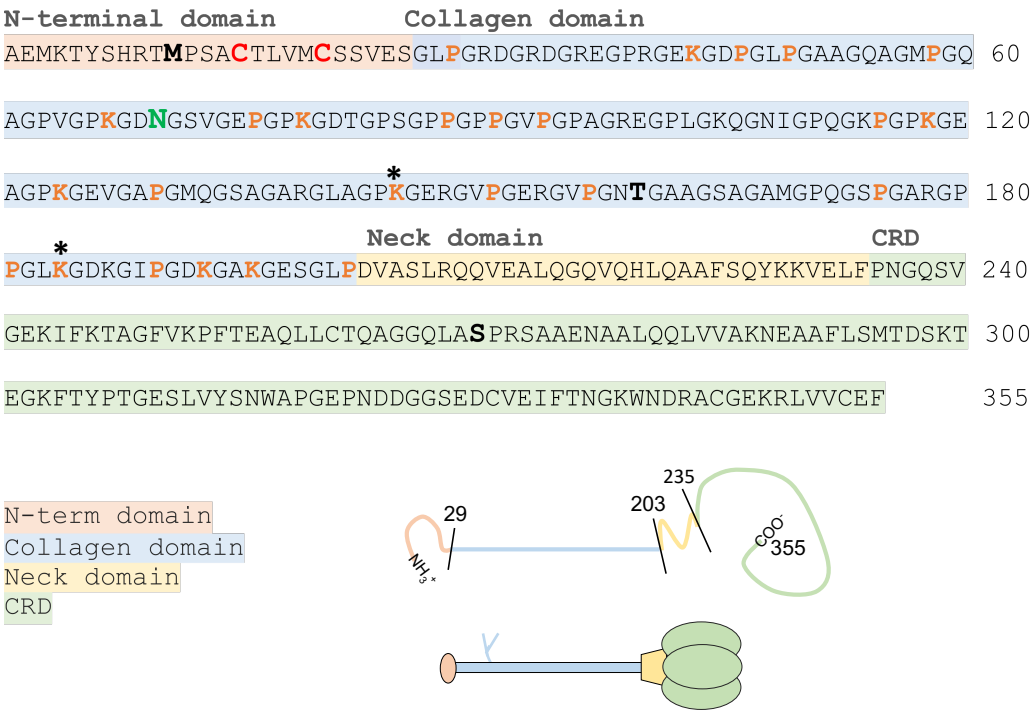

Figure 8: Amino acid sequence and domain organization of hSP-D. The segments of the sequence defining the different protein domains are shaded with different colors: N-terminal (orange), collagen (blue), neck (yellow) and CRD (green). Amino acids Met[11], Thr[160] and Ser[270] are in bold as possible genetic variants of the protein. Cysteines Cys[15] and Cys[20] are in red bold letter. Glycosylated (blue Y in the protein scheme at the bottom) residue N70 is in bold green. Hydroxylated prolines are in brown (Leth-Larsen et al., 1999). Lysines marked with the asterisk are always found O-glycosylated, the rest of lysines in bold brown can be found as partly O-glycosylated and/or hydroxylysine residues.

A. <u>N-terminal domain:</u>

The amino terminal region contains two conserved cysteines: Cys[15] and Cys[20], which are important for protein oligomerization (Crouch, 2000). These 2 cysteines form interchain disulfide bonds to stabilize SP-D trimers. It has been

observed that a truncated version of SP-D, produced by the substitution of these cysteines by serines, may form trimers but those are not stabilized and cannot assemble into larger oligomers (Brown-Augsburger et al., 1996b).

B. Collagen domain:

SP-D possesses a long collagen domain formed by 59 repetitions of the triplet G-X-Y (in which the first amino acid is always glycine and, X and Y are different amino acids) (Crouch et al., 1994b, Crouch, 2000). There are several prolines and lysines within the collagen domain that can be hydroxylated, and hydroxylysines can be further O-glycosylated. In addition, SP-D collagen domain has a N-glycosylation site in the asparagine in position 70 (Figure 8). The structure of the glycan attached to this Asn^{70} has been described as a core-fucosylated biantennary structure, containing N-acetylglucosamine (GlcNAc) and galactose (Leth-Larsen et al., 1999). Proline hydroxylation is important for the stabilization of the collagen helix, but the role of glycosylated hydroxylysines and the N-glycosylation in Asn^{70} is not fully understood. It has been described that the N-glycan is not determinant for protein secretion by cells, oligomerization or interaction with several microorganism (Brown-Augsburger et al., 1996a, Crouch, 2000).

C. Neck domain:

This short peptide has an α-helical structure and contains four heptads with hydrophobic residues at position "d", being leucine in the first three heptads and tyrosine in the last one (C-terminal side). The positions of these hydrophobic residues, as well as the consensus aromatic residues Phe^{225} and Tyr^{228}, are important to maintain a stable α-helical coiled-coil structure in trimers (Zhang et al., 2001b). It has been shown that the neck domain is critical for protein trimerization, because truncated versions lacking the complete neck domain were only found as monomers. It was proposed that the role of the coiled-coil structure is to align the collagen chains to facilitate the subsequent "zipper-like" folding of the three chains until the N-terminal domain (Zhang et al., 2001b).

D. Carbohydrate recognition domain (CRD):

This domain attributes lectin activity to SP-D. It has a globular structure with 7 β-strands and 2 α-helical segments (Figure 9A). There are four cysteines that form intrachain disulfide bonds Cys^{261}-Cys^{353} and Cys^{331}-Cys^{345}. Each CRD contains 3 calcium binding sites, where 3 calcium ions are coordinated to specific amino acids of the protein (Figure 9B). Calcium ion 1 is coordinated to the lateral chains of Glu^{321}, Asn^{323}, Glu^{329}, Asn^{341}, Asp^{342} and to the main carbonyl chain of Asp^{342}. In the

absence of a carbohydrate ligand, coordination is completed by two water molecules. In the presence of a carbohydrate ligand, such as glucose or maltose, the positions occupied by the two water molecules are substituted by the hydroxyl groups in carbons 3 and 4 of the carbohydrate hexose. Moreover, 4 protein residues coordinate with those two hydroxyl groups: Glu^{321} and Asn^{323} with O3′ atom (oxygen atom of OH-group in carbon 3) and Glu^{329} and Asn^{341} with O4′ atom; all these four amino acids are also calcium-coordinators. Calcium ions 2 and 3 are coordinated also with some CRD amino acids and water molecules, and it seems that they do not interact with ligands, at least, with monosaccharides or disaccharides. It is unknown whether they collaborate in the interaction with more complex structures. Last, when SP-D is in its trimeric form a forth calcium binding site was found within the funnel in the cavity surrounded by the 3 CRD domains (Shrive et al., 2003).

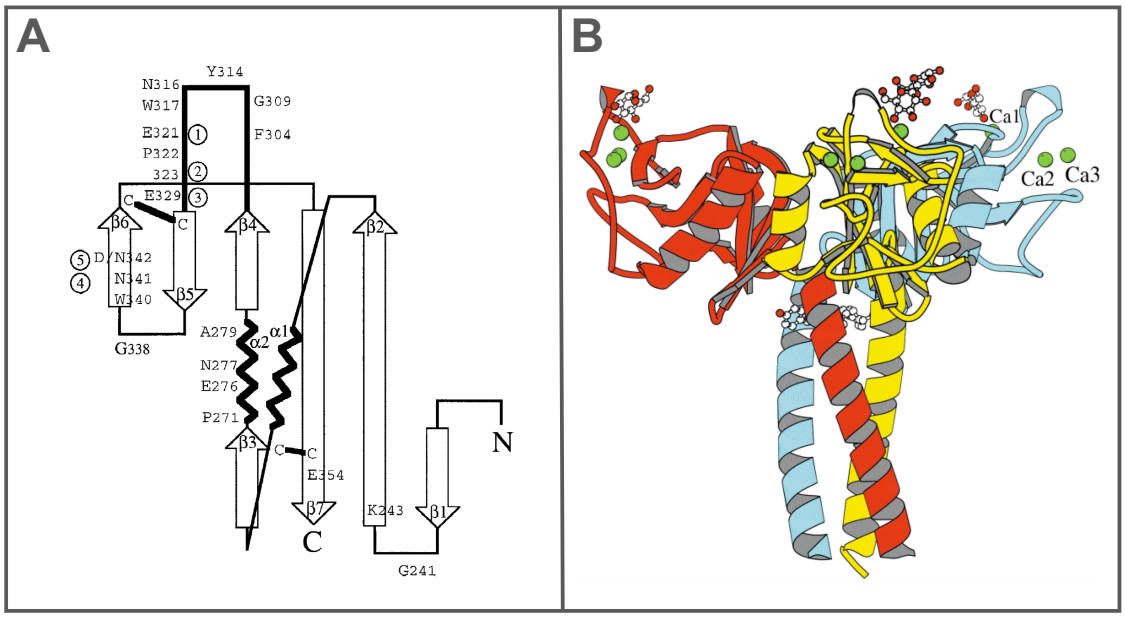

Figure 9: Structure of the carbohydrate recognition domain of SP-D. ***A***, topological representation of the secondary structure elements in C-type lectin domain of SP-D. Segments with β-strand (1-7) and α-helical (1-2) secondary structures are numbered. Amino acids denoted with encircled numbers 1-5 are the ones coordinated to the carbohydrate binding calcium ion 1. The remaining amino acids indicated in the structure are conserved among collectin proteins. Image taken from (Hakansson and Reid, 2000). ***B***, trimeric structure of a truncated version of hSP-D composed by neck and CRD domains, which is bound to maltose. Viewed perpendicular to the molecular 3-fold. Calcium ions are numbered and represented as green circles. Maltose is bound to calcium binding site 1. Image taken from (Shrive et al., 2003).

In terms of ligand recognition and binding, it is important the amino acid in position 335, a phenylalanine, due to its aromatic ring, to stablish interactions with protein ligands (Crouch et al., 2006).

Trimeric units are the minimal oligomeric form observed in SP-D. Trimers are formed through the folding of the collagen region of three monomers into a triple collagen helix and the coiled-coil formation at the neck domains level. Trimeric structures are stabilized by interchain disulfide bonds at the N-terminal domain. Four trimers are joined through the N-terminal regions and form dodecamers with a cruciform structure (Figure 7, right). Last, large oligomers, so-called fuzzy balls or asterisk-like structures, are composed by a variable number of trimeric arms from 6 to 30 or even more. The three-dimensional aspect of those large structures is not fully clear, as they have been observed deposited onto substrates by electron microscopy (EM), with an asterisk-like shape, but they could have spherical shape in solution, therefore so-called fuzzy balls (Crouch et al., 1994b, Crouch, 2000, Sorensen, 2018). Despite all the structural studies, up to now, it is not fully understood how trimers assemble into dodecamers and larger oligomers, as well as the kind of interactions leading that process.

2. Synthesis, processing and regulation of expression

Surfactant protein SP-D is encoded by a single gene with 7 exons localized in the chromosome 10, particularly at 10q22.2-23.1 region in close proximity to SP-A and MBL genes (Crouch et al., 1993b).

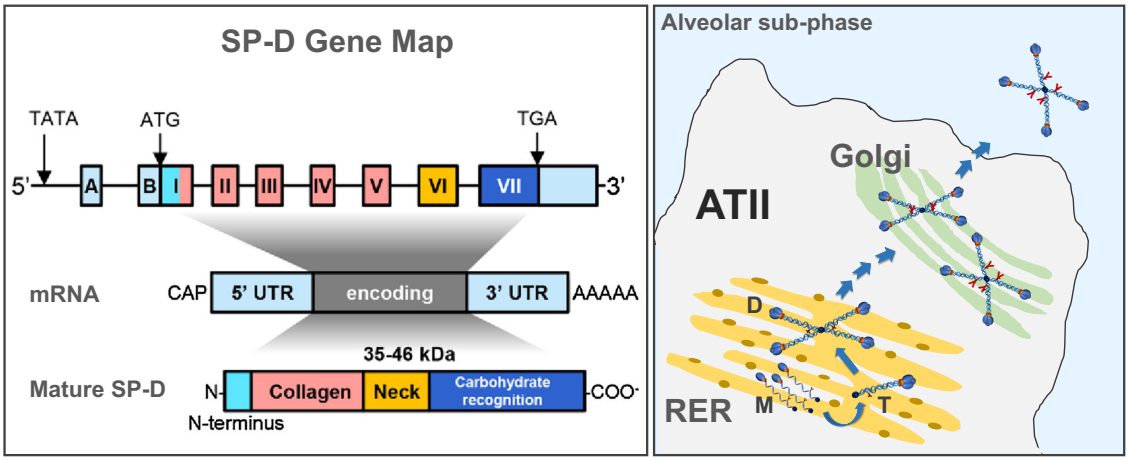

Figure 10: SP-D gene map, transcription and translational products and synthesis in ATII cells. ***Left***, chromosome exons encoding SP-D and transcription products. Modified from (Vieira et al., 2017). ***Right***, SP-D synthesis in alveolar type II cells (ATII). SP-D monomers (M) are synthetized and partly glycosylated in the rough endoplasmic reticulum (RER) and assembled into trimers (T) and dodecamers (D). From RER, SP-D goes to the Golgi apparatus where the protein is further glycosylated and then secreted to the alveolar sub-phase.

In lungs, synthesis of SP-D monomers takes place in the rough endoplasmic reticulum (RER) of type II pneumocytes and in bronchial epithelial cells, the non-ciliated Club (clara) cells (Sorensen, 2018). This includes: the folding of the C-terminal carbohydrate recognition domain, glycosylation of asparagine 70 and

hydroxylation of prolines and lysines within the collagen domain. Afterwards, trimerization is driven by neck domains and followed by the formation of the collagen triple helix, which is finally stabilized by disulfide bonds at the N-terminal domains (Figure 10). Association of trimers into dodecamers still happens in the RER and then molecules are transported to the Golgi apparatus where oligosaccharide maturation takes place prior to secretion (Brown-Augsburger et al., 1996a). To date, nothing is known about the assembly of larger oligomers, whether they are also assembled in the RER or once the protein is secreted. SP-D oligomers are secreted to the alveolar aqueous phase where the protein carries out its function.

SP-D is detected in lungs of 10-20 weeks' fetuses at low concentrations and protein levels increase during gestation until labor (Stahlman et al., 2002, Sorensen et al., 2007). Several factors have been described to regulate its expression, being increased by retinoblastoma protein, activation of the calcineurin/NFAT pathway, MAP-kinase, dexamethasone, maternal steroid treatment and TNF-α (Sorensen et al., 2007, Sorensen, 2018). On the other hand, expression was inhibited by nitric oxide synthase inhibitor (L-NAME), inhibitors of phosphoinositide 3-kinases (PI3Ks) and inhibitors of MEK1 activation (Sorensen, 2018).

In vitro, recombinant SP-D has been synthesized in several production systems, including mammalian cell lines, *E. coli* and *Pichia pastoris*. The most widely used system has been the mammalian cell line CHO-K1, which produces recombinant SP-D properly folded exhibiting the same oligomeric forms than the native protein, as well as its post-translational modifications: hydroxylations and glycosylations (Salgado et al., 2014).

3. Gene differences

Three different polymorphisms have been found in the coding sequence of human SP-D. Codons corresponding to amino acid residue 11 (Met or Thr), residue 160 (Ala or Thr), and residue 270 (Ser or Thr) (Figure 8, amino acids in black bold) (Crouch et al., 1993b, DiAngelo et al., 1999). Further studies have demonstrated that those modifications can involve structural changes in protein conformation, different protein levels in serum and altered susceptibility to various diseases (Leth-Larsen et al., 2005). Genotyping studies of serum hSP-D from Caucasian individuals have indicated a linkage between Met^{11}, Thr^{160}, and Ser^{270}, and between Thr^{11}, Ala^{160}, and Thr^{270} (Leth-Larsen et al., 2005).

Variations in amino acids at position 160 and 270 have not shown consequences in protein structure, levels and correlation with diseases. However, the presence of a methionine or a threonine at position 11 involves some changes in the protein. A study performed with a north European population showed the

allele frequency distribution as 59% methionine and 41% threonine (genotype distribution was Met/Met^{11} (35.4%), Met/Thr^{11} (47.1%), Thr/Thr^{11} (17.5%)). hSP-D expressing the Met^{11} allele contained a mixture of low (trimers) and high (dodecamers and fuzzy balls) molecular weight oligomers, whereas in the case of Thr^{11} only low molecular weight forms (trimers) were found. Besides, it was observed an implication in protein activity where the Thr^{11} showed lower activity binding to bacteria and Influenza A Virus (IAV), while the Met^{11} variant was more active (Leth-Larsen et al., 2005). Last, Met^{11} allele was associated with severe respiratory syncytial virus infection in infants (Lahti et al., 2002), while Thr^{11} could increase susceptibility to tuberculosis (Floros et al., 2000).

It has been documented by Mason and colleagues that when a threonine is found in position 11, that threonine could be also glycosylated, giving as a result an SP-D monomer with a molecular weight of 50 kDa. They suggested that this increase in molecular weight could be caused by the extra glycosylation in Thr^{11} which would not happen in the case of the Met^{11} variant (Mason et al., 1998).

Differences in SP-D amino acid sequence have been found between different species. The Asn^{70} that constitutes the N-glycosylation site, and the collagen triplet where it is contained (NGS) are conserved among many species (Figure 8). Porcine SP-D showed an extra N-glycosylation site in the Asn^{323}, located in the CRD (van Eijk et al., 2002). Variations in the most abundant oligomeric form have been shown between species, for example, dodecamers appear to be the most abundant oligomer in rat SP-D, fuzzy balls in pigs, while in humans there is a similar distribution between both (Crouch et al., 1994b, van Eijk et al., 2002, Sorensen et al., 2009). Despite these qualitative observations, due to the lack of a quantitative reproducible method, the real distribution of oligomeric forms is still unknown. The interactions and amino acids involved in the formation of large oligomers are not fully understood, as well as whether the differences in the amino acid sequences between species could influence them.

4. Functions of SP-D

SP-D participates in the host defense of lungs. It recognizes certain ligands in invading microbes and stimulates host cells to boost clearance of pathogens. Also, it regulates the innate immune response in the lungs stimulating pro- or anti-inflammatory pathways (Sorensen, 2018). Moreover, it is involved in lung surfactant homeostasis, regulating phospholipid pool sizes and accumulation in the alveolar sub-phase (Ikegami et al., 2005).

A. SP-D Ligands

Carbohydrates are the principal structures recognized by SP-D at the surface of pathogens. The carbohydrate recognition domains of the protein carry out this function, which preferentially recognize D-glucopyranosides. The carbohydrate binding preference of SP-D has been determined by solid binding assays using maltosyl-BSA to be: N-acetylmannosamine > maltose > mannose > glucose, fucose > galactose, lactose, glucosamine > N-acetylglucosamine (Crouch, 1998, Crouch et al., 2006, Haczku, 2008, Sorensen, 2018). This preference order changes between proteins from the collectin family and highly influences the ligand-specificity between the family members (Holmskov, 2000). Carbohydrates are an important component of lipopolysaccharides (LPS), which constitutes the major SP-D ligand in gram negative bacteria (Kuan et al., 1992, Lim et al., 1994). LPS is composed by the lipid A (anchor to the bacterial membrane), a core oligosaccharide structure, and the O-antigen (a repetitive glycan polymer which differs between strains) (Figure 11). LPS is referred in the literature as smooth or rough LPS, which depends on the nature of its O-antigen. When the O-antigen carbohydrate chains are reduced or eliminated, it is considered as rough LPS, whereas it is smooth LPS when the intact O-antigen is preserved. It has been published that SP-D preferentially binds to rough forms of LPS (Kuan et al., 1992, Yamazoe et al., 2008).

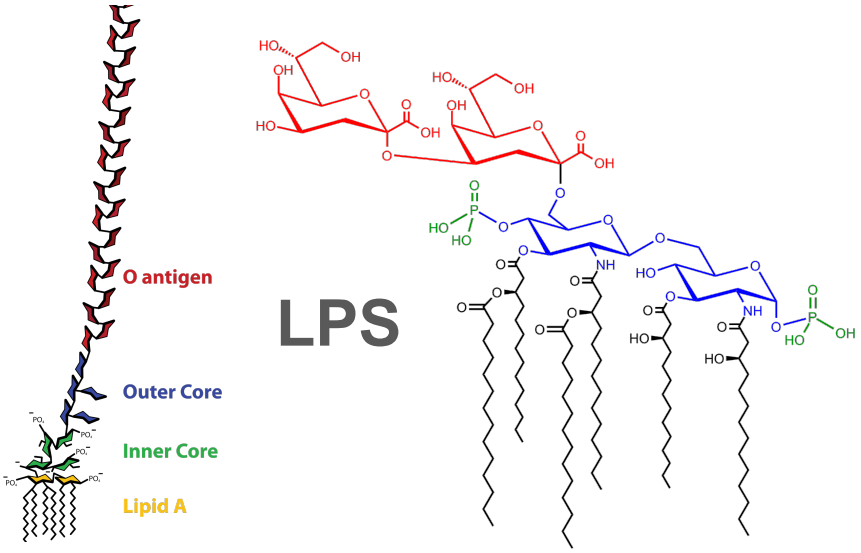

Figure 11: Lipopolysaccharide (LPS) structure. Both molecules represent LPS. O-antigen is represented in red, the LPS core in blue and green and the lipid A in yellow (left) and black (right).

SP-D also binds to other two lipid ligands: phosphatidylinositol (PI) and glucosylceramide in a calcium-dependent manner and this binding is inhibited by competing sugars (Crouch, 1998). PI seems to be the PL that allows SP-D to interact with lung surfactant membranes. It has been observed that SP-D binds to PI

(Ogasawara et al., 1992) and to glucosylceramide (Kuroki et al., 1992) on thin-layer chromatography. In addition, it has been shown that SP-D interacts with PI-containing liposomes, and that the collagen domain could be important for these interactions conferring an adequate spacing between trimeric CRDs (Ogasawara and Voelker, 1995).

Nucleic acids have been also described as SP-D ligands. SP-D binds to DNA through the collagen domain by non-covalent interactions. Although the collagen domain leads this interaction, it has been shown that in the presence of calcium this binding is stronger, so probably the CRD might contribute to it (Palaniyar et al., 2004).

Other SP-D-binding ligands have been published like proteins from the scavenger receptor cysteine rich family, such as glycoprotein-340 (GP-340) (Holmskov et al., 1997), or defensins like decorin (Nadesalingam et al., 2003).

B. Interaction with microorganisms

SP-D interacts with different strains of bacteria, viruses and fungi. The external surface of these organisms is rich in diverse polysaccharides and glycoconjugates that are recognized by SP-D.

- Bacteria

  In gram negative bacteria, SP-D binds to the core oligosaccharides (glucose and/or heptose) of LPS molecules anchored to the outer wall of bacteria (Kuan et al., 1992, Lim et al., 1994, Crouch, 2000). It has been found that SP-D binds to *Klebsiella pneumoniae, Pseudomonas aeruginosa, Haemophilus influenzae* and *Escherichia coli* (Pikaar et al., 1995, Crouch, 1998).

  In gram positive bacteria the mechanism of binding has not been completely elucidated. It seems that it could be mediated by SP-D binding to lipoteichoic acids and peptidoglycan, components of the gram-positive cell walls, as it has been demonstrated for *Staphylococcus aureus* and *Streptococcus pneumoniae* (Hartshorn et al., 1998, Crouch, 2000, Kishore et al., 2006).

  It has been also reported that SP-D binds to lipoarabinomannan in *Mycobacterium tuberculosis* (Ferguson et al., 1999).

- Viruses

  It has been observed that SP-D binds to high-mannose oligosaccharides expressed on the hemagglutinin or neuraminidase of specific strains of influenza A viruses (IAVs), and it interferes sterically with hemagglutinin activity (Hartshorn et al., 1996b).

SP-D can interact with other respiratory viruses, such as the Rous sarcoma virus, through the G protein of the virus (Hickling et al., 1999).

- Fungi

In *Pneumocystis carinii* SP-D binds to gpA, a mannosylated glycoprotein associated to trophozoites, and to the β-glucans in the cell wall. It was also reported that SP-D binds to *Cryptococcus neoformans, Aspergillus fumigatus, Candida albicans* and *Saccharomyces cerevisiae*. The interaction with those lasts is not well understood, although it has been proposed that it could be mediated by the presence of β-glucans in the cell wall (Crouch, 2000).

SP-D binding to all these pathogens mediates viral agglutination, inhibition of the hemagglutination activity of IAV, bacterial aggregation, and inhibition of bacterial growth by membrane permeation (Figure 12). All of these actions contribute to stop microbial invasion and favor their clearance. Moreover, SP-D binding can promote opsonization of the microbes that will end up in their elimination by phagocytic cells (Crouch, 2000, Ariki et al., 2012, Vieira et al., 2017).

C. Interaction with host cells and modulatory effect in immune responses

SP-D can interact with host cells and in this way, it regulates mechanisms of phagocytosis and cellular responses. One of the consequences of SP-D binding to bacteria, viruses and fungi, as well as to apoptotic cells, is their opsonization, in other words, they are marked to be deleted. Therefore, those organisms will be cleared by phagocytic cells, such as macrophages, avoiding their accumulation and harmful effects in the alveolar space.

Another important role, mediated by its opsonin function, is to avoid the accumulation of substances with antimicrobial activities that are released by different cells, and help to agglutinate microbes. This is the case of neutrophils extracellular traps (NETs) released by neutrophils under microorganism invasion. NETs are a mesh of decondensed chromatin fibers decorated with antimicrobial granular proteins, that help to capture and ensnare bacteria (Brinkmann et al., 2004). They have a defensive antimicrobial function, but their overaccumulation due to overproduction or insufficient clearance has damaging effect for lung tissues. In this way, SP-D binds to those NETs, signaling their phagocytosis by macrophages (Douda et al., 2011, Cheng and Palaniyar, 2013).

SP-D binds and regulates the expression of some cell surface receptors to induce phagocytosis or to regulate the immune responses. SP-D bound to infectious agents may interact through its collagen domain with the calreticulin-CD91

complex in phagocytic cells, driving phagocytosis and enhancing the proinflammatory response (Figure 12). Interaction of SP-D with SIRP-α (Signal-Inhibitory Regulatory Protein alpha) through its CRD, results in an inhibitory signal preventing activation of mononuclear leukocytes. However, when the CRD is already occupied by a ligand, SP-D is suggested to interact with the calreticulin-CD91 complex through the collagen domain, instead of SIRP-α, and promote inflammatory cell activation (Vieira et al., 2017, Sorensen, 2018).

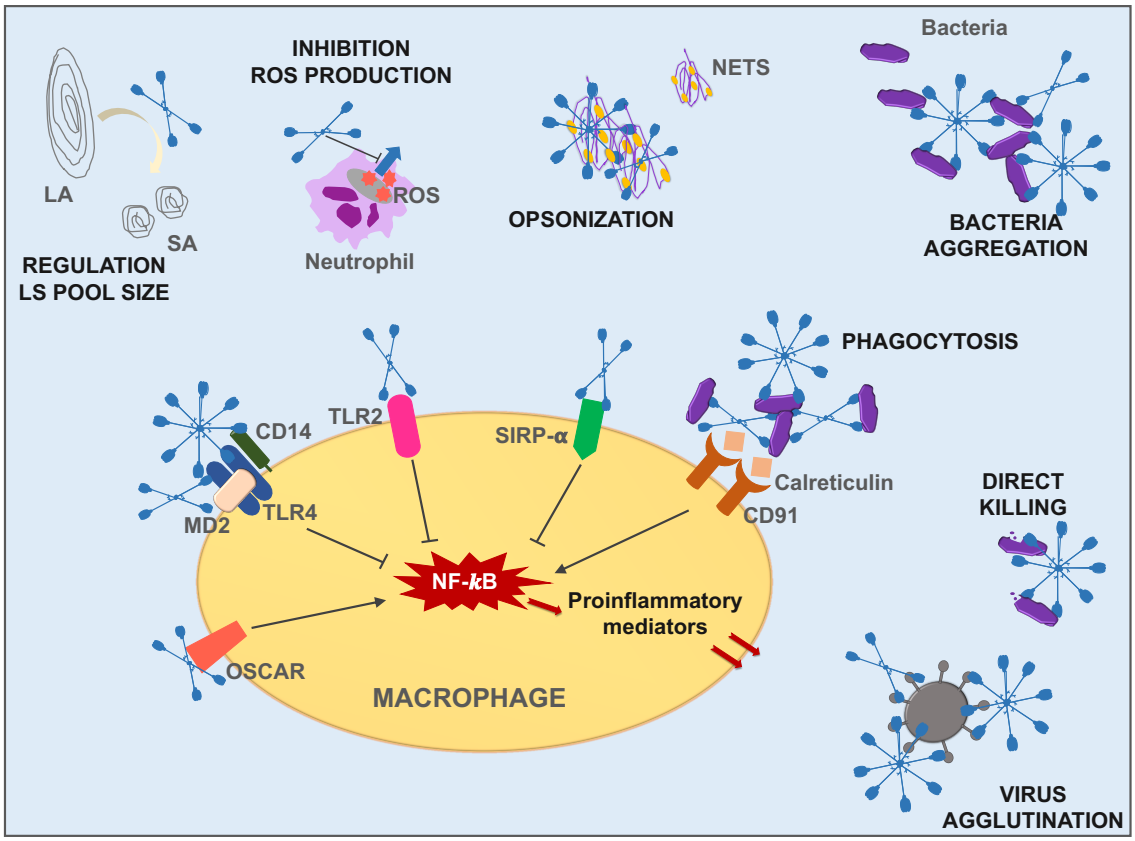

Figure 12: SP-D function in lung homeostasis. Representation of SP-D interactions with microorganism and with host cells to eliminate the pathogens and modulate the immune response. Regulation of the PL pool of LS is also represented. Elements of the figure are not in real scale. References detailed in the main text.

SP-D inhibits the inflammatory response induced by LPS. The CRD domains of SP-D bind to MD-2 in TLR4/MD-2 expressing cells, to the carbohydrate moiety of CD14 (a macrophage receptor for LPS) in CD14/TLR4 complex and to TLR2. SP-D binding to these receptors causes suppression of the inflammatory pathway and, thereby, inhibition of LPS-induced production of cytokines and inflammatory mediators (Sorensen, 2018, Vieira et al., 2017).

On the other hand, the Osteoclast-Associated Receptor (OSCAR), expressed in inflammatory monocytes, macrophages and dendritic cells can interact with the

collagen domain of SP-D and cause a pro-inflammatory response, causing the release of TNF-α and other cytokines (Vieira et al., 2017, Sorensen, 2018).

SP-D regulates the production of reactive oxygen species (ROS). Interaction of the SP-D collagen domain with the leukocyte-associated immunoglobulin-like receptor 1 (LAIR-1) results in a functional reduction of ROS production by neutrophils (Sorensen, 2018).

SP-D also interferes in the adaptive immune response. It suppresses T-cells activation and inhibits its proliferation. This finding agrees with the phenotype observed in SP-D null mice, where increased concentrations of activated lymphocytes were found, as observed by the increased proportion of CD4+ and CD8+ T cells that express CD25 and CD69 (Wright, 2005).

D. Interaction with lung surfactant lipids

Surfactant protein D participates in surfactant lipids homeostasis (Korfhagen et al., 1998). It has been found that SP-D regulates surfactant lipid pool sizes by participating in the conversion of surfactant large aggregates (LA) of LS into small aggregates (SA). In agreement with that, SP-D$^{-/-}$ mice present increased amounts of LA, and both LA and SA display abnormal structures with higher lipid density and size (Ikegami et al., 2005). It is known that ATII cells preferentially uptake SA forms of LS. As a consequence of the impaired surfactant structures and conversion to SA in SP-D$^{-/-}$ mice, LS uptake by type II pneumocytes is affected, which provokes an accumulation of surfactant lipids in the alveolar aqueous sub-phase (Ikegami et al., 2005). These alterations are restored upon administration of full-length SP-D to the null mice. It has been found that there is a direct effect of the protein over the lipid aggregates, not mediated by SP-D/ATII interactions. Interestingly, SP-D levels rise after birth and reach a peak at day 3-5 paired with PI levels. Therefore, the interaction of SP-D and PI containing vesicles has been a matter of research. It has been found that SP-D interacts and carries out a lytic activity on PI-containing vesicles, which is greater with increasing PI concentrations (Ikegami et al., 2009). In addition, the structure of LS membranes after birth is similar to those in SP-D null mice, and they change to the normal structures during the first days of life. However, the CRD and neck domains of the protein are not sufficient to carry out this function. It has been shown that the presence of full-length protein is necessary, containing dodecamers and large oligomers, to restore efficiently this dysregulation (Ikegami et al., 2009).

Despite those findings, the mechanisms by which SP-D controls surfactant lipid pools and influences ultrastructure are not fully understood. SP-D interacts

with PI through the CRD domain, but paradoxically, it is necessary to have a protein with the N-terminal domain and the collagen domain to perform this function.

Last, a protective role against PL oxidation by reactive oxygen species (ROS) has been also described for SP-D (Bridges et al., 2000). It has been proposed that SP-D directly interferes with free radical formation or propagation, protecting lung surfactant lipids and hydrophobic proteins from oxidation, which is translated into protection of LS biophysical activity.

In summary, SP-D functions are important in lung homeostasis at two levels: breathing and immune defense, with a stronger role in the last one. On the one hand, it regulates PL pools in lungs, participating in LS recycling. On the other hand, in the context of the immune defense, SP-D actions are focused to eliminate invading pathogens, in a way that the immune response will be always balanced to clear the microorganisms, without provoking an exacerbated inflammatory response that could damage lung tissues and have the opposite effect.

It should be kept in mind that some of the SP-D functions are not very specific; the protein recognizes carbohydrate structures as well as other collectins do, such as SP-A. This is the key for a rapid first response to pathogens invasion in the innate immune defense. These two collectins share several duties in lungs, but they are distinguished by a different preference of binding to diverse pathogens and receptors, and a distinct potency to carry out certain functions.

5. Surfactant protein D levels as a disease marker

SP-D levels, mainly in serum and bronchoalveolar lavage (BAL), have been found to be useful markers in several diseases.

In pulmonary alveolar proteinosis (PAP) and sarcoidosis, increased concentrations of SP-D were found in BAL and serum (Sorensen et al., 2007).

There are several pulmonary diseases where the air-capillary barrier is damaged as a consequence of the course of the disease. As a consequence, SP-D leakages from the alveolar spaces to the blood due to the loss of integrity of the barrier. This is the case of respiratory distress syndrome (RDS), acute lung injury (ALI), cystic fibrosis (CF) and chronic obstructive pulmonary disease (COPD). In all these cases, especially in advanced stages of the pathologies, a reduction of SP-D concentrations in BAL and increased levels in sera have been found compared to healthy people (Sorensen et al., 2007, Sorensen, 2018). In allergic asthmatic patients, serum and BAL SP-D levels were found to be increased (Sorensen, 2018).

Premature newborn babies have a high risk of developing bronchopulmonary dysplasia (BDP). Low levels of SP-D are found in lungs of those

patients, together with severe inflammation and impaired breathing, which is also caused by the impact of mechanical ventilation in the immature lungs of these babies. Interestingly, treatment with exogenous SP-D inhibits the lung inflammation caused by the oxygen ventilation. In this case, SP-D apart of being a disease marker, has been shown to be a potentially effective treatment for the disease (Awasthi et al., 1999, Ikegami et al., 2006, Sato et al., 2010).

6. SP-D beyond the lung

SP-D has been found in many other locations and expressed by other non-pulmonary cells in the human body. The role and functions of SP-D in those extra-pulmonary locations is under constant revision nowadays. So far, it is believed that SP-D acts as a pattern recognition molecule as in lungs, collaborating in the host defense. A very recent review written by Grith Sorensen collected and revised all human organ systems and locations for SP-D that include: the integumentary, digestive, urinary, reproductive, nervous and circulatory systems, as well as, some glands (Sorensen, 2018).

OBJECTIVES

Surfactant protein SP-D, can be found in a variety of oligomeric forms that include trimers, dodecamers and larger oligomers. It is known that disulfide bonds stabilize trimers, but the pathway and kind of interactions involved in the assembly of higher order oligomers is unclear, as well as the quantitative distribution of those in human and recombinant versions of the protein. In addition, it is still unknown whether those different oligomeric forms could affect protein activity or have different functions.

In the pulmonary context, SP-D has its essential role in the innate immune defense of the lungs, where it opsonizes pathogens that would be further cleared from the airways by immune cells. Furthermore, an alteration of lung surfactant metabolism has been reported in mice lacking SP-D (SP-D$^{-/-}$ knock out). However, how the contribution of SP-D to lung homeostasis could protect lung surfactant biophysical functions, especially under inflammatory insults, has not been properly explored.

Altogether, the main objective of this Thesis was **to characterize SP-D oligomeric forms, the kinds of interactions that drive the oligomerization pathway and the possible distinct activity of those oligomers**, using human SP-D and a full-length recombinant version of the protein. In addition, **to study the protective role of SP-D for lung homeostasis and breathing compliance under inflammatory conditions.**

The specific objectives were:

- **Characterization of SP-D oligomeric forms and its oligomerization pathway.** Identification and quantification of the distribution of the different oligomeric forms in a recombinant version of human SP-D. Study of the interactions that govern the oligomerization process and how they change under different conditions, such as pH. (Results, chapter 1).
- **Evaluation of the activity and function of the different oligomers.** Isolation of rhSP-D oligomeric forms and comparison of their activity to aggregate and bind to bacteria. (Results, chapter 2).
- **Structural and functional characterization of human SP-D.** Quantative distribution of the oligomeric forms of hSP-D purified from natural sources. Characterization of the glycan structure at the N-glycosylation site of the protein. Evaluation of the activity of two human proteins obtained from different sources and interpretation of the results according to their composition in oligomeric. (Results, chapter 3).

- **SP-D in lung homeostasis: modulation of LPS-induced NETosis and prevention of lung surfactant NETs-inactivation.** Study of the effect of SP-D in LPS induced NETosis, in *in vitro* and *in vivo* models. Analysis of the inhibitory effect of NETs in lung surfactant biophysical function and the activity of SP-D as a NET-protective agent (Results, chapter 4).

MATERIALS AND METHODS

MATERIALS

Reagents

Chemicals and reagents were purchased from Sigma Aldrich (St. Louise, MO, USA) unless otherwise indicated in the text.

Porcine lung surfactant (LS)

Bronchoalveolar lavage was carried out in fresh adult porcine lungs to obtain lung surfactant as it has been previously described (Taeusch et al., 2005). One liter of cold saline solution (0.9% NaCl) was poured into the lungs through the trachea, lungs were massaged and the solution was withdrawn. Two or three lavages were performed per respiratory apparatus (trachea and two lungs). The recovered bronchoalveolar lavage fluid (BALF) was filtered through a muslin and centrifuged (1,000 X g, 5 min, 4 ºC) to remove cells and debris and it was stored at -20 ºC until use.

In order to isolate lung surfactant lipid-protein complexes, BALF was thawed and ultra-centrifuged (100,000 X g, 1h, 4 ºC) and surfactant large aggregates were pelleted, which contain surface active components of LS. Supernatants were discarded and the pellets were resuspended in a 16% NaBr, 0.9% NaCl solution to perform a discontinuous density gradient centrifugation (120,000 X g, 2h, 4 ºC). The discontinuous gradient was formed with saline solutions that contained different concentrations of NaBr – from high to low density: 16% NaBr 0.9% NaCl, 13% NaBr 0.9% NaCl and 0.9% NaCl. After centrifugation, lung surfactant complexes, free of other cell lipids and impurities, are found in a thick white-yellowish compact layer placed between the middle dense and the lighter dense solutions. The material was carefully removed from the tubes, pooled, homogenized and diluted with 0.9% NaCl. It was frozen in liquid nitrogen and stored at -80 ºC until use.

Isolated lung surfactant was constituted by surfactant lipids, surfactant hydrophobic proteins (SP-B and SP-C) and the hydrophilic protein SP-A. Also, some traces of proteins like immunoglobulins and hemoglobin were co-purified associated with surfactant complexes. Hydrophilic protein SP-D was mostly lost in the first ultra-centrifugation.

Organic extract (OE) of lung surfactant

Organic extraction of LS was performed to remove its hydrophilic components, such as collectin proteins (SP-A and SP-D), following the protocol established by Bligh and Dyer (Bligh and Dyer, 1959). Briefly, lung surfactant, methanol and chloroform were mixed in a proportion of 1:2:1 (volume), respectively. The mixture

was vortexed thoroughly for 30 s and incubated 30 min at 37-40 ºC with gentle shaking to allow the flocculation of water-soluble proteins. Then, 1 volume of chloroform and 1 volume of water were incorporated and a biphasic solution was formed after vortex. The mixture was centrifuged (600 X g, 5 min, 4 ºC) to separate the organic from the aqueous phase. The organic phase was kept, and 2 more volumes of chloroform were added and mixed with the remaining aqueous phase, which was centrifugated again. This step was repeated twice to maximized the recovering of hydrophobic material. Pooled hydrophobic fractions were kept at -20 ºC until use. Phospholipids concentration was determined by phosphorous quantification described below (methods, page 64).

Reconstituted porcine surfactant organic extract

Organic extract reconstituted in an aqueous buffer was employed to evaluate the effect of some components in the surface-active properties of lung surfactant.

First, 335 µL of OE at 9 µg/µL (phospholipid concentration) were first dried under nitrogen flow to evaporate the organic solvents and then, under vacuum in an UNIVAP (2h at 37 ºC) to eliminate chloroform traces. Afterwards, surfactant lipids and proteins were reconstituted to a final PL concentration of 60 mg/mL in a 2 consecutive steps incubation process, where incubations were done with intermittent shaking (10 min shaking/10 min repose at 1400 rpm):

1st step - 25 µL of buffer 150 mM NaCl, 5 mM Tris (pH 7.4) were added, fully mixed and incubated at 45 ºC for 30 min.

2nd step - 25 µL of purified NETs (see page 58) resuspended in RPMI media with a DNA concentration of 0.65 µg/mL were also added, mixed and incubated in this case at 37 ºC for 30 min.

To assess whether SP-D could restore NETs-inhibited surfactant function, 25 µL of hSP-D (page 58) in 150 mM NaCl, 20 mM Tris (pH 7.4), 5 mM EDTA at 808 µg/mL were added instead of buffer (final SP-D concentration in the sample respect to PL was 0.67% (w/w)) in the first step. EDTA concentration in SP-D buffer was compensated to zero with 1 M $CaCl_2$, before incorporating the protein to the mixture.

Reconstituted samples were diluted to a PL concentration of 20 mg/mL with purified NETs in RPMI media and incubated 30 min at 37 ºC prior to use them. Samples reconstituted in the first and second steps with RPMI media without NETs and also with protein buffer without SP-D were prepared as controls.

Lung surfactant from PBS or LPS-instilled mice

Balb/c wild type (WT) SP-D$^{+/+}$ and Knock out (KO) SP-D$^{-/-}$ mice (generated by Dr. S. Hawgood, UCSF) were bred in the Toronto Centre for Phenogenomics (TCP), Canada. Mice of two ages, ~15 weeks or ~35 weeks, were used in this study. All procedures were performed in accordance with TCP approved protocols and ethical guidelines.

- Mice instillation

For airway instillation, mice were anesthetized with 2-4% isofluorane with O_2 at 1000 mL/h until they fell sleep. Then, 5 μg of LPS (0182:B12) from *E.coli* in 25 μL of sterile PBS or 25 μL of sterile PBS (negative control) were instilled intranasally. 24 hours after instillation, mice were sacrificed with an intraperitoneal injection of 0.1 mL of Euthanyl (Bimeda-MTC, Cambridge, ON, Canada).

- Bronchoalveolar lavage (BAL)

The chest of the animal was opened. An intratracheal catheter was tied into the proximal trachea and 1 mL of cold buffer (NaCl 150 mM, Tris 5 mM (pH 7.4)) was flushed into the lungs and withdrawn by a syringe three time. Three lavages of 1 mL each were carried out per animal, obtaining around 2.5 mL of BALF from each mouse. BAL samples were frozen in dry ice and kept at -80 ºC until use.

- Lung surfactant isolation

BALs were thawed at 37 ºC and centrifuged for 10 min at 400 X g and the pellets were discarded. An aliquot of 400 μL of BAL-supernatant was saved and frozen for further experiments (citH3, total protein and DNA concentrations in BAL). 2 mL of BAL-supernatants were ultra-centrifuged (100,000 X g, 1h, 4 ºC) to pellet lung surfactant components. LS pellets were resuspended in 10 μL of buffer (150 mM NaCl, 5 mM Tris 5 mM (pH 7.4)) and PL concentration was determined with the phosphatidylcholine quantification kit as stated in methods (page 63). Before evaluating their biophysical function in the CBS, samples were diluted with the same buffer as before to reach a PC concentration of 10 mg/mL. BALs from mice were not pooled, but the LS from each single mouse was evaluated individually.

The animal work described in this section (instillation and BAL) was carried out at the Toronto Centre for Phenogenomics and the laboratory of Dr. Nades Palaniyar at the Department of Translational Medicine in SickKids Hospital (Toronto, Canada).

Neutrophils extracellular traps (NETs) from human neutrophils

Neutrophils were isolated from human blood and stimulated with agonists *in vitro* to produce and release NETs.

- Human peripheral neutrophil isolation

The study protocol was approved by the Ethics Committee of the Hospital for Sick Children, SickKids Hospital (Toronto, Canada). All methods were performed in accordance with the relevant guidelines and regulations. Peripheral blood from healthy male donors was collected in K2 EDTA blood tubes (Becton, Dickinson and Co.) after obtaining informed consent. Polymorph Prep (Axis-Shield) protocol was used for separating polymorphonuclear neutrophils from blood, as previously described elsewhere (Naffah de Souza et al., 2017, Khan et al., 2017). Red blood cells were lysed with a 0.2% NaCl hypotonic solution for 30 s, followed by restoring the isotonic condition by adding an equal volume of 1.6% NaCl, 20 mM Hepes (pH 7.2) solution. Cellular debris were removed performing two consecutive washes with 0.85% NaCl, 10 mM Hepes (pH 7.2) buffer. Last, neutrophils were resuspended in RPMI medium (Invitrogen; Carlsbad, CA, USA) containing 10 mM HEPES (pH 7.2). Cells were counted and viability was checked by Trypan blue using a hemocytometer. Purity of neutrophils was determined by Cytospin preparation and imaging. Neutrophil preparations with > 95-98% pure alive cells were used for NETs production and NETosis experiments.

- NETs preparation and purification

NETosis was induced in neutrophils using LPS (0182:B12) from *E.coli* as agonist. LPS was added to 100,000 human neutrophils in 1 mL of Roswell Park Memorial Institute (RPMI) medium to reach a final concentration of 5 µg/mL. Samples were incubated four hours at 37 ºC, 5% CO_2 with intermittent gentle mixing by inverting the tubes, so avoid the sedimentation of the cells. After the incubation, samples were centrifuged at 400 X g for 10 minutes. Supernatants were collected and frozen in dry ice. DNA concentration in the purified NETs was determined with Quant-iT PicoGreen dsDNA Kit (Invitrogen, Carlsbad, CA, USA) following manufacturer´s instructions.

Human surfactant protein D (hSP-D) isolation

Human SP-D was purified from two different sources, BAL of proteinosis patients and amniotic fluid (AF) from cesareans at term pregnancy. The purification protocols were different, but the isolation was based in SP-D carbohydrate binding properties in both cases.

- hSP-D isolated from proteinosis BAL

Human SP-D was obtained from therapeutic BALs of individuals suffering from pulmonary alveolar proteinosis (PAP) as previously described elsewhere (Strong et al., 1998). BAL was filtered through a membrane of 0.22 µm pore size and solutions of 1M Tris (pH 7.4) and 1M $CaCl_2$ were added to reach a final

concentration of 20 mM and 10 mM, respectively, followed by adjusting pH to 7.4. Then, BAL was mixed with maltose-agarose beads, incubated and stirred overnight at 4 ºC. SP-D binds through its CRD to the carbohydrate ligands present in the beads in a calcium-dependent manner. After incubation, the beads were poured into an empty column and the column was packed and washed with 1 M NaCl to remove nonspecifically bound components on an AKTA FPLC system (G.E. Healthcare; L. Chalfont, UK). SP-D was eluted with a Tris-$MnCl_2$ buffer: 20 mM Tris (pH 7.4), 100 mM $MnCl_2$.

Fractions containing SP-D were pooled and concentrated using Amicon filter units (10 kDa-pore size membrane) and further purified with a Superose 6 gel filtration column (10x300 mm; Amersham Biosciences; L. Chalfont, UK) in 150 mM NaCl, 20 mM Tris (pH 7.4), 5 mM EDTA buffer. SP-D eluted as the first sharp peak in the void volume, followed by a broaden peak which corresponded to SP-A. Protein purity was examined by reducing PAGE-SDS and Coomassie staining, SP-D monomer was observed as a ~ 43 kDa band (Figure 13).

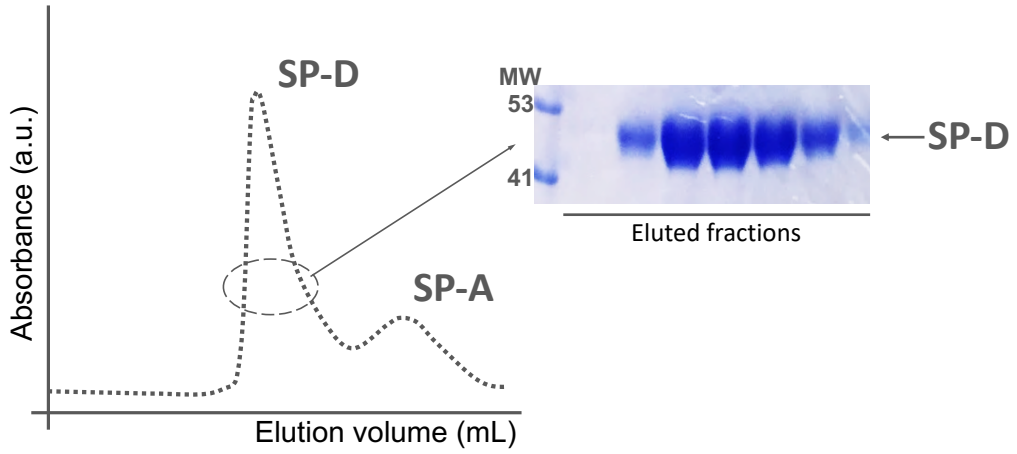

Figure 13: Schematic representation of SP-D elution profile from Superose 6 column. Inset, Coomassie staining of PAGE-SDS for the fractions within the SP-D peak.

- hSP-D isolated from amniotic fluid

Amniotic fluid was collected from women at term pregnancy (≥ 37 weeks) in programmed cesareans at the Gynecology and Obstetrics Service of "Hospital 12 de Octubre" (Madrid, Spain) in a collaboration with Drs. Emma Batllori and Alberto Galindo. Protocols were approved by the Ethics Committee of the Hospital and informed consent was signed by the donors.

Centrifuge tubes, bottles, resins and columns used in the purification were either bought sterile and LPS-endotoxin free or sanitized with 0.2 M NaOH.

Amniotic fluid samples were filtered through a muslin and centrifuged (1000 X g, 5 min, 4 ºC) to remove cell debris, followed by ultra-centrifugation (100,000 X g, 1h, 4 ºC) to remove lipids and surfactant proteins associated to lipids (SP-B, SP-

C and the major fraction of SP-A). Supernatants were frozen and stored at -80 ºC until employed.

Prior to affinity chromatography, supernatants were pooled and 1M Tris (pH 7.4) and 0.5 M EDTA were added to reach a concentration of 20 mM and 5 mM, respectively. The fluid was then stirred for 1h at 4 ºC and filtered, first, through a strainer of 100 μm-pore and then, in filter bottles with a 0.45 μm-pore size membrane. Then, 1 M $CaCl_2$ was incorporated to get a final concentration of 10 mM and the pH was checked and adjusted to 7.4. The sample was loaded into a column with Superdex®-75 beads equilibrated with buffer 100 mM NaCl, 20 mM (Tris pH 7.4), 10 mM $CaCl_2$. SP-D binds to the beads through its CRD domains in a calcium-dependent manner, as explained before. The column was washed with a high salt solution 1 M NaCl, 20 mM Tris (pH 7.4), 10 mM $CaCl_2$ to remove any non-specifically bound proteins, such as albumin (Strong et al., 1998). Last, SP-D was eluted with a Tris-$MnCl_2$ buffer: 20 mM Tris (pH 7.4), 100 mM $MnCl_2$ in 1 mL fractions. PAGE-SDS under reducing conditions developed by silver staining, was carried out with 10 μL of each sample to check for fractions that contain SP-D and protein purity. Fractions that contained higher concentration of SP-D were dialyzed overnight against 200 mM NaCl, 20 mM Tris (pH 7.4), 1 mM EDTA. Afterwards, they were aliquoted, frozen in liquid nitrogen and stored at -80 ºC until use.

Production and purification of recombinant human SP-D (rhSP-D)

Full length rhSP-D (Met^{11}, Thr^{160}, Ser^{260}) was synthesized by Chinese hamster ovary (CHO) cells and purified in two-steps chromatography columns.

- Cell culture

Stably transfected CHO cells expressing SP-D were stored and ready to start the cell culture growth produced in Cincinnati Children's Hospital as previously described (Ikegami et al., 2006). Briefly, a dihydrofolate reductase-deficient (DHFR) CHO cell line was transfected with a cDNA encoding full length SP-D. Transfected cells were selected with increasing concentrations of methotrexate and high expressing clones were selected, cloned and stored in liquid nitrogen.

For protein production, SP-D expressing CHO cells were grown in Iscove's Modified Dulbecco's Medium (IMDM) (Lonza; Basel, Switzerland) supplemented with 10% heat-inactivated fetal bovine serum (FBS), glutamine and antibiotics (penicillin and streptomycin) (all from Gibco, Thermo Fischer Sci.; Waltham, MA, USA). Cell passages were carried out when confluence was 80%, by trypsin treatments, until cells were grown in 2L-roller bottles. For bioproduction, cell media was switched to serum free Ex-cell® chemically defined CHO media. Cells secrete rhSP-D to the media that was harvested to start SP-D isolation.

- rhSP-D purification

Chromatography equipment, bottles, resins and tubes used in this purification where LPS-decontaminated with 0.2 M NaOH or bought sterile and LPS-free. Moreover, water for injections (US Pharmacopeia) was employed to prepare the buffers.

Cell harvested media was supplemented with EDTA (3mM) and stirred 40 min at 4 ºC, before centrifugation (10,000 X g, 40 min, 4 ºC). Supernatants were filtered through 0.22 μm-pore membranes and diluted 1:1 with 25 mM Tris (pH 7.4). An anion exchange chromatography was carried out with ceramic Q hyperD resine (Pall Corp, NY, USA) that was equilibrated with 60 mM NaCl, 20 mM Tris (pH 7.4), 0.01% Tween-80 in a column. The media was loaded into the column followed by extensive washing with 60 mM NaCl, 20 mM Tris (pH 7.4) to remove impurities. Elution of the protein was carried out with 800 mM NaCl, 20 mM Tris (pH 7.4). Fractions that contained the protein were identified by dark color and PAGE-SDS developed by silver staining. Moreover, protein concentration in the fractions was determined by BSA assay (methods section). Protein concentration obtained by this method was significantly high, although purity was low.

- rhSP-D from Airway Therapeutics LLC. (Cincinnati, OH, USA)

The structural characterization of rhSP-D described in Chapter 1 was carried out with a rhSP-D preparation provided by Airway Therapeutics LLC. (Cincinnati, OH, USA) that was produced by Drs. A. Jain and W.H. Brondyk in Sanofi (Boston, MA, USA). The production and purification methods were described in (Arroyo et al., 2018), being the foundation of the method the same as described above.

SP-D proteins used in this Thesis

SP-D	Source	Purified in	Experiments (Chapter)
hSP-D	BAL proteinosis	Palaniyar's lab	4
	BAL proteinosis	Kingma's lab	1 and 3
	AF	Perez-Gil's lab	3
rhSP-D	CHO cells	Kingma's lab	2
	CHO cells	Airway Therapeutics – Sanofi	1

Table 1: List of the different surfactant proteins D (SP-D) preparations used in the present Thesis. hSP-D from Kingma's lab was a gift and rhSP-D from Airway Therapeutics was obtained thanks to a collaboration project. Other were produced and purified as part of the experiments of this Thesis.

Isolation of the different oligomeric forms of rhSP-D by size exclusion chromatography (SEC)

Separation of rhSP-D oligomers was addressed by gel filtration chromatography using a Sepharose CL-6B equilibrated in 200 mM NaCl, 20 mM Tris (pH 7.4), 10 mM EDTA. The rhSP-D preparation used in these experiments was the one purified with the ceramic Q hyperD resine. 1 mL of rhSP-D at 4-5 mg/mL was applied into the column (1.5 x 90 cm). The elution fractions were collected and analyzed by ELISA and AFM (methods section) to identify the isolated SP-D oligomers. Fractions of trimers, hexamers and fuzzy balls were identified and used for further experiments.

A shorter column (1.5 x 40 cm) with the same resin, equilibrated and run with the same buffers was used for assessing protein redistribution assays.

METHODS

Protein quantification

- BCA Assay

Purified SP-D was quantified with Pierce™ BCA Protein Assay Kit (ThermoFisher Sci.; Waltham, MA, USA). In this assay, protein quantification is based on Biuret reaction where Cu^{2+} is reduced to Cu^{1+} in the presence of proteins under alkaline conditions. Then, bicinchoninic acid (BCA) chelates Cu^{1+} and forms a colored complex which absorbs at 562 nm (λ = 562 nm) (Smith et al., 1985). The stoichiometry of the reaction is shown in figure 14.

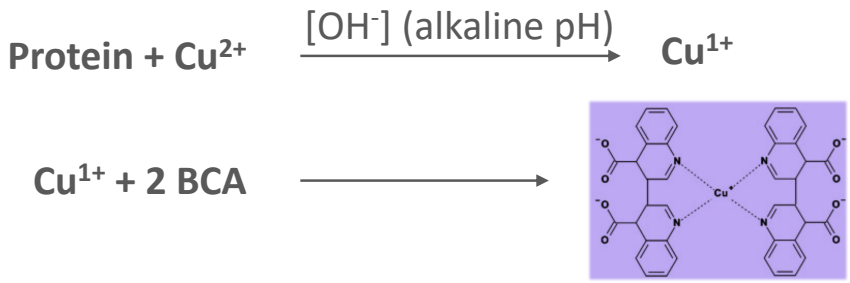

Figure 14: Chemical reactions that take place in the BCA assay.

Quantification was performed following manufacture's protocol for microplate procedure.

- ELISA

Fractions eluted from the SEC column were assessed by ELISA, with the aim to identify the fractions that contained isolated rhSP-D oligomers. It was also applied to quantify protein concentration in those fractions that contained the oligomers.

Microtiter plate wells were coated with 100 µL of a mouse antiSP-D monoclonal antibody (2D12A88-Seven Hills Bioreagents; Cincinnati, OH, USA) diluted 1:5000 in 100 mM $NaHCO_3$-Na_2CO_3 (pH 9.6) buffer, overnight at 4 ºC. Plates were washed 5 times between incubations and all washes and dilutions from this point were carried out with dilution buffer (0.05% TBS-tween, 5 mM $CaCl_2$). Wells were blocked with 1% BSA in dilution buffer for 1 hour at RT. After washing, 50 µL of protein samples and appropriate dilutions of standards were added in duplicates and incubated for 1 hour. Plates were washed and 50 µL of rabbit anti-mouse SP-D antiserum (dilution 1:7500) were incorporated and incubated for 1 hour. After washing, 100 µL of a goat anti-rabbit IgG HRP-conjugated antibody (1:10000) were added and incubated for 1 hour. Wells were washed and 100 µL of TMB (3,3',5,5'-tetramethybenzidine) (BioFX® Surmodics; E. Prairie, MN, USA) were added for 2 minutes and the reaction was stopped with 100 µL of 2N H_2SO_4. Plates were read at 450 nm (λ = 450 nm) (Kingma et al., 2006).

The fractions that contained higher levels of rhSP-D in the first ELISA were further quantified by a second ELISA-kit (Biovendor; Brno, CZ) that was more sensitive.

Phospholipis quantification

- Phosphatidylcholine (PC) quantification

PC represents ~80% of phospholipid concentration in lung surfactant (Veldhuizen et al., 1998). For this reason, PC concentration in LS from mice was determined as a reference of phospholipids concentration in those samples, using a commercial kit (Spinreact; Girona, ES). Briefly, PC was hydrolyzed by phospholipase D to choline and phosphatidic acid. Choline was oxidized to betaine and hydrogen peroxide (H_2O_2) by choline oxidase. Finally, a colorimetric reaction took place between H_2O_2, phenol and 4-aminophenazone to produce a colored substance (quinonimine). The absorbance of the sample was measured in a spectrophotometer at 505 nm (λ = 505 nm) and it was proportional to the PC concentration.

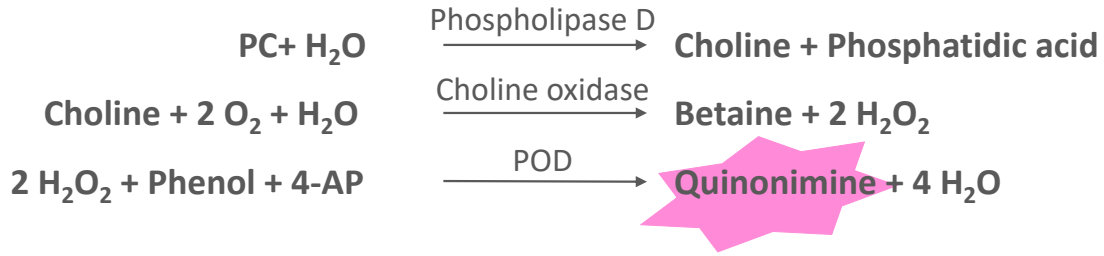

Figure 15: Chemical reactions involved in quantification of PC concentration by the commercial Kit used.

Lung surfactant samples from mice were diluted 1:10 and manufacturer's protocol was performed.

- Phosphorus assay

Total phospholipid concentration in organic extract from LS was determined by phosphorus quantification (Rouser et al., 1966). Samples were dried in glass tubes in a sand bath, 0.45 mL of 70% perchloric acid were added and incubated (260 ºC, 30 min) to allow phosphorus mineralization. While incubation, tubes were capped with glass ampoules to avoid acid evaporation. Then, 3.5 mL of miliQ water and 0.5 mL of 2.5% ammonium molybdate (w/v) were added and vigorously mixed, followed by addition of 0.5 mL of 10% ascorbic acid (w/v) and incubation at 100 ºC, 7 min. The reaction of phosphorus with ammonium molybdate generates phosphomolybdic acid, which is reduced by ascorbic acid to phosphomolybdate that possesses a blueish color. Samples were placed in ice to stop the color reaction and measured in a spectrophotometer at 820 nm (λ = 820 nm). Samples with a known PL concentration were also assessed to build a standard curve, from where the concentrations of the unknown samples were interpolated. The values were transformed to PL concentrations considering 734 Da as the average molecular mass of surfactant lipids.

Cholesterol quantification

Cholesterol quantification was addressed with a commercial kit (Spinreact; Girona, ES), where a colored compound (quinonimine) was generated after oxidation of cholesterol with several coupled reactions. Therefore, intensity of the color was proportional to the cholesterol concentration in the sample. Briefly, cholesterol esters in samples were broken down to free cholesterol and fatty acids with cholesterol esterase (CHE) enzyme. Cholesterol was oxidized by cholesterol oxidase (CHOD) to 4-cholestenona and hydrogen peroxide (H_2O_2), which was transformed to quinonimine by the peroxidase (POD) enzyme in presence of phenol and 4-aminophenazone (4-AP). The absorbance of the sample was measured in a spectrophotometer at 505 nm (λ = 505 nm).

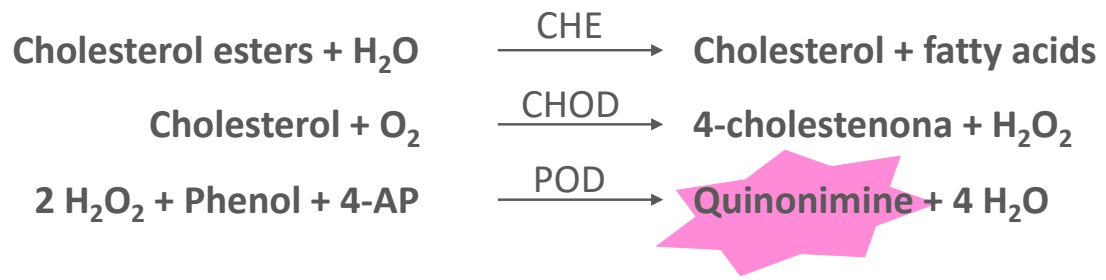

Figure 16: Chemical reactions involved in cholesterol concentration quantification assessed by the commercial kit, described in the text.

Cholesterol concentration in LS samples from mice (diluted 1:5) was determined following manufacturer's kit protocol and all values obtained were reported relative to the PC concentration in those samples.

Limulus Amebocyte Lysate (LAL) Assay

Endotoxin concentrations in purified SP-D were determined with LAL Assay (Lonza; Basel, Switzerland). In this method, the endotoxin catalyzes the transformation of a proenzyme found in LAL to its active form in a concentration dependent manner (Young et al., 1972). Then, the activated enzyme catalyzes the release of a color substance (p-nitroaniline) from the substrate that will be measured photometrically at 405–410 nm, once the reaction is stopped. Absorbance and endotoxin concentration are linear in the 0.1–1.0 EU/mL range.

Manufacturer's protocol was followed to determine the endotoxin levels in purified SP-D.

Atomic Force Microscopy (AFM)

The atomic force microscopy belongs to the family of Scanning Probe Microcopies. It was first described by Binnig and colleagues (Binnig et al., 1986) and its operation principle is based on the tip-sample interactions . Up to now, it has been widely applied to characterize the structure of different materials, among them, many biological systems (Carvalho and Santos, 2012, de Pablo and Carrion-Vazquez, 2014).

- Components of the microscope

The cantilever that scans the surface of the sample has a triangular or pyramidal shape commonly, and in its free-end holds what it is referred as the tip. The chemical composition of the cantilever defines its hardness. They are made of silicon (Si) or silicon nitride (Si_3N_4), being the ones composed by Si the hardest, more appropriate for experiments in air. This cantilever is excited by a small piezo in the cantilever holder device and it oscillates at the resonance frequency. The mechanical movement of the cantilever is defined by the Hooke's law:

$$\vec{F} = k\vec{x} \quad \textbf{(eq. 1)}$$

Where, k represents the spring constant of the cantilever and it is relevant in the sensitivity of the measurement (de Pablo and Carrion-Vazquez, 2014).

The laser, which has a wavelength of λ = 633 nm, is focused on the tip of the cantilever and it is reflected to a four quadrants photodiode. The laser must be also aligned with the center of the photodiode, so in non-contact regime the zero of lateral and vertical forces correspond to the center of the photodiode.

A magnetic disc that holds the sample is placed onto a piezoelectric tube, which allows the movement of the sample in the direction X, Y and Z with nanometric precision.

The electronics receives information from the photodiode, it sends it to the computer and back to the piezo to respond to the topographic changes in the sample. Last, the computer, with a proper signal digital processor.

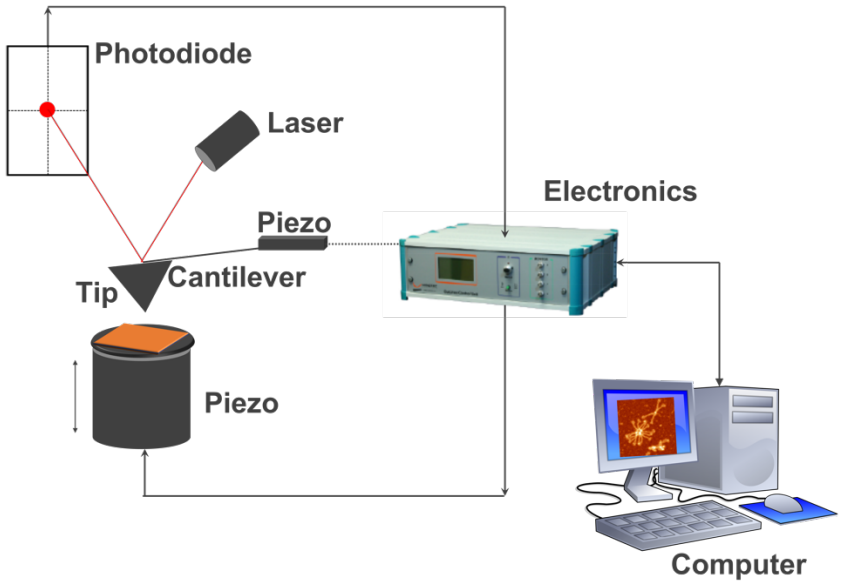

Figure 17: Schematic representation of AFM main components described in the text.

- Contact and dynamic AFM operational modes

In contact mode, the tip is permanently in touch with the sample while scanning (Binnig et al., 1986). It produces higher resolution images, but it is not advisable for biological samples because the higher forces applied over the tip can damage and break biological structures.

In dynamic mode, the cantilever has a sinusoidal oscillation while scans the sample and the tip occasionally contacts the sample (de Pablo and Carrion-Vazquez, 2014). This mode is characterized by the oscillation amplitude and the oscillation frequency of the cantilever, and the phase difference between the input and the output signal after the feedback of the cantilever. Two dynamic modes have been described according to the variable that is controlled by the system: Amplitude-Modulation (AM-AFM) or *tapping* and Frequency-Modulation (FM-AFM) modes. In t*apping* mode, the oscillation amplitude is the variable controlled by the system and kept constant along the measurements. In these experiments, when the tip faces a structure with different height during the scanning of samples, the oscillation amplitude changes; this information is received by the feedback

system, that compensates the change increasing or decreasing the voltage that the piezo applies. Therefore, the sample is moved up or down in Y-direction to adjust the sample-tip distance and restore the oscillation amplitude. Thus, a topographic image of a sample is obtained with the information reported by the movements of the piezo to keep the oscillation amplitude constant.

Only AM-AFM is described here, not FM-AFM, because it was the mode used in the present Thesis.

- Sample preparation

Atomically flatten substrates are needed for AFM experiments. Mica moscovita is a phyllosilicate mineral that can be exfoliated in a reproducible way, producing atomically flatten surfaces. It was the material used in the present thesis.

In this Thesis, 20 µL a of protein solution at 0.85 ng/µL was incubated for 4-5 min onto freshly cleaved mica. The surface was thoroughly rinsed with 6-7 mL of deionized water to remove buffer components. Finally, the sample was dried under nitrogen air flow. Samples at acidic and basic pH were prepared in the same way, but pH was previously changed by dilution up to the final protein concentration (0.85 ng/µL), with citrate buffer (200 mM NaCl, 20 mM citrate, 1 mM EDTA) when shifting to acid pH or Tris buffer 200 mM NaCl, 20 mM Tris (pH 8.5), 1 mM EDTA for basic pH. Protein was incubated at 4 °C during a minimum of 30 min before use.

AFM experiments were performed in Dr. Fernando Herrero Moreno's laboratory at the Centro Nacional de Biotecnología (CNB-CSIC), in Madrid, Spain. The samples were scanned under an AFM from Nanotec (Nanotec Electrónica, Madrid, Spain) using PointProbePlus tips, type PPP-NCH (Nanosensors, Neuchâtel, Switzerland). Amplitude modulation mode (AM-AFM, tapping) was used for imaging in air, at room temperature and low humidity. The system was isolated from mechanical vibrations and thermal variations. The software employed to control the system, imaging processing (general plane subtraction, line flattening) and height profiles was the WsxM freeware (Horcas et al., 2007).

Cryo-TEM

Cryo-TEM implies traditional transmission electron microscopy (TEM) with a cryo-sample holder and a specific protocol for preparation of the samples. It is a high-resolution technique which allows the observation of unaltered molecular structures, because fixation and staining agents are not needed.

Samples for cryo-TEM are prepared in two steps: i) the solution with the molecules is loaded into a holey carbon grid and the excess of solution is removed by blotting, ii) the grid is rapidly frozen by plunging it into a cryogen substance. As

a result, samples are covered by a thin layer of vitrified water and are kept at cryogenic temperatures all the process, even in the microscope holder (Czarnocki-Cieciura and Nowotny, 2016, Stark and Chari, 2016).

Then, the structures are observed in a TEM where an electron beam is generated and focused on the sample through condenser electromagnetic lens. Some electrons are scattered and others go through the sample, which depends on the density of the sample. Unscattered electrons hit a fluorescent screen at the bottom of the microscope, giving the final image displayed in different grey colors according to the density of the components.

Different dilutions of rhSP-D in the range 0.02-0-04 μg/μL were applied to holey carbon copper grids (R2/2; Quantifoil, DE) and vitrified using a Cryoplunge (Gatan; CA, USA). The grids were imaged in a JEM-1230 transmission electron microscope (JEOL; Tokyo, JP) operated at 100 kV and recorded at a final magnification of 5.68 Å/pixel using an F416 CMOS camera from TVIPS (Gauting, DE).

Confocal microscopy

Chamber slides with 12 wells (Ibidi; Munich, DE) were seeded with 100 μL of RPMI media containing 50000 neutrophils. The same method described above was used for preparing the agonists or agonist with SP-D prior to add them to the cells. In this case, two final calcium concentrations were tested: 0.5 mM and 2mM. After stimulation, cells were placed at 37 ºC, 5% CO_2 incubator for 2 hours. Then, cells were fixed with 4% (w/v) PFA overnight at 4 ºC. After fixation, samples were washed three times with PBS and then permeabilized with 0.05% (w/v) Triton X-100 for 10 minutes. Cells were washed three times with PBS again and primary antibodies were added to the samples followed by incubation at 4 ºC overnight. The antibodies used were anti-myeloperoxidase mouse antibody (ab25989, Abcam; EN, UK) at 1:500, used for staining MPO (with secondary antibody conjugated with a green fluorescence Alexa fluor 488 dye; 1:5000 dilution; ThermoFisher Sci.; Waltham, MA, USA), while rabbit anti-citrullinated histone 3 antibody (ab5103; Abcam, EN, UK) at 1:500 dilution was used for detecting the presence of citrullinated histone H3 (CitH3, with secondary antibody conjugated with a far-red fluorescence dye Alexa fluor 647; 1:5000 dilution; ThermoFisher Sci.; Waltham, MA, USA). DNA was stained with DAPI (1:100 dilution). After incubation with the secondary antibody, slides were washed and mounted by glass cover slips (ThermoFisher Sci.; Waltham, MA, USA) with anti-fade fluorescent mounting medium (Dako; CA, USA). The images were taken using an Olympus IX81 inverted fluorescence microscope with a Hamamatsu C9100-13 back-thinned EM-CCD camera and

Yokogawa CSU × 1 spinning disk confocal scan head with Spectral Aurora Borealis upgrade, four separate diode-pumped solid-state laser lines (Spectral Applied Research, 405, 491, 561, and 642 nm). Samples were imaged at 40×/0.95 magnification and images were processed by Volocity software (version 6.3, Cell Imaging Perkin-Elmer).

Gel electrophoresis and Western Blot

- Native PAGE (polyacrylamide gel electrophoresis)

Native electrophoresis was carried out in the absence of chemical denaturing agents and heating shock. Protein samples were prepared with loading buffer (5X) containing 5% Blue G-250 and 1 M 6-aminocaproic acid. Electrophoresis was performed in 4-15% polyacrylamide precast gels (BioRad; CA, USA) at 4 ºC at 110V for 30 minutes, followed by 2 hours at 180 V (Schagger, 2001).

- SDS-PAGE

For non-reducing conditions, loading buffer (5X) containing 10% SDS, 312.5 mM Tris (pH 6.8), 50% glycerol, 0.15% bromophenol blue, prepared in miliQ water was added to the sample. For reducing conditions, 20% β-mercaptoethanol was added to the previously described non-reducing loading buffer. Samples were heated at 99 ºC for 10 minutes prior to load them into the gels.

Gels that contained a different percentage of polyacrylamide were used according to the different proteins tested. SP-D was run in 4-15%, 4-20%, 8% acrylamide gels; SP-A, SP-B and SP-C were run in 4-20% or 16% acrylamide gels; for citH3 12% acrylamide gels were used.

Electrophoresis were run at 110 V for 10 min and then the voltage was increased to 150-180 V until completion.

- Cross-linking

Protein cross-linking was performed with glutaraldehyde (GA) (Merck-Millipore, MA, USA) at a final concentration of 0.5% or 1% (v/v) for 2, 15 or 30 minutes, according to a protocol modified from (Leitner et al., 2010). Reaction was stopped by adding non-reducing loading buffer and heating at 99 ºC for 10 minutes.

- Silver staining

Gels were fixed for 30 min in fixing solution (40% ethanol, 10% acetic acid) and then placed for 30 min in sensitising solution (30% ethanol, 0.5% glutaraldehyde, 12.6 mM sodium thiosulphate, 0.8 M sodium acetate). Afterwards, three 5-min washes with miliQ water were performed to remove the excess of the previous solutions. Gels were immersed in a silver solution (0.6 mM silver nitrate, 0.04% formaldehyde) for 20 min and after a quick wash with miliQ water, protein

bands were developed with developing solution (0.2 M sodium carbonate, 0.02% formaldehyde). Color development reaction was stopped with stop solution (50 mM EDTA (pH 8.0)) for 10 min.

- Coomassie staining

Gels were fixed and stained with a solution of 1mg/ml Coomassie Brilliant Blue R-250, 50% MeOH, 10% acetic acid for 20 min. Protein bands were visualized upon destaining with a 10% acetic acid, 45% MeOH solution.

Antibodies and dilutions used

Primary antibody	Dilution	Reference	Supplier	Secondary Antibody	Dilution	Supplier
SP-A	1:10000	-	Dr. Joanna Floros	Rabbit	1:10000	Dako
SP-B	1:5000	WRAB-48604	Seven Hills Bioreagents	Rabbit	1:5000	Dako
SP-C	1:5000	WRAB-76694	Seven Hills Bioreagents	Rabbit	1:5000	Dako
SP-D	1:2500	WMAB-1A10A9	Seven Hills Bioreagents	Mouse	1:5000	Cell Signaling
	1:5000	WMAB-2D12A88	Seven Hills Bioreagents	Mouse	1:5000	Cell Signaling
citH3	1:500	Ab5103	Abcam	Rabbit	1:5000	Dako

Table 2: Primary antibodies and their associated secondary antibody, both with their working dilutions and suppliers are listed in this table.

- Western Blot (WB)

Proteins were transferred from the gel to nitrocellulose (Amersham Biosciences; L. Chalfont, UK) or PVDF (BioRad; Hercules, CA, USA) membranes. In the case of SP-A, B and C, PVDF membranes were preferred while for SP-D and citH3 nitrocellulose membranes were used. Two transfer systems were employed: i) a humid chamber, in the case of surfactant proteins (A, B, C, D), where the transfer was carried out at 350 mA, 1h, 4 ºC; ii) a semidry Trans-Blot® Turbo™ Transfer System (BioRad, Hercules, CA, USA), for citH3 and some WBs of SP-D, where the transfer was conducted at 1.3 A, 7 min, room temperature.

Membranes were blocked with 5% milk in 0.1% PBS-Tween (PBS-T) for 2 hours at room temperature. The primary antibody was diluted to optimal concentration (Table 2) in the previous buffer and incubated at 4 ºC overnight. Four washes of 10 min with PBS-T were carried out to eliminate the unbound antibody, and the secondary antibody was incubated for 1 h at room temperature. After repeating the washes, protein bands were developed using chemiluminescent

detection, the membrane was incubated 1 min in Immobilion Western Chemiluminescent HRP substrate solution (Merck-Millipore, Burlington, CA, USA) and the images were recorded in ImageQuant LAS500 (GE Healthcare; L. Chalfont, UK).

Dot Blot

LPS (0182:B12) dilutions at 2.5, 5, 10, 20, 60 and 80 μg/mL were dotted (2 μL) onto a nitrocellulose membrane (Amersham Biosciences; L. Chalfont, UK). 370 ng of SP-D and SP-D buffer were also applied as positive and negative controls. After drying at room temperature, membranes were blocked with 5% BSA in TBST-Ca buffer (150 mM NaCl, 50 mM Tris (pH 7.4), 0.02% Tween, 5 mM $CaCl_2$) at 4 ºC overnight. Three washes with TBST-Ca buffer were done and the different membranes were incubated with 5 μg/mL or 15 μg/mL of SP-D in TBST-Ca or 5 μg/mL of SP-D in TBST-EDTA 20 mM for 5 hours at room temperature. A control with TBST-Ca without SP-D was also performed. After incubation, membranes were washed four times with TBST-Ca and incubated with SP-D antibody (Cocalico Biologicals, PA, USA) at 1 μg/mL at 4 ºC overnight, followed by four washes with TBST-Ca. Membranes were then incubated for 1 hour with the secondary antibody, donkey anti-rabbit IgG-HRP (ThermoFisher Sci.; Waltham, MA, USA) dilution 1:10000 and antibody was washed away as described above. SP-D complexes were detected by ECL (Millipore).

Sytox Green kinetics assay

Sytox green (Life Technologies; Carlsbad, CA, USA), a cell-impermeable nucleic acid binding dye, was used for monitoring NETosis over time. Microplates of 96-wells were seeded with 100 μL suspension containing 50000 neutrophils and 5 μM Sytox green. Agonists (positive control), or agonists with SP-D (at 10, 20, 40 μg/mL), or RPMI with protein buffer (negative control) were prepared in 10 μL of media and incubated for 30 minutes at 37 ºC, 5% (v/v) CO_2. Calcium concentration in SP-D was adjusted prior to use to 5 mM $CaCl_2$. After the appropriate incubation time, the mixture (10 μL) was added to the cells and the fluorescence intensity of the dye was tracked at 30-minute time intervals up to 240 minutes after cell activation, using a POLARstar OMEGA fluorescence plate reader. Between plate readings the plate was kept at 37 ºC, 5% (v/v) CO_2. Final calcium concentration in the experiment was 0.5 mM. The final concentrations of the different agonists in these experiments were 25 nM PMA, 2.5 μM Ionomycin and 5 μg/mL LPS. For dose-response LPS curves, different LPS concentration were tested. The green fluorescence at time 0 min was subtracted from the fluorescence at each time point

and was then divided by the fluorescence values of cell lysed with 0.5% (v/v) Triton X-100 (100% DNA – total DNA present in the cell).

Deglycosylation experiments

Two μg of SP-D were treated with 500 U of PNGase F enzyme. (New England Biolabs Inc., Ipswich, MA, USA) according to the manufacturer's protocol. In some cases, it was further treated with 0.025 U of neuraminidase (sialidase) from *Arthrobacter ureafaciens* from Sigma (St. Louise, MO, USA), also following the manufacturer's protocol.

Results were analysed by AFM and PAGE-SDS developed with silver staining.

N-glycan profiling

Hydrophilic interaction ultra-performance chromatography with fluorescence detection coupled electrospray injection quadrupole time-of-flight tandem mass spectrometry (HILIC-UPLC-FLD-ESI-Q-TOF MS/MS) was performed to carry out the characterization of the glycan attached to Asn^{70} of SP-D. First, the purified protein was denatured and N-Glycans were released during incubation with N-glycanase F. Then, free N-glycans were labeled with a fluorophore (RapiFluor, Waters; MA, USA) at the reducing end, followed by a purification step employing a HILIC solid phase extraction. An I-class system with fluorescence detection (Waters) was used for HILIC-UPLC. The mixture of purified fluorescently tagged N-glycans was separated on an an Acquity UPLC BEH Glycan column (150x2.1mm, 1.7u, Waters) at 60°C with a flowrate of 0.5mL/min. 100% acetonitrile (A) and 100mM ammoniumformiate, pH4.5, were used as the eluent system and the gradient of 22%B to 44%B in 82min was applied. The fluorescence wavelength settings were: λ_{ex} 265nm and λ_{em} 425nm.

A coupled Bruker Impact HD ESI-Q-TOF-MS(MS) was used for N-glycan identification in positive ion mode. N-glycans were identified according to molecular masses in combination with fragment analyses. Quantification of N-glycan structures was performed from fluorescence peak areas. N-glycan parameters were calculated from the relative molar amounts of the identified N-glycans.

N-glycan profiling was carried out in collaboration with Glycotope GmbH (Berlin, DE).

pH experiments and thermal denaturation of rhSP-D

For protein stability experiments against thermal denaturation, rhSP-D was diluted to the final required concentration with citrate buffer at pH 4.2 (200 mM

NaCl, 20 mM citrate, 1 mM EDTA) and incubated in ice for 30 minutes. Then, samples were heated at desired temperature (35, 40, 45, 50, 55, or 60 ºC) for 15 minutes and crosslinked as described above. Electrophoresis was performed under non-reducing conditions and AFM samples were prepared and scanned as described above.

Carbohydrate binding preference assay

SP-D binding preference to maltose, N-acetylglucosamine (GlcNAc), glucose or galactose, was assessed by competitive binding of the protein to mannan agarose beads, in the presence of the different competitors at several concentrations. SP-D binding to mannan agarose beads depends on the affinity of the protein for the competitor agent. The method was slightly modified from a microplate assay previously described elsewhere (Palaniyar et al., 2004, Kingma et al., 2006)

Mannan agarose beads were washed and resuspended in TBS three times, and the number of beads in the final suspension was counted with a hemocytometer. Reaction mixes were prepared by adding in every tube: 5,000 beads, different concentrations of the carbohydrate competitor (0.01-200 mM), 2 µL of 250 mM $CaCl_2$ and the necessary volume of TBS to reach 100 µL as final volume in each tube. Last, 300 ng of SP-D were added and the samples were incubated in a thermomixer at 4 ºC for 2 hours with constant shacking at 600 rpm. It was important to compensate EDTA concentration with $CaCl_2$ in protein buffer before adding the protein to the reaction mix. A positive control without mannan beads and a negative control in the presence of 20 mM EDTA were also conducted.

After incubation time, unbound SP-D was separated from SP-D bound to the beads by centrifugation (13,000 X g, 1 min, 4 ºC). Fifty µL of the supernatant, containing the unbound protein, were collected and concentrated in an UNIVAP at 37-40 ºC to reduce the final volume to 6-8 µL. In order to quantify the unbound protein, PAGE-SDS of the samples under reducing conditions was carried out in 4-15% acrylamide gels. Protein bands were developed by silver staining and densitometry analysis was performed with ImageJ software. The percentage of unbound SP-D for each condition was obtained from densitometry of the bands, and all values were reported relative to the intensity of the band when 20 mM EDTA was added to the reaction mixture (100% unbound SP-D). The percentage of bound SP-D was calculated by difference (equation 2) and represented against its competitor concentration.

$$\%\boldsymbol{Bound_{SP-D}} = \mathbf{100} - \%\boldsymbol{Unbound_{SP-D}} \quad \text{(eq. 2)}$$

SP-D *E. coli* binding assay

An ELISA-like binding assay was developed to determine the binding affinity of SP-D to the gram-negative bacteria *E. coli*.

Microtiter plates were coated with a suspension of *E. coli DH5α* at $5x10^8$ cells/mL in 50 mM $NaHCO_3$-Na_2CO_3 (pH 9.6) buffer. Then, 200 µL of the bacterial suspension were pipetted into the wells and the plate was incubated at 4 ºC, overnight. Plates were washed 5 times between incubations and all washes and dilutions from this point were carried out with dilution buffer (0.05% TBS-tween, 5 mM $CaCl_2$). Wells were blocked with 2% BSA in dilution buffer for 2 hours at RT. After washing, samples of serial diluted (1:2) SP-D (from 1µg/µL to 2.3 ng/µL) were added to the wells in duplicates to obtain a standard curve. Protein was incubated for 1 hour, washed and 50 µL of mouse anti-SP-D antibody (dilution 1:5000) (Seven Hills Bioreagents, Cincinnati, OH, USA) were incorporated and incubated for 1 hour. After washing, 100 µL of a horse anti-mouse IgG horseradish peroxidase (HRP)-conjugated antibody (1:7500) (Cell Signaling, Danvers, MA, USA) were added. One hour later, plates were washed and 100 µL of TMB/E (3,3',5,5'-tetramethybenzidine) (Merck-Millipore; MA, USA) were added for 3 minutes and the reaction was stopped with 100 µL of 2N H_2SO_4. Plates were read for absorption at 450 nm.

A modified version was also developed with different antibodies. Rabbit anti-SP-D primary antibody (1:100) (Santa Cruz; Dallas, TX, USA) and anti-rabbit Ig HRP-conjugated antibody (1:1000) (Dako; S. Clara, CA, USA) were used. The epitope for this anti-SP-D is located in the N-terminal domain of the protein, instead of the CRD domain. In this case, incubation with TMB substrate was maintained for 15 minutes before stopping the color reaction.

Bacterial aggregation assay

SP-D aggregation activity was determined by measuring light transmission through a suspension of *E. coli DH5α* after addition of the protein. The method was slightly modified from (Kingma et al., 2006).

Bacterial cultures were grown at 37 ºC overnight. Then, cells were centrifuged (1,000 X g, 5 min, 4 ºC) and the supernatant was discarded. One wash was performed by resuspending the cells in 5 mL of 150 mM NaCl, 20 mM Hepes (pH 7.4) and repeating the centrifugation step. Finally, bacteria were diluted with the previous buffer until an optical density at 700 nm (OD_{700nm}) of ~ 1.1. Calcium concentration was adjusted to 5 mM in the final reaction by adding the required volume of 1 M $CaCl_2$ solution (Hartshorn et al., 1998).

Samples were prepared in spectrophotometer cuvettes with 650 µL that contained:

- 470 µL of bacterial suspension
- 180 µL that contained: i) SP-D to reach the final concentration assessed (concentrations ranged from 10 µg/mL to 0.1 µg/mL) and ii) 200 mM NaCl, 20 mM Hepes (pH 7.4) buffer.

The absorbances of samples were read every 2.5 min at OD_{700nm} during 2-3 hours. The decreased in optical density through the time indicates the extent of bacterial aggregation. In order to compare the activity of SP-D from different sources or different oligomeric forms, the percentage (%) of aggregated bacteria at different SP-D concentrations was calculated from the absorbance decay in samples at specific time points. All values were relative to the absorbance at t = 0 of the bacterial suspension without SP-D, considered as 100% absorbance = 0% aggregation.

Captive Bubble Surfactometer (CBS)

Captive Bubble Surfactometer (CBS) is a non-commercial device that was originally designed by Dr. Samuel Schürch (Schurch et al., 1989). It allows to evaluate the surface activity of materials adsorbed to the air-liquid interface of an air-bubble that is confined in a chamber under controlled conditions. The surface tension (γ) can be calculated from the shape (volume, diameter and height) of the bubble, which is monitored and recorded during the experiment, and the CBS software will transform those measurements in surface tension values (Schoel et al., 1994). The major advantage of the equipment is that it somehow mimics, *in vitro*, the physiological situation of a single alveolus in the lung during breathing. This characteristic makes it particularly useful to evaluate the performance of lung surfactant samples under different physiological or pathological conditions.

The air bubble is created in a cylindric glass chamber filled with buffer. The chamber has a small (2 mm) hole at the bottom, to allow the entry of a thin capillary and air to create the bubble (0.035-0.040 cm^3). The composition of the buffer that fills the chamber is 150 mM NaCl, 5 mM Tris (pH 7.4), containing 10% sucrose (w/v) to increase the density and avoid mixing and dilution of the introduced lung surfactant samples within the buffer. The opposite side of the chamber is sealed with a 1% agarose (w/v) cap that separates the bubble from a piston, which will be moved up and down by the system to compress and expand the space in which the bubble is confined. The glass chamber is inserted in a bigger chamber, with two transparent walls, where a water bath is created to control the temperature by a

feedback system and an external source of heat. Prior to the injection of the sample, the buffer inside the chamber is subjected to degasification by pressure and heat.

Experiments in the CBS are characterized by three steps:

- Initial adsorption (IA)

Once the bubble has been created and centered, injection of the sample is executed introducing in the chamber a transparent capillary connected to a syringe. Typically, 150 nL of the sample are applied near the surface of the bubble and the surface tension is monitored during the adsorption of the material, for 5 min.

In this step, it is observed the ability of lung surfactant to reach the interface and form a film capable of reducing air-water surface tension (~70 mN/m) to equilibrium surface tension (typically for lung surfactant ~22-23 mN/m), in a few seconds.

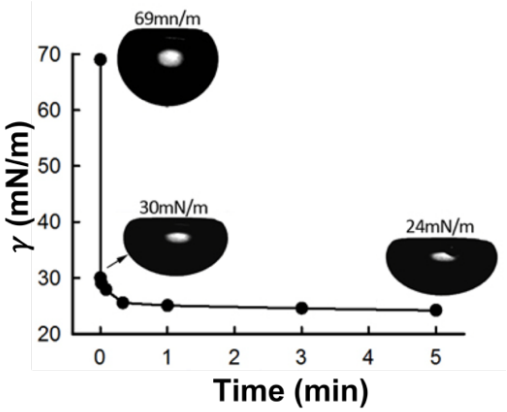

Figure 18: Changes in the bubble shape due to decrease of surface tension (γ) upon injection of the material during initial adsorption (IA). Within the first seconds after application of the sample, the surface tension goes down to values close to 22-25 mN/m, which is reflected in the shape of the bubble that becomes flatter.

- Post expansion adsorption (PEA)

After IA, the chamber is sealed and the bubble is rapidly expanded to 0.15 cm^3 by the movement of the piston controlled by the software. Surface tension of the bubble is monitored during further 5 min, where reorganization, transfer and spreading of surfactant into the expanded interface can be analyzed.

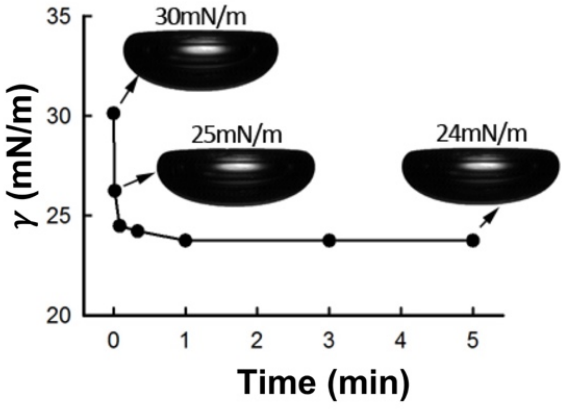

Figure 19: Changes in the bubble shape due to decrease of surface tension (γ) upon rapid expansion of the bubble during post expansion adsorption (PEA). Within the first seconds after expansion of the bubble, the surface tension goes down to values close to 22-25 mN/m which is reflected in the shape of the bubble that becomes flatter.

♦ Q-static compression-expansion cycling

Four slow step-wise compression and expansion cycles are applied to the bubble. Cycles are performed with 1 second delay between compression steps, each reducing 20% its previous volume. Maximum volume is set during post-expansion and minimum volume is set manually during each cycle. During this slow compression-expansion cycles, the film undergoes relaxation and reorganization processes. First Q-static cycle often shows a plateau with a decrease in area and little change in surface tension during compression, a process known as "squeeze-out", which consists in a partial depuration of the less active material out from the interface. During expansion steps, similar isotherms to that from compression are observed, but during the first Q-stat cycle the reorganization of the material at the interface originates isotherms with different tilt during compression and expansion, with some hysteresis. The area enclosed by the compression and expansion isotherms illustrates the ability of the material to reorganize during the compression and expansion cycles, which represents the hysteresis of the cycle, meaning the energy spent by the compression-expansion process. The subsequent cycles exhibit progressively reduced hysteresis, indicating that the refinement of the material at the interface is irreversible.

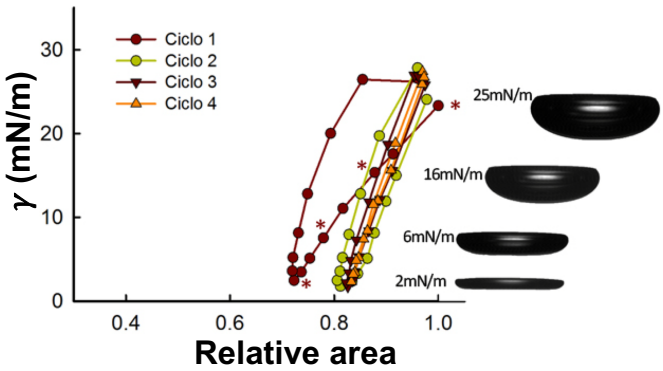

Figure 20: Changes in the bubble shape associated with surface tension (γ) during Q-static compression-expansion cycles. Compression-expansion isotherms for Q-static cycles 1, 2, 3 and 4 show the changes in surface tension upon reducing and increasing the area of the bubble. The image illustrates how the shape of the bubble changes during the first Q-static compression.

♦ Compression-expansion dynamic cycling

The bubble is finally subjected to fast compression-expansion cycles, which mimics breathing at physiological rates, typically at 20 cycles/min for humans and for mice the maximum speed that the device reaches 30 cycles/min, although mouse breathing rate is much higher. The surface tension of the bubble is monitored during cycling by the software and represented in the compression-expansion isotherms that plot the changes in surface tension, as a function of the relative area of the bubble. The area enclosed by the compression and expansion isotherms represents the hysteresis of the cycle, and thus, the energy spent by the compression-expansion process. Good lung surfactants exhibit reduced or no

hysteresis and reduced compression is needed for they to reach the characteristic minimum surface tensions (~2mN/m).

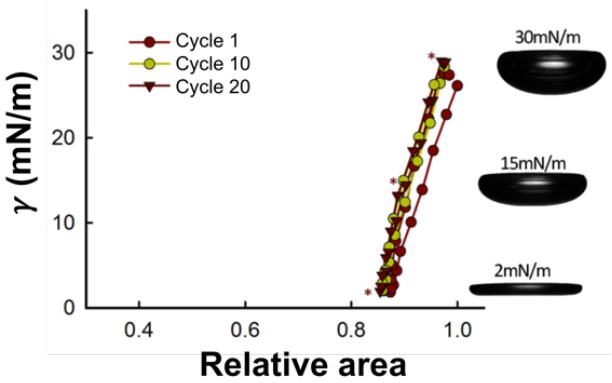

Figure 21: Changes in the bubble shape associated with surface tension (γ) during dynamic compression-expansion cycles. Compression-expansion isotherms for cycles 1, 10 and 20 show the changes in surface tension upon reducing and increasing the area of the bubble. The image illustrates how the shape of the bubble changes during the first dynamic compression.

Statistics analysis

All statistical analyses were performed on GraphPad Prism 7. Two-way ANOVA with Bonferroni post-test, One-way ANOVA with Tukey's post-test and t-test were done as appropriate. Significant differences were considered with a p-value of <0.05(*), ≤0.01(**), ≤0.001(***), ≤0.0001(****).

RESULTS

Chapter 1

Structural characterization of the supramolecular assembly of rhSP-D

The recombinant human rhSP-D used in this chapter was provided by Airway Therapeutics LLC. and the experiments were done in collaboration with the company, supervised by Dra. Jan Rosenbaum.

The AFM experiments included in the present chapter were done in collaboration with Dr. Fernando Moreno-Herrero at the "Centro Nacional de Biotecnología" (CNB-CSIC). Cryo-TEM samples were obtained and imaged in the Electron Microscopy Facility (EMF) of the Biological Research Center (CIB-CSIC, Madrid). The results were published in the following article:

Arroyo, R., Martin-González, A., Echaide, M., Jain, A., Brondyk, W.H., Rosenbaum, J., Moreno-Herrero, F., Perez-Gil, J. "**Supramolecular Assembly of Human Pulmonary Surfactant Protein SP-D".**

Journal of Molecular Biology, 430 (2018), 1495-1509,

DOI: 10.1016/j.jmb.2018.03.027

Introduction

SP-D was first described as CP4 protein by Persson and colleagues in 1988 (Persson et al., 1988). They characterized a 43 kDa product from type II pneumocytes, composed of collagenous and non-collagenous domains and the presence of asparagine-N-linked carbohydrates (Persson et al., 1988, Persson et al., 1989). Numerous structural and functional studies have been carried out since then to further characterize SP-D from several organisms. Moreover, different recombinant versions of SP-D have been produced, with Chinese hamster ovary (CHO) cells being the most widely-used system to produce the human recombinant protein (rhSP-D) (Hartshorn et al., 1996a, Ikegami et al., 2006).

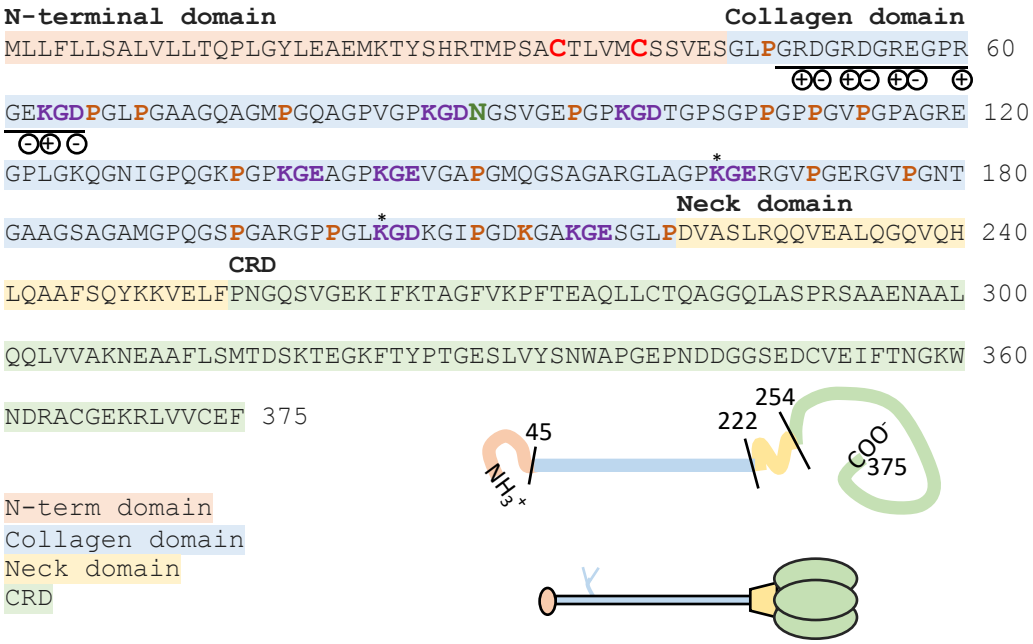

Figure 1.1: Amino acid sequence and domain organization of hSP-D. The segments of the sequence defining the different protein domains are shaded with different colors: N-terminal (orange), collagen (blue), neck (yellow) and CRD (green). Cysteines C15 and C20 are in red bold letter. Glycosylated (blue Y at the protein scheme) residue N70 is in bold green. Hydroxylated prolines are in brown (Leth-Larsen et al., 1999). Amino acid triplets in purple represent triples prone to form ionic interactions between triple helices in the collagen region. Lysines marked with the asterisk are always found O-glycosylated, the rest of lysines within these triples can be found as partly O-glycosylated and/or hydroxylysine residues. The underlined amino acid sequence constitutes the so-called "charged patch", with the expected charge of the amino acids at pH 7 indicated below.

The SP-D monomer contains 355 amino acids (43 kDa) arranged in four structural domains (Figure 1.1), including: i) an N-terminus domain, where two conserved cysteines (C15 and C20) are important for protein oligomerization (Zhang et al., 2001a), ii) a collagen domain, characterized by a series of Gly-X-Y triplet sequence repeats, iii) an α-helical coiled-coil neck region and, iv) a globular domain, the carbohydrate recognition domain (CRD). The CRD contains four additional cysteine residues implicated in intramolecular disulfide bonds (Brown-

Augsburger et al., 1996a), and four calcium-binding sites important for its calcium-dependent immune activity (Crouch et al., 1994b, Crouch, 1998, Shrive et al., 2003). The sequence of SP-D also contains an asparagine in position 70 (N70), which is glycosylated, and a number of lysines that are partially O-glycosylated (Leth-Larsen et al., 1999). Most prolines within the collagen domain are at least partially hydroxylated when located in third residue position (G-X-P) of the characteristic G-X-Y collagen domain triplets.

Three monomers form trimers through the folding of the collagenous region into triple helices and the assembly of a coiled-coil bundle of α-helices in the neck region. Two disulfide bonds between cysteines 15 and 20 stabilize this trimeric structure (Crouch, 1998). It has been described that trimers either associate into higher order oligomers such as dodecamers, which are structures formed by four trimers, or the so-called "asterisk-like" or "fuzzy balls", larger oligomers composed by 6 or more trimers, existing in a wide and variable range of sizes. It is currently unknown whether the different oligomeric forms of SP-D might provide selective contributions to the various aspects of SP-D physiology. It is also unknown how such oligomerization-function relationships could be modulated by physiologically relevant factors. This gap in knowledge is in part due to the difficulties of characterizing the conformational diversity of SP-D under different environmental constraints in a manner that provides both qualitative and quantitative outputs. New tools are also needed to identify and discriminate the protein domains or regions and the nature of the interactions involved in the formation and stabilization of the different protein oligomers.

In this chapter, we present a detailed analysis of the structure of a recombinant human SP-D produced in CHO cells, with the goal of providing both a qualitative and quantitative assessment of the conformational diversity and the determinants defining the oligomerization pathway of the protein. Using high-resolution atomic force microscopy (AFM) and electrophoresis methodologies, we have described the different SP-D oligomeric forms, defined and quantitatively characterized some of their relevant features. The distribution of oligomeric forms of rhSP-D has been for the first time quantified as a function of pH. Our results indicate that rhSP-D is assembled in four oligomeric states: trimers, hexamers, dodecamers and larger oligomers (fuzzy balls), with dodecamers being the most abundant structure in all experimental conditions tested. We have developed a cross-linking protocol to detect the presence of SP-D dodecameric forms by PAGE-SDS, in which dodecamer is only visualized after chemical crosslinking and in the presence of denaturing agents, indicating the importance of ionic and hydrophobic interactions in dodecamer formation and stabilization.

Results

Qualitative and quantitative analysis of rhSP-D oligomeric forms by AFM

Atomic force microscopy of rhSP-D samples deposited onto mica surfaces at pH 7.4 revealed that rhSP-D is assembled in a variety of different oligomeric structures including trimers, hexamers, dodecamers, and larger aggregates, usually described as asterisk-like or fuzzy balls, composed by a variable number of trimers (Figure 1.2A). Details of the four different oligomeric species observed are shown in figures 1.2B and 1.2C. Different clones of rhSP-D were studied. Some differences in the oligomeric forms distribution were found between them, that could be caused by the purification process and buffers. For this reason, it was important to obtain human SP-D as a control (Chapter 3), to figure out which one was the most similar to native protein. One representative clone of those assessed was chosen for this study. The dodecamer was the most abundant structure in this and other rhSP-D clones studied.

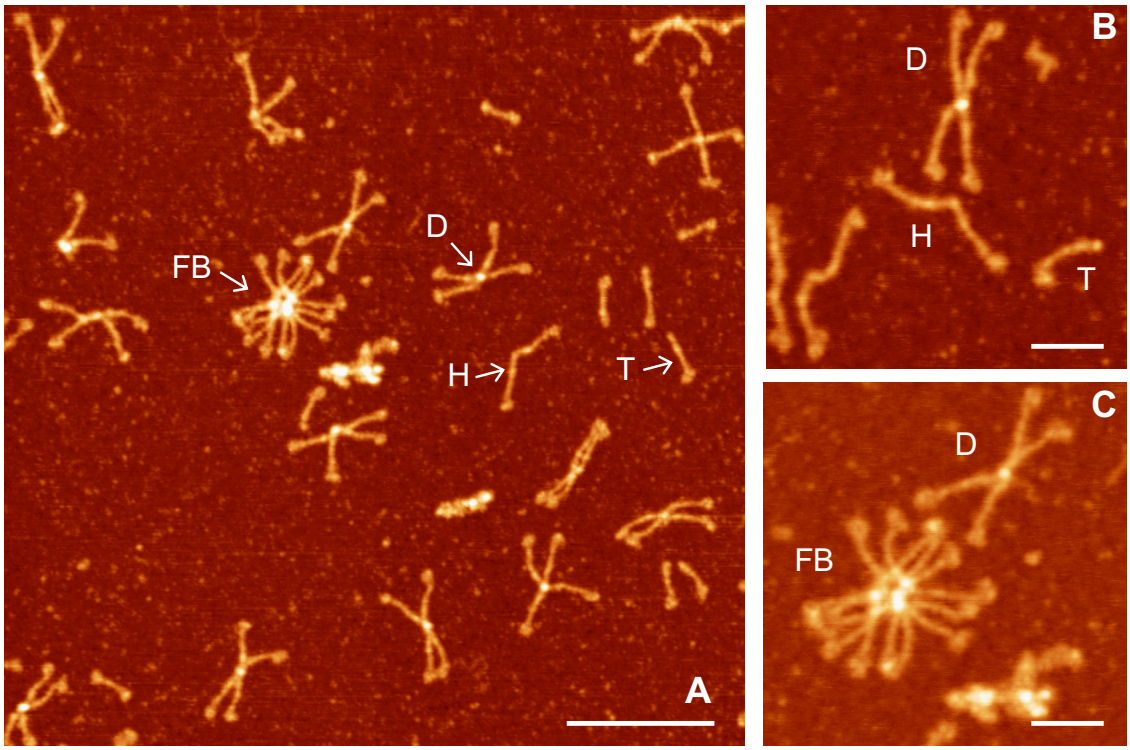

Figure 1.2: AFM images of rhSP-D at pH 7.4. ***A-C***: AFM images of rhSP-D, where illustrative examples of different oligomeric forms can be observed, including trimers (T), hexamers (H), dodecamers (D), and fuzzy balls (FB). ***A***, 1-µm scan, the scale bar represents 200 nm. ***B*** and ***C***, 300 nm scan; the scale bar represents 60 nm.

To perform a quantitative analysis, a collection of high-quality images of 1 µm-scan area was taken among different sample preparations and regions, a set of which can be observed in Figure 1.3. Molecules were counted and classified into

groups according to their oligomeric state. Table 1.1 and Figure 1.4 summarize the results obtained for a total of 660 molecules identified.

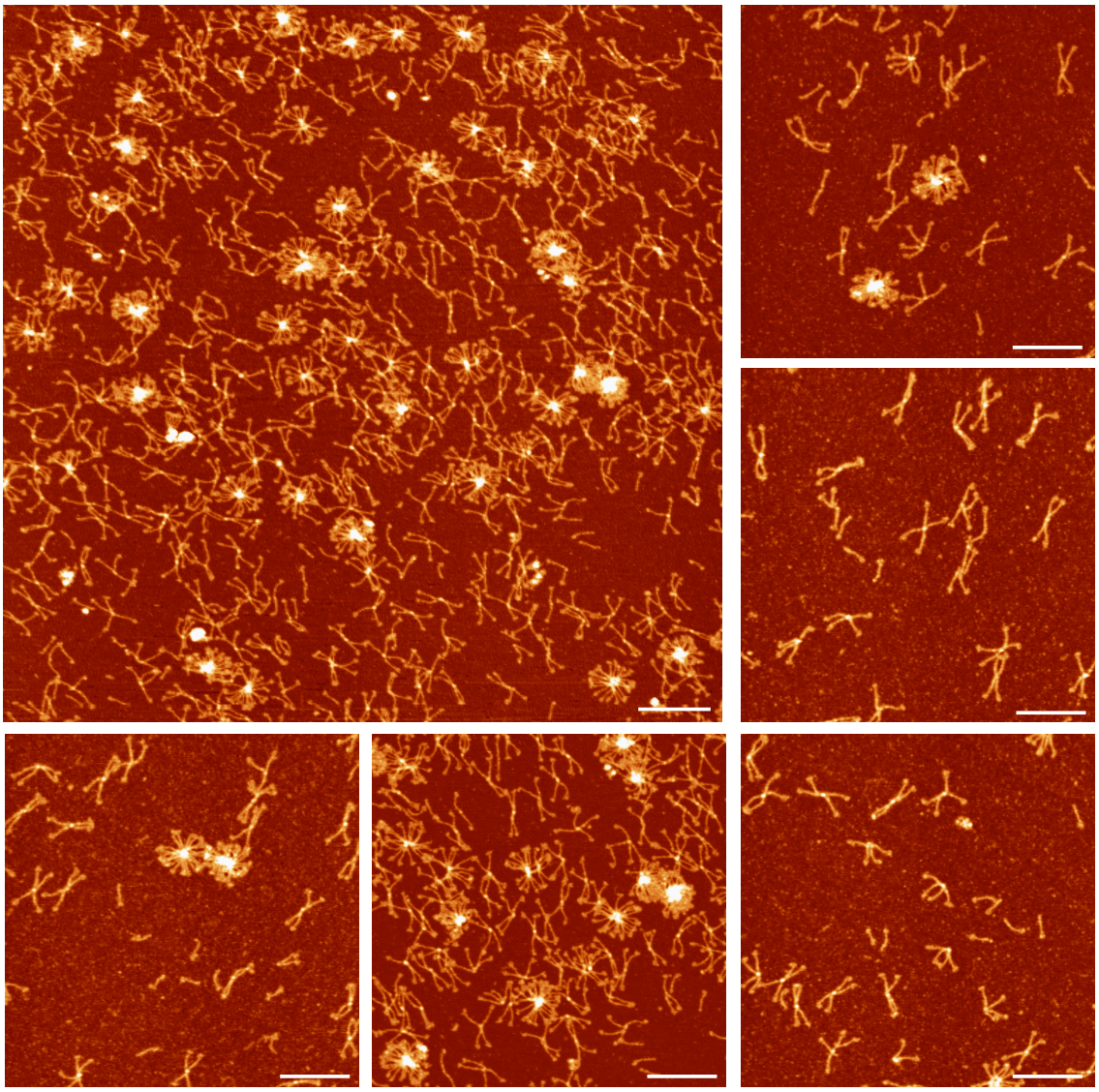

Figure 1.3: Set of AFM images of rhSP-D at pH 7.4. AFM images of rhSP-D, where the different oligomeric forms previously mentioned can be observed along all the preparation. *Top left image,* 2-μm scan, while the rest are 1-μm scan. The scale bar represents 200 nm.

A relative distribution of the different protein oligomers was calculated considering three different parameters: i) % molecules, from the number of individual molecules within each oligomerization state, ii) % weight, from the amount of total protein mass across each of the 4 groups considering the molecular weight of each oligomer, defined as 43,000 Da/monomer unit times the number of monomer units per oligomer; and iii) % trimers, from the amount of trimers contained per oligomeric form group. According to these results, 41% of molecules and 51% of mass of rhSP-D is assembled as dodecamers, with dodecamers being the major single oligomeric species constituent of this recombinant protein. The

heterogeneous higher order oligomers ('fuzzy balls') are the second most abundant species (29%) in mass, and trimers and hexamers constitute minor components, with 11% and 9%, respectively, of protein mass.

Table 1.1: Quantitative distribution of different oligomeric forms of SP-D as determined from individual molecules observed under AFM at pH 7.4

Oligomeric Form	Nº Molecules	% Molecules	Weight (MDa)	Weight (g)	% Weight	Nº Trimers	% Trimers
Total	660	100	278.2	4.62E-16	100	2169	100
Trimer	244	37	31.5	5.23E-17	11	244	11
Hexamer	100	15	25.8	4.28E-17	9	200	9
Open	76	11	19.6	3,26E-17	7	152,00	7
Closed	24	4	6.2	1,03E-17	2	48,00	2
Dodecamer	273	41	140.9	2.34E-16	51	1092	50
Fuzzy Balls	45	7	80.1	1.33E-16	29	633	29

Weight (MDa), % molecules and % weight are defined as described in Results. Weight (g) is defined as weight in daltons/Avogadro's number.

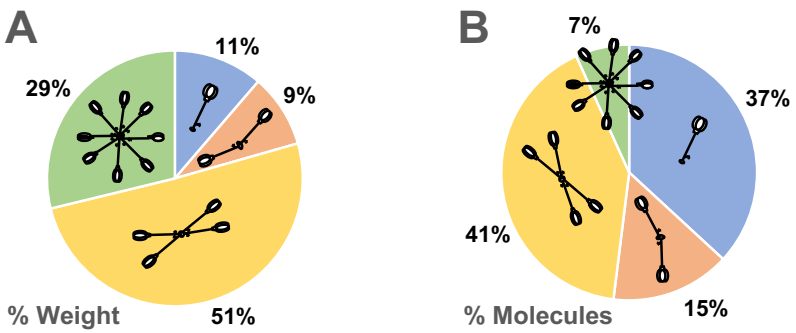

Figure 1.4: Quantitative distribution of oligomers. The distribution of oligomers has been represented as the percentage of molecules (***A***) and the percent by mass (***B***) of the different populations.

Structural characterization of rhSP-D oligomeric forms

To further characterize the distinct oligomeric forms, we measured the position and size of relevant structural features from AFM height profiles of individual trimers, hexamers, dodecamers, and other higher-order structures (Figure 1.5).

- Trimers: rhSP-D trimer images in figure 1.5A show the carbohydrate recognition domain with unprecedented resolution, enough to differentiate its three individual globular domains. Previous results published in the literature showed only a solid bright white spot at the end (Crouch et al., 1994a, Leth-Larsen et al., 2005, Hartshorn et al., 2008). A bright protuberance was observed at 47 ± 5 nm from the C-terminal end, which likely corresponds to the N-glycosylation site of the molecule, located at residue N70 in the collagen domain (Leth-Larsen et al., 1999).

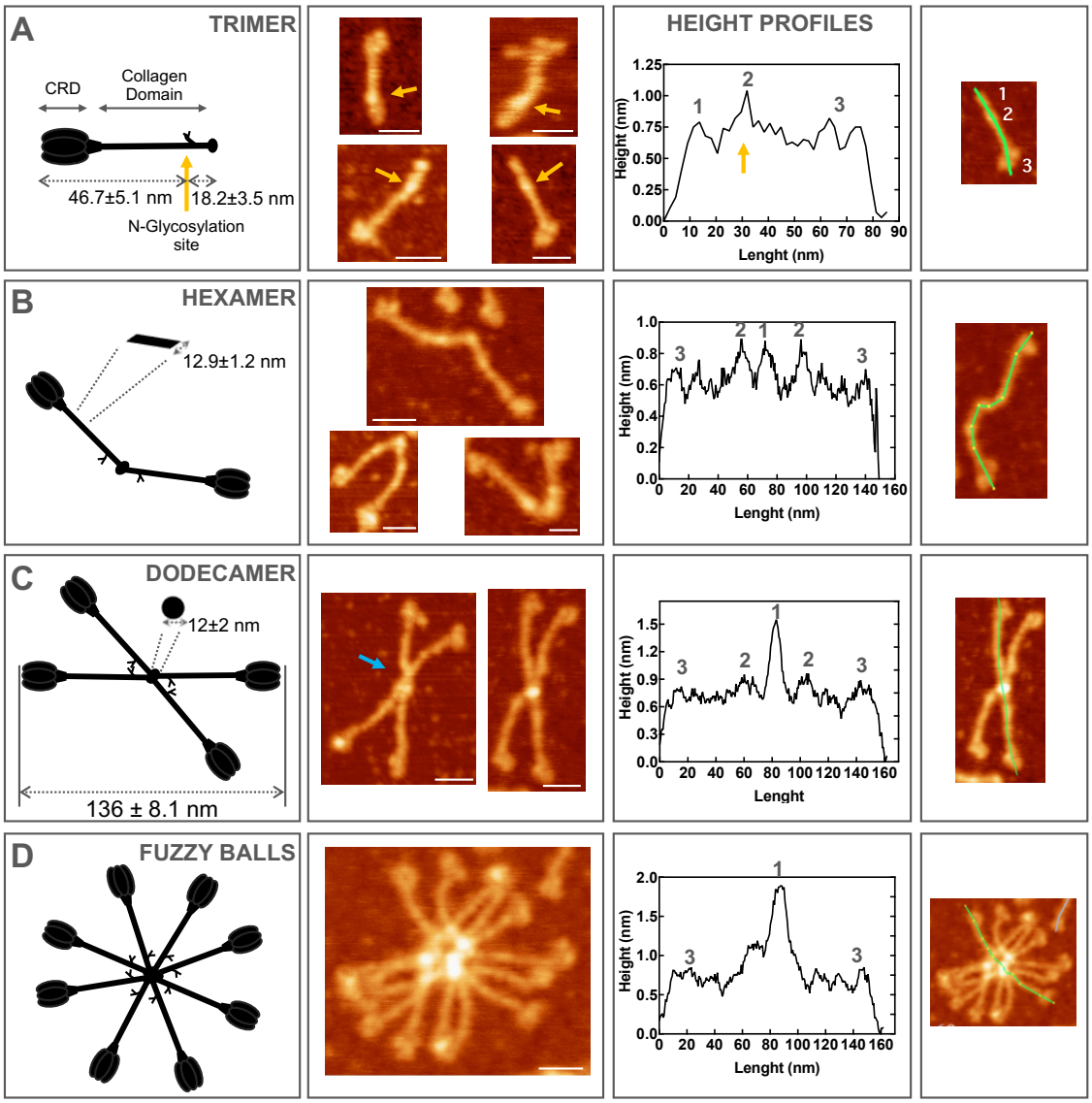

Figure 1.5: Structural analysis of the oligomeric forms of rhSP-D. The *first column* contains a schematic drawing of each type of oligomer that has been analyzed and includes representative characteristic parameters calculated from the AFM images. The position of the glycosylation site is indicated by a "Y". All parameters were calculated after measuring and averaging 50 individual molecules, and the average and its standard deviation are shown. The *second column* illustrates representative AFM images from each type of SP-D oligomer; the scale bar represents 30 nm. Yellow arrows mark the bright spot at the N-glycosylation site (N70). The blue arrow points to the segment overlapping two clearly distinct hexamers within a dodecamer. The *third column* illustrates the height profiles taken from each oligomer along the green line drawn in the images of the *fourth column*. The numbers above the profile indicate 1: N-terminal domain, 2: N-glycosylation site; 3: CRD.

To prove that the rhSP-D used in these experiments was N-glycosylated, de-glycosylation experiments were carried out with PNGase F, which removes the sugar core attached to an asparagine residue through an N-acetyl-glucosamine group (see Figure 1.6). A consistent shift to a lower electrophoretic mobility was found between intact rhSP-D and PNGaseF-cleaved rhSP-D (Figure 1.6A) accompanied by a disappearance of the majority of the bright protuberances in AFM images of the protein (Figure 1.6B), confirming that the recombinant human

rhSP-D is N-glycosylated. The AFM height profile of the trimer (Figure 1.5A) additionally confirmed the three relevant features (numbered 1-3), corresponding to the N-terminal end, the N-glycosylation site and the CRD, respectively. In addition, we often observed several conspicuous, regularly spaced, and bright segments along the collagen domain, which could correspond to the collagen triple helical twists. However, resolution limitations precluded the unequivocal assignment.

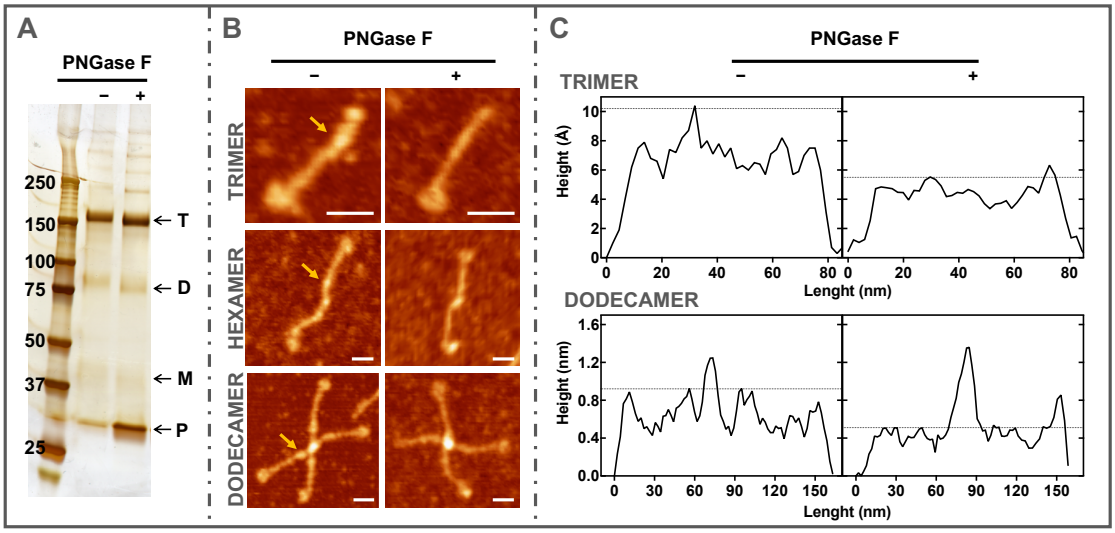

Figure 1.6: De-glycosylation of rhSP-D. ***A***, silver staining non-reducing SDS-PAGE analysis of rhSP-D treated (+) or not (-) with PNGase F; T (trimer), D (dimer), M (monomer), P (PNGase F). *Panel* ***B*** shows AFM images of trimers, hexamers and dodecamers before (-) and after (+) PNGase F treatment. The yellow arrow indicates the N-glycosylation site seen as a bright protrusion in the glycosylated protein. The scale bar represents 25 nm. ***C,*** Height profiles of trimers (*top*) and dodecamers (*bottom*) before (*left*) and after (*right*) PNGase F treatment. Horizontal dotted lines have been traced at the height of the N-glycosylation site height.

- Hexamers: rhSP-D hexamers are structures consisting of two trimers linked by the N-terminal domain (Figure 1.5B). Two populations of hexamers with different shapes were found: hexamers with a closed conformation (V-like) and hexamers with an open (rod-like) configuration, with the latter being the most abundant as quantitated in Table 1.1. The presence of hexamers opens the possibility that these oligomers could be a structural intermediate between trimers and dodecameric forms, especially considering the way the N-terminal regions of dodecamers are seen under AFM. The maximal observed distance between two opposed CRD domains in the hexamers contained into the dodecamer molecule was 136 ± 8 nm (Figure 1.5C), slightly longer than published data for rat SP-D (114 ± 3 nm) (Crouch et al., 1994b). The symmetrical height profile of the dodecamer exhibited the highest point in the middle of the molecule, which

matches with the N-terminal domain of both hexamers constituting the interaction point (Figure 1.5C, height profile).

- Dodecamers: The rhSP-D dodecamer appears to be formed by close association of two hexamers, although the part of the molecules that would be responsible for this interaction is not fully clear. The central junction exhibited a radius of 12 ± 2 nm and an apparent height of 1.0 ± 0.4 nm as determined from the AFM profile (Figure 1.5C). In the dodecamers, it is quite frequent to observe a close apposition of the zone between N-glycosylation sites from the two possible different hexamers at one or even at both sides of the N-terminal domain (see Figure 1.7C and F). It is not known whether this interaction could have an influence in protein oligomerization because in other cases is not observed (Figure 1.7A, E). An open question is whether "V-like" and "rod-like" hexamers might promote formation of different types of higher order oligomeric structures.

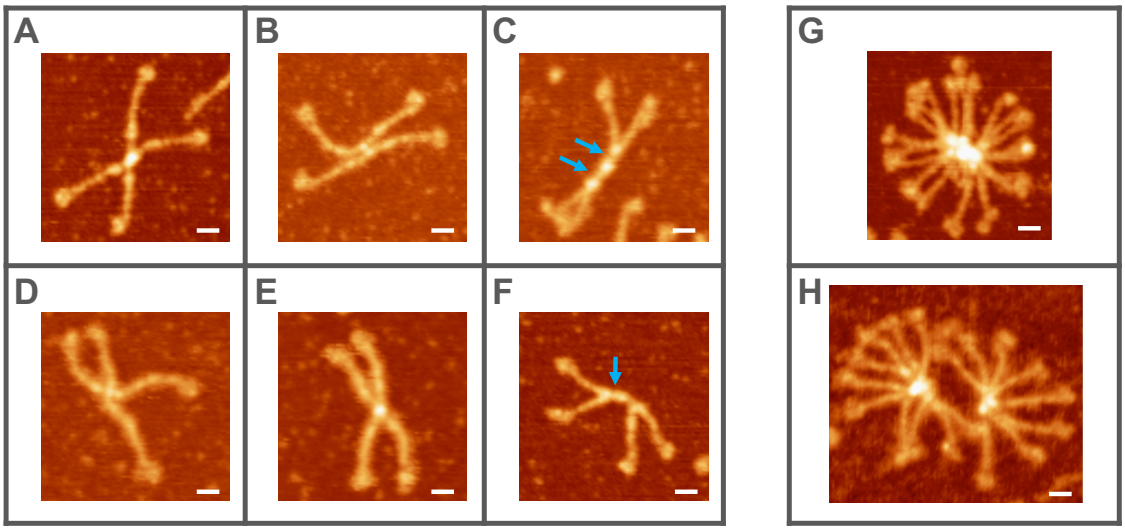

Figure 1.7: AFM images of rhSP-D. ***A-F:*** magnifications of some dodecamers. The blue arrow points to the segment overlapping two clearly distinct hexamers within a dodecamer. ***G-H:*** magnification of fuzzy balls. ***A-H,*** the scale bar represents 20 nm.

- Higher order oligomers: They include heterogeneous higher order asterisk- or fuzzy ball-like oligomers composed of a variable number of trimeric arms, usually in a range between 6 and more than 20, as it is observed in figure 1.3 and 1.5D. They adopted a circular disposition once adsorbed onto the mica-substrate with a diameter similar to that of dodecamers. It is apparent that the center of fuzzy balls is not a solid unique junction, but a cluster of several small nearby centers, which could correspond to the N-terminal domain of trimers pre-associated in dodecamers or hexamers (Figure 1.7G). The width and the height of the central structure increased with the number of trimers contained in the fuzzy ball, while the total diameter of the full complex remained constant (Figure

1.8). Most fuzzy balls presented well-separated pairs of trimers around the central interacting region, suggesting that these structures are built from hexamers in their closed (V-like) conformation.

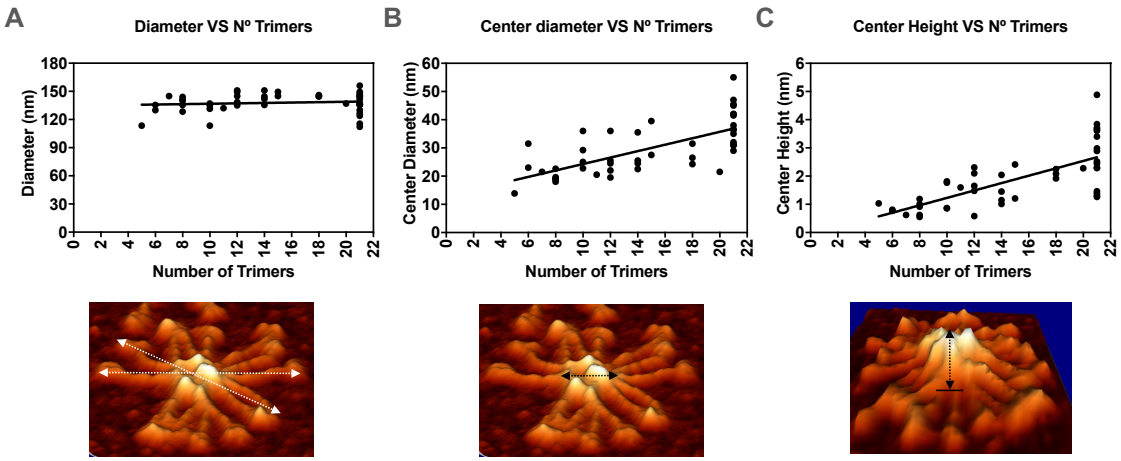

Figure 1.8: Structural characterization of rhSP-D fuzzy balls. Some parameters of fuzzy balls were measured and plotted against the number of trimers per molecule. ***A***, total diameter of the whole molecule, taken as the average of two diameters measured for each molecule. ***B***, the center diameter, taken as the average of two measurements of the central stem of each molecule, as indicated by the black arrow. ***C***, the height of the center (N-terminal domain) of each fuzzy ball, measured as indicated.

Characterization of rhSP-D by Cryo-TEM

Despite the fact that AFM is a powerful technique, which allowed us to observe in detail many of the structural determinants of the protein and quantify the distribution of the oligomeric forms, molecules observed were restricted to a 2 dimensional (2D) planar conformation defined by its interaction with the mica surface. This was a limitation to figure out the conformation of rhSP-D oligomers in solution, particularly the conformation of fuzzy balls. Cryo-TEM was used then in an attempt to sort out this question. Figure 1.9 shows molecules selected from the images obtained. Despite the difficulty to identify them, some clusters where trimers are branching out from a central point can be observed, which we attributed to fuzzy balls (Figure 1.9, top panel left and zooms). In addition, some dodecamers were identified (Figure 1.9, bottom panel). The conformation of SP-D oligomers and their arrangement in the sample supposed an obstacle to identify dodecamers and small oligomers. When they were arranged perpendicular to the plane only their CRDs could have been identified and, when parallel to the plane it was challenging to recognize their thin collagen arms.

These results did not allow us to discern unequivocally the 3D conformation of fuzzy balls. Although they looked like circles in most of the images, which corresponds to spheres in solution, the limited resolution impeded us from distinguishing the molecules and their terminal ends properly and figuring out the

real conformation. Moreover, in the case of dodecamer and lower order species, we cannot ignore that probably we were only identifying a few examples of them. Further optimization of the experimental conditions to improve resolution is required to complete the characterization of the configuration of SP-D in solution.

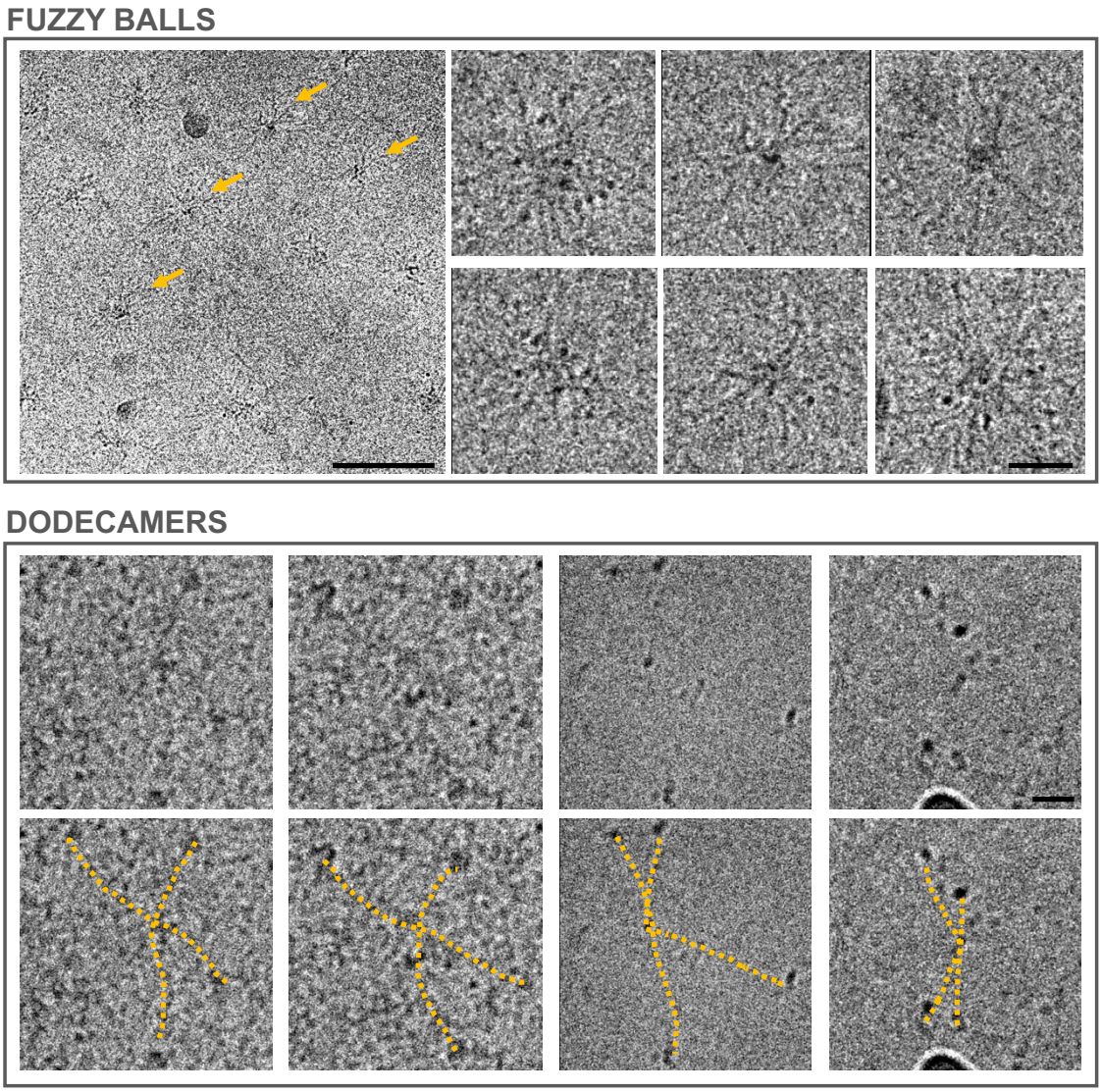

Figure 1.9: Cryo-TEM micrographs of rhSP-D. *Top panel, left,* image obtained in Cryo-TEM, arrows indicate some identified fuzzy balls, scale bar 100 nm; *right,* selected particles from the images were zoomed, the scale bar represents 25 nm. *Bottom*, selected dodecamers from the images were zoomed, the first and second row contain the same images, but in the second row the molecules have been traced with a yellow dotted line to help to assist identification; the scale bar represents 25 nm.

Electrophoretic analysis of rhSP-D

In order to gain insight about the type of interactions leading to formation of different rhSP-D oligomers and to confirm the presence of the structures observed by AFM in the samples examined in bulk, a biochemical analysis using PAGE with gradient polyacrylamide gels was conducted. The rupture of interchain disulfide bonds with βME totally transformed all oligomeric species into monomeric form,

as deduced by its electrophoretic behavior (Figure 1.10A). Under non-reducing conditions and in the presence of SDS, the sample was found to consist mainly in trimers (Figure 1.10A). Blue native electrophoresis was carried out to analyze the protein native state. We expected to see protein bands principally at the theoretical mobilities corresponding to the molecular weights of hexamer, dodecamer and at least smaller sized fuzzy balls in the gels, but the experiments revealed that under such conditions most of the protein was not able to enter into the gel, remaining in the well (Figure 1.10B, first lane in the gel). It was necessary to add SDS to the sample to allow the protein to enter the gel, but rhSP-D was then only observed primarily in the form of trimers (Figure 1.10B left and 1.10C).

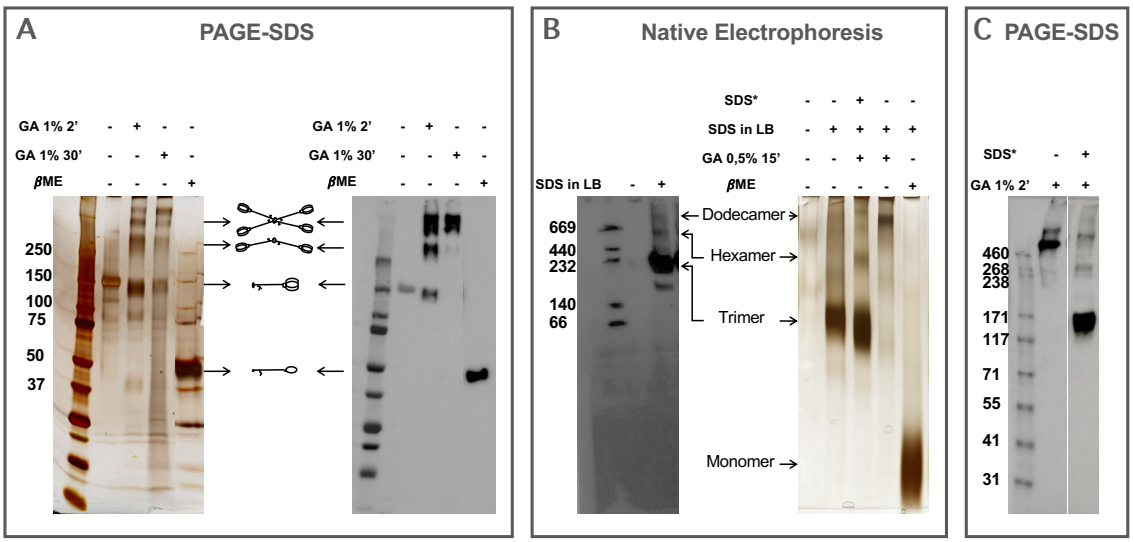

Figure 1.10: Biochemical analysis of rhSP-D by electrophoresis. The quaternary structure of rhSP-D has been analyzed by PAGE-SDS (*A and C*) and native electrophoresis (*B*). The different conditions and reagents used for treating each sample are indicated above the gels and membranes. ***A***, the gel on the left has been developed by silver staining and the WB-membrane on the right side has been developed with anti-SP-D antibody as indicated in Methods. ***B***, the membrane on the left is an anti-SP-D WB, while the gel on the right has been revealed by silver staining. ***C***, western blot anti-SP-D. SDS* means that SDS was added to the sample before crosslinking with GA. The molecular weight of the protein standards is indicated to the left of the gels and membranes.

In order to detect higher order oligomeric conformations, we subjected the rhSP-D native structure to crosslinking by glutaraldehyde (GA), a bifunctional reagent that binds and interconnects neighboring reactive groups within the protein and between protein chains. After 2 minutes of GA crosslinking reaction, PAGE performed under non-reducing conditions revealed protein bands with mobilities corresponding to hexameric and dodecameric structures; whereas after 30 min of crosslinking reaction, substantially lower amounts of hexamer were apparent (Figure 1.10A, see WB). Fuzzy balls oligomers were not seen in these gels and membranes after cross-linking, probably because their big size does not allow them

to penetrate into the gels. Cross-linked samples were also subjected to a modified native electrophoresis, where the typical native loading buffer was substituted by non-reducing loading buffer (which contains SDS), in order to push the protein through the pores (Figure 1.10B right, third lane). On the contrary, no protein bands were observed in the gel when the experiment was carried out with cross-linked samples and native loading buffer.

Effect of pH on the conformation and oligomerization of rhSP-D

To further characterize the oligomerization pathway of SP-D and the type of interactions involved, the effect of acidic and basic pH on rhSP-D structure was studied. Protein was diluted to the desired concentration for AFM experiments with buffers at different pHs (8.5, 5.5, 4.2 and 3.0). AFM imaging of these samples was carried out followed by a quantitative analysis of the distribution of oligomeric forms (Figure 1.11).

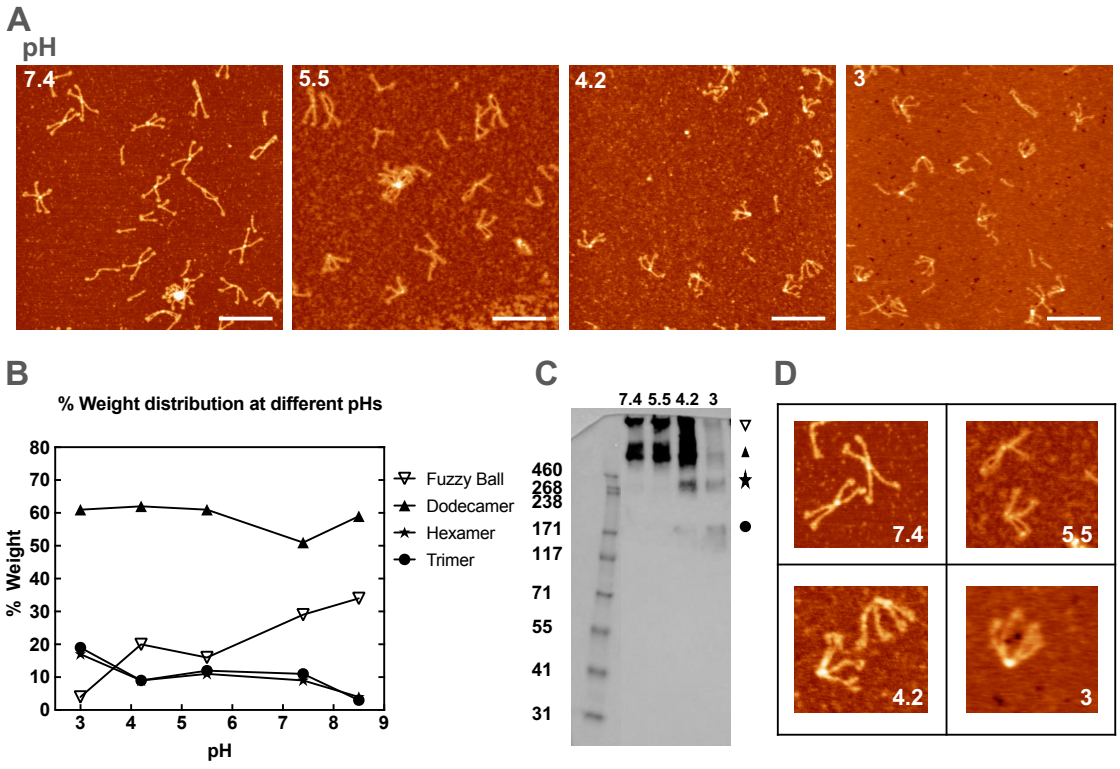

Figure 1.11: Effect of pH on the conformation and oligomeric distribution of rhSP-D. ***A,*** representative AFM images taken from rhSP-D samples at the different pHs indicated; the scale bar represents 200 nm. ***B,*** percentage by mass of the different oligomeric forms of rhSP-D at the different pHs (after assigning and counting 218 molecules at pH 3.1, 154 at pH 4.2, 175 at pH 5.5, 660 at pH 7.4 and 310 at pH 8.5). ***C,*** the effect of pre-incubation at different pH conditions on the electrophoretic behavior of the protein was evaluated after the samples were subsequently crosslinked with GA 0.5% for 15 minutes. Different symbols indicate the different types of oligomers: fuzzy balls (*open triangle*), dodecamer (*triangle*), hexamer (*star*) and trimer (*circle*). ***D***, magnified representative images of the dodecamer conformation observed under different pH conditions.

The results revealed that the proportion of protein assembled as dodecamers was higher in a more acidic environment, concomitant to a reduction in the percentage of fuzzy balls. We found that at pH 5.5 and 4.2 there is a reduction of 10-15% by weight in the proportion of fuzzy balls compared to that at pH 7.4, together with an increase in dodecamers, but not in trimers (Figure 1.11B). This supports the hypothesis that dodecamers are joined by weak interactions to create fuzzy balls, instead of being formed directly by covalent interactions between trimers, with all of them linked together by the N-terminal end, a possibility previously suggested (Crouch et al., 1994b, Brown-Augsburger et al., 1996a). At pH 3.0, the increase in dodecamer content was similar (10%), but a higher decrease in fuzzy ball-like oligomers (25%) was observed. This was accompanied in this case by a 9% increase in both trimers and hexamers, suggesting that at extremely low pH, fuzzy balls could start to dissociate into dodecamers and further into hexamers and/or trimers. At basic pH (8.5), a reduction in the proportion of trimers and hexamers was observed, accompanied by an increase in dodecamer content and in large oligomers (34%). The content in higher order fuzzy ball-like oligomers seems to continuously increase from pH 3 to pH 8.5, indicating that the more alkaline pH promotes formation of larger oligomers beyond the dodecamer. Changes in the distribution of oligomers due to acidic pH were confirmed by electrophoresis, where rhSP-D samples at different pHs were subsequently crosslinked with GA (Figure 1.11C). The most prominent dodecamer band was observed at pH 4.2.

Interestingly, a conspicuous change in the conformation of dodecamers was clearly observed in the AFM images as a consequence of acidic pH (Figure 1.11D). At the most acidic pHs (4.2 and 3.0) most of dodecamer molecules appeared in a sort of closed configuration, with the four trimers and the 4 trimeric CRD domains clustered in a nearby space. These cryptic structures appeared in all possible orientations and only at these pHs, discarding any artifact from the washing and drying sample preparation procedures. At pH 5.5, an intermediate state between those at pH 7.4 and 4.2 was observed, with some dodecamers attaining a closed conformation and others in a standard X-like open conformation (Figure 1.11A). In order to better quantitate the characterization of this structural conversion, the four angles present within each dodecamer were measured, and data were pooled for each pH condition, and represented as histograms (Figure 1.12A, top).

At pH 7.4, the histogram was composed of two main angle populations, one corresponding to acute angles of 30º-50º and the other to obtuse angles of 140º-150º, indicating that the dodecamers exhibit an X-like shape. Interestingly, the two acute angles were not identical in each X-like dodecamer. The ratio α_1/α_2

calculated for 273 dodecamers, where α_1 is the smallest acute angle in the molecule and α_2 the biggest acute angle, peaked at 0.7 (Figure 1.13). This suggests that dodecamers are likely composed of two hexamers in open (rod-like) conformation as the assembly by two hexamers in closed conformation would have provided a value closer to 1.0.

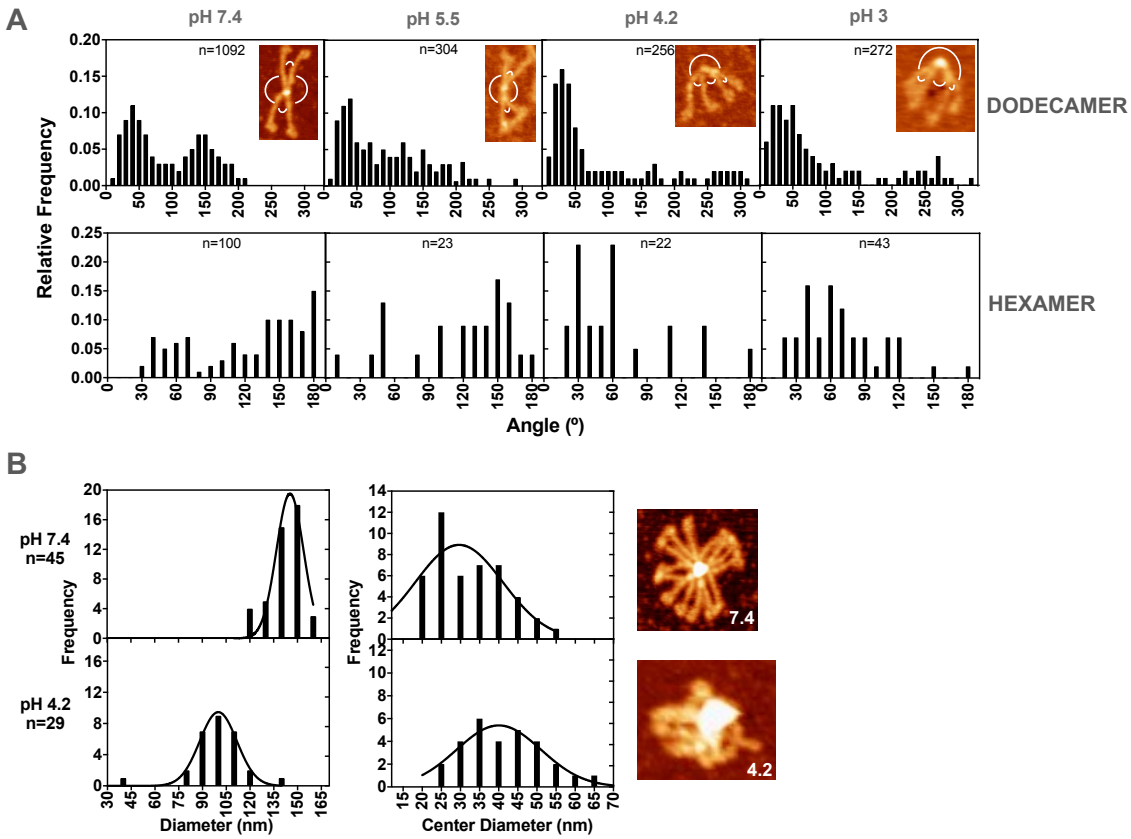

Figure 1.12: Effect of pH on the conformation of rhSP-D oligomers as evaluated by measurement of the angles defined by the position of their trimeric arms. ***A***, the four angles formed by the relative position of the individual trimeric arms within each dodecamer (*A, top*) were measured and pooled, and their relative frequencies represented with a histogram at each of the different pHs . Inside each of the graphs, a representative picture of a dodecamer with the typical configuration at the corresponding pH has been included, indicating the angles measured. "n" is the total number of angles measured for each condition. A similar analysis was performed for the angle enclosed by the two trimers within each hexamer (*A, bottom*). ***B***, to analyze the pH-induced changes in the conformation of the fuzzy balls, the frequency distribution of the total molecule diameter and the center diameter (N-terminal domain) is illustrated at pH 7.4 (*top panels*) and 4.2 (*bottom panels*). The histograms have been fitted to a Gaussian distribution. A representative AFM image of a fuzzy ball at each pH condition is showed on the right.

At pHs 4.2 and 3.0, the histograms of angles only show one main peak around acute angles of 20º-40º and a large dispersion of different values of obtuse angles. These data reflect how most dodecamers are in a closed conformation. At pH 5.5, an intermediate state is observed, where the peak of acute angles is present and the incidence of obtuse angles with values between 100º to 180º is still significant, but the peaks are not as prominent as observed at pH 7.4. This indicates that some

dodecamers are changing to a closed conformation while others are still in a X-like conformation.

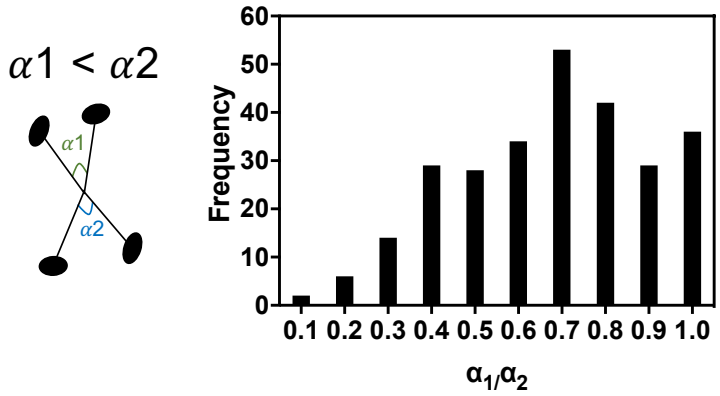

Figure 1.13: Ratio of acute angles α_1/α_2 in rhSP-D dodecamers. Frequency distribution of the ratio between the two acute angles in each of 273 dodecameric rhSP-D molecules, determined at pH 7.4.

The angle formed by each hexamer (as a result of the relative position between its two trimers) was also measured and data was compiled in histograms (Figure 1.12A, bottom) showing the same trend as that observed in dodecamers.

Changes in conformation between pH 7.4 and 4.2 were also studied in fuzzy balls. In this case, the parameters evaluated were the total molecule diameter and the center diameter. The results revealed that fuzzy balls at pH 4.2 are characterized by a shorter total molecule diameter and larger center diameter than at pH 7.4. These results are in agreement with dodecamer conformational changes and imply that fuzzy balls are formed from hexamers and/or dodecamers in a closed conformation at acidic pH (Figure 1.12B).

Effect of calcium on the conformation and oligomerization of rhSP-D

SP-D encloses four calcium binding sites in the CRD, which are important for its innate immune activity (Crouch, 1998, Shrive et al., 2003). To determine whether the presence of calcium could influence rhSP-D structure, its conformation and the distribution of oligomeric forms, AFM experiments were carried out at pH 7.4 in the presence of $CaCl_2$ 5 mM, instead of EDTA 1mM. The addition of calcium did not show conspicuous differences when compared to the EDTA condition. The distribution of oligomeric forms was similar in both cases, as well as the histogram of the angles enclosed within dodecamers (Figure 1.14). Although calcium affects the disposition and conformation of some protein segments within the CRD domain to allow the interaction of some amino acids with their ligands (Shrive et al., 2003), it does not seem to have substantial impact on the supramolecular structure and conformation of SP-D.

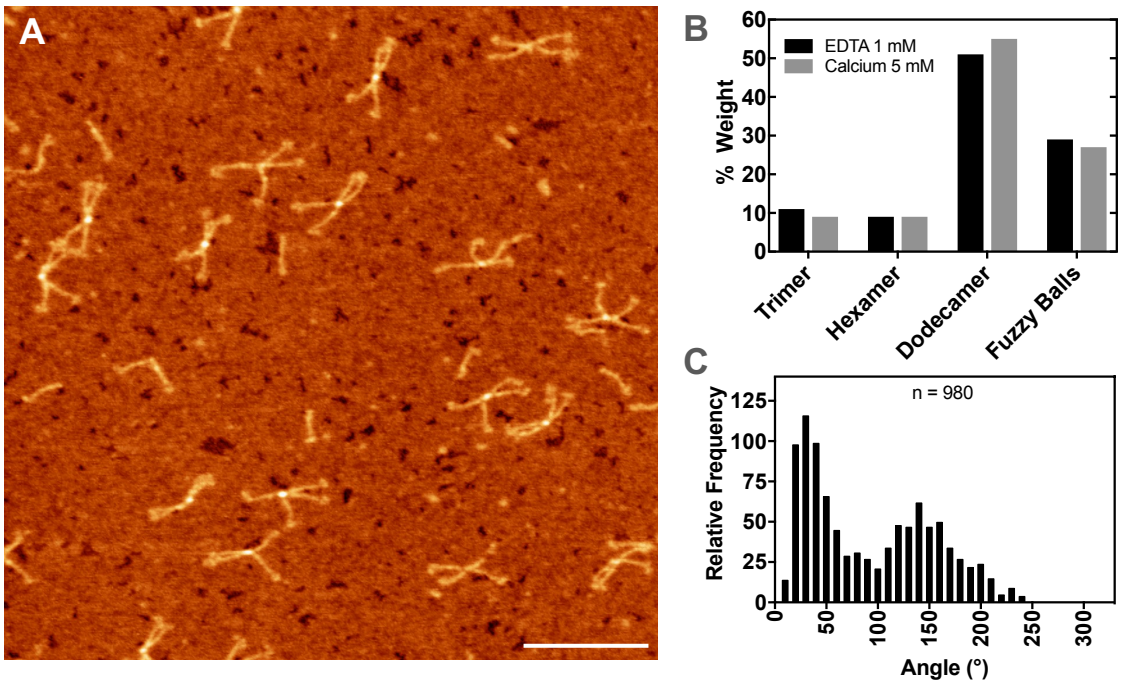

Figure 1.14: Structure and distribution of oligomeric forms of rhSP-D in the presence of 5 mM calcium. ***A***, representative AFM image of rhSP-D in 5 mM calcium. The scale bar represents 200 nm. ***B***, distribution of oligomeric forms of rhSP-D at pH 7.4 in 200 mM NaCl, 20 mM Tris, 1 mM EDTA, (black bars) (n=660) or 200 mM NaCl, 20 mM Tris, 5 mM $CaCl_2$ (grey bars) (n=520). ***C***, relative frequency of distribution of the four angles enclosed within dodecamers in the presence of 5 mM calcium (n=980).

Thermal stability of rhSP-D at neutral and acidic pH

The thermal stability of the structure of rhSP-D, especially of dodecamers, was examined by gel electrophoresis and AFM at pH 7.4 and 4.2, and the results are shown in figure 1.15. The structure of rhSP-D is more resistant to thermal denaturation in an acidic environment than at neutral pH. When heated to 40-45 ºC at pH 4.2 it is still possible to observe bands in the gels corresponding to hexamers and dodecamers; while at pH 7.4, the bands of these oligomeric forms are not clearly defined at the same temperatures. It appears that the conformational changes occurring in the protein at pH 4.2 make it more resistant to thermal denaturation. AFM imaging of rhSP-D at pH 7.4 and 45 ºC show how the SP-D is disassembled and many collagen triple helical domains are unstructured (i.e. marked by a dotted circle in figure 1.15). In contrast, at the same temperature at pH 4.2, hexamers are the most abundant species observed in AFM images, followed by trimers, all of them composed of properly assembled collagen triple helices (see figure 1.15, solid-line circles). AFM images therefore confirm that rhSP-D thermal stability is highly dependent on collagen thermal stability.

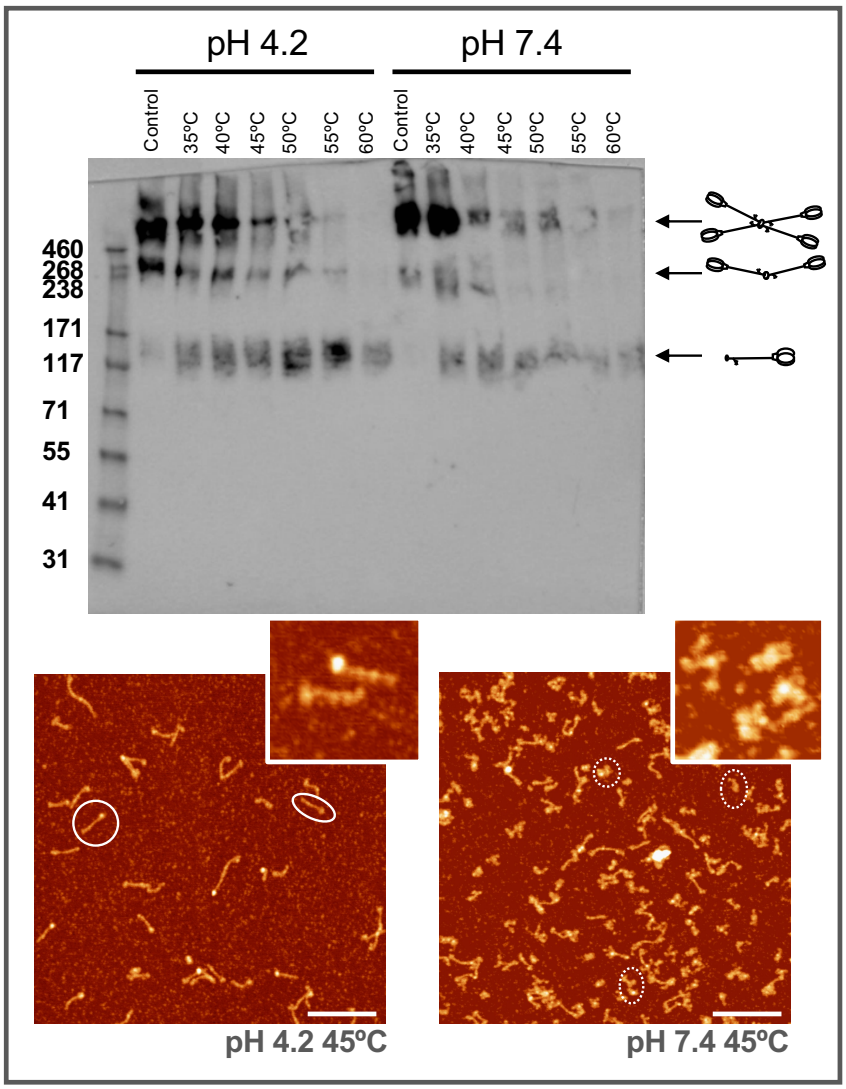

Figure 1.15: Thermal denaturation of rhSP-D. ***Top***, a PAGE-SDS gel followed by western blot of rhSP-D after exposure to different temperatures at pH 7.4 or 4.2 prior to crosslinking as described in the methods section. The pH and temperature of treatment of each sample are indicated at the top of the WB membrane, the assigned oligomeric states of each band is on the right, and the molecular weight of standards on the left. ***Bottom***, representative AFM images of rhSP-D after incubation at 45º at pH 4.2 (*left*) or 7.4 (*right*). Structures enclosed in white solid circles are examples of intact trimers with a preserved native structure, while structures enclosed in dotted circles are examples of disassembled trimers due to thermal stress. The scale bar represents 200 nm.

Discussion

Trimers, dodecamers and higher order oligomers have been described as the different oligomeric forms of SP-D (Crouch et al., 1994b, Crouch et al., 1994a, Hartshorn et al., 1996a, Brown-Augsburger et al., 1996a, Leth-Larsen et al., 2005). However, the actual distribution and function of these different forms still remain as open questions. The particular shape of dodecamers and higher order oligomers known as 'asterisk-like' or 'fuzzy balls' makes difficult to separate and quantify the different fractions using conventional chromatographic procedures (Crouch et al., 1994b, Ogasawara and Voelker, 1995, Leth-Larsen et al., 2005). Electrophoresis

experiments have failed to catch SP-D structures larger than trimers. Even in electron microscopy, SP-D cannot be observed under-close-to-native conditions due to the fixing and shadowing treatment required for sample observation that always occurs under vacuum (Crouch et al., 1994b, Hartshorn et al., 1996a). Plain electron microscopy images, typically obtained in the absence of specimen tilting and tomography make also impossible to determine whether some or all of the largest aggregates are closer to flat ("asterisk"-like) or spheric ("fuzzy ball"-like) three-dimensional assemblies when they are free in solution. For all these reasons, a quantitative analysis of the oligomeric distribution of SP-D under different conditions remains a challenge. In the current chapter, we have used AFM as a tool to analyze, both qualitatively and quantitatively, the structures of rhSP-D produced in CHO cells under close to native conditions. Previous AFM observations had provided a rather qualitative description of SP-D structure (Leth-Larsen et al., 2005, Hartshorn et al., 2008). We have found that rhSP-D is a mixture of trimers, hexamers, dodecamers and higher order oligomeric species. The variety and morphology of the structures observed are similar to those previously reported by transmission electron microscopy (Hartshorn et al., 1996a), except that the dodecamer is confirmed as the most abundant species in the rhSP-D studied here. Dodecamers had been already described as the most abundant oligomeric structure of rat SP-D and its recombinant version (rrSP-D) as examined by electron microscopy (Crouch et al., 1994a, Crouch et al., 1994b).

However, it is relevant that the conspicuous presence of a population of hexamers in the previous studies (Hartshorn et al., 1996a, Leth-Larsen et al., 2005, Hartshorn et al., 2008) was either ignored (Leth-Larsen et al., 2005, Hartshorn et al., 2008), or considered as a possible artifact of the assembly of SP-D (Hartshorn et al., 1996a). We propose here that the hexamer is likely an intermediate in dodecamer and fuzzy ball assembly. In the model proposed in figure 1.16, three monomers associate into trimers, which are stabilized by disulfide bonds; trimers then form hexamers and these are subsequently paired into dodecamers. These two last structures are found associated into higher order oligomers of variable mass, termed 'fuzzy balls' based on their dandelion-like appearance on the surface of the mica in the AFM images illustrated herein. We propose that the oligomerization process that take trimers to fuzzy balls is governed by different non-covalent interactions at the different oligomerization levels.

The high-quality AFM images obtained in the current study have allowed the observation of unprecedented structural details, including individual CRD domains in trimers, defined N-glycosylation sites, presumed collagen triple helical twists and the junction points around the N-terminal region in dodecamers and fuzzy balls.

The repeated observation of hexamers in different sample preparations and the fact that dodecamers observed on the surface of the mica seem to be composed of two hexamers (see Figure 1.7), raise the question of what kind of interactions could be involved in the assembly of hexamers to form dodecamers. Moreover, the identification of segmented fuzzy ball centers, possibly corresponding to individual dodecamers and/or hexamers, suggests that the assembly of the higher order oligomeric structures is a reversible and dynamic process that might contribute to the modulation of SP-D function in response to local conditions within the cell or tissue under different physio-pathological contexts.

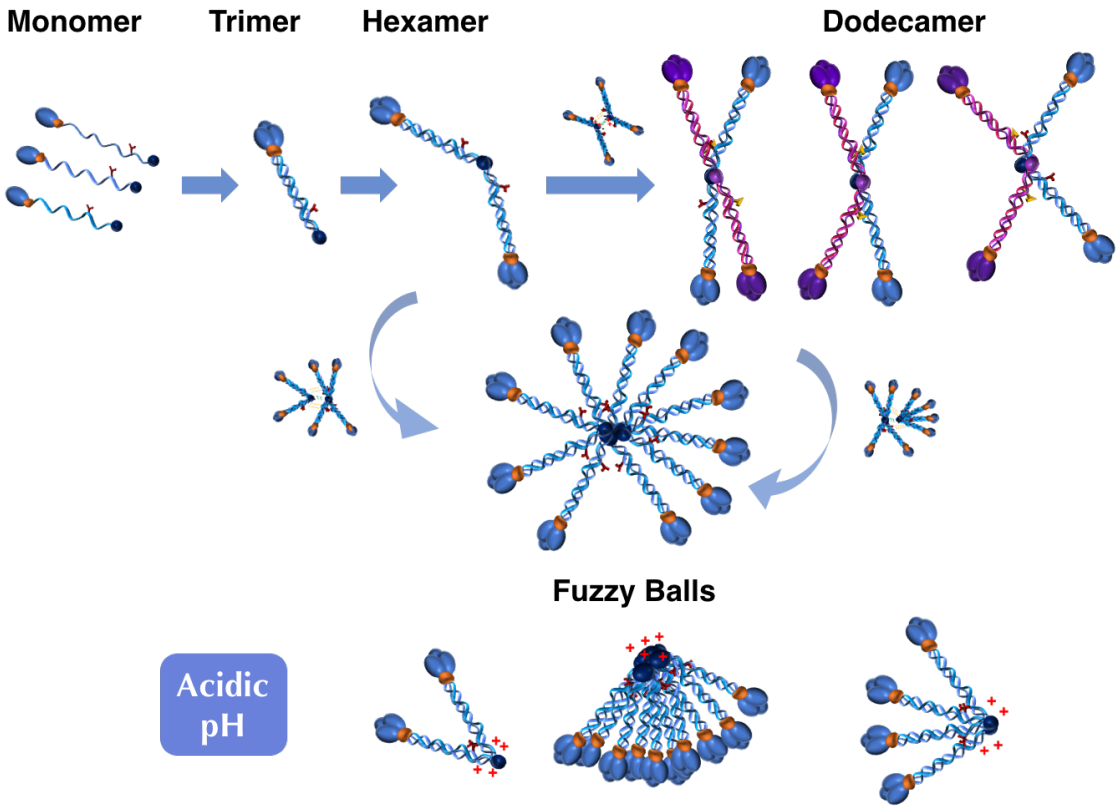

Figure 1.16: Proposed model for rhSP-D oligomerization pathway. Three monomers of rhSP-D first associate through the folding of the collagenous sequence segment into triple helices and the assembly of a coiled-coil bundle of α-helices in the neck region. These trimers are stabilized by two disulfide bonds in the cysteine-rich N-terminal domain (Brown-Augsburger et al., 1996a). Two trimers would then form hexamers with the participation of non-covalent interactions, such as ionic interactions, between the two N-terminal domains. The next step would be the association of two hexamers into dodecamers by ionic and hydrophobic interactions, which could present sugars from opposed hexamers for interaction, at one or both sides of the N-terminal domain. Fuzzy balls would be formed by association of dodecamers and/or hexamers through weaker non-covalent interactions, most likely involving hydrophobic interactions. At extreme acidic pH, the configuration of the hexamers, dodecamers and fuzzy balls changes from open to closed, which could influence the whole assembly pathway because it is accompanied by an increase in the proportion of dodecamers and lower order species and a decrease in the amount of fuzzy balls.

Using truncated versions of SP-D, Zhang and colleagues showed that the neck domain is indispensable for trimer formation (Zhang et al., 2001b). Based on the study of mutant vs. wild type proteins, it was proposed that residues C15 and C20 at the amino terminal domain of SP-D are crucial to establish interchain covalent interactions, which then allow the assembly of trimers into higher order oligomers (Crouch et al., 1994b, Brown-Augsburger et al., 1996a, Brown-Augsburger et al., 1996b). On the other hand, the role of the collagen domain in protein assembly is still not fully clear. Ogasawara and Volker showed that the absence of the collagen domain prevents a recombinant rat protein from forming higher order oligomers (Ogasawara and Voelker, 1995); in contrast, Kingma and colleagues reported association of 4 trimers in a collagen-deleted SP-D mutant expressed in mice, attributing to the N-terminal domain the leading role in the assembly of higher order oligomers (Kingma et al., 2006). The cross-linking protocol developed in the current work is a useful tool that could complement future studies to clarify this question.

Our results provide additional evidence on the oligomerization of SP-D. Trimers are the minimal structural unit observed in AFM images (Figure 1.2 and 1.3). The length of the collagen domain as measured under AFM, 48 ± 5 nm, agrees well with its expected theoretical length, 51 nm, considering a distance of 8.6 Å per G-X-Y collagen domain triplet (Beck and Brodsky, 1998, Okuyama, 2008). The position of the N-glycosylation site relative to the beginning of the collagen domain was determined at 9.2 ± 2.5 nm, a bit shorter than the theoretical value of 12.9 nm that could be expected only considering the position of the glycosylation site in the sequence and standard geometric considerations of the collagen triple helix. This indicates that specific interactions and condensing effects may modulate the structure of the collagen domain region at a local scale.

The possible existence of SP-D hexamers was mentioned in only two previously published studies. Crouch and colleagues suggested the possible existence of paired SP-D trimers associated in overlapping antiparallel arrangements (Crouch et al., 1994b) and Leth-Larsen et al. found a peptide of 15-16 kDa after collagenase digestion which dissociated into six polypeptide chains after reduction (Leth-Larsen et al., 1999). AFM images of rhSP-D (Figures 1.2 and 1.5) show the conspicuous presence of hexamers composed of two trimers joined through their N-terminal domains. Several lines of evidence obtained from these images indicate that hexamers are a necessary intermediate state in the oligomerization process: i) the absence of Y-shaped structures formed by three trimers, ii) the conspicuous association of two hexamers in some dodecameric assemblies, which do not exhibit a unique solid central hub at the N-terminal region (see blue arrow in Figure 1.5C,

and panels B and D of Figure 1.7), and iii) the parallelism between angle values formed by the trimeric arms in hexamers and dodecamers (Figure 1.12A).

In addition, we propose that dodecamers would be formed by two hexamers (Figure 1.16) and stabilized by a combination of non-covalent interactions between two hexamers at the N-terminal domain and the beginning of the collagen stem. In figure 1.1 the segment in rhSP-D sequence at the beginning of the collagen domain is marked as a charged patch, which contains a high density of basic and acidic residues and is highly conserved among different species. It is reasonable to consider that these residues could form ionic inter-chain links between triple helices from different hexamers. It has been published that in human collagen I the frequently found Lys-Gly-Asp/Glu triplets are highly stabilized by salt bridges (Persikov et al., 2005a, Persikov et al., 2005b), through formation of favorable ion pairs (Freudenberg et al., 2007). The amino acid sequence of rhSP-D contains eight of these triplets (Figure 1.1, purple residues), three of them close to the N-terminal region. Those triplets might establish inter-triple helix ionic bonds, due to its close proximity around the N-terminal region, contributing to dodecamer formation and stabilization. This idea is supported by AFM images (Figure 1.2 and blue arrow in figure 1.5C, figure 1.7) where the two hexamers in some dodecamers are observed with those regions (from N-terminal to the N-glycosylation site) interacting or closely apposed. Electrostatic interactions between carbohydrates linked to N70 could also play a complementary role in oligomerization.

The higher order oligomers observed in SP-D samples, typically described as 'fuzzy-ball' assemblies, could be the result of the association of dodecamers and/or hexamers. These assemblies have been traditionally interpreted as the result of the coalescence of multiple trimeric arms with a nearly spherical geometry. However, our images illustrate how, once deposited onto mica, they adopt a conformation with the N-terminal region protruding out from the mica (Figure 1.8C). This supports the existence of specific interactions between the collagen segments close to the N-terminal domains of different hexamers and/or dodecamers. Consequently, these higher order SP-D oligomers should probably not be seen as truly spherical arrangements –as the 'fuzzy ball' term may suggest- but as widespread arrangements of hexamers and dodecamers in a bouquet joined through the N-terminal ends. Unfortunately, the low resolution of rhSP-D molecules in cryo-TEM, which shows protein structure without being deposited onto any substrate, did not contribute to elucidate fuzzy balls conformation in the three dimensions. The stability of the fuzzy balls could be weak compared to that of dodecamers, being more sensitive to environmental conditions such as pH (see figure 1.11), a probable consequence of the key role of ionic interactions in the supratrimeric protein

oligomerization of SP-D. Interestingly, there is also a parallelism in the behavior of surfactant collectins SP-A and SP-D upon exposure to acidic pH. A conformational change, from open-arms to a tight closed-structure with the collagen domains grouped in a "stem-like" region and a shorter diameter of the CRD domains, has been reported for SP-A as a function of changes in pH or in the ionic environment (Efrati et al., 1987, Ridsdale et al., 1999, Palaniyar et al., 2001).

We have observed by gel electrophoresis and AFM experiments that acidic pH promotes changes in SP-D conformation that include an increase in the thermal stability of the protein. Previously published data showed a dependence of collagen thermal stability on pH (Bianchi et al., 1967, Freudenberg et al., 2007), suggesting that the higher stability of SP-D at pH 4.2 could be associated with a higher stability of its collagen domain segments. In fact, thermal denaturation of the protein as observed under AFM (see figure 1.15) seems to include a conspicuous denaturation of putative collagen domain triple helices, which appear unstructured at 45 ºC at pH 7.4.

A precise characterization of the distribution of SP-D oligomeric forms is the first step to address why SP-D exists as a variety of oligomeric forms, something that has been provided for recombinant human rhSP-D in this chapter. However, considering that trimers, hexamers, dodecamers and fuzzy balls have all been observed here and in previous structural studies with protein from different sources (Crouch et al., 1994b, Hartshorn et al., 1996a, van Eijk et al., 2002, Leth-Larsen et al., 2005, Hartshorn et al., 2008), it seems reasonable to propose that SP-D exists in a dynamic equilibrium between these different oligomeric forms, sensitive to the surrounding environment, with the hexamers playing a key role in the assembly process. It has been described that higher order multimers are more effective to promote influenza virus aggregation *in vitro* (Hartshorn et al., 1996a). Along the same line, structures larger than trimers, probably dodecamers and fuzzy balls, are required for binding to bacteria (Leth-Larsen et al., 2005) and for lung surfactant homeostasis (Zhang et al., 2001a). Further findings will be provided in the next chapter regarding activity of the different oligomeric forms, as well as a structural analysis of native human SP-D from two different sources (Chapter 3), to confirm that the structures observed in this chapter in rhSP-D are present in native protein and are not artifacts of the recombinant protein production process.

It is unknown whether the conformational changes observed here under acidic conditions may have any functional implication. It has been published that the pH in the lung fluid may become acidic under disease or inflammation (Ng et al., 2004), down to around 6.5. The effect of pH on SP-A function and structure has been studied (Ruano et al., 1998, Ruano et al., 1999), but not much is known about

its effect on SP-D. The closed conformation and higher proportion of dodecamers could be particularly important for the fate of the protein along secretory or endocytic pathways, where it may reach organelles with acidic pH (close to 5.5) (Demaurex, 2002). Dodecamers in closed conformation are somehow similar to fuzzy balls, described as the most active species against certain pathogens, suggesting that this conformational change could lead to a more active molecule with the CRD domains grouped in an orientation to simultaneously bind a higher number of ligands or receptor subunits clustered at the same surface.

In summary, in this chapter we have presented the characterization of the different oligomeric forms of a recombinant human SP-D and determined its quantitative distribution. We propose a model for SP-D assembly that includes hexamers as an essential intermediate in the pathway to dodecamer assembly. The importance of environmental conditions such as pH on SP-D oligomerization and its three-dimensional configuration has been also demonstrated. Moreover, it was shown that the presence of calcium, which is crucial for some activities of SP-D, does not influence protein oligomerization and conformation at the supramolecular level.

RESULTS

Chapter 2

Isolation and functional characterization of the different oligomeric forms of recombinant human rhSP-D

Part of the experiments included in this chapter were performed during a short-term stay in the laboratory of Dr. Paul Kingma at Cincinnati Children's Hospital Medical Center (Cincinnati, OH, USA) assisted and supervised by Paul Kingma, Ph.D., MD. AFM images were obtained in the laboratory of Dr. Fernando Moreno Herrero in "Centro Nacional de Biotecnología" (CNB-CSIC) (Madrid, Spain).

Introduction

Up to date, it has been described that surfactant protein SP-D is assembled in trimers, dodecamers and large oligomers (fuzzy balls) (Crouch et al., 1994b, Crouch, 2000). The results described in chapter 1 of this Thesis have added hexamers as an additional oligomeric form of the protein.

Previous studies have attempted to isolate SP-D oligomers. In one of them, the isolation was performed using hSP-D purified from amniotic fluid, but the resolution was limited to distinguish between low oligomeric forms, trimers and possibly hexamers, and high molecular weight oligomers: dodecamers and fuzzy balls (Leth-Larsen et al., 2005, Sorensen et al., 2009). In another study, Hartshorn and colleagues isolated recombinant human rhSP-D dodecamers and fuzzy balls, but no clear quantitative evidences were showed to demonstrate that this separation was actually achieved (Hartshorn et al., 1996a).

Influenza A virus (IAV) and some bacterial species, such as *Escherichia coli*, have been defined as SP-D ligands *in vivo* (Crouch, 1998, Crouch, 2000). SP-D recognizes carbohydrate structures at microbial surfaces and binds to them, which causes aggregation and opsonization of the infectious particles (Sano and Kuroki, 2005, Vieira et al., 2017). Therefore, both, bacteria and virus have been used for evaluating protein activity. The functional activity of isolated oligomeric forms of SP-D has been assessed mainly by binding assays to purified ligands, like LPS or carbohydrates, IAV and bacteria. Also, virus aggregation assays have been performed. In general terms, the main conclusion obtained seem to be that large oligomers have a higher affinity for binding to the bacteria strains tested and to IAV (Leth-Larsen et al., 2005), with the large fuzzy balls exhibiting higher potency to aggregate IAV compared to dodecamers (Hartshorn et al., 1996a).

The objective in this thesis chapter was to isolate the different oligomeric forms of recombinant human rhSP-D in order to evaluate and compare their functional activity. Also, we pursued to achieve a higher degree of fractionation than just separating low and high molecular weight oligomeric forms, obtaining if possible isolated trimers, hexamers, dodecamers and fuzzy balls in sufficient amount to carry out functional assays. An additional objective was to define whether the hexamers found in chapter 1 were functional structures or just an intermediate in protein oligomerization. The results of these experiments demonstrated that it is possible to obtain fractions highly enriched in trimers, hexamers and fuzzy balls. However, dodecamers were found dispersed within the fractions between fuzzy balls and hexamers, contaminated with those two species. Fuzzy balls were the most active oligomeric form with respect to bacterial binding and aggregation

assays. Also, hexamers triggered bacteria aggregation, although with less pontency than fuzzy balls.

Results

Production and purification of recombinant human SP-D

Recombinant human SP-D (rhSP-D), variant Met^{11} Thr^{160} Ser^{270}, was produced in mammalian CHO cells, as described in methods.

Purification of rhSP-D is usually performed by two consecutive chromatographic steps. First, an anion exchange column, which allows us to concentrate the sample and remove glucose from cell media. Second, a carbohydrate affinity column, which removes non-specific proteins and specifically binds SP-D, eluting pure SP-D at the end (Ikegami et al., 2006).

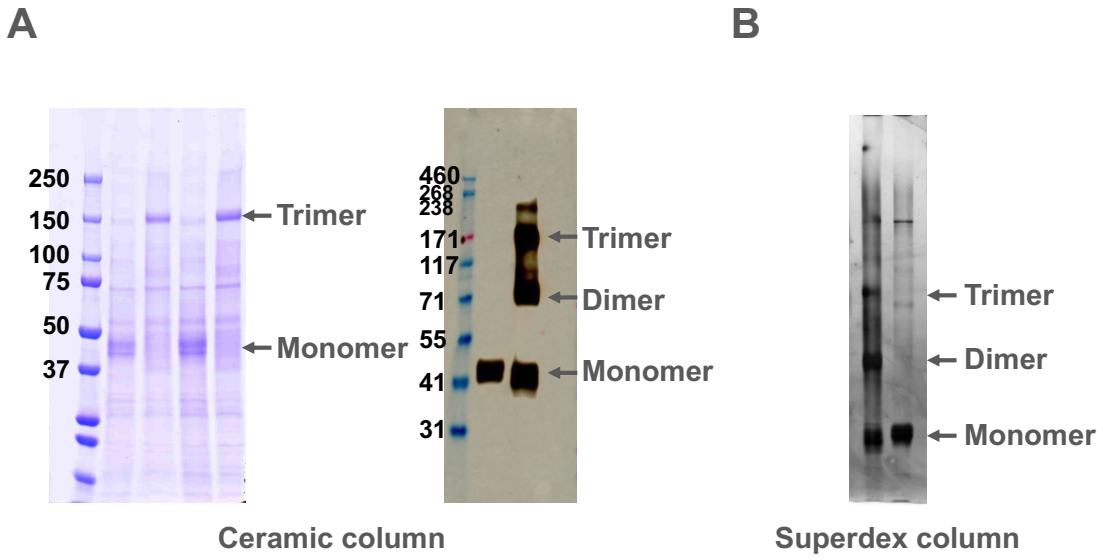

Figure 2.1: Electrophoretic analysis of rhSP-D purified produced by CHO cells. ***A***, protein purified through an anionic exchange chromatography, evaluated by PAGE-SDS developed with Coomassie blue (*left*) and by WB (*right*) with anti-SP-D in the presence or absence of reducing conditions. ***B***, protein purified by two consecutive chromatographic steps. First, an anionic exchange chromatography and second, an affinity chromatography in a Superdex matrix. The final purified protein was analyzed by PAGE-SDS developed with silver staining, in the presence or absence of reducing conditions.

A complete purification procedure was performed with a first batch of rhSP-D, meaning that the two columns were run and pure SP-D was obtained (Figure 2.1B). However, the protein yield obtained with this procedure was too low for the purpose of the study, a total amount of 600-700 µg diluted in 4-5 fractions. Hence, a modified approach was followed using only the first column (anionic exchange) and then, applying the partly purified protein in a gel filtration column (sizing column), with the goal to fractionate the different rhSP-D oligomeric forms and separate them from other proteins in a single step. The protein yield obtained from

the ion exchange ceramic column was high, recovering as much as several 1mL-fractions with a concentration of protein of around 3-5 mg/mL, although not all this protein was SP-D. The electrophoretic analysis of fractions eluted from this ceramic column revealed the presence of rhSP-D trimers, that were reduced to monomers in the presence of β-mercaptoethanol (Figure 2.1A). When these samples were observed under AFM, rhSP-D was found to be assembled into the different species described in chapter 1: trimers, hexamers, dodecamers and fuzzy balls (Figure 2.2). As expected, samples presented also a high amount of impurities, probably unspecific proteins, observed as small bright balls in AFM images (see round bright spots in Figure 2.2, left).

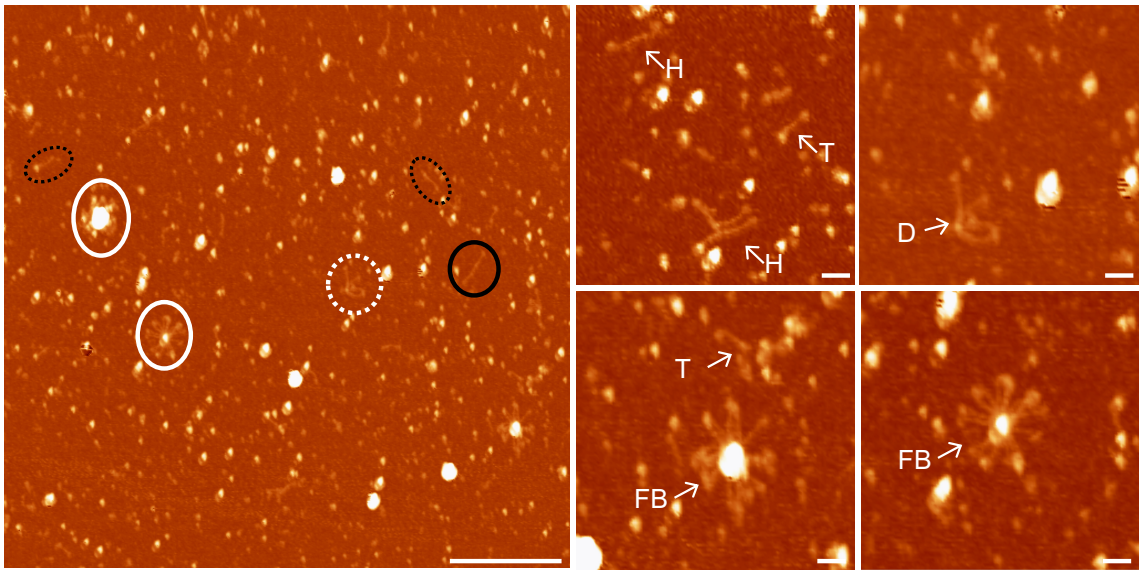

Figure 2.2: rhSP-D obtained after 1-step ion exchange chromatography. rhSP-D produced by CHO cells and purified through an anionic exchange chromatography (ceramic column) was imaged by AFM. *Left*, scan area of 2 μm, where white solid circles mark the presence of fuzzy balls, white dotted circles indicate dodecamers, black solid circles enclose hexamers and black dotted circles, trimers. The scale bar represents 200 nm. *Right*, magnifications of AFM images showing illustrative examples of different oligomeric forms: trimers (T), hexamers (H), dodecamers (D) and fuzzy balls (FB). The scale bar represents 50 nm.

On the whole, we were able to produce rhSP-D by CHO cells and purify it with a ceramic anion exchange column, obtaining high protein (SP-D) yields that contained some amounts of co-eluting unspecific proteins. Moreover, rhSP-D purified in this way presented all the oligomeric forms previously described.

Isolation of recombinant human rhSP-D oligomeric forms

Size exclusion chromatography (SEC) was carried out to separate trimers, hexamers, dodecamers and fuzzy balls. Sepharose CL-6B was poured and equilibrated into a long column (90 cm) to ensure an efficient separation between the different oligomers. Chromatography was performed as stated in methods,

applying onto the sizing column around 4 mg of protein obtained from the ceramic column. Eluted fractions were assessed by SP-D ELISA to quantitate the protein concentration and to obtain a column elution profile (Figure 2.3A). In spite of the fact that the column profiles did not show very defined peaks, the pattern observed was repetitive after comparing more protein samples resolved by SEC. The profiles always exhibited a main peak around 60 mL elution volume, with a characteristic shoulder at 65-67 mL and small peaks at subsequent elution volumes (Figure 2.3A).

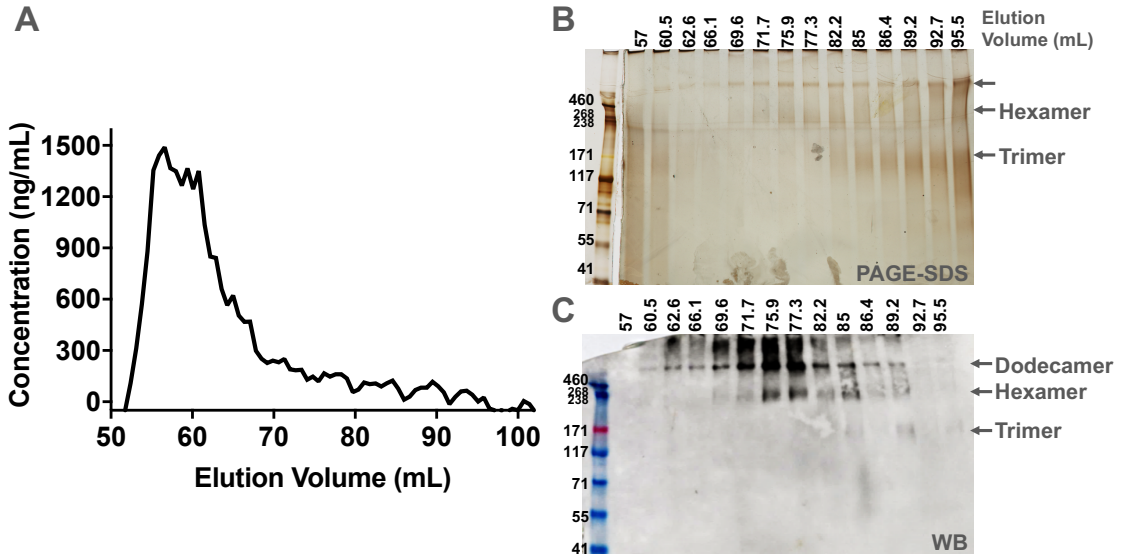

Figure 2.3: Size exclusion chromatography (SEC) of rhSP-D. ***A***, elution profile of rhSP-D in a Sepharose CL-6B column, obtained with SP-D ELISA. ***B-C***, electrophoresis analysis after cross-linking of selected fractions eluted from the column at increasing elution volumes (the elution volume of each fraction is indicated above the gels). ***B***, polyacrylamide gradient (4-15%) gel developed by silver staining. ***C***, western-blot developed with anti-SP-D (1A10A9). The position in the gels of the different protein oligomeric forms are indicated on the right.

A calibration of the sizing column was performed with standard globular proteins of different size, and the expected elution volumes for different rhSP-D oligomers were calculated according to their theoretical molecular mass. However, the flexible and fibrous structure of SP-D oligomers, far from the structure of globular proteins, likely implies very distinct hydrodynamic properties, making these standard references useless. Only the determination of the column void volume was useful to estimate the elution volume of the large fuzzy balls. Therefore, other methods were necessary to identify rhSP-D oligomer peaks.

Selected samples, corresponding to some of the vague, but repetitive, peaks along the profile were examined by electrophoresis and AFM. PAGE-SDS and WB of rhSP-D crosslinked with glutaraldehyde (GA) were performed using polyacrylamide gradient (4-15%) gels. According to these results (Figure 2.3B), dodecamers were spread over the eluted fractions (see silver stained gel and WB). The band with the mobility of hexamers became more evident at volume 75.9 and

77.3, and the band of trimers started at volume 85 (more obvious in the silver stained gel than in the WB, Figure 2.3B-C). The presence of fuzzy balls in gels was not expected, as they do not penetrate into gels due to its size and molecular mass. Silver staining and WB are very sensitive techniques that detect species even if they are at very low concentration. These techniques provide an estimation of where each of the oligomers elute in the chromatography, but they do not discern whether the fractions contained a majority of each form. Hence, protein samples were analyzed by AFM. Selected images of fractions that correspond to the indicated elution volumes are shown in Figure 2.4. It was found that fraction eluted at 60.5 mL (V60.5) contained only fuzzy balls, sample eluting at V77.3 mL enclosed mainly hexamers, and that at V89.2 mL, trimers. It is remarkable that those eluted fractions were significantly enriched in one type of oligomer.

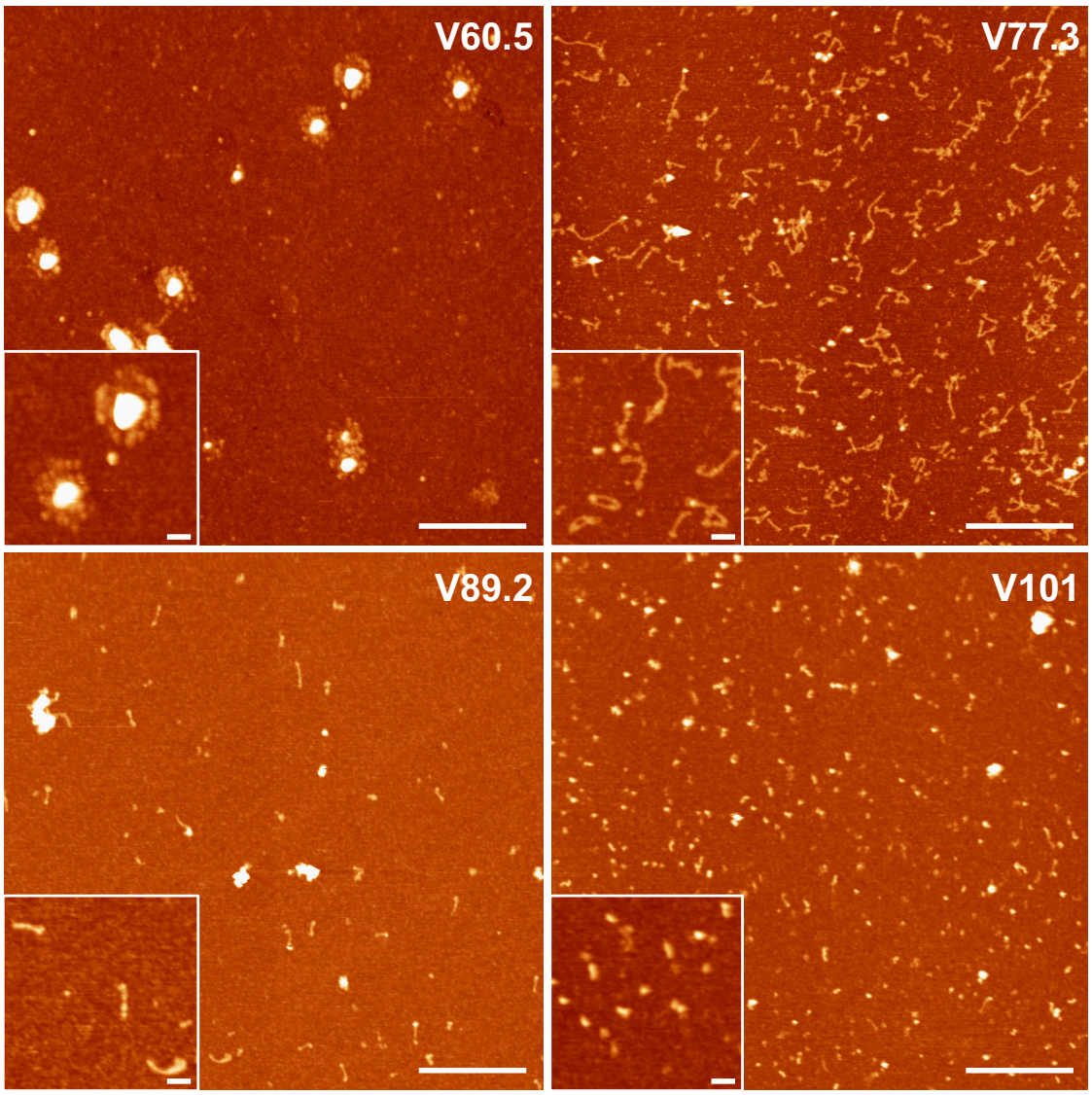

Figure 2.4: AFM images of samples from selected eluted fractions from SEC. Representative AFM images of rhSP-D corresponding to elution volumes V60.5 (fuzzy balls), V77.3 (hexamers), V 89.2 (trimers) and V101 (unspecific proteins). The scale bar represents 200 nm in the largest images and 50 nm in the insets.

Quantification of the distribution of oligomeric forms, as percentage of protein mass, was performed with images taken from samples of these selected elution volumes. Fuzzy balls constituted 95% of the protein in V60.5, hexamers accounted for 74% in V77.3 and trimers constituted 80% in V89.2 (see Figure 2.6A). Unfortunately, isolated dodecamers were not found. Eluted fractions from 60.5 mL to 75 mL of the chromatographic profile were carefully examined, especially those around volume 66 mL, matching with the shoulder observed in the elution profile at the right-side of the main peak (Figure 2.3A). Some of these fractions exhibited a mixture of dodecamers and hexamers, but none of them had a significant amount of dodecamers to be considered pure. AFM images of samples at V66 are shown in Figure 2.5. The quantification of the distribution of oligomeric forms in that fraction revealed a distribution of 20% trimers, 28% hexamers, 38% dodecamers and 14% fuzzy balls. Dodecamers were the most abundant oligomer, but they constituted only around 40% of the total protein mass.

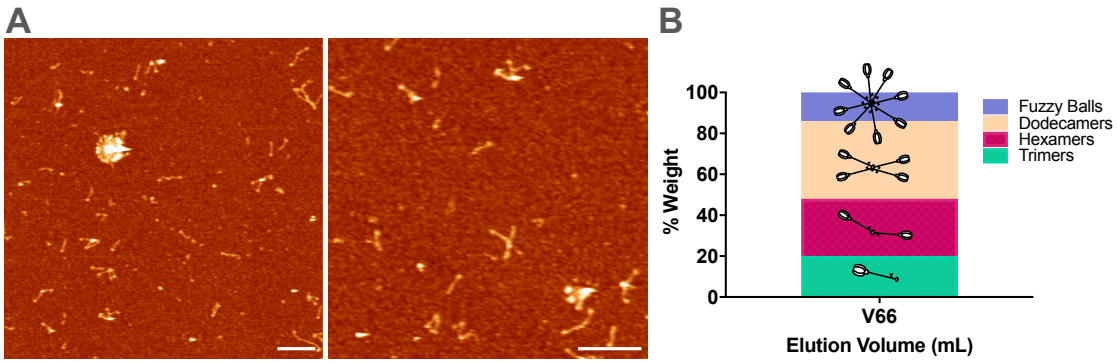

Figure 2.5: AFM images and quantification of the distribution of the oligomeric forms in fraction V66. ***A,*** representative AFM images of rhSP-D corresponding to elution volume V66. The scale bar represents 200 nm. ***B***, quantitative analysis of the distribution of oligomeric forms in fraction V66 by percentage of protein mass (% weight).

The presence of dodecamer bands in the electrophoretic analysis at the latest elution volumes, when they were not observed in those fractions under AFM, was contradictory. Therefore, the electrophoretic analysis was only used as a guide to estimate where the different oligomeric forms were and, which fractions should be examined under AFM. From our experience, AFM results are more relevant than electrophoresis; besides, AFM images allowed us to classify and count the different molecules in order to obtain the percentage of distribution. We could not discard that the cross-linking agent – glutaraldehyde - could promote some oligomerization. Regarding trimer bands in the WB, they can be observed but are not really well defined when compared to those revealed by silver staining. An explanation was found later, as the antibody used for this WB, anti-SP-D 1A10A9 (see table 2 in methods section), sometimes does not recognize the trimer

efficiently, but it does it with the dodecamer (Airway Therapeutics LLC., personal communication).

The concentration of recombinant rhSP-D in fractions enriched in trimers, hexamers and fuzzy balls was quantified with a commercial ELISA kit that was more sensitive and precise in order to do further experiments. Routinely, SP-D concentration is quantified by BCA. In our case, we wanted to specifically quantify SP-D, avoiding the possible interference of the small amounts of contaminants still observed in the AFM images at the later fractions. Besides, the elution of the sizing column provides low protein concentrations. For this reason, we used in this chapter the ELISA kit as quantification method instead of the BCA assay.

The second goal pursued with the sizing column, to increase protein purity removing those unspecific proteins observed as bright spots in figure 2.3B, was achieved successfully. The band pattern observed in figure 2.2A (gel, two first lanes), with bands at lower molecular weights than rhSP-D monomer, was not seen in the fractions eluted from the sizing column (Figure 2.3B). Selected fractions eluted around volume 100 mL were analyzed by AFM (Figure 2.4, V101) and contained the bright spots with a ball-shape that were identified as contaminants in Figure 2.2, before running the sizing column.

In summary, rhSP-D trimers, hexamers and fuzzy balls were efficiently isolated with enough purity grade (Figure 2.6). Fractions enriched in dodecamers were not found, although they were observed spread along the elution fractions between volumes ~ 63-74 mL by cross-linking and electrophoresis.

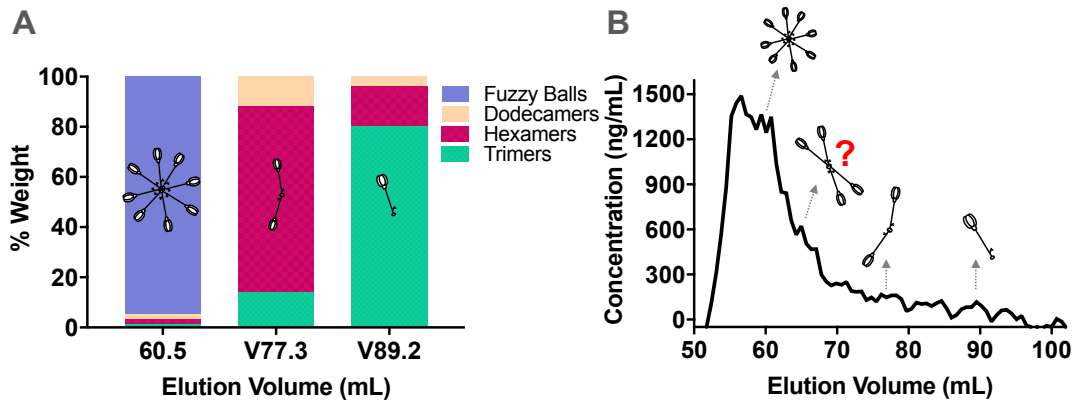

Figure 2.6: Identification of the eluted fractions that were significantly enriched in the different oligomeric forms of rhSP-D. ***A***, quantitative analysis of the distribution of oligomeric forms in the indicated fractions by percentage of protein mass (% weight). ***B***, position of the fractions containing isolated fuzzy balls, hexamers and trimers in the elution profile of a Sepharose CL-6B column (sizing column).

Redistribution of SP-D Oligomeric forms

rhSP-D exhibits a mixture of different oligomeric forms, as studied in chapter 1 and found also in the experiments of this chapter. Since hexamers, dodecamers and

fuzzy balls are assembled through non-covalent interactions, it might be possible that when oligomers are isolated and stored, they could progressively redistribute to end in a close to "native" distribution of oligomeric forms. The potential redistribution of isolated fuzzy balls was assessed after 3 hours, 24 h and 5 days of storage at 4 ºC. The quantity of hexamers and trimers isolated was low compared to fuzzy balls, so they were rather preserved for functional studies.

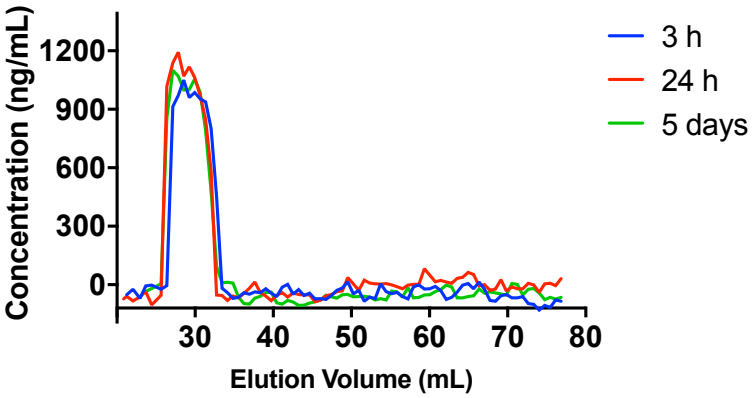

Figure 2.7: Size exclusion chromatography of a preparation of purified rhSP-D fuzzy balls after different incubation times at 4 ºC. Column elution profiles were obtained by SP-D ELISA of fractions resulting from the size exclusion chromatography in Sepharose CL-6B of rhSP-D fuzzy balls, after different incubation times: 3 hours (blue), 24 h (red) and 5 days (green) at 4 ºC.

To assess potential oligomeric forms redistribution, the same resin (Sepharose CL-6B) was poured into a shorter column (~ 40 cm) and ~ 150 µg of rhSP-D isolated fuzzy balls were applied onto the column. Column elution profiles were built with SP-D ELISA, as described before. Experiments at the different times were repeated twice and the average of two replicates was represented to show the elution profiles. The profiles of the protein after all incubation times (3h, 24h and 5 days) showed a main peak at the void volume (~ 29-30 mL), which corresponded to the elution of fuzzy balls (Figure 2.7), without displaying any significant shift in the elution profile. Therefore, we concluded that there was no significant redistribution. It could be still possible that longer incubation times at 4 ºC or shorter times at room temperature might induce some redistribution.

Binding of the different oligomeric forms to *Escherichia coli*

To address whether different isolated recombinant human rhSP-D oligomers (trimers, hexamers and fuzzy balls) could exhibit different affinity of binding to bacteria, one of the protein ligands *in vivo*, binding assays to *Escherichia coli* strain DH5α were performed in an ELISA-like assay.

Different concentrations of rhSP-D oligomers were incubated into microtiter plate wells coated with bacteria. Protein binding was measured by SP-D ELISA. It was found that fuzzy balls had higher binding affinity to bacteria, compared to

hexamers and trimers (Figure 2.8A). There were no apparent differences between hexamers and trimers. However, when absorbance values were relativized considering as 100% the maximum absorbance obtained at 2000 ng/mL of rhSP-D fuzzy balls, significant differences were found between hexamers and trimers at the highest SP-D concentration tested (Figure 2.8B). The experiments were performed with two anti-SP-D antibodies that differed in their protein epitope. In one case the epitope was located in the CRD of SP-D, while in the second case, it was at the N-terminal domain. SP-D binds to bacteria through the CRDs. If the epitope of the antibody is located in the CRD of the protein, it could be blocked when SP-D is bound to bacteria, leading to a potential underestimation of the protein bound. The differences observed between the oligomeric forms of rhSP-D with respect to their ability to bind to *E. coli* were repetitive with both antibodies, although the one that binds to the CRD showed better reactivity. Therefore, there were no issues with the protein recognition by these two antibodies. Results showed here were obtained with the antibody that recognizes the epitope at the CRD of the protein.

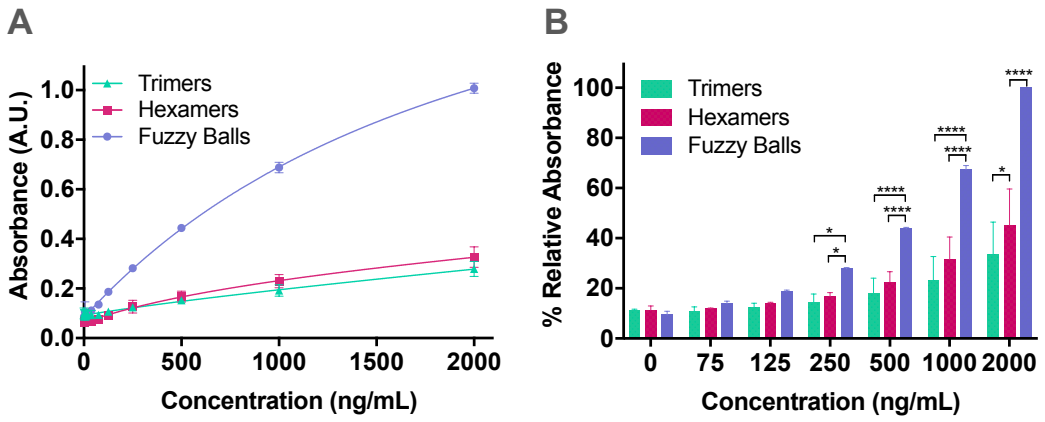

Figure 2.8: Binding of trimers, hexamers and fuzzy balls of rhSP-D to *E. coli*. Plates were coated with bacteria and incubated with 2-fold dilutions starting at 2000 ng/mL of each rhSP-D isolated oligomeric form. Bound SP-D was detected with antibodies in an ELISA-like assay. ***A***, representation of the absorbance of bound SP-D at the different SP-D concentrations tested (n = 2), Two-way ANOVA with Tukey's post-test was performed, differences between fuzzy balls and hexamers and trimers were significant from 125 ng/mL of SP-D ****$p<0.0001$. The difference between hexamers and trimers at 2000 ng/mL was significant **, p=0.0096. ***B***, relative absorbance considering 100% the value obtained for fuzzy balls at an SP-D concentration of 2000 ng/mL. Two-way ANOVA with Tukey's post-test was performed *, $p<0.05$; ****, $p<0.0001$.

Bacterial aggregation induced by the different oligomeric forms of recombinant human rhSP-D

In lungs, one of the functions accomplished by SP-D is the agglutination of invading pathogens, such as bacteria, which facilitates their clearance via mucociliary escalator. Therefore, bacterial aggregation assays of *E. coli* were carried out to evaluate *in vitro* the activity of isolated rhSP-D oligomers.

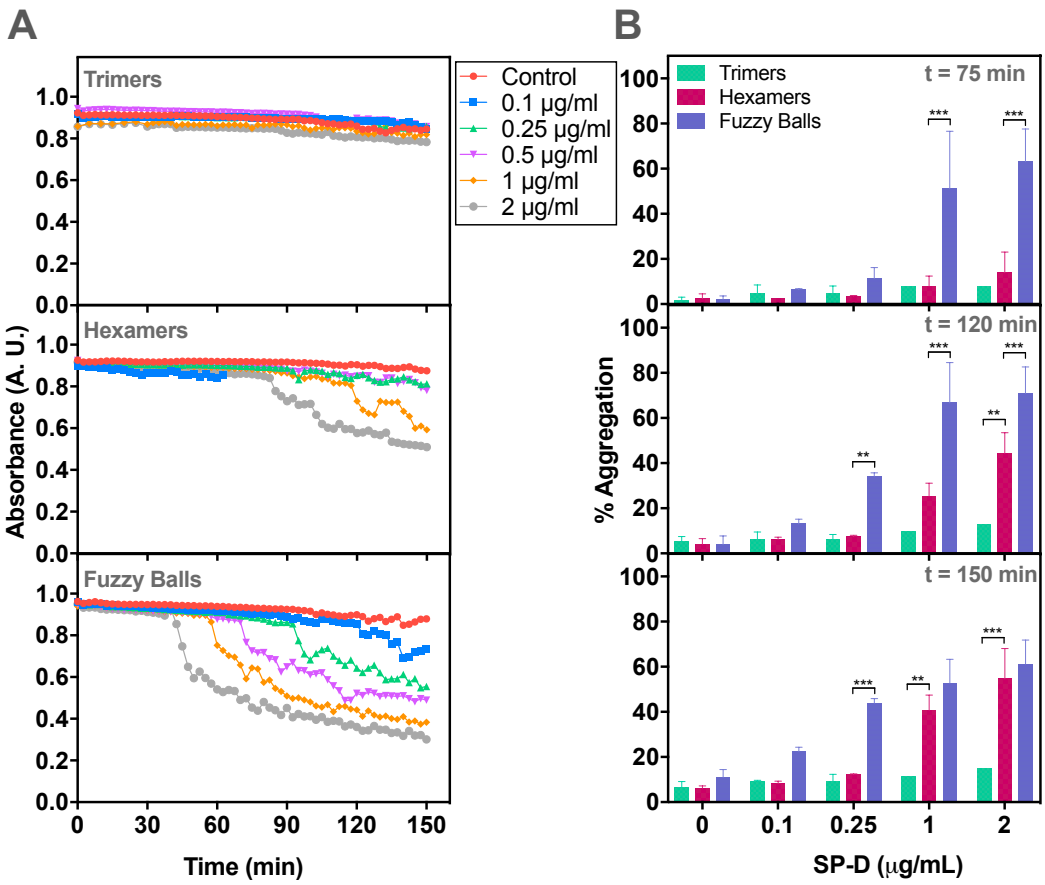

Figure 2.9: Bacterial aggregation by the different oligomeric forms of rhSP-D. Bacterial suspensions of *E. coli DH5α* were incubated with or without (control) different concentrations of rhSP-D isolated oligomeric forms. ***A***, absorbance values (λ = 700 nm) were monitored during 150 minutes upon addition of trimers (*top*), hexamers (middle panel) or fuzzy balls (*bottom*). ***B***, percentage of aggregated bacteria determined at three time points (t = 75, t = 120 min and, t = 150 min), as stated in methods, after addition of four different concentration of SP-D trimers (*top*), hexamers (*middle*) or fuzzy balls (*bottom*). Two-Way ANOVA with Tukey's post-test: **, p≤0.01; ***, p≤0.001.

The ability of rhSP-D trimers, hexamers and fuzzy balls to aggregate bacteria was tested at different protein concentrations (0.1 µg/mL – 2 µg/mL), by monitoring light transmission through a suspension of *E. coli* after the addition of protein over 150 minutes. Trimers did not display bacterial aggregation even at the highest concentration tested, 2 µg/mL (Figure 2.9A, top graph). Hexamers started to show activity at protein concentration of 1 µg/mL (Figure 2.9A, middle graph), while fuzzy balls were the most active oligomeric form, starting to trigger bacterial aggregation in less than 60 min at 2 µg/mL (Figure 2.9A, bottom graph). Even at low protein concentrations, such as 0.1 and 0.25 µg/mL, aggregation started after 2 hours (see blue and green lines, bottom graph in Figure 2.9A). The percentage of aggregated bacteria was calculated for the different species at three time points (Figure 2.9B): 75 min, 120 min, and at the final time point (150 min). At early times, 75 minutes, only fuzzy balls showed significant aggregation of bacteria compared to trimers and hexamers (Figure 2.9B, top). After two hours (120 min), significant

differences were also observed at low concentrations (0.25 µg/mL) between fuzzy balls and hexamers (Figure 2.9B, middle graph). Interestingly, at 2 µg/mL of protein concentration, the percentage of aggregated bacteria was significantly higher in hexamers compared to trimers, phenomenon that was also observed at 1 µg/mL of SP-D at the final time point (150 min) (Figure 2.9B, bottom graph). On the contrary, at final time point (150 min), the differences in activity between hexamers and fuzzy balls, at higher protein concentrations (1-2 µg/mL), became less significant than at earlier time points.

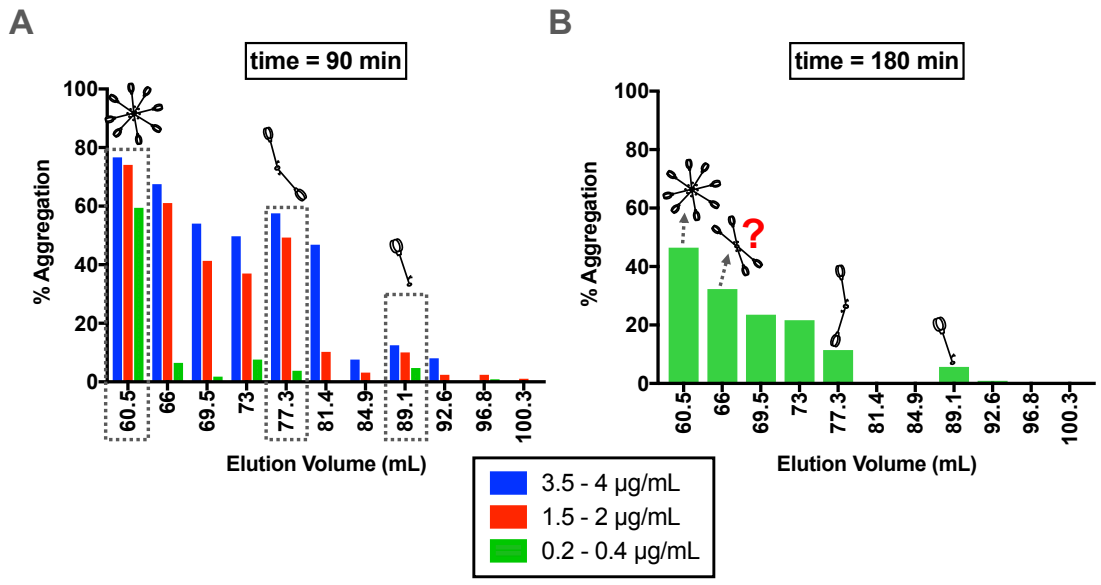

Figure 2.10: Percentage (%) of aggregated bacteria by selected fractions eluted from the SEC column. The % of aggregated bacteria was calculated at two different time points (A, left: t = 90 min; B, right: t = 180 min) at different protein concentrations (indicated by colors). The peaks assigned to fuzzy balls, hexamers and trimers are indicated by dashed boxes and schematic drawings.

Figure 2.10A shows how the % of aggregated bacteria varies as promoted by the different column fractions, including those with isolated fuzzy balls (V60.5), hexamers (V77.3) and trimers (V89.2), at three protein concentration ranges, 90 minutes after protein incorporation. It is remarkable that only fuzzy balls are active at the lowest concentration tested (green bars) at this time point. Moreover, at the other two concentration ranges (blue and red bars), the percentage of aggregated bacteria was maximum in the fraction that corresponded to fuzzy balls and also peaked in the fraction that matched with hexamers. Interestingly, fraction V66 (Figure 2.5), which corresponds to the shoulder observed in the column elution profile (Figure 2.6) and it was the region where we expected to find dodecamers, showed lower activity than fuzzy balls, but higher than hexamers. This was also observed at the final time point (Figure 2.9B, time 180), where a progressive

decrease in protein activity was observed from fuzzy balls to trimers. Despite these findings, our AFM and electrophoresis results did not allow us to confirm accumulation of isolated dodecamers in that fraction (V66), as observed in the quantification of the distribution of oligomeric forms illustrated in Figure 2.5B.

In summary, we have shown that fuzzy balls are the most potent oligomeric forms of rhSP-D with respect to their ability to trigger *E. coli* aggregation; hexamers were also active and the activity of trimers was negligible.

Discussion

The activity of the different oligomeric forms of SP-D has been a matter of discussion since it was found that the protein is assembled in different structures. Herein we have been able to separate trimers, hexamers and fuzzy balls of a recombinant human rhSP-D. It has been found that fuzzy balls are the most potent oligomer in the functional assays performed, binding and aggregation of *E. coli*. Trimers have shown a lower affinity of binding to bacteria and were not able to aggregate them. It is remarkable that the hexamers described in chapter 1 could be isolated and have shown to be functional oligomers, displaying an intermediate grade of activity between trimers and fuzzy balls, facts that demonstrate that they are SP-D entities and not artifacts of the production or purification processes.

The degree of separation obtained in previous studies allowed authors to differentiate between high and low molecular weight oligomeric forms using a Superose 6 column (molecular weight (MW) separation range for globular proteins and dextrans in the 5 – 5000 kDa range) (Leth-Larsen et al., 2005), and between fuzzy balls and dodecamers with a column with a matrix constituted by 4% crosslinked agarose (Hartshorn et al., 1996a). They compared binding and IAV aggregation, finding that fuzzy balls were the most active oligomeric form in all the experiments performed.

In our study, using a Sepharose CL-6B column, where the resin matrix is formed by 6% of crosslinked agarose with a MW separation range for globular proteins and dextrans of 10 – 4000 kDa, we have achieved a higher degree of separation. We have been able to obtain most of the different oligomeric forms of SP-D: trimers, hexamers and fuzzy balls. Different fractions were highly enriched in each of the oligomeric forms, as shown by the quantitative study (Figure 2.6A). Despite numerous attempts, it was not possible to isolate pure dodecamers. Several facts could contribute to this failure. First, the rhSP-D produced probably had a higher proportion of fuzzy balls than the one observed in chapter 1. This idea was also discussed for a rhSP-D produced by other authors (Hartshorn et al., 1996a), where they obtained similar amounts of both dodecamers and fuzzy balls, and, we have

also observed it in hSP-D purified from amniotic fluid (seen in Chapter 3). Although we did not observe a dramatically increased proportion of fuzzy balls when we imaged the starting material in the AFM (rhSP-D obtained from ceramic column, Figure 2.2B), more fuzzy balls were observed compared to the recombinant version studied in chapter 1. Second, dodecamers were spread over all the eluted fractions from the fuzzy balls peak to the hexamers peak. The flexible structure of dodecamers likely allow them to display different conformations, as we observed in chapter 1, implying variations in their hydrodynamic properties. If we imagine the sphere that would contain the dodecamer, the diameter of this sphere changes along different dodecamer conformations: opened, closed and intermediate states. It might be possible that opened structures (with a larger diameter) would not penetrate resin pores, eluting earlier than partly bended structures or completely closed conformations. In addition, the column flow rate could influence protein conformation. Their flexibility could likely promote that some dodecamers randomly penetrate the pores and as a result, they could change to close conformations to be able to go through the column pores as pushed by the liquid flowing into the column; others could migrate faster without entering into the pores in their opened conformation. Third, we observed some fractions in which dodecamers appeared mixed with hexamers. The similarities in conformation between hexamers and dodecamers, with similar molecule diameter, might be translated into an analogous behavior due to also similar hydrodynamic volumes. In this line we only obtained pure hexamers at later fractions. In principle, one could expect finding isolated dodecamers at the earlier fractions after the fuzzy balls peak, but it did not happen. Therefore, the isolation of dodecamers remains as a challenge. They are present in our rhSP-D because they can be found in the starting material.

The total concentration of protein isolated in the form of trimers was low, in agreement with the quantitative data from chapter 1, but it was still enough to perform some functional assays. Up to now, the evaluation of the activity of trimers had been carried out with truncated versions of the protein that prevented oligomerization to larger structures, such as substitution of cysteines 15 and 20 by serines, that served to show that trimers were not sufficient to cause viral aggregation, or, with mutated versions composed only by trimeric CRDs and neck domains (Brown-Augsburger et al., 1996a, Brown-Augsburger et al., 1996b, Zhang et al., 2001a, Tecle et al., 2008). Also, binding properties of trimeric forms of hSP-D have been analyzed, but in those studies isolated trimers were constituted mainly by the Thr^{11} variant (Leth-Larsen et al., 2005, Sorensen et al., 2009), whereas our rhSP-D trimers contain Met^{11} in their sequence. In both cases, our rhSP-D trimers

and the low molecular weight forms in the study by Leth-Larsen et al. (2005) showed lower binding to bacteria than higher order oligomers.

SP-D has shown therapeutic effects in animal models, i.e. preventing endotoxin shock in newborn preterm lambs (Ikegami et al., 2006). From a physiological point of view, it is important to know whether all the oligomeric forms found in SP-D are functional, and which one is the most active, particularly, if one considers recombinant human rhSP-D as a possible therapeutic option. We have studied the activity of rhSP-D trimers, hexamers and fuzzy balls in terms of binding to one of its physiological ligands, *E. coli*, and their potential to aggregate it, as one of the *in vivo* functions of SP-D. Fuzzy balls showed higher binding affinity to *E. coli* than hexamers and trimers. Increased concentrations of the two last ones did not increase the rate of protein bound to bacteria, and only hexamers, at the highest concentration tested (2000 ng/mL), exhibited greater binding than trimers (Figure 2.8B). These results agreed with previous findings comparing high and low molecular weight forms of hSP-D (Leth-Larsen et al., 2005). On the contrary, affinity of binding of low molecular weight forms of SP-D to isolated LPS was found to be higher than in the case of high molecular weight forms (Leth-Larsen et al., 2005, Sorensen et al., 2009). The bacterial strain tested in our experiments is gram negative, with LPS exposed in their external wall available to be recognized by SP-D. In our hands, trimers of SP-D did not significantly bind to *E. coli*, suggesting that they bind poorly to the LPS on the outer membrane. A possible explanation to this fact would be that when LPS is anchored on a bacterial wall, trimers are not able to interact with LPS due to its distribution and steric disposition. This idea was also discussed by Hakansson and Reid (2000). A lower affinity of SP-D for binding to LPS "in situ" might require a synergistic cooperation of more than one trimeric CRD domain to sustain binding, explaining why trimers with one single trimeric CRD do not practically bind. Hexamers, with two trimeric CRD domains might constitute the minimal unit with the capacity to exhibit binding cooperativity. Fuzzy balls, with their higher number of trimers and CRD domains would exhibit maximal cooperativity, maximal affinity and maximal probability of interacting with the LPS even when it is arranged in a specific conformation on bacterial wall.

In the case of bacterial aggregation, it is even more evident that rhSP-D needs to be assembled in structures larger than trimers to trigger aggregation (Figure 2.9), and that fuzzy balls are the most active oligomeric form to do this. Similar results had been previously obtained for viral aggregation (Hartshorn et al., 1996a). As mentioned before, SP-D binds bacteria and viruses through its trimeric CRDs. It is logical that in order to aggregate pathogens, SP-D molecules need to be constituted by at least two trimers in order to be able to group together two bacteria, where

one trimer contained in the protein molecule would bind to one bacterium and another trimer to another bacterium. Again, fuzzy balls, with their multiple trimeric CRDs, would be the perfectly suited to promote the highest aggregation extent when compared to other protein oligomeric forms.

In this chapter, we have also analyzed the potential redistribution of SP-D oligomeric forms *in vitro*. Hartshorn and colleagues did not find any processing or storage condition that influence multimerization or dissociation (Hartshorn et al., 1996a). On the contrary, it has been reported that storage of SP-D multimers at 4 ºC during one week induces dissociation into trimers, which is more dramatic and happens earlier at room temperature, although it was prevented when SP-D was stored at -20 ºC (Sorensen et al., 2009). The same study also showed that protein dilution favors an increase in the proportion of trimers. We did not find dissociation of fuzzy balls after 5 days of storage at 4 ºC (Figure 2.7), neither upon the dilution required for AFM imaging (Figure 2.4), so our data agreed better with the first report. In addition, it has been found that binding to N-acetyl-D-mannosamine agarose when this was employed as resin to purify SP-D by affinity chromatography, promoted oligomerization of trimers into protein multimers (Sorensen et al., 2009). Thus, this finding opens the question whether ligand binding *in vivo* could promote oligomerization of the protein, which could be linked to a progressive displacement to the most active forms and a stimulation of function.

In summary, in this chapter we have achieved the separation of recombinant human rhSP-D oligomeric forms. Isolation of trimers, hexamers and fuzzy balls was particularly efficient. Fuzzy balls presented a higher affinity of binding and a higher potency to aggregate bacteria, which postulate them as the most active oligomeric form with respect to those protein functions that depend on the lectin activity. How much this is also the case for other biological functions of SP-D, such as its role in surfactant homeostasis or the regulation of the immune responses by SP-D has to be investigated. It could be that the versatility in SP-D oligomeric forms could be related to the versatility of SP-D in protein functions.

RESULTS

Chapter 3

Structural and functional characterization of human pulmonary surfactant protein SP-D from amniotic fluid and proteinosis BAL

The AFM experiments included in the present chapter were done at the laboratory of Dr. Fernando Moreno Herrero in "Centro Nacional de Biotecnología" (CNB-CSIC; Madrid, Spain). Glyco-profiling of hSP-D was performed by Glycotope GmbH (Berlin, DE). Amniotic fluid was obtained from the Gynecology and Obstetrics Service of "Hospital 12 de Octubre" (Madrid, Spain) in a collaboration with Drs. Emma Batllori Badia and Alberto Galiento Izquierdo.

Introduction

In chapter 1, rhSP-D isolated from culture medium of CHO cells has been used for characterizing the structure of this protein and determining the quantitative distribution of rhSP-D oligomeric forms. Besides, in chapter 2, a functional study to compare the activity of isolated different rhSP-D oligomeric forms has been performed. However, up to now, the quantitative distribution of SP-D oligomeric forms of the human protein obtained from natural sources (hSP-D) is unknown. It also remains to be stablished whether structures, such as hexamers, are secreted and are present or not as intermediates assemblies *in vivo*. These findings would be relevant to validate CHO cells as an appropriate system to produce rhSP-D similar in structure and activity to the native protein.

Human SP-D (hSP-D) has been routinely obtained from bronchoalveolar lavages of patients that suffer from pulmonary alveolar proteinosis (PAP), a disease characterized by altered surfactant production and metabolism. The most common type of PAP courses with an alteration of the granulocyte macrophage-colony stimulating factor (GM-CSF). This protein is important for lung surfactant recycling and catabolism by alveolar macrophages. Hence, its alteration causes accumulation of surfactant proteins and lipids that also show protein aggregates and altered phospholipid composition, including increased concentrations of cholesterol (Suzuki and Trapnell, 2016) (Ballester, et al., 2018). It has been described in the literature that SP-D produced by PAP patients is found in higher amounts, and is composed largely of higher order oligomeric forms, as a consequence of the disease (Crouch et al., 1993a). Thus, it is an open question how much this protein, which comes from a pathological condition, reflects the actual structure and functional behavior of the native protein in healthy human mucosae. Alternatively, previous works have obtained non-pathological hSP-D from amniotic fluid (AF) from cesareans at term pregnancy (Strong et al., 1998, Nadesalingam et al., 2003, Leth-Larsen et al., 2005). Human SP-D has been detected in amniotic fluid as early as 26 weeks' gestation, and its concentration levels progressively increase until labor (Miyamura et al., 1994, Stahlman et al., 2002). Therefore, hSP-D from AF could be a good control for structural studies. Three polymorphisms have been reported in hSP-D, with differences in the amino acid sequence at residues 11 ($Met^{11}Thr$), 160 ($Ala^{160}Thr$) and 270 ($Ser^{270}Thr$). It is known that the amino acid present in position 11 is relevant for protein oligomerization: when it is a methionine, hSP-D is found in both low and high molecular weight forms. However, when a threonine is occupying this position, the protein lacks high molecular weight oligomers (Leth-Larsen et al., 2005). Moreover, it is also known that the amino acid Asn^{70} of human SP-D is glycosylated in its amide, as it is in

rhSP-D, with biantennary structures and fucose attached to the glycan core (Leth-Larsen et al., 1999, Ito et al., 2015).

In chapter 2, fuzzy balls showed an increased activity in the functional assays performed, when compared to hexamers and trimers. In this line, the activity of hSP-D from PAP and AF has been previously characterized, especially in terms of binding and agglutination of influenza A virus (IAV), but never in a comparative way (Hartshorn et al., 1996a, Leth-Larsen et al., 2005). A different behavior could be expected in terms of activity, particularly, considering the expected differences in the distribution of the oligomeric forms between these two proteins, in line with the results obtained in chapter 2.

In the present chapter, we have characterized the structure of hSP-D obtained from PAP and AF and quantified the distribution of oligomeric forms of AF-hSP-D to compared them with the recombinant protein produced by CHO cultures. Moreover, the characterization of the glycan attached to the asparagine in position 70 has been addressed, with highly sensitive technologies available nowadays. Last, the activity of hSP-D from AF and PAP to bind and aggregate bacteria, as well as their carbohydrate binding preference have been assessed and compared. We found that hSP-D from AF is also formed by trimers, hexamers, dodecamers and fuzzy balls, being the proportion of fuzzy balls slightly higher than that of dodecamers. The combination of dodecamers and fuzzy balls represented ~70% of the total protein mass obtained from AF. It was found that the N-glycan structure was biantennary, core-fucosylated with partial galactosylation and sialylation, as well as bisecting GlcNAc. To our knowledge sialylation of SP-D has not been reported before. hSP-D from AF and PAP were both active in the functional assays performed, being PAP-hSP-D more effective, probably as a consequence of its abnormal increased proportion of large oligomers.

Results

Isolation of human SP-D from amniotic fluid by affinity chromatography

Human SP-D was obtained from two different sources to carry out the studies in the present chapter. First, hSP-D purified from bronchoalveolar lavage of patients suffering from pulmonary alveolar proteinosis (PAP) was provided by Dr. Paul Kingma (Cincinnati Children's Hospital; Cincinnati, Ohio). As this protein comes from a pathological situation in the lungs, hSP-D was also purified from amniotic fluid (AF) obtained in cesareans at term pregnancy.

Superdex-75® resine was applied to purify hSP-D from AF. In the presence of calcium, SP-D binds through its CRD domains to the dextrans covalently bound to a matrix composed of crosslinked agarose. Superdex has better flow rates than

maltose-agarose, and covalently bound dextrans allow high efficiency of protein binding when compared to plain crosslinked agaroses. SP-D purification was carried out as described in the methods section. Fractions eluted from the column were examined by electrophoresis under reducing conditions and developed by silver staining to find those that contained the protein (Figure 3.1A).

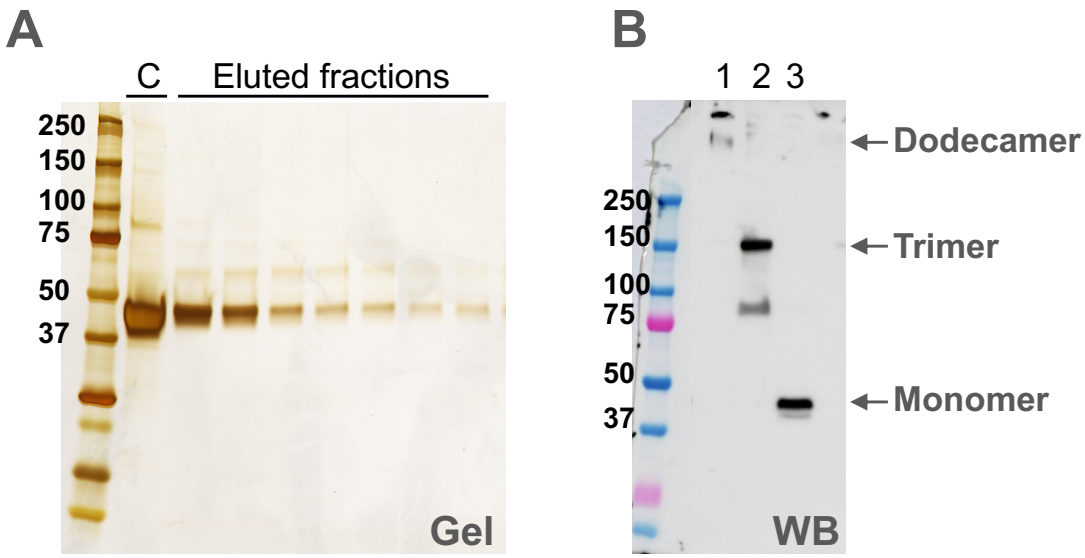

Figure 3.1: Purification of human SP-D from amniotic fluid (AF). ***A***, PAGE-SDS of fractions eluted from Superdex®-75 column under reducing conditions, including a control (C) of rhSP-D; the gel was developed by silver staining. ***B***, western blot of one column fraction (lanes 1-3) developed with anti-SP-D (1A10A9). In lane 1 hSP-D was crosslinked with GA, lane 2 non-reducing conditions, lane 3 reducing conditions.

hSP-D monomer from AF showed an electrophoretic mobility corresponding to an approximate molecular weight of ~ 43,000 Da (Figure 3.1A, B), as previously reported by other authors (Miyamura et al., 1994, Strong et al., 1998, Leth-Larsen et al., 2005). Western blot of a selected fraction from the affinity column was carried out to confirm that the protein was in fact SP-D, and to observe its different oligomeric forms. SP-D was found as a monomer under reducing conditions (Figure 3.1B, lane 3) and mainly as trimer (MW of 150 kDa) under non-reducing conditions (Figure 3.1B, lane 2). When the protein was crosslinked with GA, the dodecamer band was observed (Figure 3.1B, lane 1), but due to the size of the pores in the acrylamide gels, it was not possible to detect the presence of larger oligomers. The endotoxin content was determined with LAL assay, being its concentration < 1 EU/mL.

Two purifications were performed in this study starting from different volumes of pooled AF from cesareans. SP-D harvested from each of them is compiled in table 3.1. Although high amounts of amniotic fluid are needed to obtain a

reasonable protein yield, SP-D was efficiently purified from amniotic fluid with Superdex resin.

Table 3.1: Efficiency of hSP-D purification

Purification	Volume AF (mL)	Donors	hSP-D purified (µg)
1	450	2	90
2	2000	7	400

Structural characterization and quantification of the different oligomeric forms in hSP-D

To confirm that the oligomeric forms observed in rhSP-D produced by CHO cells, characterized in chapters 1 and 2, are present in the human protein and that the distribution of those oligomers is similar, a structural analysis was performed with the human protein obtained from AF and PAP.

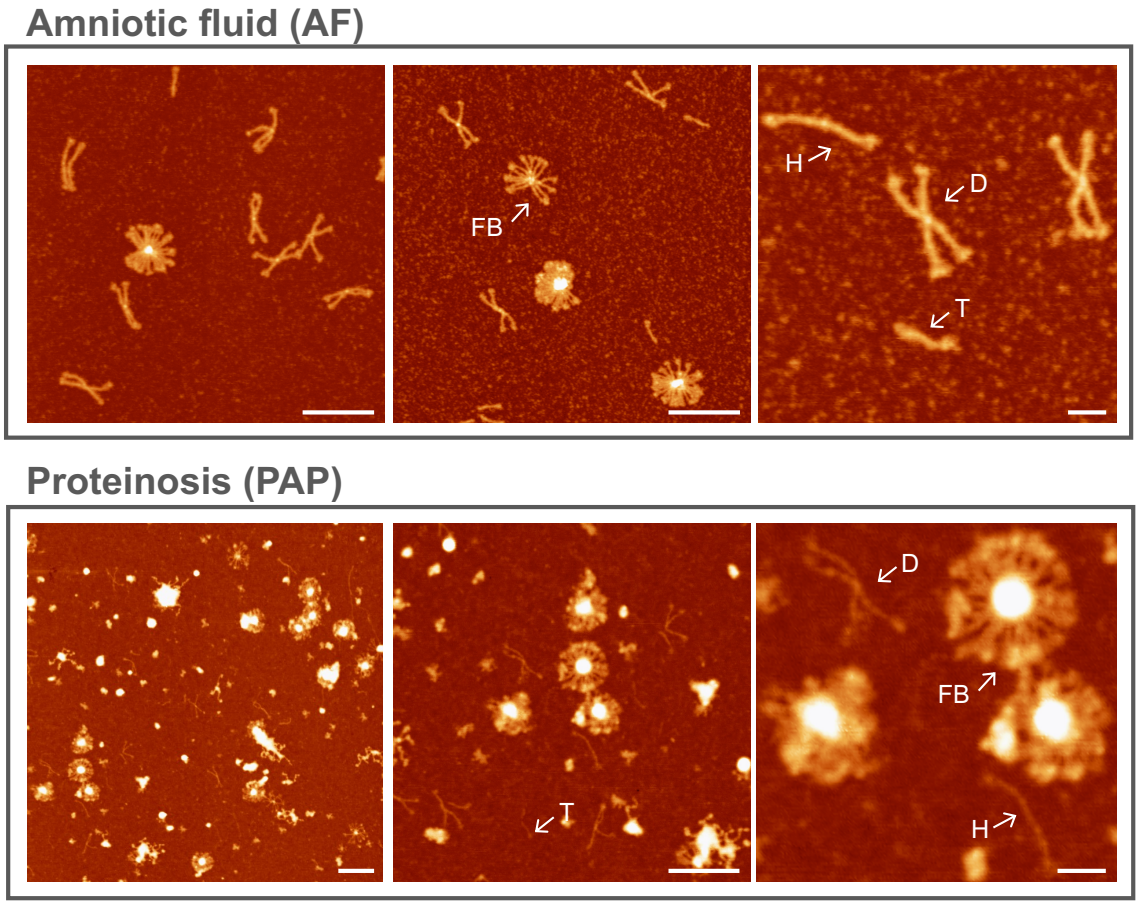

Figure 3.2: AFM images of hSP-D from amniotic fluid and proteinosis BALs. AFM images of hSP-D from AF (*top*) and proteinosis (*bottom*) contained trimers (T), hexamers (H), dodecamers (D) and fuzzy balls (FB); the scale bar represents 200 nm in images on the left and middle columns and, 50 nm in the images on the right column.

AFM was the technique chosen to observe and quantify hSP-D structures. The protein was found as a mixture of trimers, hexamers, dodecamers and large oligomers (fuzzy balls) in both cases (Figure 3.2). It is remarkable the presence of hexamers in the native human protein as it was observed in rhSP-D in chapter 1, something that has been ignored or considered an artifact up to now. In the case of hSP-D from PAP, the most abundant species found were the heterogeneous higher order oligomers (fuzzy balls) (Figure 3.2, bottom row). The exact quantitative distribution of oligomeric forms was not assessed in the SP-D from PAP because these preparations were much less clean, and it was often difficult to unequivocally assign each molecule to a defined oligomerization group. Besides, it has been already described in the literature that SP-D from PAP patients has higher amount of large oligomeric forms, as a consequence of this disease (Crouch et al., 1993a).

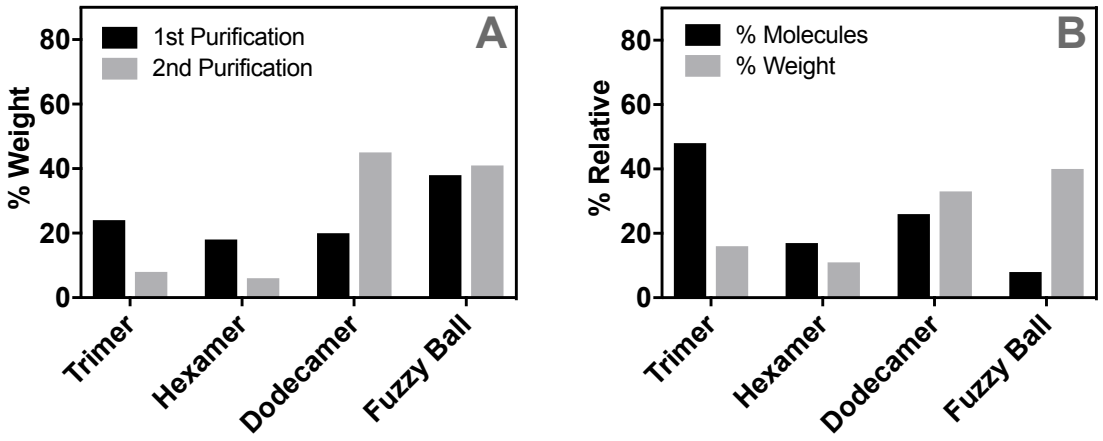

Figure 3.3: Quantification of the distribution of oligomeric forms in hSP-D from AF. ***A-B***, quantitative distribution of the different oligomeric forms in hSP-D (from AF) as determined from individual molecules observed under AFM. Percentage of weight and % of molecules were defined as described in results. ***A***, the number of molecules assigned and counted were 367 for the first purification and 273 for the second one. ***B***, distribution by % of weight of pooled molecules from both purifications (n = 650).

Hence, quantification was performed with hSP-D from AF. Several samples of purification batches 1 and 2 were prepared and imaged to count a significant number of molecules as in chapter 1. Interestingly, there were differences in the distribution of species between the material obtained from the two purifications (Figure 3.3A). These discrepancies could be attributed to the diverse protein polymorphisms described in humans, especially regarding that of amino acid in position 11 (Leth-Larsen et al., 2005). Further characterization is needed to determine other factors that could also contribute to variations in the oligomeric state of SP-D, which possibly reflects the rich dynamic nature of this protein and its potential connection with particular physio-pathological contexts. When

quantitative data from both purifications were pooled, dodecamers and fuzzy balls were the most abundant oligomers by percentage in weight with respect to total protein mass (% weight) (Figure 3.3B). Trimers were the most abundant structure referred to individual molecule distribution (% molecules).

Altogether, these data show that hSP-D is composed by a mixture of trimers, hexamers, dodecamers and larger oligomers, confirming that the oligomeric forms observed in the rhSP-Ds produced by CHO cells are also present in human protein, obtained from natural sources. Moreover, fuzzy balls were the most abundant structures in hSP-D (40% by % weight), closely followed by dodecamers (33% by % weight). These results validate CHO cells as a good system to produce recombinant human rhSP-D similar to hSP-D and, provide for the first time, a reference for the oligomeric forms distribution in human protein.

N-glycosylation of asparagine 70 in hSP-D obtained from amniotic fluid

To deeply characterize hSP-D, it was investigated whether the asparagine in the amino acid 70 of hSP-D sequence was N-glycosylated, as it was shown in the recombinant rhSP-D in chapter 1 and published before by other authors (Leth-Larsen et al., 1999). This glycosylation was observed as a bright protrusion in the rhSP-D AFM images (chapter 1, Figure 1.6). Although this point near the N-terminal domain did not look very prominent in hSP-D AFM images (Figure 3.2, top row), the height profiles of single molecules confirmed its existence. Height profiles for a total of 50 molecules were measured, revealing that the height of the region corresponding to the N-glycosylation site was 0.6 ± 0.2 nm (average ± SD) taller than the mere collagen triple helix (Figure 3.4).

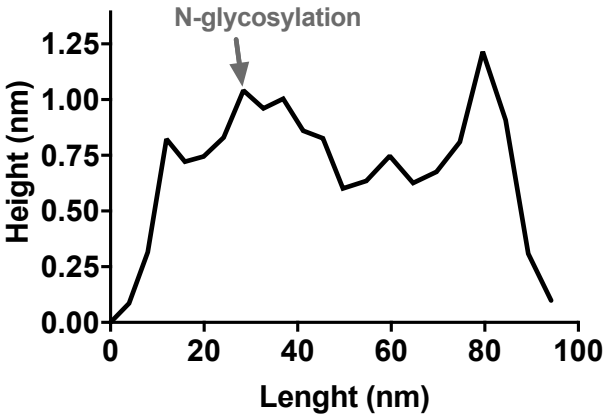

Figure 3.4: Height profile of hSP-D trimer measured by AFM. A representative height profile of the trimers observed in hSP-D from amniotic fluid is shown. The peak that corresponds to the N-glycosylation site is indicated.

Moreover, de-glycosylation experiments were carried out with PNGase F, which removes the carbohydrate core attached to asparagine, to further confirm protein N-glycosylation. Results in Figure 3.5 showed a shift in the electrophoretic mobility of the protein monomer after treatment with the enzyme (gel on the right). It should be noted that hSP-D monomer was already found resolved in two bands after electrophoresis, with the upper band being more conspicuous before de-glycosylation (black arrow) and the lower band after de-glycosylation (blue arrow). These data agreed with the observation of other authors (Leth-Larsen et al., 2005), showing that hSP-D was constituted by a mixture of its N-glycosylated and de-glycosylated forms, being the glycosylated the most abundant. The protein was further de-glycosylated with neuraminidase, which removes sialic acids, and a larger shift was observed in the band (Figure 3.5, left gel, green arrow). This protein sample showed a band pattern that contained more bands at lower molecular weights, probably due to denaturation of the neuraminidase by the reducing buffer of electrophoresis. When de-glycosylation was performed under non-reducing conditions, it was not possible to observe differences between the electrophoretic mobility of the bands (Figure 3.5, left gel, bands that correspond to trimers). We suspect that these enzymes might not have full access to the region when the protein is assembled in higher order oligomers.

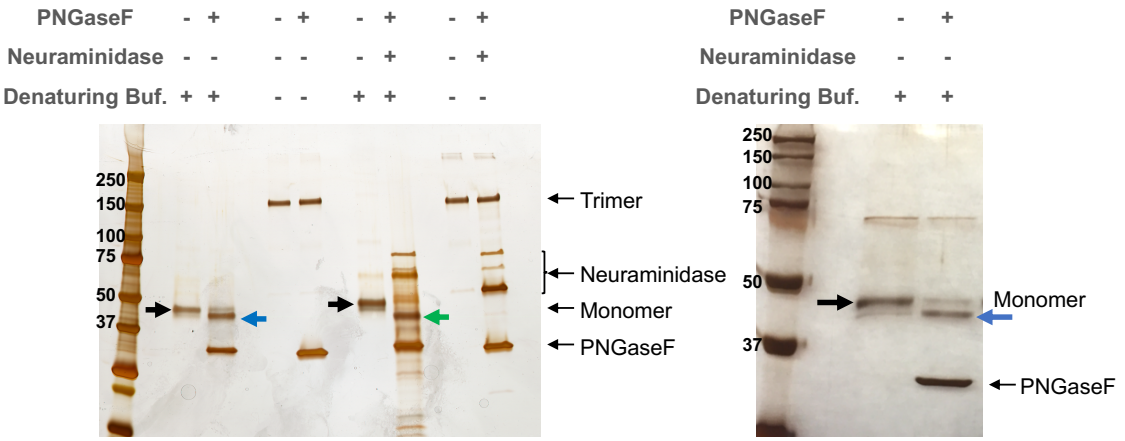

Figure 3.5: De-glycosylation experiments of hSP-D. hSP-D from AF was treated with PNGase and/or neuraminidase in the presence or absence of denaturing buffer. Conditions for each lane are indicated above the gels. *Left*, polyacrylamide gradient (4-15%) gel. *Rigth*, 8%-acrylamide gel. Black arrows indicate the band of the glycosylated form of SP-D, the blue arrow that of the de-glycosylated form after PNGaseF, and the green arrow that of the de-glycosylated form after PNGaseF and neuraminidase. Both gels were developed by silver staining.

Once N-glycosylation of Asn-70 was confirmed, we wondered about the sugars that constitute the actual structure. Some studies have addressed this issue in the past. However, new developed tools available nowadays, enabled us to obtain a deeper insight. Therefore, N-glycan profiling was carried out using a hydrophilic

interaction ultra-performance chromatography with fluorescence detection (HILIC-UPLC-FLD) coupled to electrospray ionization quadrupole time-of-flight tandem mass spectrometry (ESI-Q-TOF MS/MS). Results (Figure 3.6) showed that core-fucosylation was high (~ 80%) (Figure 3.6, "F" component in Table). Besides, high degrees of galactosylation were determined (>90%) ("G0-G4"in Table of Figure 3.6), in combination with a medium-high degree of sialylation (~ 65%) which was mainly monosialylation ("S1"). Thus, 80% of N-glycans comprising one or more antennae were terminated with galactose ("tG1-4" component in the Table of Figure 3.6). The degree of high mannose was low (6%) and no hybrid type glycans were found. There was a 15% N-glycans bearing bisecting terminal GlcNAc ("B" in the Table of Figure 3.6).

F	oF	B	S0	S1	S2	S3	S4	G0	G1	G2	G3	G4	GalNAc0	GalNAc1	GalNAc2	A1	A2	A3	A4	Le^A/Le^X	HB	M	tG0	tG1	tG2	tG3	tG4	tGalNAc0	tGalNAc1	LacNAc1
76.9	0.0	14.8	34.5	37.8	22.7	5.1	0.0	9.0	7.8	66.4	16.8	0.0	100.0	0.0	0.0	0.0	77.4	16.8	0.0	0.0	0.0	5.8	37.0	39.4	17.6	6.0	0.0	100.0	0.0	0.0

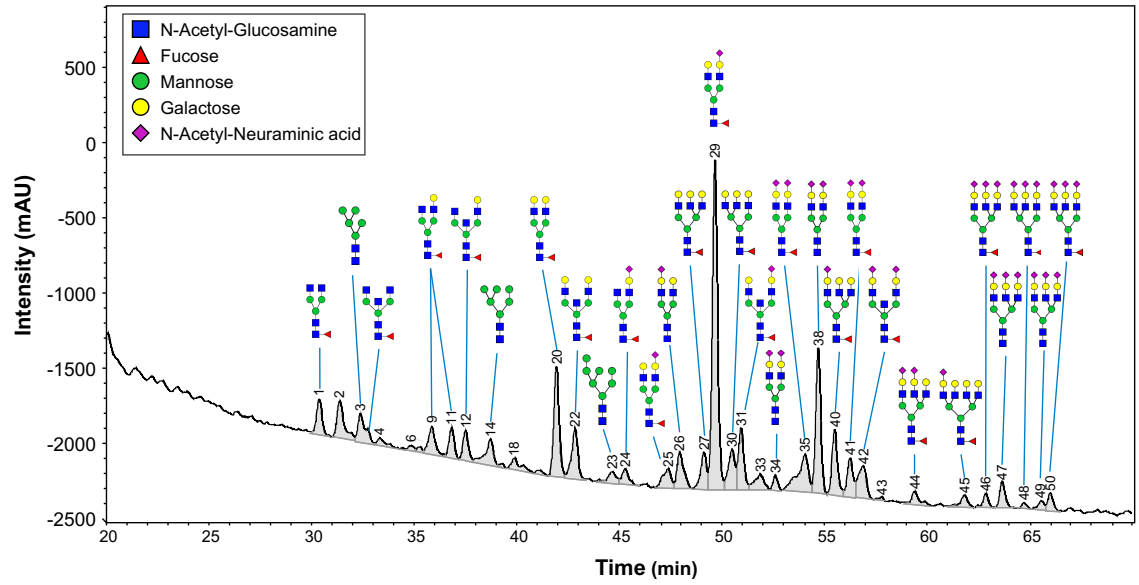

Figure 3.6: Carbohydrate-profiling of the glycan attached to the asparagine 70 of hSP-D. Glycan at the N-glycosylation site of hSP-D from AF was removed with PNGase F and further analyzed as described in the methods section to identify the sugars that it contained. The ***Table*** at the top indicates the amount of the different carbohydrates enclosed within the glycan structure. ***Glycan-Profile (bottom)***, The identified peaks are numbered in the chromatogram and the carbohydrates assigned to those peaks are represented following the Symbol Nomenclature for Glycans (SNFG) (Varki et al., 2015) . **Table legend: F**: core-fucose; **oF**: outer arm fucose; **B**: bisecting GlcNAc; **S0-S4**: non- to tetrasialylated complex type; **G0-G4**: non- to tetragalactosylated complex type; **GalNAc0-GalNAc2**: zero to two N-acetylgalactosamine residues; **A1-A4**: mono- to tetraantennary complex type N-glycans; **LeA/LeX**: Lewis-A or Lewis-X glyco-epitopes; **HB**: hybrid type; **M**: highmannose type; **tG0-tG1**: zero or one terminal galactose residues; **tGalNAc0-tGalNAc 2**: zero to two terminal N-acetylgalactosamine residues; **LacNAc1**:LacNAc repeat (GlcNAc-Gal attached to terminal Gal).

In summary, these findings confirmed N-glycosylation of Asn-70 in hSP-D and characterized the carbohydrate structure with unprecedent detail. It was shown that

N-glycan was biantennary, core-fucosylated with partial galactosylation and sialylation as well as bisecting GlcNAc.

hSP-D from amniotic fluid (AF) and proteinosis (PAP) binds and aggregates bacteria with different potency

An important question that should be addressed is whether the differences observed in the proportion of fuzzy balls in hSP-D obtained from AF or PAP, would correlate with differences in protein function, in terms of activity. In chapter 2, we already saw that isolated fuzzy balls were more active than hexamers and trimers, in the case of rhSP-D.

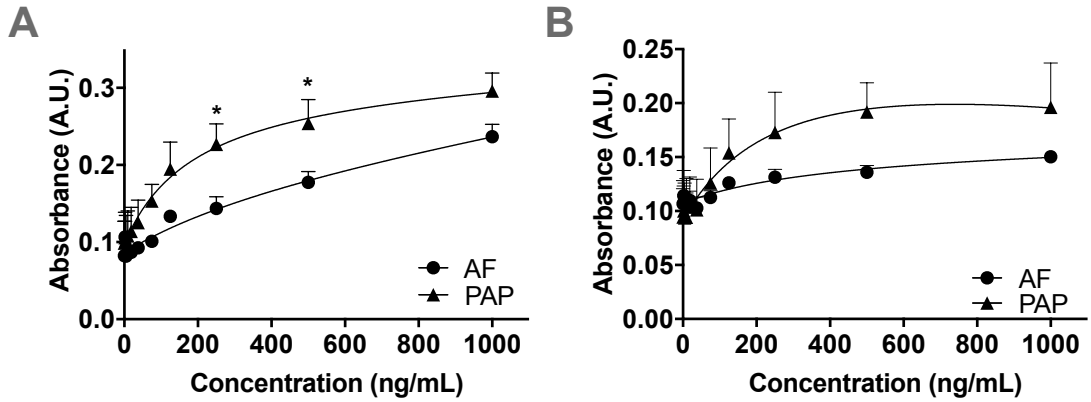

Figure 3.7: Binding assay of hSP-D from AF or PAP to *E. coli*. Plates were coated with bacteria and incubated with 2-fold dilutions starting at 1000 ng/mL of hSP-D from each of the two sources. Bound SP-D was detected with antibodies in an ELISA-like assay; (n = 2), Two-way ANOVA with Bonferroni's multiple comparison post-test was performed: *, $p<0.05$. ***A***, monoclonal anti-SP-D against an epitope in the CRD, ***B***, against an epitope in the N-terminal domain of hSP-D.

First, binding of hSP-D to *E. coli* was assessed in a solid-phase assay. *E. coli* is one of the typical bacterial ligands of hSP-D *in vivo*. Microtiter plates were coated with *E. coli DH5α* and incubated with different hSP-D concentrations, starting at 1000 ng/mL and making progressive two-fold dilutions of the two hSP-D preparations in the presence of calcium 5 mM. The experiment was performed twice with two different monoclonal anti-SP-D antibodies, to demonstrate that the antibodies used did not interfere in the results. It is known that SP-D binds to bacteria through its CRD domains, where the epitope for many anti-SP-D antibodies is also located (Hartshorn et al., 2010). Once SP-D is bound to bacteria, the epitope in the CRD recognized by the antibody could be not accessible, which would be translated into an underestimation of the concentration of bound protein. Therefore, as in chapter 2, one antibody towards an epitope enclosed in the CRD (Figure 3.7A) and another with its epitope in the N-terminal domain (Figure 3.7B) of the protein were tested. Similar results were obtained for both of them. Both preparations, PAP-hSP-D and AF-hSP-D, bound in a concentration-dependent manner to *E. coli*. In all

concentrations tested, PAP-hSP-D showed a significant (*t*-test, $p = 0.0005$) higher degree of binding to bacteria than AF-hSP-D.

Second, SP-D promoted *E. coli* aggregation assays were performed to determine the activity of the protein to aggregate, as a previous step to clearance, potentially pathogenic entities such as bacteria. Bacterial suspensions were incubated with different concentrations of AF-hSP-D or PAP-hSP-D and light transmission (turbidity) through each sample was monitored during 2 hours. hSP-D from PAP aggregated bacteria more efficiently than protein from AF (Figure 3.8A). It was necessary to dilute PAP-hSP-D concentrations to 0.1 µg/mL to observe a decay in activity, while AF-hSP-D already showed less activity at 1 µg/mL. Moreover, higher concentrations of AF-hSP-D were required to reach the maximum aggregation activity than in the case of PAP-hSP-D. The percentage of aggregated bacteria referred to the control (in the absence of protein) was calculated for both proteins at 3 different concentrations and at two time points (Figure 3.8B). Striking differences were observed especially at t = 60 min, where PAP-hSP-D aggregated almost 50% of the bacteria at all concentrations tested, whereas AF-SP-D needed 2.5 µg/mL to start showing some activity (Figure 3.8B, top). At final time point (t = 120 min), AF-SP-D activity was improved, but still less than PAP-SP-D at low protein concentrations (Figure 3.8B, bottom).

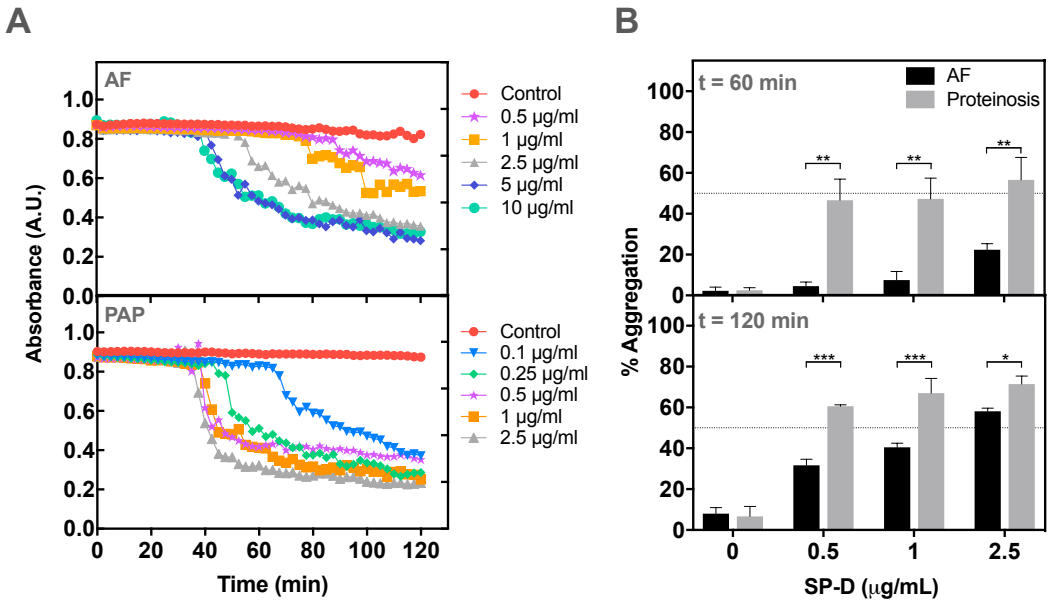

Figure 3.8: Bacterial aggregation assay induced by hSP-D from AF and PAP. Bacterial suspensions of *E. coli DH5α* were incubated with or without (control) different concentrations of hSP-D from AF (*top*) or PAP (*bottom*). ***A***, absorbance values (λ = 700 nm) were monitored during 2 hours. ***B***, % of aggregated bacteria was determined at two time points (t = 60 and t = 120 min), as stated in methods, at three different concentration of SP-D; a dotted line has been traced at 50% aggregation. Two-Way ANOVA with Bonferroni's post-test: *, $p<0.05$; **, $p\leq0.01$; ***, $p\leq0.001$.

These data illustrate that both hSP-Ds were functional and active in the assays performed, but PAP-hSP-D showed apparently higher activity than AF-hSP-D, presumably due to its higher proportion of large fuzzy balls oligomers, as it has been documented for viral particles (Hartshorn et al., 1996a, Leth-Larsen et al., 2005) and as we demonstrated for rhSP-D in chapter 2.

Carbohydrate binding preference of hSP-D

To further characterize differences between hSP-D obtained from AF or PAP, binding properties of hSP-D to different carbohydrates were assessed. We allowed hSP-D from the two sources to bind to mannan-coated beads in the presence of maltose, glucose, galactose or N-acetyl-glucosamine (GlcNAc) at different concentrations, to see how efficiently those different sugars compete to prevent binding of SP-D to mannose on a reference ligand.

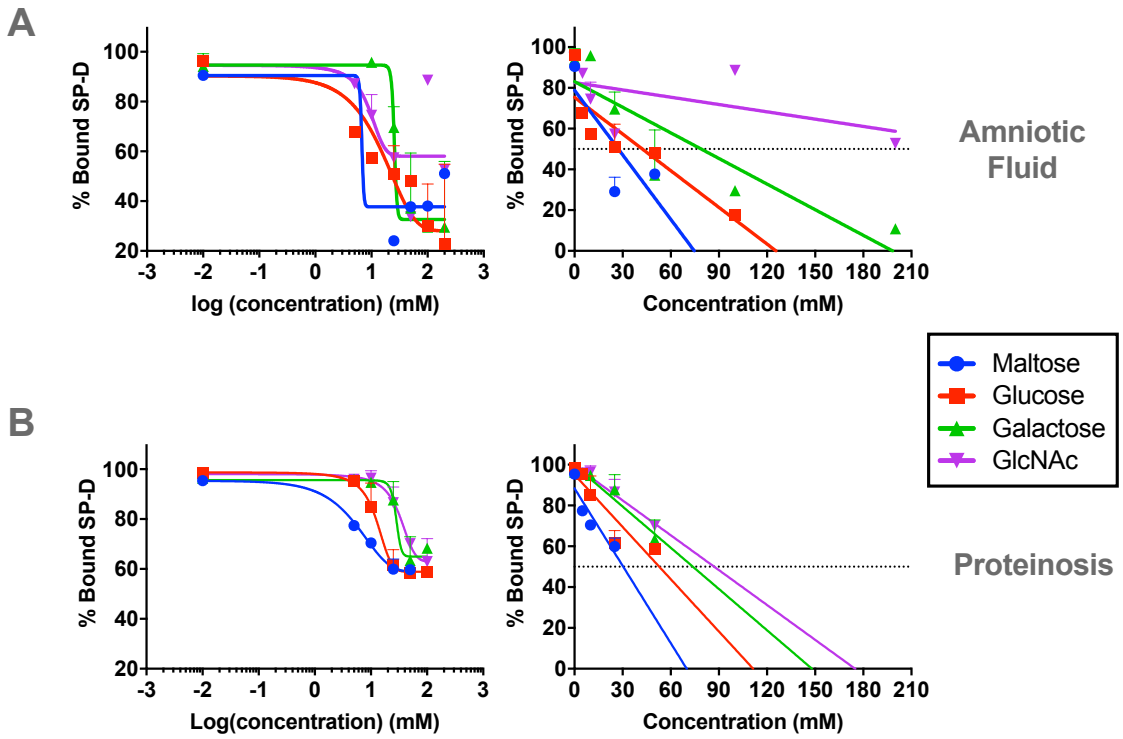

Figure 3.9: Binding competition of hSP-D to carbohydrates. The effect of different concentrations (0.01, 10, 25, 50, 100, 200 mM) of maltose, glucose, galactose and N-acetyl-glucosamine (GlcNAc) on the binding of hSP-D from AF (***A***) or PAP (***B***) to mannan was determined. The percentage of SP-D bound to mannan-coated beads in the presence of different concentrations of the competitors is represented in both A and B. ***A***, data represented were fitted to a sigmoidal dose-response model. ***B***, lines in the graph represented the linear regression of the points for the different competitors, a dotted line indicates where the 50% of inhibition is reached.

With both proteins, AF-SP-D and PAP-SP-D, maltose and glucose inhibited SP-D binding to mannan at lower concentrations than galactose and N-acetyl-glucosamine (Figure 3.9). In addition, PAP-hSP-D needed lower concentrations of competitors to suppress 50% hSP-D binding to mannan-beads than AF-hSP-D.

Carbohydrate binding preference assays of hSP-D obtained from amniotic fluid have been previously conducted, and the results obtained in this work were coincident (Holmskov, 2000, Palaniyar et al., 2004).

These results also agreed with our previous functional assays, indicating that PAP-hSP-D is more active than the protein isolated from amniotic fluid.

Discussion

In previous chapters, protein conformation and the distribution of oligomeric forms were evaluated in a recombinant human rhSP-D preparation under different conditions. However, a quantitative study performed with the human natural protein was not available, which could be used as a reference of what should be considered as standard values of the different oligomeric forms.

We first showed that hSP-D from PAP was mainly composed by large oligomers (Figure 3.2B), as it has been already observed by other authors (Crouch et al., 1993a, Hartshorn et al., 1996a), which is probably associated with the disease condition. Therefore, it is questionable whether this protein preparation could be used as a reference protein for quantitative studies of proteins produced by alternative approaches. As an alternative to this pathological source, hSP-D from AF was obtained to perform the analysis. It has been reported that SP-D in AF at term pregnancy comes from type II pneumocytes from the fetus (Stahlman et al., 2002) and from the internal layer of the placenta, part of the human amniotic membrane (Lemke et al., 2017). After quantification of the different oligomeric forms, discrepancies were observed between the two purifications performed, from two pools of different donors. The proportion of trimers and hexamers was markedly higher in purification 1, while that of dodecamers was lower compared to purification 2 (Figure 3.3A). These differences might be attributed to possible genetic variations that contribute to different polymorphisms of hSP-D among population. It was described for a Caucasian population that the distribution frequency of the amino acid at position 11, in hSP-D from serum, was 59% Met and 41% Thr. In addition, it was observed that a predominance of low molecular weight oligomers existed for hSP-D in the individuals with Thr^{11} (Leth-Larsen et al., 2005). Purification 1 was performed from a pool of amniotic fluid from only two individuals, while purification 2 was from a pool obtained from 7 donors (Table 3.1). One could expect a higher influence of polymorphisms when amniotic fluid is obtained from a low number of donors, while this effect should be diluted out when the AF pool is constituted by a higher number of individuals. Different polymorphisms have been also observed between ethnic groups (Liu et al., 2003), but in our case all donors were Caucasians. Many other factors could contribute to

differences in protein oligomerization and in the proportion of the different forms, a source of variability that should be explored in detail, as a possible way for this protein to respond to environmental conditions during lung and mucosa homeostasis. On the other hand, the proportions obtained from rhSP-D in chapter 1 included 50% of dodecamers and 30% of fuzzy balls, numbers that are similar to the results obtained for AF-hSP-D from purification 2 (Figure 3.3A). Moreover, rhSP-D was assembled into dodecamers and fuzzy balls that summed a total of 80% of the protein, similar to the 70% observed in AF-hSP-D total data (Figure 3.3B).

It has been published that the degree of fucosylation of the glycan core, attached to the N-glycosylation site (Asn^{70}) of hSP-D purified from serum, differs between COPD and healthy individuals (Ito et al., 2015). The glycan profiling of lung hSP-D from AF performed in the present study, with more sensitive methods than the ones available a few years ago, allowed us to identify and describe in more detail the sugars attached to the protein. We confirmed a biantennary structure, with galactose and GlcNAc (Leth-Larsen et al., 2005) and we found also a significant amount of sialic acids and high core-fucosylation. The new data could be useful to identify markers of different diseases as it was shown with the degree of fucosylation in serum SP-D.

Last, in chapter 2, differences in activity of isolated rhSP-D oligomeric forms were found. SP-D activity was greater for the protein forms with higher degree of multimerization. Hence, after observing differences in the oligomeric distribution between AF-SP-D and PAP-hSP-D, we evaluated whether the differences in structure could be also translated into differences in protein activity. We showed that the increased number of large oligomers in PAP-hSP-D is associated with a greater binding affinity of SP-D to *E. coli* and to different carbohydrates, when it was compared with hSP-D from amniotic fluid, where the proportion of fuzzy balls was lower and similar to that of dodecamers. Moreover, PAP-hSP-D was also more efficient to aggregate bacteria. This confirms that the degree of oligomerization of hSP-D and the quantitative distribution of the different oligomeric forms influence protein activity, at least, in those functions that depends on the CRD domain. These results are consistent with those from a study where the activity of isolated fuzzy balls was compared with that of a rhSP-D with qualitatively more dodecamers. The protein with higher content in fuzzy ball-like aggregates was more active, in terms of binding and agglutination of influenza A virus, than the one with more dodecamers (Hartshorn et al., 1996a). However, this should be interpreted carefully. It cannot be concluded that the protein, in the pathological context of proteinosis *in vivo*, is more active just because it contains a higher proportion of large oligomers. There are many other potential factors possibly derived from the

pathological context, which that could affect its function *in vitro* and *in vivo*. In other words, an individual suffering from proteinosis, with a reactive situation in lungs, where SP-D has a high proportion of fuzzy balls, is not necessarily more protected against infections than a healthy newborn baby with lower amounts of fuzzy balls.

In summary, we have characterized the quantitative distribution of human SP-D from a non-pathological source, amniotic fluid, and analyzed the differences with respect to a protein from a disease condition, like PAP. Moreover, we have seen the effect of the proportion of oligomers of human native SP-D in protein function, which confirmed the results obtained in chapter 2. hSP-D from AF and PAP were both active, but it could be concluded that the greater amount of fuzzy balls, the greater potency in protein activity, at least in those functions that rely on the CRD domain.

RESULTS

Chapter 4

SP-D modulates LPS-induced NETosis and protects lung surfactant from NETs

Part of the experiments included in the present chapter were performed during a short-term stay in the laboratory of Dr. Nades Palaniyar in SickKids Hospital (Toronto, ON, Canada). This short-stay was funded by a fellowship from the Spanish Ministry of Education Culture and Sport (EST16/00922). Mouse work was performed in the facilities of the Toronto Centre for Phenogenomics (TCP) (Toronto, ON, Canada). Confocal images were obtained and imaged in the Imaging Facility at SickKids Hospital.

The results have been sent for publication to Nature Communications.

Introduction

During respiratory infections by different pathogens, capillary alveolar neutrophils infiltrate to airway alveolar spaces after sensing microbial insults (Cheng and Palaniyar, 2013). LPS is a key bacterial component responsible for inducing the formation of neutrophil extracellular traps (NETs), a process known as NETosis. NETs are a mesh of decondensed chromatin fibers decorated with antimicrobial granular proteins, that help to capture and ensnare bacteria (Brinkmann et al., 2004). The complete regulatory mechanism of NETosis is still elusive. So far, NADPH oxidase 2 (NOX)-dependent and –independent types of NETosis have been described. NOX-dependent NETosis, triggered by bacterial components (e.g. LPS) or phorbol myristate acetate (PMA), courses with ROS production (Khan et al., 2017, Khan and Palaniyar, 2017), while NOX-independent NETosis needs an increase in intracellular calcium concentration (e.g. caused by ionophores or ionomycin secreted by *Streptomyces conglobatus*) to drive NETosis. Influx of the intracellular calcium forms a complex with peptidylarginine deiminase 4 (PAD4) that translocates to the nuclei and citrullinates histone 3 leading to the formation of NETs (Li et al., 2010, Khan and Palaniyar, 2017, Papayannopoulos et al., 2010). Citrullination is the posttranslational enzymatic conversion of arginine residues to peptidylcitrulline, which is catalized by PAD4 (Konig and Andrade, 2016). The modification of arginine residues results in a loss of positive charge, increasing its hydrophobicity, which in the case of histones promotes chromatin decondensation, leading to the formation of NETs (Wang et al., 2009).

Although NETs are beneficial for controlling infection, an excess in NET formation is deleterious to surrounding tissues and associated with lung injury and inflammatory lung diseases, such as cystic fibrosis (CF), where it affects lung function and exacerbates disease conditions (Cheng and Palaniyar, 2013). The biophysical function of lung surfactant (LS), which allows compression and expansion of alveoli during normal breathing without collapse, could be compromised by the presence of increased NETs in the airways, which could be a potential contribution to respiratory failure in lung pathologies, as it happens when there is an overproduction of other inflammatory components (Echaide et al., 2017). On the contrary, the innate immune function of lung surfactant, where SP-A and SP-D play key roles (Kishore et al., 2006), could help to counteract exacerbated NETosis and its deleterious effects, especially with the action of SP-D. As it was described in the introduction, SP-D opsonizes particles to be further cleared by immune cells (Crouch, 2000). It has been stablished that SP-D binds to lipopolysaccharides (LPS) of some bacterial strains through the CRD domain in a calcium-dependent manner (Lim et al., 1994). Moreover, it has been also found

that SP-D can interact with DNA (Palaniyar et al., 2004) and NETs (Douda et al., 2011), through ionic interactions. Though calcium is not essential, these interactions are stronger when it is present (Palaniyar et al., 2004). It was also described that SP-D enhances the clearance of DNA from the airways by macrophages (Palaniyar et al., 2005). Interestingly, in some lung diseases where an excess of NETs causes disease exacerbation, such as cystic fibrosis or ARDS, a relationship between low SP-D levels and exacerbated NETs in bronchoalveolar lavages (BAL) has been found (Sorensen, 2018, Sorensen et al., 2007, Nishikiori et al., 2014, Cheng and Palaniyar, 2013, Saffarzadeh et al., 2012).

However, whether SP-D has a role in modulating NET formation during LPS-induced NETosis or whether SP-D could protect LS function from potential NET-mediated inhibition is unknown.

With these antecedents, this chapter has addressed:

- Whether SP-D could modulate LPS-induced NETosis
- The probable mechanism for SP-D to modulate NETosis
- The potential inhibition of LS function by NETs
- The consequences of NETs release on respiratory mechanics

These findings should help to understand the role of SP-D in regulating the development of NETosis and in protecting lung compliance when neutrophils are released to the airways.

Results

SP-D binds LPS and suppresses LPS-mediated NETosis in neutrophils

The LPS (0128:B12) strain used in this chapter is different from other strains previously tested elsewhere (Khan et al., 2017), which differs in the O-antigenic polysaccharide chain (the sugar constituents, their sequence and their mode of linkage) that determines the serological O-specificity. Hence, in a first step, we have determined the potential of the LPS (0128:B12) strain to trigger NETosis by using a SytoxGreen dye based assay in human neutrophils. The results showed that this LPS strain induces NETs release in a dosage dependent manner (Figure 4.1A). Based on these results, 5 μg/mL of LPS was chosen as the optimal working concentration for most of the experiments.

Then, the ability of SP-D to interact with LPS (0182:B12) was determined. For this purpose, we used a dot blot analysis. Different concentrations of LPS (2.5 to 80 μg/mL; 2μL) were placed as dots on a membrane, and incubated with 5 μg/mL or 15 μg/mL of SP-D, in the presence of 5 mM calcium or 20 mM EDTA. A negative control experiment was carried out in the same conditions without SP-D. The

amount of SP-D bound to LPS was determined by developing the blot after detecting the SP-D with anti-SP-D antibodies. Blot images showed that SP-D binds to this LPS in a dose dependent manner (Figure 1A). Moreover, calcium was required for this interaction, suggesting that SP-D binds LPS through its CRD domains, as it has been previously shown with other LPS strains as well (Ohya et al., 2006, Yamazoe et al., 2008).

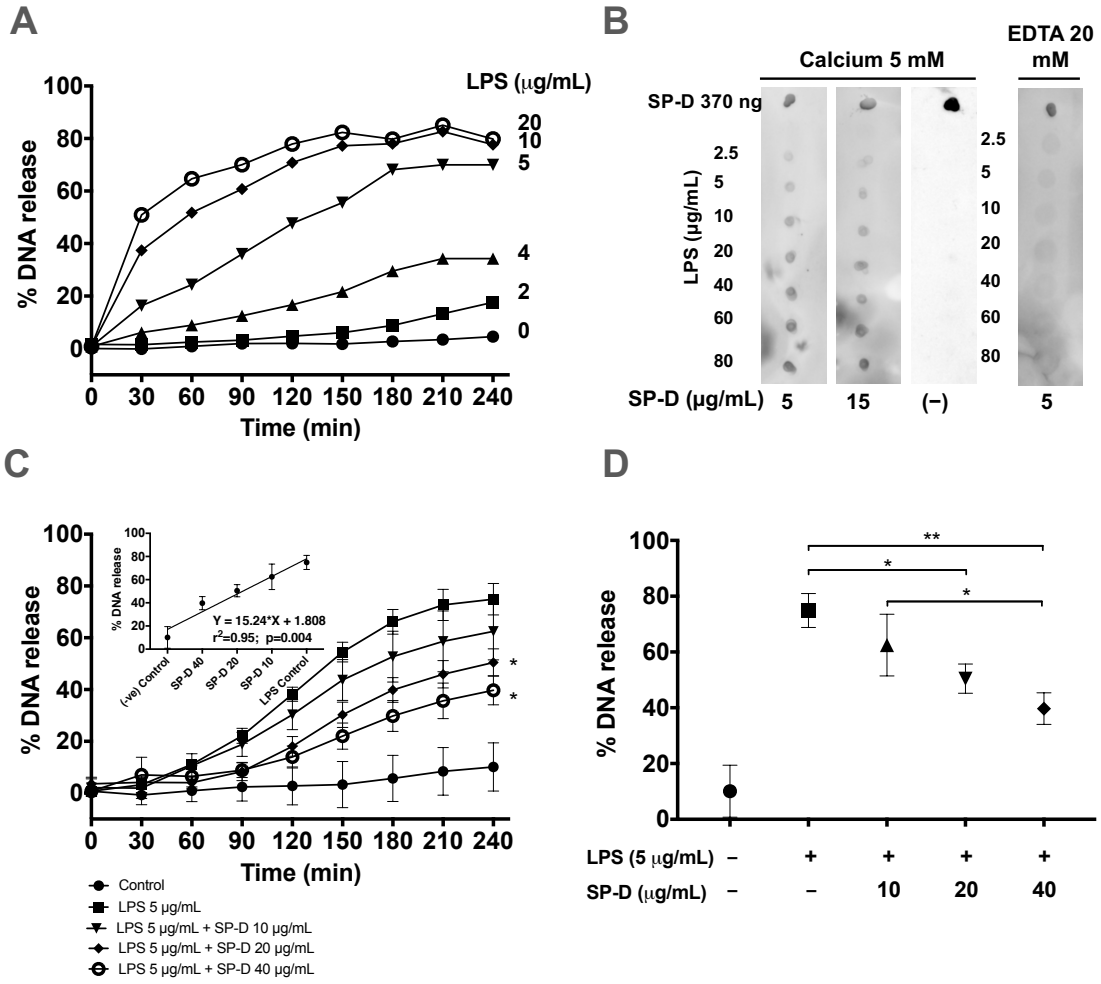

Figure 4.1: SP-D binds LPS (0128:B12) and suppresses LPS-induced NETosis. ***A, C-D***, NETosis kinetics assessed by Sytox Green plate reader assays, where the %DNA released in the presence of 0.5% (v/v) Triton was considered as 100%. ***A***, LPS dose dependently induces NETosis. LPS at concentrations ≥5 μg/mL produced substantial degree of NETosis. ***B***, Dot blot showing that SP-D binds to LPS. LPS (0128:B12) at different concentrations was dotted onto a membrane, which was later incubated with SP-D at different concentrations in the presence of 5 mM calcium or 20 mM EDTA. ***C***, SP-D dose-dependently suppresses LPS (5 μg/mL)-induced NETosis (n=3; Two-way ANOVA with Bonferroni's multiple comparison post-test: *, $p<0.05$). The regression graph in the inset represents the values at time 240-min, showing a linear decrease of NETosis with increase in the concentration of SP-D. ***D***, the percent differences of DNA released at 240-min time points shown in panel C (n=3, One Way ANOVA with Tukey's multiple comparison post-test: * $p<0.05$; **, $p\leq0.01$). Error bars represent standard deviation.

After determining that SP-D binds to LPS (0128:B12), we investigated whether the presence of SP-D could modulate LPS-induced NETosis. For that, a Sytox Green

assay was conducted upon exposure of neutrophils to 5 µg/mL LPS concentration in the presence or absence of different SP-D concentrations. Before adding LPS to the cells, the agonist was first incubated with SP-D at a final calcium concentration of 0.5 mM. The percentage of DNA release data showed that SP-D reduces DNA release in a dosage dependent manner (Figure 4.1C). The decrease in DNA release was significantly higher at higher protein concentrations, leading to a significant reduction of 35% in the presence of 40 µg/mL of SP-D (Figure 4.1D).

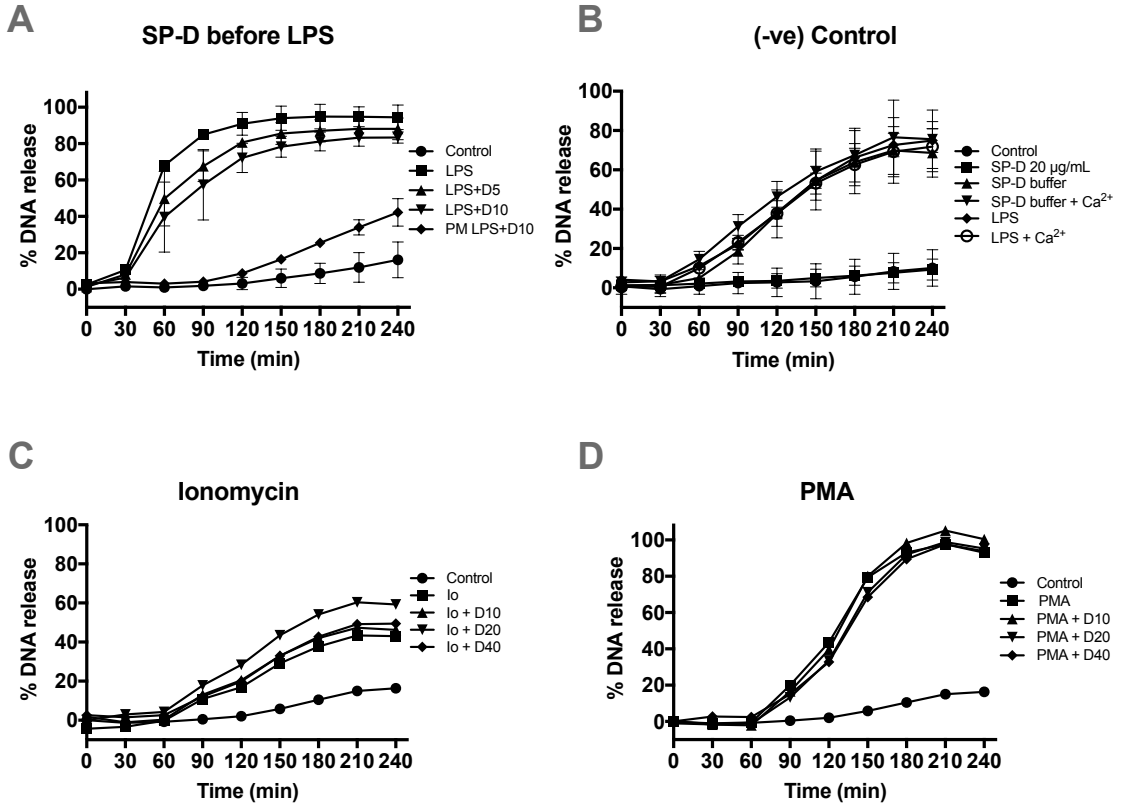

Figure 4.2: Kinetics of NETosis induced by LPS and other agonists, where SP-D did not show any effect. ***A-D***, NETosis kinetics assessed by Sytox Green assay, where the %DNA released in presence of 0.5% (v/v) Triton was considered as 100%. ***A***, SP-D was first added to the cells and incubated for 30 minutes. After incubation, LPS agonist was added at 5 µg/mL and NETosis kinetics was monitored, as previously described; (n=2), error bars represent SD. ***B***, controls to discard any effect of SP-D on neutrophils in the absence of LPS or any effects of SP-D buffer components to reduce LPS-induced NETosis. LPS concentration was 5 µg/mL; (n=3), error bars represent SD. ***C*** *and* ***D***, no effect of SP-D (at 10, 20 or 40 µg/mL) modulating NETosis was observed when NETosis was induced by 25 mM of PMA (*B*) or 2.5 µM of Ionomycin (*C*).

On the other hand, when different concentrations of SP-D were pre-incubated with the cells before adding LPS, no effect was observed in the release of DNA (Figure 4.2A). Therefore, direct binding of LPS by SP-D is defining the mechanism of action. The batch of SP-D used in these experiments was different; for that reason, a control with the pre-incubation procedure, explained in methods section, was also included (PM-LPS + SP-D10 µg/mL), which showed that this batch of SP-D worked well at 10 µg/mL. This effect of SP-D was shown to be specific for LPS, as

it is shown in Figure 4.2 (B-D). NETosis induced by other agonists like PMA (NOX-dependent NETosis) or Ionomycin (NOX-independent NETosis) was not modulated by SP-D: neutrophils underwent NETosis and the percentage of DNA release was not altered by the presence of SP-D.

Altogether, these findings showed that SP-D binds to LPS (0128:B12) in a dose dependent manner and as a consequence, LPS-induced NETosis is suppressed by SP-D. Moreover, calcium is required for this protein function. PMA- or ionomycin-mediated NETosis are not altered by the presence of SP-D. These findings suggest that SP-D binds to LPS and suppresses LPS-induced NETosis.

Confocal microscopy confirms that SP-D suppresses LPS-mediated NETosis

To directly examine the effect of SP-D on LPS-mediated NET formation, we stained the specimen for DNA and immunostained them for myeloperoxidase (MPO), containing neutrophils treated with LPS, in the presence or absence of SP-D.

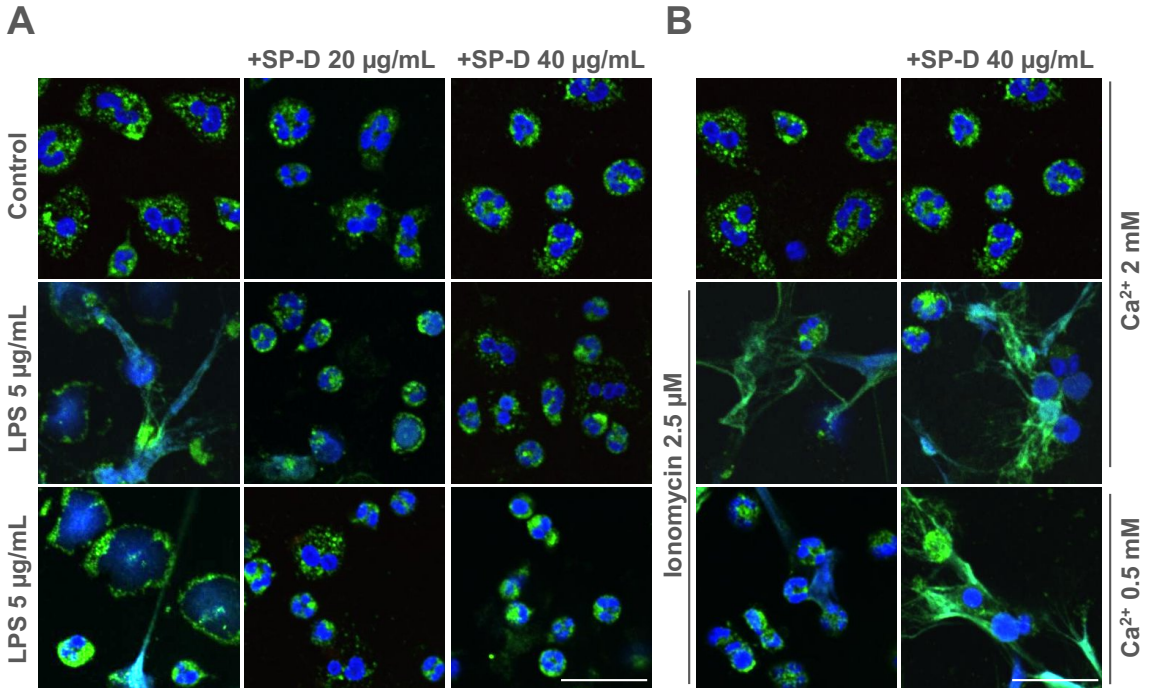

Figure 4.3: Confocal microscopy images confirm that SP-D suppresses LPS-mediated NETosis. ***A-B***, neutrophils were activated for 2 hours by LPS (*A*) or Ionomycin (*B*) with or without SP-D at two calcium concentrations, and imaged after immunostaining for myeloperoxidase (MPO)-green and staining with DAPI for DNA-blue. MPO co-localized to NET-DNA upon stimulating neutrophils with LPS or Ionomycin. ***A***, preincubation of indicated concentrations of SP-D with LPS showed that SP-D suppresses NETosis. ***B***, SP-D did not suppress NETosis induced by ionomycin. (n=2, scale bar 20 µm).

Confocal microscopy images of neutrophils stained for DNA (DAPI; blue) and MPO (green) confirmed the effect of SP-D on LPS-mediated NETosis (Figure 4.3). Neutrophils stimulated with 5 µg/mL of LPS showed decondensed nuclei and DNA

strings colocalized with MPO in the cytoplasm, confirming the release of NETs. Also, some NETs were observed protruding out from the cell. By contrast, the control condition (unstimulated neutrophils) showed intact nuclei with MPO granules in the cytoplasm. In the presence of SP-D, NETs were almost absent and neutrophils morphology was similar to control cells. No differences were observed in the suppressive effect at the two calcium concentrations tested (Figure 4.3A). Neutrophils treated with Ionomycin did not show any response to SP-D, where similar amounts of NETs were observed in the presence and absence of SP-D (Figure 4.3B).

Collectively, confocal images confirmed the release of NETs by LPS and the suppressive effect of SP-D only in LPS-mediated NETosis, but not in the induced by other ligands such as PMA and ionomycin.

SP-D suppresses histone 3 citrullination induced by LPS in human neutrophils

Certain agonist can induce PAD4-mediated citrullination of histone 3 to facilitate NETosis (Li et al., 2010, Papayannopoulos et al., 2010, Douda et al., 2015, Khan and Palaniyar, 2017).

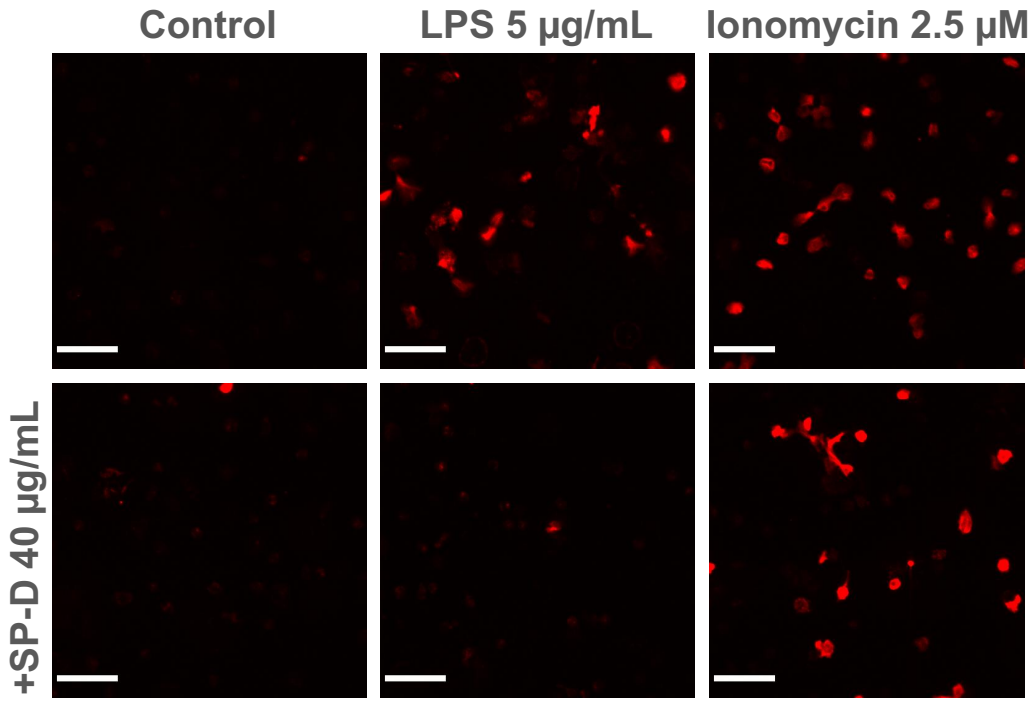

Figure 4.4: LPS (0128:B12) induces citrullination of histone 3 (citH3) during NETosis and SP-D prevents LPS-induced citH3 formation. Neutrophils were activated for 2 hours with buffer control, LPS or ionomycin with (*bottom row*) or without (*top row*) 40 µg/mL of SP-D. The specimens were immunostained and imaged for citrullinated histone 3 – red. LPS and ionomycin, but not buffer control, induced citH3 formation. SP-D suppressed LPS-mediated, but not ionomycin-mediated citH3 formation (n=2, scale bar 40 µm).

To determine whether LPS (0128:B12) provokes citrullination of the histone H3 (citH3) in neutrophils, and assess the regulatory effect of SP-D, the specimens were immunostained for citH3 (red) and imaged by confocal microscopy. Ionomycin was used as positive control to induce citH3 formation.

Neutrophils treated with LPS showed the immunostaining of citH3, while this staining was almost absent in the control condition (Figure 4.4). When 5 μg/mL of LPS were preincubated with SP-D at a concentration of 40 μg/mL, it showed reduced citH3 immunostaining (least staining), indicating the suppressive effect of SP-D. Interestingly, the citH3 suppressive effect of SP-D was not observed in ionomycin treated cells (Figure 4.4, bottom row).

Results determined the presence of citH3 in LPS and ionomycin treated cells while again, the presence of SP-D only suppressed citrullination during LPS-, but not the calcium ionophore (ionomycin)-induced NETosis.

LPS instillation induces exacerbated NETosis in the airways of SP-D$^{-/-}$ (KO) mice

With the aim to address whether SP-D has any modulatory role during NETs release in the lungs under inflammatory conditions, we performed an *in vivo* experiment, where we instilled LPS in both SP-D Knock-out (KO) and wild type (WT) mice.

Total protein concentration in bronchoalveolar fluid (BAL) was determined by BCA assay, as a landmark for airway inflammation. Data showed that the protein concentration was higher in LPS given mice than in the PBS-instilled mice, and a slightly increased amount was found in KO LPS mice compared to WT LPS mice (Figure 4.5A). Additionally, the BAL samples from these instilled mice were examined for the presence of DNA and citH3 to assess the presence of NETs. PicoGreen DNA binding fluorescence dye was employed to quantify the NETs DNA in BAL-supernatants. LPS-instilled mice showed higher amounts of DNA in BAL-supernatants compared to PBS-instilled mice (Figure 4.5B). Moreover, the DNA concentration values were significantly higher in BAL from KO LPS mice than in that from WT LPS, especially for a subgroup of animals within the KO LPS condition, suggesting an important protecting role for SP-D against NETosis in mice airways. CitH3 was found in LPS-instilled mice samples (Figure 4.5C, left panel), being greater the degree of citrullination in KO mice with respect to WT mice (Figure 4.5C, right panel).

These *in vivo* data reveal that LPS induces NETosis in neutrophils in mice airways and also support *ex vivo* data, showing again an important role for SP-D to prevent LPS-induced NETosis in mouse lungs.

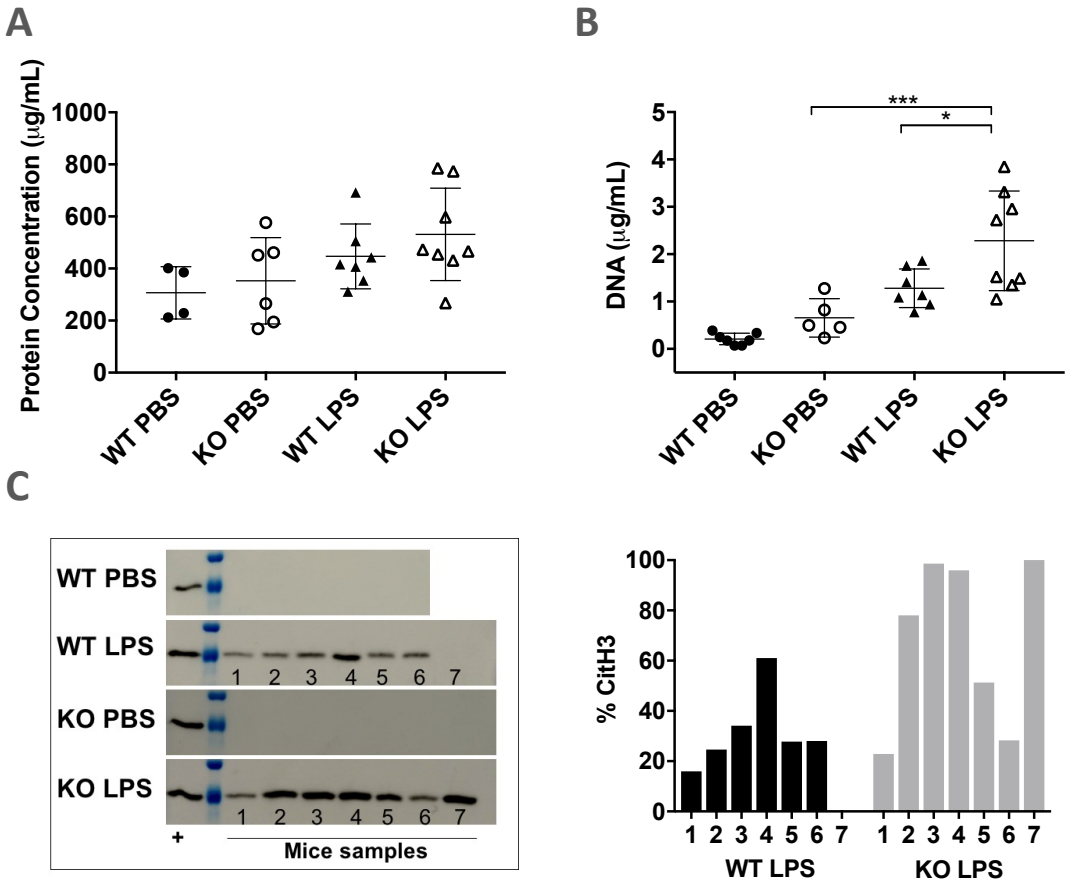

Figure 4.5: SP-D$^{-/-}$ (KO) mice suffered exacerbated NETosis after LPS instillation compared to WT mice. ***A***, total protein concentrations in BAL for the different mouse groups. Symbols represent averaged values (n=2). One-way ANOVA with Tukey's multiple comparison post-test, p=0.0776 (no significant). ***B-C***, cell free DNA concentration and citH3 in BAL were determined as markers of the presence of NETs. Higher amounts of NETs were found in KO-LPS mice compared with WT-LPS. ***B***, DNA concentrations in BAL assessed by PicoGreen assay. Symbols represent averaged values (n=2). One-way ANOVA with Tukey's multiple comparison post-test: *, p<0.05; ***, p≤0.001. ***C***, *left panel*: WB anti-citH3 for all mouse groups; *right panel*: densitometry of the bands in LPS-instilled mice.

Lack of SP-D worsen surfactant biophysical function and efficiency of breathing in LPS-instilled mice

The biophysical activity of lung surfactant (LS) pelleted from BAL-supernatants was evaluated in the captive bubble surfactometer (CBS) for individual mouse samples. This setup somehow mimics, *in vitro*, the *in vivo* situation of a single alveolus during breathing. LS is applied directly onto the air-liquid interface of an air-bubble inside a chamber filled with buffer, which upon adsorption of surfactant, can be compressed and expanded like the alveolus is in the lung. Repetitive compressions-expansions are called dynamic cycles and in this work were performed at 30 cycles/min, trying to mimic mouse breathing rate, although it is known that mouse breathing is even faster (Irvin and Bates, 2003, Zehendner et al., 2013).

In terms of surfactant initial adsorption to the interface, adsorption of the surfactants obtained from all the experimental groups was excellent; no differences were observed between surfactants obtained from the different mouse groups (Figure 4.6, left). In all cases, surfactant rapidly produced equilibrium surface tensions around 22 mN/m. Nevertheless, when testing post expansion adsorption, which analyses the ability of the surface film to re-spread and replenish the interface upon expansion, some mouse samples from KO LPS group were not able to re-stablish the equilibrium surface tension, even though the differences were not significant.

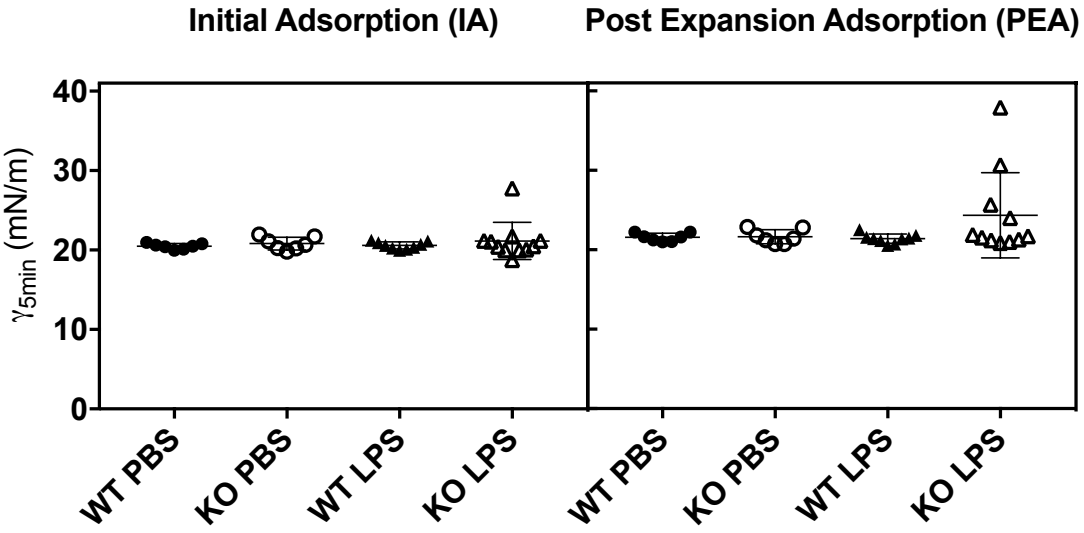

Figure 4.6: Adsorption properties of LS from mice evaluated in the CBS. 150 nL of LS at a PL concentration of 10 mg/mL were applied with a capillary inside the chamber near the surface of the air bubble. Adsorption of the material to the air-water interface was evaluated initially at Initial Adsorption (IA) and Post-Expansion (PEA). The shape of the bubble was monitored and recorded during 5 minutes to assess changes in the surface tension (γ). Data in the graph correspond to values of surface tension at the end of the IA and PEA period for individual mouse samples. One-way ANOVA with Tukey's multiple comparison post-test: p=0.7599 (IA), p=0.1385 (PEA) (no significant).

Regarding the behavior of surfactant during dynamic cycles, WT mice instilled either with PBS or LPS and KO mice instilled with PBS had a competent surfactant to reach very low minimum surface tensions <2 mN/m, while maintaining maximum surface tensions around 30 mN/m (Figure 4.7, top row), which are common values for a LS that works well (Schurch et al 2010). Interestingly, KO mice instilled with LPS had LS whose function was severely affected. During compression, it was unable to reach the low surface tensions that are required for efficient breathing. Surfactant impairment was already evident at the first cycle, but became worse after 20 compression-expansion cycles (Figure 4.7, top row). Maximum surface tensions exhibited by these surfactant films were too high when compared to other mouse groups, indicating that LS was not efficiently

reincorporated to the interface during the periods of expansion of the bubble, which mimic inspiration *in vivo* (Figure 4.7, bottom row). Again, these differences were more significant once the material went through repetitive compression-expansion cycles (see data from cycle 20 compared to cycle 1), likely as a consequence of the cumulative losses of LS towards the interface.

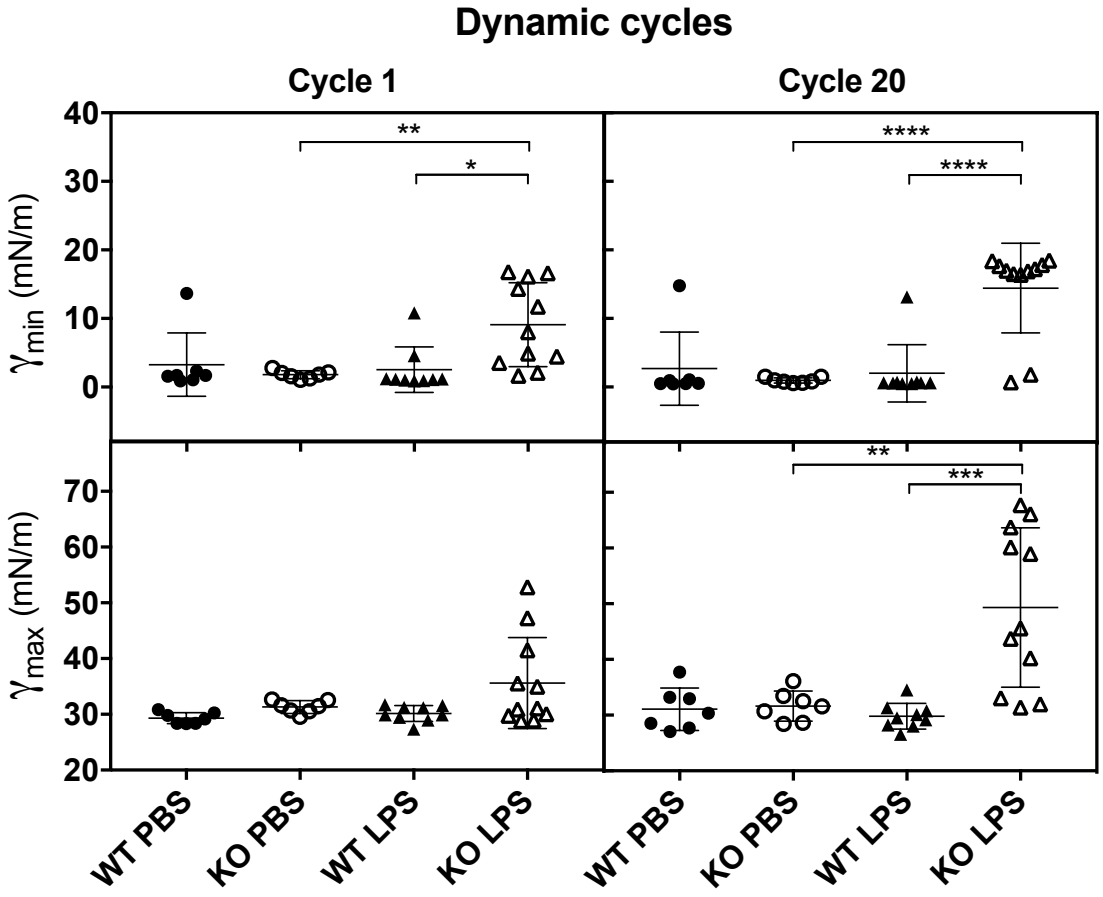

Figure 4.7: Dynamic behavior of surfactant films from different mice groups. Minimum (γ_{min}) and maximum (γ_{max}) surface tension produced by LS (10 mg/mL) from the different mouse groups during compression-expansion cycling. Symbols represent data obtained from individual mouse (average of three replicates.) WT-PBS (n=7), KO-PBS (n=7), WT-LPS (n=9), KO-LPS (n=11); (One-way ANOVA with Tukey's multiple comparison post-test: **, p≤0.01; ***, p≤0.001; ****, p<0.0001).

Representative replicates of the CBS isotherms from all the individual mouse samples have been summarized in Figure 4.8. Initial adsorption to the air-liquid interface of LS from KO LPS mice was delayed 5-10 seconds in some cases (see for example Figure 4.8; first and third IA graphs of KO-LPS samples). In addition, post-expansion adsorption was also retarded and even not able to reach minimum surface tension in some mice (see for example Figure 4.8; first, third and two last columns in PEA graphs of KO-LPS samples). Thus, although final surface tension values after 5 min adsorption of surfactant from KO LPS were not significantly different compared to other mice groups (Figure 4.6), initial adsorption was actually

affected, being retarded in some cases or not even able to reach the equilibrium surface tension (~ 20-22 mN/m) after post expansion adsorption (PEA).

Taking into consideration these data, we conclude that there is a significant difference in the surfactant biophysical activity when comparing WT and KO mice challenged by LPS. Therefore, it seems that SP-D counteracts and regulates the NETosis process within the lungs. Thus, SP-D contributes to the protection of surfactant membranes from the inhibition caused by NETs and other inflammatory components released from cells, such as neutrophils, as a consequence of LPS stimulation.

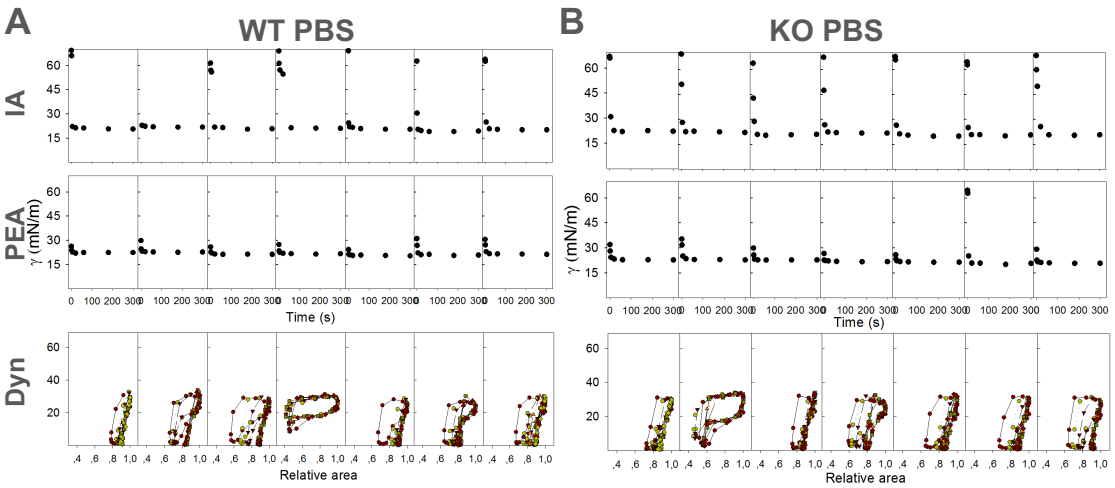

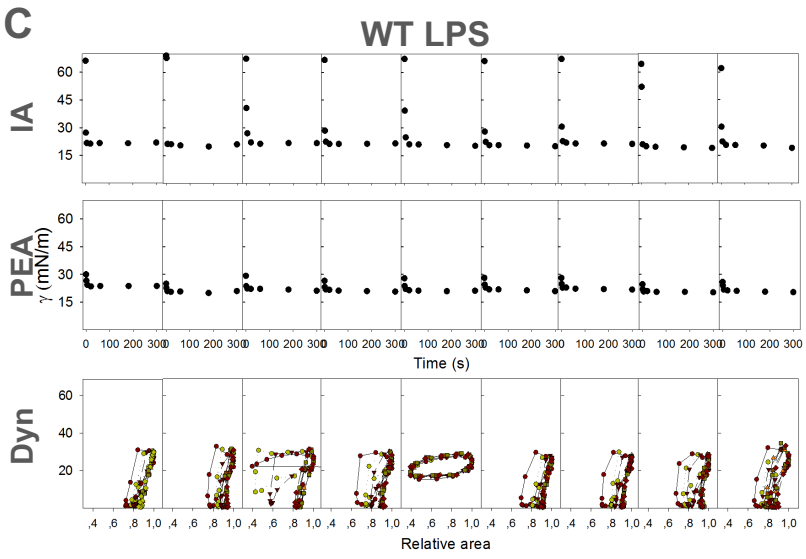

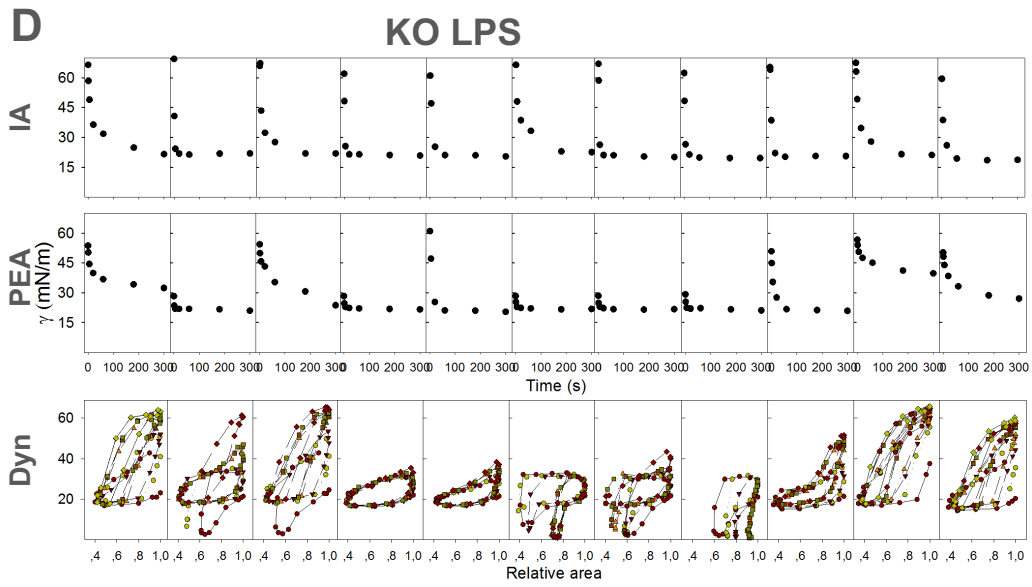

Figure 4.8: Surface activity of lung surfactant from WT or KO mice instilled with PBS or LPS. Surface activity is represented as isotherms obtained from the CBS, thermostated at 37 ºC. One replicate from each individual mouse is represented for WT PBS (***A***), KO PBS (***B***), WT LPS (***C***) and KO LPS (***D***) mouse groups. For all mouse groups, the *top row* shows isotherms of IA into the air-water interface of a bubble over a 5 min period. *Middle row* compares post expansion adsorption (PEA) over a 5 min period. *Bottom row*, dynamic compression-expansion cycling isotherms at 30 cycles/min. PL concentration in LS was 10 mg/mL.

SP-D$^{-/-}$ (KO) mice showed higher cholesterol and reduced SP-A and SP-C levels

To determine whether there were differences in SP-A, SP-B and SP-C levels between LS from the different mouse groups, which could be associated with the differences observed in their biophysical activity, western blots of these proteins were carried out.

Figure 4.9A shows the results for the complete set of samples, while representative WBs for each surfactant protein are shown in Figure 4.9B. Results showed that SP-D KO mice had significantly lower levels of SP-A and SP-C than WT mice while no differences were observed in SP-B levels (Figure 4.9A). Similar differences in surfactant protein composition have been reported previously, in experiments in which the mice were not subjected to instillation (Ikegami et al., 2000). In the current work, the possibility that PBS or LPS instillation could modify surfactant protein levels was also explored. SP-B and SP-C levels in surfactant from WT mice were significantly reduced as a consequence of LPS instillation. However, no significant changes of the already reduced levels of SP-B and SP-C were observed upon instillation of LPS in KO mice, neither in the levels of SP-A from all mouse groups (Figure 4.9A).

The proportion of cholesterol in LS has been associated with surfactant inactivation in cases of lung injury and ARDS (Markart et al., 2007). Determination of cholesterol revealed that LS from KO mice had higher proportions of cholesterol

with respect to PC than LS from WT mice (3.3-3.7% compared to 2-2.4%) (Figure 4.9C).

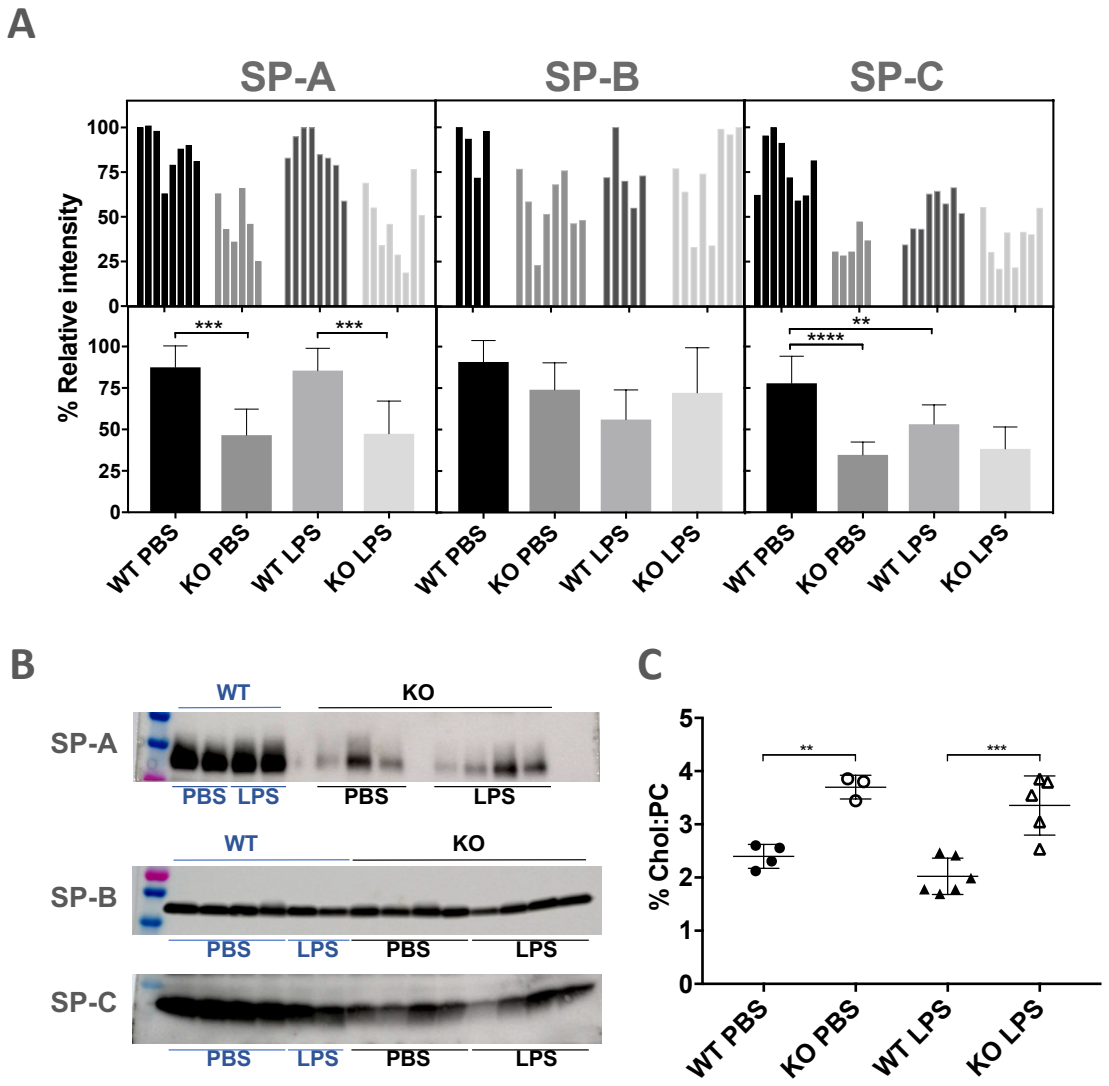

Figure 4.9: Differences in SP-A, SP-B and SP-C and cholesterol levels in LS in the surfactant of SP-D$^{+/+}$ (WT) and SP-D$^{-/-}$ (KO) mice. ***A***, densitometry of the bands of surfactant proteins (SP-A, -B and -C) shown in Western blots for LS samples from all mice; One-way ANOVA with Tukey's multiple comparison post-test: **, p≤0.01; ***, p≤0.001; ****, p<0.0001. ***B***, representative Western blots for SP-A, SP-B and SP-C from the different mouse groups. ***C***, [cholesterol]/[phosphatidylcholine] (w/w) ratio, One-way ANOVA with Tukey's multiple comparison post-test: **, p≤0.01; ***, p≤0.001. These differences do not explain the differences in SP-D-mediated effect on surface active properties of surfactant (see text).

These data show that in SP-D$^{-/-}$ KO mice, lung surfactant contains a higher proportion of cholesterol and a reduced amount of surfactant proteins SP-A and SP-C. No significant differences were observed in SP-B levels between WT and KO groups, neither within KO mice as a consequence of LPS or PBS instillation.

SP-D protects lung surfactant complexes from the inhibitory effects of NETs

The overproduction of NETs by neutrophils and its harmful effects in lungs have been well described as a consequence of infectious and inflammatory conditions (Cheng and Palaniyar, 2013), but nothing is known about the possibility that NETs could interfere directly with the surface active properties of surfactant complexes. The organic extract (OE) of porcine lung surfactant, which is depleted of collectin proteins and is the base of clinical surfactants (Echaide et al., 2017), was used as an *in vitro* model to study the direct effect of NETs in LS biophysical function. Reconstituted OE material was combined with purified NETs from human neutrophils and its biophysical activity was evaluated in the CBS. Surfactant function was completely inhibited by the presence of NETs. Surface tensions after initial (IA) and post expansion (PEA) adsorption were no lower than ~50 mN/m (Figure 4.10 and Table 4.1), when a good surfactant reaches values close to ~20 mN/m (Schurch et al 2010).

Table 4.1: Parameters defining the behavior of surfactant films when its function is inhibited by NETs and restored by the presence of SP-D

Sample	IA[1]	PE[2]	Q-STAT Cycle 4		DYN Cycle 20		
			γmin^3	γmax^4	γmin^5	γmax^6	ΔA^7
	γmin(mN/m)	γmin(mN/m)	(mN/m)	(mN/m)	(mN/m)	(mN/m)	
OE	26.8±10	23.1±0.8	2.3±0.7	27.4±1.6	1.9±0.4	35.2±7.3	0.2±0.1
OE + NETs	50.3±2.0	53.4±2.4	15.1±7.1	33.4±7.8	8.0±7.0	54.6±4.9	0.5±0.1
OE + SP-D + NETs	37.7±13.8	30.3±11.2	2.4±0.2	28.0±1.4	2.1±0.7	32.1±4.5	0.2±0.05

[1]Minimal surface tension after 5 min of IA.
[2]Minimal surface tension after 5 min of PEA.
[3]Minimal surface tension after 4 quasi-static compression-expansion cycles.
[4]Maximal surface tension after 4 quasi-static compression-expansion cycles.
[5]Minimal surface tension after 20 dynamic compression-expansion cycles (at 20 cycles/min).
[6]Maximal surface tension after 20 dynamic compression-expansion cycles (at 20 cycles/min).
[7]ΔA: Reduction in relative area needed to reach minimal surface tension.
All, n= 4, average of 4 replicates, being 2 of them from a different sample. One-way ANOVA with Tukey's multiple comparison post-test, p-values: <0.05 (*), ≤0.01(**), ≤0.001(***).

The dynamic behavior of surfactant films exposed to NETs, once subjected to compression-expansion dynamics, was also affected and minimum and maximum surface tensions reached after quasi static and dynamic cycles were high, far from the minimal values of ≤2 mN/m and ~25 mN/m, respectively, produced by a fully operative surfactant film. SP-D was found to counteract the inhibitory effect of NETs. When SP-D was added to the organic extract (OE) material prior to their exposure to NETs, as described in methods, surface tension values upon adsorption and after CBS cycling were significantly improved (Table 4.1).

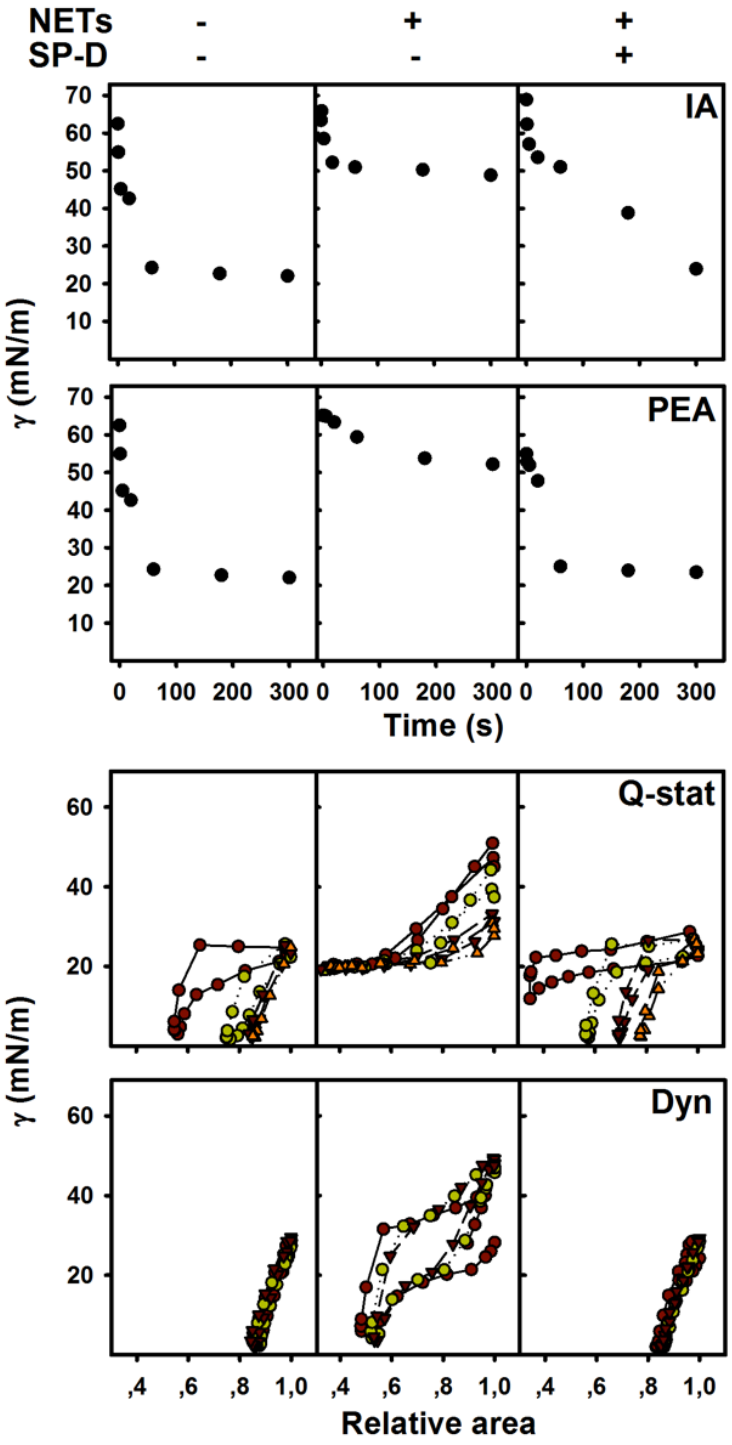

Figure 4.10: Effect of SP-D on the susceptibility of pulmonary surfactant to inhibition by NETs. Surface activity is assessed by the isotherms obtained from the CBS, thermostated at 37 ºC. Representative isotherms from each group of samples were chosen. Surfactant films were formed upon injection of a suspension of porcine surfactant OE reconstituted at 20 mg/mL in the absence or in the presence of NETs, as described in methods, and in the absence (*middle column*) or presence (*right column*) of SP-D at 0.67% (w/w with respect to phospholipid). The *upper set* of isotherms show initial (IA; *top row*) and post-expansion (PEA; *bottom row*) adsorption to the air-water interface of a bubble over a 5 min period. The *lower set* of isotherms illustrate Q-static (*top row*) and dynamic (*bottom row*) compression-expansion cycling at 20 cycles/min.

These experiments revealed for the first time that NETs can directly inhibit surfactant biophysical function, suggesting that NETosis should be considered as an additional mechanism that impairs surfactant function during lung inflammation. Besides, a novel role for SP-D in LS biophysical function was found because it protects LS against NETs inhibitory effects.

Discussion

SP-D plays an important role in the immune defense of the lungs and LS homeostasis (Sorensen, 2018). In infectious and inflammatory lung diseases, NETosis has been described as one of the processes that takes place (Cheng and Palaniyar, 2013). Furthermore, SP-D/NETs interaction has been reported (Douda et al., 2011), but the consequences of this interaction in alveolar homeostasis and pulmonary mechanics, for example at the level of lung surfactant function, remained unknown. In this chapter, we studied the regulatory effect of SP-D on the mechanism of NETosis induced by a new strain of LPS. Moreover, we investigated how SP-D attenuates NETs damaging effects on LS *in vivo*, which affects lung compliance during breathing, using a SP-D$^{-/-}$ Knock out mice model. The results obtained have demonstrated that SP-D i) suppresses LPS-induced NETosis *ex vivo*, ii) modulates NETosis *in vivo* and, iii) protects lung surfactant performance from NETs-inhibition during breathing-like interfacial mechanics.

Previous studies have reported some relationships between SP-D and NETs. First, it was reported that SP-D binds to different LPS strains (Yamazoe et al., 2008, Lim et al., 1994), which may act as a NETosis agonists. Second, bronchoalveolar lavage (BAL) from LPS-instilled mice, designed as an animal model for NETosis, was found to present increased levels of SP-D when compared to mice that did not undergo NETosis (Douda et al., 2011). Last, some inflammatory lung diseases, such as ARDS and cystic fibrosis, that course with exacerbated NETosis, were characterized by low SP-D levels in the BAL (Sorensen, 2018, Sorensen et al., 2007, Cheng and Palaniyar, 2013, Saffarzadeh et al., 2012, Nishikiori et al., 2014). Altogether these findings suggest that SP-D might have a role modulating NETs production and clearance. It has been previously shown that SP-D indeed participates in the clearance of DNA, the major component of NETs, by macrophages (Palaniyar et al., 2005). On the top of that, we have demonstrated that SP-D can reduce NETs production by neutrophils (Figure 4.1 and 4.3), stablishing a clear role for SP-D to prevent or at least ameliorate the development of LPS-induced NETosis. We show evidences here that this regulation takes place via a direct binding of the protein to LPS.

The negative effects of exacerbated NETs in the lungs have been studied in terms of lung inflammatory response and lung tissue injury (Cheng and Palaniyar, 2013). However, whether NETs could impair lung compliance, associated with a distortion of surfactant biophysical function, remained as an open question. Herein, we have shown that NETs exert a direct inhibitory effect on LS *in vitro* and that SP-D can prevent that inhibition (Figure 4.10). Moreover, surfactant inactivation was also found *in vivo*, in LS from mice suffering from exacerbated NETosis in the absence of SP-D, after LPS-instillation (Figure 4.7 and 4.8). Although we cannot ignore the possible contribution of other inflammatory components, such as liberation of ROS and/or other pro-inflammatory components to LS inhibition, we propose that NETs have a major role in the inhibition of LS biophysical function, at least in this model. Serum proteins leaked to the airways during lung injury have been reported to inactivate lung surfactant (Zuo et al., 2008), but total protein concentrations in BAL from our LPS-instilled mice were low compared to the concentrations that were previously reported to cause inhibition (Sato et al., 2010).

In addition, it has been described that SP-D$^{-/-}$ (KO) mice have higher amounts, but with altered composition, of LS lipids together with lower relative proportions of SP-A and SP-C proteins (Ikegami et al., 2000). Our data agreed with those findings (Figure 4.9), but we also found that LS from KO mice had a higher concentration of cholesterol (ratio chol:PC), also documented previously for those BALs from mice (Botas et al., 1998). However, we do not think that in our model, the altered content cholesterol and SP-C (high levels of cholesterol and lower levels of SP-C) contribute significantly to the LS inhibition observed because: i) when SP-D KO mice were PBS-instilled, the same phenotype (low SP-C, high cholesterol) was found with no detrimental effect on LS function, ii) *in vitro* NETs-inhibition experiments showed inhibition of organic extract (OE), which has normal concentrations of SP-C and cholesterol and only lacks collectin proteins (Blanco and Perez-Gil, 2007), indicating that unaltered concentrations of SP-C and cholesterol did not prevent LS inhibition by NETs; and iii) it has been reported that cholesterol concentrations of at least 20 % (w/w) with respect to PL are needed to abolish surfactant function (Gunasekara et al., 2005), whereas in KO mice cholesterol concentrations only raised to 4% as a maximum that is not enough to inhibit LS. It should be noted that SP-B has been described as the most critical protein for LS biophysical function (Schurch et al., 2010, Olmeda et al., 2013). We did not observe differences in SP-B levels between the different mouse groups studied (Figure 4.9). Last, it has been reported that SP-D protects surfactant lipids from oxidation *in vitro* (Bridges et al., 2000), and that oxidation of PL and hydrophobic proteins contribute both to impairment of LS biophysical function

(Rodriguez-Capote et al., 2006). Therefore, ROS generated in LPS-induced NETosis could also contribute to LS inhibition.

The implications of the reduced levels of SP-A observed in SP-D KO mice are unknown (Ikegami et al., 2000). However, SP-A/DNA interaction (Palaniyar et al., 2004) and the participation of SP-A in DNA clearance by macrophages (Palaniyar et al., 2005) have been shown to be low when compared to the activities of SP-D. So, in principle, we would not expect important effects of SP-A on modulating LPS-induced NETosis, neither in the protection of LS from NETs. Further experiments with SP-A$^{-/-}$ mice should confirm or discard this possibility.

Considering all the data, we propose that in the absence of SP-D, lung injury and inflammation could lead to a sustained over-accumulation of NETs in the lungs, where ionic interactions between negatively charged DNA in NETs and LS positively charged components, such as hydrophobic surfactant proteins, could lead to disruption of the multilayered surfactant structures and impairment of their function (figure 4.11). In the presence of SP-D, NETs would be opsonized by the protein and cleared by macrophages, preventing the interference with LS membranes. Besides, SP-D could avoid exacerbation of NETosis by its binding to LPS.

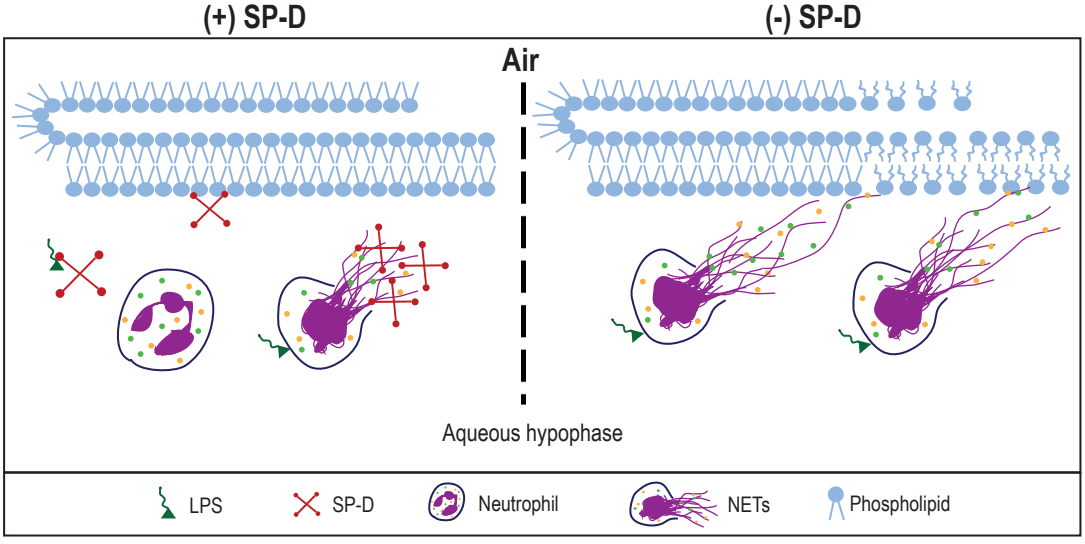

Figure 4.11: A model summarizing the effect of SP-D on LPS-mediated NETosis and NET-mediated inhibition of surfactant. In the presence of SP-D (+SP-D), SP-D sequesters LPS and suppresses LPS-mediated induction of NETosis; any NETs formed by the neutrophils will be coated with SP-D. These two effects of SP-D would suppress NET formation and NET-mediated inactivation of lung surfactant. In the absence of SP-D (-SP-D), LPS would directly interact with neutrophils and induce NETosis. NETs released from these neutrophils will inhibit the surface-active properties of the surfactant. Our data sets indicate that SP-D significantly contributes to the protective effects seen in our *in vitro*, *ex vivo* and *in vivo* experiments. The keys are listed at the bottom of the diagram.

In summary, in the present chapter it has been determined that SP-D regulates LPS-induced NETosis at different levels. First, reducing NETs release by neutrophils because SP-D binds to LPS and reduces its agonist effect. Second, once NETosis is developed in the lungs, SP-D prevents overproduction or overaccumulation of NETs in the airways and thus it protects lung surfactant biophysical function during breathing. These findings could have relevance in the context of the pathophysiological mechanism of severe lung diseases, which course with strong inflammation, accumulation of NETs and reduced levels of SP-D, such as cystic fibrosis (Cheng and Palaniyar, 2013), the current results suggest that treatment of these patients with exogenous SP-D (Sorensen, 2018) could improve some aspects of these diseases.

GENERAL DISCUSSION

Since surfactant protein SP-D was discovered in rat bronchoalveolar lavage in the late eighties, first named as CP4 (Persson et al., 1988) and then as SP-D (Persson et al., 1989), structural and functional studies have been performed to understand its functions in different organs and tissues, but mainly in lungs, where the role of SP-D in the innate immune defense has been well documented.

The observation of purified SP-D from different species has revealed that the protein is assembled in trimers, dodecamers and large oligomers, so called fuzzy balls or asterisk-like structures (Crouch et al., 1994b, Crouch, 2000). Results presented in this Thesis have included hexamers, constituted by the association of two trimers, as an additional oligomeric form and as an intermediate state between trimers and dodecamers or fuzzy balls (Chapter 1). Studies with SP-D obtained from different animals and with human proteins from two different sources, amniotic fluid (AF) and bronchoalveolar lavage of patients suffering from proteinosis (PAP), have shown some level of variability in the distribution of SP-D oligomeric forms among them. Although previous studies did not perform quantitative measurements like those included in this Thesis, it was already proposed that rat SP-D assembles mainly as dodecamers (Crouch et al., 1994b), while fuzzy balls seem the most abundant form in the case of porcine SP-D (van Eijk et al., 2002). In humans, SP-D from PAP was principally found as fuzzy balls (Chapter 3 and (Crouch et al., 1993a), whereas in AF both dodecamers and fuzzy balls were the most abundant structures in a proportion close to 1:1, as observed in Chapter 3. Several aspects can be discussed to interpret the variability observed in the distribution of SP-D oligomeric forms.

First, the kind of interactions defining protein oligomerization. It has been reported that neck domains are essential for protein trimerization (Zhang et al., 2001b) to align three monomers in which their collagen domains fold following a zipper-like mechanism (Hakansson and Reid, 2000). Trimers are further stabilized by disulfide bonds between cysteines within the N-terminal domains (Brown-Augsburger et al., 1996b). Disulfide bonds are not essential for protein secretion as trimers (Brown-Augsburger et al., 1996a), but they are necessary for secretion of higher order oligomers, even though these are not bound by disulfide bridges as observed in Chapter 1. However, formation of disulfide bonds could promote the exposition of certain residues that would favor the assembly of hexamers through non-covalent interactions at the N-terminal domains, and afterwards, of higher order oligomers. As we observed in Chapter 1, beyond trimers, the whole oligomerization process is governed by non-covalent interactions, which would be more sensitive to amino acid sequence variations and external conditions, being

translated into different distributions of the oligomeric forms of the protein among different species.

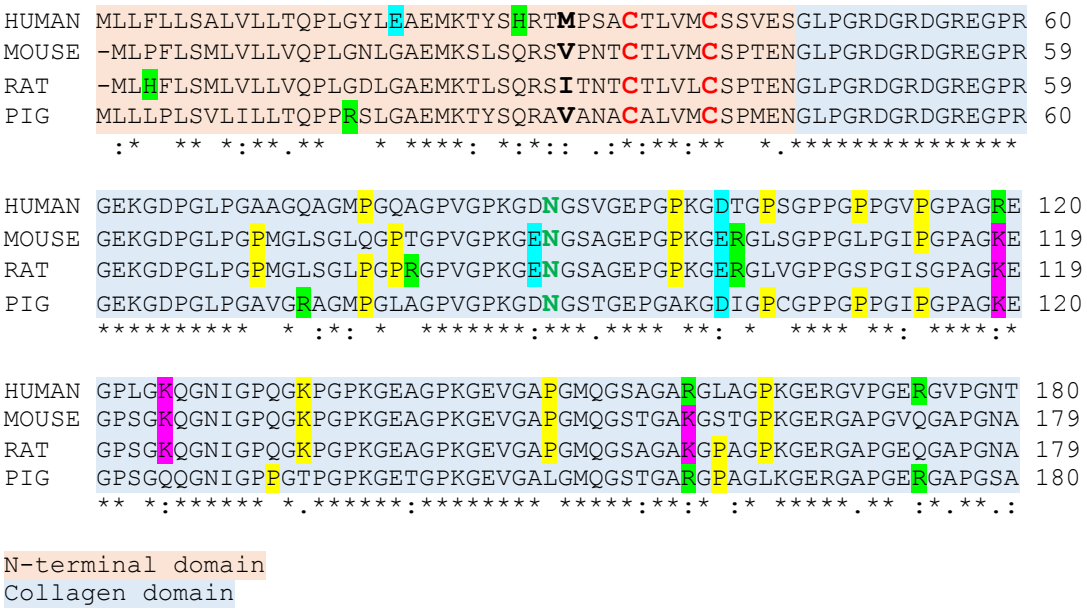

Figure 22: Alignment of SP-D sequences from different species. The N-terminal domains and part of the collagen domains of human, mouse, rat and pig SP-D have been aligned. Black bold: amino acid in position 11, corresponding to the numeration of hSP-D. In red bold, cysteines at the N-terminal domain. In green bold, asparagine, which is N-glycosylated in the collagen domain. Prolines which are non-conserved among species have been highlighted in yellow, lysines in pink. Other basic amino acids non-conserved are highlighted in green and acids in blue.

Second, variations between species in non-conserved amino acids residues within the N-terminal and collagen domains near the N-terminal end, which are the regions implicated in the assembly of hexamers, dodecamers and fuzzy balls, could cause a distinct specie-specific degree of protein oligomerization. The alignment of amino acid sequences from rat, mouse, pig and human SP-D in Figure 22 showed some divergences in their non-conserved amino acids (Figure 22). It has been described that the first exon codifying for the collagen domain, which contains the "charged patch" as defined in Chapter 1, is more hydrophilic than the rest (Crouch, 2000). Modifications in amino acids within this region could introduce variations in the local charge and influence oligomerization. Also, hydroxylation of prolines and lysines and subsequent glycosylation of lysines at the collagen domain, could be altered and have implications in the development of larger oligomers. Last, the N-glycosylation site could affect protein oligomerization, as we have observed dodecamers interacting also through these points in some AFM images. Altogether, the particular amino acid sequence and consequently, the local charge in the N-terminal and the first region of the collagen domains, seem critical for the establishment of non-covalent interactions that drive protein

oligomerization. Interestingly, conglutinin - a bovine collectin- possesses a similar structure to the one of SP-D, with a 78% of identity in the amino acid sequence and an assembly also into cruciform-like oligomers (Strang et al., 1986, Lu et al., 1993, Holmskov, 2000). In PAGE-SDS under non-reducing conditions, conglutinin has been found as a main band of 260-300 kDa, which coincides with the molecular weight expected for hexamers (Lu et al., 1993). The amino acid sequence of the protein has a cysteine in position 38 in the collagen domain, which forms disulfide bonds and may stabilize hexamers. However, structures larger than dodecamers have not been observed in conglutinin (Strang et al., 1986). It should be noted that the position of Cys^{38} in conglutinin collagen domain coincides with the area we proposed in SP-D as important for dodecamer formation, although SP-D lacks a cysteine residue in the collagen domain. Other interactions and mechanisms, like the ones we have proposed should be implicated in dodecamer formation by human SP-D, but the parallelism between SP-D and conglutinin oligomerization is remarkable.

Third, influence of the surrounding conditions in the distribution of oligomeric forms of SP-D. As a result of the non-covalent character of interactions that keep dodecamers and fuzzy balls associated, a variation in their proportion as a consequence of the external conditions, could be expected. This was the case of the changes in pH described in Chapter 1 or, in a disease condition such as proteinosis as seen in Chapter 3. Thus, the malleable character of SP-D oligomerization could be an advantage to respond to challenging situations in lungs. *In vivo*, the alveolar sub-phase could be subjected to changes, for example, in response to inflammation, affecting the oligomers distribution of SP-D. This has been also observed in Chapter 3, comparing human SP-D from a particular healthy situation, amniotic fluid, with that from a disease one, pulmonary alveolar proteinosis, where the protein is immersed in a more reactive pathological environment that could promote oligomerization to fuzzy balls. Interestingly, the total amount of dodecamers and fuzzy balls in recombinant human rhSP-D (81%) (Chapter 1) was similar to that in hSP-D from AF (73%) (Chapter 3), although the most abundant structures were dodecamers in rhSP-D and fuzzy balls in hSP-D. The rhSP-D used in Chapter 2 probably presented a higher proportion of fuzzy balls than rhSP-D in Chapter 1. Therefore, an additional level of variation could exist, affecting the distribution of oligomeric forms as a function of production and purification processes. Still in all batches of rhSP-D obtained, the protein was very similar to hSP-D, validating CHO cells as a good system to produce recombinant SP-D.

Collectin proteins possess carbohydrate recognition domains with lectin activity, which is calcium-dependent (Hakansson and Reid, 2000, Holmskov, 2000). The lectin activity of SP-D is involved in most of its functions, where trimeric CRDs are essential (Crouch, 2000, Sorensen, 2018). However, several protein activities have been described where collagen and N-terminal domains are important (Palaniyar et al., 2002, Kingma et al., 2006). In some cases, binding to ligands takes place through the collagen domain, such as in DNA binding (Palaniyar et al., 2004). In other cases, such as in the effect of SP-D on surfactant ultrastructure, homeostasis and recycling, the collagen domain is required, although whether it only provides an appropriate spacing between trimeric CRDs or it is implicated itself in these functions is unknown (Kingma and Whitsett, 2006, Korfhagen et al., 1998). N-terminal domains are critical for the transformation of surfactant large aggregates into small aggregates (Palaniyar et al., 2002, Ikegami et al., 2005), likely because higher order oligomers rather than trimers are needed to this function, and the N-terminal domain is essential as a junction hub of dodecamers and fuzzy balls (Zhang et al., 2001a). Moreover, modified recombinant proteins carrying on the substitution or deletion of any single domain of the protein have failed to correct foamy enlarged macrophages typical in SP-D$^{-/-}$ mice, where only full-length SP-D has been able to correct this issue (Ikegami et al., 2009).

Apart from the role of each SP-D domain in protein functions, the implication of the different oligomeric forms (trimers, dodecamers and fuzzy balls) in protein activity and function has been also discussed. In this Thesis, functions related to bacteria binding and aggregation were assessed with isolated trimers, hexamers and fuzzy balls. We were able to distinguish between activity of trimers and hexamers for the first time. The results revealed that hexamers are the minimal unit necessary to produce bacteria aggregation and that fuzzy balls are the most potent and active structure (Chapter 2). These findings agreed with results obtained in previously published viral aggregation assays, where fuzzy balls were the most active oligomer (Hartshorn et al., 1996a). However, affinity of binding to bacteria was similar in the case of trimers and hexamers and significantly higher for fuzzy balls. Previous studies have shown similar outcomes, but with less differentiation between protein oligomeric forms (Leth-Larsen et al., 2005). Moreover, protein activity trends were consistent with the behavior of two human SP-Ds with a different oligomeric form distribution. Proteinosis hSP-D, with fuzzy balls as the most abundant structure, showed higher activity in the functional assays performed than amniotic fluid SP-D, with a similar content of dodecamers and fuzzy balls (Chapter 3). Perhaps, from the comparison of these two cases, it might be interpreted that fuzzy balls exhibit higher activity than dodecamers, at least in terms of bacteria aggregation and

binding, functions that depend on the lectin activity contained in the carbohydrate recognition domains. Thus, AF-hSP-D that contains a proportion close to 1:1 between fuzzy balls and dodecamers showed less activity than PAP-hSP-D, where fuzzy balls are significantly increased in detriment of dodecamers. It should be kept in mind that these assays were done *in vitro* with isolated protein. Therefore, it should not be interpreted that proteinosis patients could be somehow more protected against infections than babies inside the uterus. *In vivo*, the distribution of SP-D oligomeric forms could be more dynamic attending to changes in the surrounding environment, for example, promoting association into fuzzy balls in response to bacterial infection. Last, we have only evaluated the activity of isolated trimers, hexamers and fuzzy balls for SP-D functions mediated by lectin activity. Further experiments would be required to analyze and compare their behavior in SP-D surfactant homeostasis related functions. It has been reported that trimers are not sufficient to restore phospholipid metabolism in SP-D$^{-/-}$, but SP-D trimers used in those studies were obtained by mutation of cysteines 15 and 20 to serine. The situation could be different for true native wild-type trimers. Hexamers are the minimal unit that provide a proper spacing between two trimeric CRDs, being less complex than dodecamers and fuzzy balls, and it would be interesting to see their potential influence in surfactant ultrastructure and homeostasis.

In proteinosis disease, a similar altered context has been found with respect to lipid accumulation than in SP-D$^{-/-}$ phenotype (Ikegami et al., 2000). Considering that SP-D participates in surfactant recycling, and that in PAP there is an accumulation of SP-D – mainly assembled as fuzzy balls- in the alveolar sub-phase (Chapter 3), SP-D should not contribute to accumulation of lipids in PAP lungs. However, it has been demonstrated that the alteration in PL homeostasis in SP-D$^{-/-}$ differs from the one found in PAP, where the problem resides in the GM-CSF gene and the lack of surfactant catabolism by macrophages (Ikegami et al., 2001). SP-D is implicated in surfactant recycling by ATII cells, while GM-CSF mediates PL catabolism by macrophages.

Up to date, the interest in SP-D functions has been mainly focused on immune functions of the protein. Although SP-D is a surfactant protein, not many studies have been conducted on its possible role to sustain surfactant biophysical functions. It seems that SP-D only interacts with phosphatidylinositol (PI) among surfactant phospholipids (Ogasawara et al., 1992). Despite influencing surfactant ultrastructure (Poulain et al., 1999) and homeostasis (Korfhagen et al., 1998), mediating PL uptake by ATII cells (Ikegami et al., 2005), it is believed that SP-D does not in principle interfere in surfactant biophysical function, directly or indirectly. However, some evidences in the literature showed that it could have an

indirect role, protecting LS membranes from disturbing agents that could cause impairment of their function. In several lung diseases, such a cystic fibrosis, low SP-D levels in bronchoalveolar lavage has been found, along with an exacerbated inflammatory response in lungs with high cytokines, neutrophil extracellular traps (NETs), ROS, etc., which provokes tissue damage (Sorensen, 2018, Cheng and Palaniyar, 2013, Sorensen et al., 2007). The release of those inflammatory mediators may interfere with surfactant phospholipids and hydrophobic proteins, inhibiting lung surfactant biophysical function, impairing its ability to sustain low surface tensions at the end of expiration (Echaide et al., 2017, Zuo et al., 2008). We have investigated the role of SP-D to protect lung surfactant biophysical function, using an *in vivo* mice model of airway inflammation. Wild type ($SP\text{-}D^{+/+}$) and SP-D knock out ($SP\text{-}D^{-/-}$) mice were instilled with LPS causing NETosis, which was exacerbated in the case of KO mice (Chapter 4). The biophysical activity of LS from mice subjected to different conditions was evaluated and showed that surfactant from LPS-instilled KO mice was inactivated, being unable to reach low surface tensions during breathing dynamics. We attributed this inhibition mainly to NETs released to the airway spaces, as we also found direct inhibition of LS by NETs *in vitro*. The presence of SP-D turned out to protect lung surfactant from NETs inhibition, which may occur at two levels. First, SP-D suppresses LPS-induced NETosis by sequestering LPS, mediated by the lectin activity of CRDs (Chapter 4), which also brought to light a modulatory role of SP-D in NETosis development. Second, it has been reported that SP-D binds NETs through the collagen domain of the protein (Douda et al., 2011). In this way, SP-D would opsonize NETs, preventing their interference with surfactant components and also its inhibition. This would be supported by findings in Chapter 4, where the presence of SP-D prevented surfactant inactivation by NETs *in vitro* and *in vivo*. A protective effect of SP-D in lung surfactant biophysical function in the presence of plasma proteins has been also reported previously (Sato et al., 2010). Thus, SP-D may influence surfactant biophysical function indirectly, without necessarily interacting with surfactant phospholipids, but keeping surfactant membranes free of disrupting components, especially under inflammatory conditions. Last, the SP-D used for *in vitro* experiments was obtained from proteinosis BAL, hence, it was mainly assembled as fuzzy balls. Performance of SP-D was good binding LPS, which agrees well with the functional assays performed in Chapters 2 and 3. Moreover, it was functional interacting with NETs, in principle mediated by the collagen tails.

In summary, we have characterized SP-D oligomeric forms, investigated the oligomerization pathway from monomers to fuzzy balls and studied the kind of

interactions involved in protein assembly, which are principally governed by non-covalent interactions in higher order oligomers. Moreover, isolated trimers, hexamers and fuzzy balls have been functionally evaluated and compared, being fuzzy balls the most active oligomer in functions mediated by lectin activity. These studies have been performed with recombinant human rhSP-D and further validated with human hSP-D from amiotic fluid and proteinosis BAL, where the different oligomeric forms of rhSP-D were also present with a functional activity consistent with the functional behavior described for specific oligomeric forms distribution. Last, we have gone further to assess the function of SP-D *in vivo* modulating NETosis, a *in vivo* process implicated in the immune response and with important consequences in lung surfactant biophysical behavior. The results allowed us to determine the protective role of SP-D against LS inhibition mediated by NETs and its modulatory effect on NETosis triggered by neutrophils.

CONCLUSIONS

The research presented in this Doctoral Thesis provides new insights into the structure and oligomerization pathway of surfactant protein SP-D. It also reveals further details about the structural-function relationships of the different oligomeric forms of the protein. In addition, the implication of SP-D in lung homeostasis has been demonstrated at the level of the immune defense of the lungs and the biophysical function of lung surfactant. Taking all the results into consideration we may conclude that:

- Surfactant protein SP-D is assembled into trimers, hexamers, dodecamers and larger order oligomers (Known as fuzzy balls). Beyond trimers, which are stabilized by disulfide bonds, the oligomerization pathway is governed by non-covalent interactions that take place between the N-terminal domains and the nearest collagen regions.
- The quantification of the distribution of oligomeric forms of SP-D revealed that dodecamers and fuzzy balls are the most abundant species, being the proportion sensitive to the surrounding conditions, such as pH, which also affect protein conformation and thermal stability.
- The study of human SP-D obtained from amniotic fluid has served as a reference to validate CHO cells as a good system to produce recombinant human rhSP-D. The types of oligomers observed were the same in both cases and hSP-D presented a proportion close to 1:1 of dodecamers and fuzzy balls.
- The glycosylation site is observed in human and recombinant SP-D as protrusion in the collagen domain near the N-terminal domain. The glycan structure in hSP-D is biantennary, core fucosylated and it contains sialic acids and galactose.
- Fuzzy balls are the most active oligomeric forms in protein functions that rely on the lectin activity of SP-D, at least with respect to binding and aggregation of bacteria. Hexamers are functional structures, although their activity is lower compared to fuzzy balls. Trimeric structures are not sufficient to aggregate bacteria.
- Human SP-D from proteinosis BAL is mainly assembled as fuzzy balls, while hSP-D from amniotic fluid presents a predominance of fuzzy balls, but closely followed by dodecamers. Purified human SP-D from proteinosis is more active than hSP-D from amniotic fluid, probably due to its higher content in fuzzy balls.
- SP-D suppresses LPS-induced NETosis. SP-D binds in a calcium-dependent manner to LPS through its trimeric CRD domains, therefore it reduces free LPS to trigger NETosis by neutrophils. Absence of SP-D *in vivo* implies

exacerbated NETosis, and the excess of NETs contributes to functional impairment of lung surfactant. *In vitro*, NETs directedly inhibits lung surfactant biophysical function, which can be prevented in the presence of SP-D. Thus, SP-D protects lung surfactant from NETs inhibition.

REFERENCES

ARIKI, S., NISHITANI, C. & KUROKI, Y. 2012. Diverse functions of pulmonary collectins in host defense of the lung. *J Biomed Biotechnol,* 2012**,** 532071.

ARROYO, R., MARTIN-GONZALEZ, A., ECHAIDE, M., JAIN, A., BRONDYK, W. H., ROSENBAUM, J., MORENO-HERRERO, F. & PEREZ-GIL, J. 2018. Supramolecular Assembly of Human Pulmonary Surfactant Protein SP-D. *J Mol Biol,* 430**,** 1495-1509.

AVERY, M. E. & MEAD, J. 1959. Surface properties in relation to atelectasis and hyaline membrane disease. *AMA J Dis Child,* 97**,** 517-23.

AWASTHI, S., COALSON, J. J., CROUCH, E., YANG, F. & KING, R. J. 1999. Surfactant proteins A and D in premature baboons with chronic lung injury (Bronchopulmonary dysplasia). Evidence for an inhibition of secretion. *Am J Respir Crit Care Med,* 160**,** 942-9.

BALLESTER, C., ECHAIDE, M., PEREZ-GIL, J. 2018. Pulmonary alveolar proteinosis. A compositional and biophysical functional analysis of its effects on lung surfactant. ATS (A73).

BAN, N., MATSUMURA, Y., SAKAI, H., TAKANEZAWA, Y., SASAKI, M., ARAI, H. & INAGAKI, N. 2007. ABCA3 as a lipid transporter in pulmonary surfactant biogenesis. *J Biol Chem,* 282**,** 9628-34.

BANGHAM, A. D., MORLEY, C. J. & PHILLIPS, M. C. 1979. The physical properties of an effective lung surfactant. *Biochim Biophys Acta,* 573**,** 552-6.

BATES, S. R. 2010. P63 (CKAP4) as an SP-A receptor: implications for surfactant turnover. *Cell Physiol Biochem,* 25**,** 41-54.

BECK, K. & BRODSKY, B. 1998. Supercoiled protein motifs: the collagen triple-helix and the alpha-helical coiled coil. *J Struct Biol,* 122**,** 17-29.

BIANCHI, E., CONIO, G., CIFERRI, A., PUETT, D. & RAJAGH, L. 1967. The role of pH, temperature, salt type, and salt concentration on the stability of the crystalline, helical, and randomly coiled forms of collagen. *J Biol Chem,* 242**,** 1361-9.

BINNIG, G., QUATE, C. F. & GERBER, C. 1986. Atomic force microscope. *Phys Rev Lett,* 56**,** 930-933.

BLANCO, O. & PEREZ-GIL, J. 2007. Biochemical and pharmacological differences between preparations of exogenous natural surfactant used to treat Respiratory Distress Syndrome: role of the different components in an efficient pulmonary surfactant. *Eur J Pharmacol,* 568**,** 1-15.

BLIGH, E. G. & DYER, W. J. 1959. A rapid method of total lipid extraction and purification. *Can J Biochem Physiol,* 37**,** 911-7.

BORIE, R., DANEL, C., DEBRAY, M. P., TAILLE, C., DOMBRET, M. C., AUBIER, M., EPAUD, R. & CRESTANI, B. 2011. Pulmonary alveolar proteinosis. *Eur Respir Rev,* 20**,** 98-107.

BOTAS, C., POULAIN, F., AKIYAMA, J., BROWN, C., ALLEN, L., GOERKE, J., CLEMENTS, J., CARLSON, E., GILLESPIE, A. M., EPSTEIN, C. & HAWGOOD, S. 1998. Altered surfactant homeostasis and alveolar type II cell morphology in mice lacking surfactant protein D. *Proc Natl Acad Sci U S A,* 95**,** 11869-74.

BRIDGES, J. P., DAVIS, H. W., DAMODARASAMY, M., KUROKI, Y., HOWLES, G., HUI, D. Y. & MCCORMACK, F. X. 2000. Pulmonary surfactant proteins

A and D are potent endogenous inhibitors of lipid peroxidation and oxidative cellular injury. *J Biol Chem,* 275**,** 38848-55.
BRINKMANN, V., REICHARD, U., GOOSMANN, C., FAULER, B., UHLEMANN, Y., WEISS, D. S., WEINRAUCH, Y. & ZYCHLINSKY, A. 2004. Neutrophil extracellular traps kill bacteria. *Science,* 303**,** 1532-5.
BROWN, E. S. 1957. Lung area from surface tension effects. *Proc Soc Exp Biol Med,* 95**,** 168-70.
BROWN-AUGSBURGER, P., CHANG, D., RUST, K. & CROUCH, E. C. 1996a. Biosynthesis of surfactant protein D. Contributions of conserved NH2-terminal cysteine residues and collagen helix formation to assembly and secretion. *J Biol Chem,* 271**,** 18912-9.
BROWN-AUGSBURGER, P., HARTSHORN, K., CHANG, D., RUST, K., FLISZAR, C., WELGUS, H. G. & CROUCH, E. C. 1996b. Site-directed mutagenesis of Cys-15 and Cys-20 of pulmonary surfactant protein D. Expression of a trimeric protein with altered anti-viral properties. *J Biol Chem,* 271**,** 13724-30.
CARVALHO, F. A. & SANTOS, N. C. 2012. Atomic force microscopy-based force spectroscopy--biological and biomedical applications. *IUBMB Life,* 64**,** 465-72.
CHENG, O. Z. & PALANIYAR, N. 2013. NET balancing: a problem in inflammatory lung diseases. *Front Immunol,* 4**,** 1.
CHEONG, N., ZHANG, H., MADESH, M., ZHAO, M., YU, K., DODIA, C., FISHER, A. B., SAVANI, R. C. & SHUMAN, H. 2007. ABCA3 is critical for lamellar body biogenesis in vivo. *J Biol Chem,* 282**,** 23811-7.
CLARK, J. C., WERT, S. E., BACHURSKI, C. J., STAHLMAN, M. T., STRIPP, B. R., WEAVER, T. E. & WHITSETT, J. A. 1995. Targeted disruption of the surfactant protein B gene disrupts surfactant homeostasis, causing respiratory failure in newborn mice. *Proc Natl Acad Sci U S A,* 92**,** 7794-8.
CLEMENTS, J. A. 1957. Surface tension of lung extracts. *Proc Soc Exp Biol Med,* 95**,** 170-2.
CROUCH, E., CHANG, D., RUST, K., PERSSON, A. & HEUSER, J. 1994a. Recombinant pulmonary surfactant protein D. Post-translational modification and molecular assembly. *J Biol Chem,* 269**,** 15808-13.
CROUCH, E., PERSSON, A. & CHANG, D. 1993a. Accumulation of surfactant protein D in human pulmonary alveolar proteinosis. *Am J Pathol,* 142**,** 241-8.
CROUCH, E., PERSSON, A., CHANG, D. & HEUSER, J. 1994b. Molecular structure of pulmonary surfactant protein D (SP-D). *J Biol Chem,* 269**,** 17311-9.
CROUCH, E., RUST, K., VEILE, R., DONIS-KELLER, H. & GROSSO, L. 1993b. Genomic organization of human surfactant protein D (SP-D). SP-D is encoded on chromosome 10q22.2-23.1. *J Biol Chem,* 268**,** 2976-83.
CROUCH, E. C. 1998. Structure, biologic properties, and expression of surfactant protein D (SP-D). *Biochim Biophys Acta,* 1408**,** 278-89.
CROUCH, E. C. 2000. Surfactant protein-D and pulmonary host defense. *Respir Res,* 1**,** 93-108.
CROUCH, E. C., SMITH, K., MCDONALD, B., BRINER, D., LINDERS, B., MCDONALD, J., HOLMSKOV, U., HEAD, J. & HARTSHORN, K. 2006.

Species differences in the carbohydrate binding preferences of surfactant protein D. *Am J Respir Cell Mol Biol,* 35**,** 84-94.

CRUZ, A., CASALS, C., PLASENCIA, I., MARSH, D. & PEREZ-GIL, J. 1998. Depth profiles of pulmonary surfactant protein B in phosphatidylcholine bilayers, studied by fluorescence and electron spin resonance spectroscopy. *Biochemistry,* 37**,** 9488-96.

CZARNOCKI-CIECIURA, M. & NOWOTNY, M. 2016. Introduction to high-resolution cryo-electron microscopy. *Postepy Biochem,* 62**,** 383-394.

DE PABLO, P. J. & CARRION-VAZQUEZ, M. 2014. Imaging biological samples with atomic force microscopy. *Cold Spring Harb Protoc,* 2014**,** 167-77.

DEMAUREX, N. 2002. pH Homeostasis of cellular organelles. *News Physiol Sci,* 17**,** 1-5.

DIANGELO, S., LIN, Z., WANG, G., PHILLIPS, S., RAMET, M., LUO, J. & FLOROS, J. 1999. Novel, non-radioactive, simple and multiplex PCR-cRFLP methods for genotyping human SP-A and SP-D marker alleles. *Dis Markers,* 15**,** 269-81.

DOUDA, D. N., JACKSON, R., GRASEMANN, H. & PALANIYAR, N. 2011. Innate immune collectin surfactant protein D simultaneously binds both neutrophil extracellular traps and carbohydrate ligands and promotes bacterial trapping. *J Immunol,* 187**,** 1856-65.

DOUDA, D. N., KHAN, M. A., GRASEMANN, H. & PALANIYAR, N. 2015. SK3 channel and mitochondrial ROS mediate NADPH oxidase-independent NETosis induced by calcium influx. *Proc Natl Acad Sci U S A,* 112**,** 2817-22.

ECHAIDE, M., AUTILIO, C., ARROYO, R. & PEREZ-GIL, J. 2017. Restoring pulmonary surfactant membranes and films at the respiratory surface. *Biochim Biophys Acta,* 1859**,** 1725-1739.

EFRATI, H., HAWGOOD, S., WILLIAMS, M. C., HONG, K. & BENSON, B. J. 1987. Divalent cation and hydrogen ion effects on the structure and surface activity of pulmonary surfactant. *Biochemistry,* 26**,** 7986-93.

FEHRENBACH, H. 2001. Alveolar epithelial type II cell: defender of the alveolus revisited. *Respir Res,* 2**,** 33-46.

FERGUSON, J. S., VOELKER, D. R., MCCORMACK, F. X. & SCHLESINGER, L. S. 1999. Surfactant protein D binds to Mycobacterium tuberculosis bacilli and lipoarabinomannan via carbohydrate-lectin interactions resulting in reduced phagocytosis of the bacteria by macrophages. *J Immunol,* 163**,** 312-21.

FLOROS, J., LIN, H. M., GARCIA, A., SALAZAR, M. A., GUO, X., DIANGELO, S., MONTANO, M., LUO, J., PARDO, A. & SELMAN, M. 2000. Surfactant protein genetic marker alleles identify a subgroup of tuberculosis in a Mexican population. *J Infect Dis,* 182**,** 1473-8.

FLOROS, J., WANG, G. & MIKEROV, A. N. 2009. Genetic complexity of the human innate host defense molecules, surfactant protein A1 (SP-A1) and SP-A2--impact on function. *Crit Rev Eukaryot Gene Expr,* 19**,** 125-37.

FREUDENBERG, U., BEHRENS, S. H., WELZEL, P. B., MULLER, M., GRIMMER, M., SALCHERT, K., TAEGER, T., SCHMIDT, K., POMPE, W. & WERNER, C. 2007. Electrostatic interactions modulate the conformation of collagen I. *Biophys J,* 92**,** 2108-19.

GEORGE, G. & HOOK, G. E. 1984. The pulmonary extracellular lining. *Environ Health Perspect,* 55**,** 227-37.

GIESSIBL, F. J. 2003. Advances in atomic force microscopy. *Rev. Mod. Phys.*, 75, 949.

GLASSER, S. W., BURHANS, M. S., KORFHAGEN, T. R., NA, C. L., SLY, P. D., ROSS, G. F., IKEGAMI, M. & WHITSETT, J. A. 2001. Altered stability of pulmonary surfactant in SP-C-deficient mice. *Proc Natl Acad Sci U S A,* 98**,** 6366-71.

GLASSER, S. W., DETMER, E. A., IKEGAMI, M., NA, C. L., STAHLMAN, M. T. & WHITSETT, J. A. 2003. Pneumonitis and emphysema in sp-C gene targeted mice. *J Biol Chem,* 278**,** 14291-8.

GOERKE, J. 1998. Pulmonary surfactant: functions and molecular composition. *Biochim Biophys Acta,* 1408**,** 79-89.

GUNASEKARA, L., SCHURCH, S., SCHOEL, W. M., NAG, K., LEONENKO, Z., HAUFS, M. & AMREIN, M. 2005. Pulmonary surfactant function is abolished by an elevated proportion of cholesterol. *Biochim Biophys Acta,* 1737**,** 27-35.

GUNTHER, A., SCHMIDT, R., FEUSTEL, A., MEIER, U., PUCKER, C., ERMERT, M. & SEEGER, W. 1999. Surfactant subtype conversion is related to loss of surfactant apoprotein B and surface activity in large surfactant aggregates. Experimental and clinical studies. *Am J Respir Crit Care Med,* 159**,** 244-51.

HACZKU, A. 2008. Protective role of the lung collectins surfactant protein A and surfactant protein D in airway inflammation. *J Allergy Clin Immunol,* 122**,** 861-79; quiz 880-1.

HAKANSSON, K. & REID, K. B. 2000. Collectin structure: a review. *Protein Sci,* 9**,** 1607-17.

HAN, S. & MALLAMPALLI, R. K. 2015. The Role of Surfactant in Lung Disease and Host Defense against Pulmonary Infections. *Ann Am Thorac Soc,* 12**,** 765-74.

HARTSHORN, K., CHANG, D., RUST, K., WHITE, M., HEUSER, J. & CROUCH, E. 1996a. Interactions of recombinant human pulmonary surfactant protein D and SP-D multimers with influenza A. *Am J Physiol,* 271**,** L753-62.

HARTSHORN, K. L., CROUCH, E., WHITE, M. R., COLAMUSSI, M. L., KAKKANATT, A., TAUBER, B., SHEPHERD, V. & SASTRY, K. N. 1998. Pulmonary surfactant proteins A and D enhance neutrophil uptake of bacteria. *Am J Physiol,* 274**,** L958-69.

HARTSHORN, K. L., REID, K. B., WHITE, M. R., JENSENIUS, J. C., MORRIS, S. M., TAUBER, A. I. & CROUCH, E. 1996b. Neutrophil deactivation by influenza A viruses: mechanisms of protection after viral opsonization with collectins and hemagglutination-inhibiting antibodies. *Blood,* 87**,** 3450-61.

HARTSHORN, K. L., WEBBY, R., WHITE, M. R., TECLE, T., PAN, C., BOUCHER, S., MORELAND, R. J., CROUCH, E. C. & SCHEULE, R. K. 2008. Role of viral hemagglutinin glycosylation in anti-influenza activities of recombinant surfactant protein D. *Respir Res,* 9**,** 65.

HARTSHORN, K. L., WHITE, M. R., RYNKIEWICZ, M., SORENSEN, G., HOLMSKOV, U., HEAD, J. & CROUCH, E. C. 2010. Monoclonal antibody-assisted structure-function analysis of the carbohydrate

recognition domain of surfactant protein D. *Am J Physiol Lung Cell Mol Physiol,* 299**,** L384-92.

HERRIGES, M. & MORRISEY, E. E. 2014. Lung development: orchestrating the generation and regeneration of a complex organ. *Development,* 141**,** 502-13.

HICKLING, T. P., BRIGHT, H., WING, K., GOWER, D., MARTIN, S. L., SIM, R. B. & MALHOTRA, R. 1999. A recombinant trimeric surfactant protein D carbohydrate recognition domain inhibits respiratory syncytial virus infection in vitro and in vivo. *Eur J Immunol,* 29**,** 3478-84.

HILLS, B. A. 1999. An alternative view of the role(s) of surfactant and the alveolar model. *J Appl Physiol (1985),* 87**,** 1567-83.

HITE, R. D., GRIER, B. L., WAITE, B. M., VELDHUIZEN, R. A., POSSMAYER, F., YAO, L. J. & SEEDS, M. C. 2012. Surfactant protein B inhibits secretory phospholipase A2 hydrolysis of surfactant phospholipids. *Am J Physiol Lung Cell Mol Physiol,* 302**,** L257-65.

HOLMSKOV, U., LAWSON, P., TEISNER, B., TORNOE, I., WILLIS, A. C., MORGAN, C., KOCH, C. & REID, K. B. 1997. Isolation and characterization of a new member of the scavenger receptor superfamily, glycoprotein-340 (gp-340), as a lung surfactant protein-D binding molecule. *J Biol Chem,* 272**,** 13743-9.

HOLMSKOV, U. L. 2000. Collectins and collectin receptors in innate immunity. *APMIS Suppl,* 100**,** 1-59.

HORCAS, I., FERNANDEZ, R., GOMEZ-RODRIGUEZ, J. M., COLCHERO, J., GOMEZ-HERRERO, J. & BARO, A. M. 2007. WSXM: a software for scanning probe microscopy and a tool for nanotechnology. *Rev Sci Instrum,* 78**,** 013705.

HOWARD, M., FARRAR, C. A. & SACKS, S. H. 2018. Structural and functional diversity of collectins and ficolins and their relationship to disease. *Semin Immunopathol,* 40**,** 75-85.

IKEGAMI, M., CARTER, K., BISHOP, K., YADAV, A., MASTERJOHN, E., BRONDYK, W., SCHEULE, R. K. & WHITSETT, J. A. 2006. Intratracheal recombinant surfactant protein d prevents endotoxin shock in the newborn preterm lamb. *Am J Respir Crit Care Med,* 173**,** 1342-7.

IKEGAMI, M., GRANT, S., KORFHAGEN, T., SCHEULE, R. K. & WHITSETT, J. A. 2009. Surfactant protein-D regulates the postnatal maturation of pulmonary surfactant lipid pool sizes. *J Appl Physiol (1985),* 106**,** 1545-52.

IKEGAMI, M., HULL, W. M., YOSHIDA, M., WERT, S. E. & WHITSETT, J. A. 2001. SP-D and GM-CSF regulate surfactant homeostasis via distinct mechanisms. *Am J Physiol Lung Cell Mol Physiol,* 281**,** L697-703.

IKEGAMI, M., NA, C. L., KORFHAGEN, T. R. & WHITSETT, J. A. 2005. Surfactant protein D influences surfactant ultrastructure and uptake by alveolar type II cells. *Am J Physiol Lung Cell Mol Physiol,* 288**,** L552-61.

IKEGAMI, M., WHITSETT, J. A., JOBE, A., ROSS, G., FISHER, J. & KORFHAGEN, T. 2000. Surfactant metabolism in SP-D gene-targeted mice. *Am J Physiol Lung Cell Mol Physiol,* 279**,** L468-76.

IRVIN, C. G. & BATES, J. H. 2003. Measuring the lung function in the mouse: the challenge of size. *Respir Res,* 4**,** 4.

ITO, E., OKA, R., ISHII, T., KOREKANE, H., KURIMOTO, A., KIZUKA, Y., KITAZUME, S., ARIKI, S., TAKAHASHI, M., KUROKI, Y., KIDA, K. & TANIGUCHI, N. 2015. Fucosylated surfactant protein-D is a biomarker candidate for the development of chronic obstructive pulmonary disease. *J Proteomics,* 127**,** 386-94.

JOHANSSON, J. & CURSTEDT, T. 1997. Molecular structures and interactions of pulmonary surfactant components. *Eur J Biochem,* 244**,** 675-93.

JOHANSSON, J., CURSTEDT, T. & JORNVALL, H. 1991. Surfactant protein B: disulfide bridges, structural properties, and kringle similarities. *Biochemistry,* 30**,** 6917-21.

JOHANSSON, J., SZYPERSKI, T., CURSTEDT, T. & WUTHRICH, K. 1994. The NMR structure of the pulmonary surfactant-associated polypeptide SP-C in an apolar solvent contains a valyl-rich alpha-helix. *Biochemistry,* 33**,** 6015-23.

KEATING, E., ZUO, Y. Y., TADAYYON, S. M., PETERSEN, N. O., POSSMAYER, F. & VELDHUIZEN, R. A. 2012. A modified squeeze-out mechanism for generating high surface pressures with pulmonary surfactant. *Biochim Biophys Acta,* 1818**,** 1225-34.

KHAN, M. A., FARAHVASH, A., DOUDA, D. N., LICHT, J. C., GRASEMANN, H., SWEEZEY, N. & PALANIYAR, N. 2017. JNK Activation Turns on LPS- and Gram-Negative Bacteria-Induced NADPH Oxidase-Dependent Suicidal NETosis. *Sci Rep,* 7**,** 3409.

KHAN, M. A. & PALANIYAR, N. 2017. Transcriptional firing helps to drive NETosis. *Sci Rep,* 7**,** 41749.

KINGMA, P. S. & WHITSETT, J. A. 2006. In defense of the lung: surfactant protein A and surfactant protein D. *Curr Opin Pharmacol,* 6**,** 277-83.

KINGMA, P. S., ZHANG, L., IKEGAMI, M., HARTSHORN, K., MCCORMACK, F. X. & WHITSETT, J. A. 2006. Correction of pulmonary abnormalities in Sftpd-/- mice requires the collagenous domain of surfactant protein D. *J Biol Chem,* 281**,** 24496-505.

KISHORE, U., GREENHOUGH, T. J., WATERS, P., SHRIVE, A. K., GHAI, R., KAMRAN, M. F., BERNAL, A. L., REID, K. B., MADAN, T. & CHAKRABORTY, T. 2006. Surfactant proteins SP-A and SP-D: structure, function and receptors. *Mol Immunol,* 43**,** 1293-315.

KONIG, M. F. & ANDRADE, F. 2016. A Critical Reappraisal of Neutrophil Extracellular Traps and NETosis Mimics Based on Differential Requirements for Protein Citrullination. *Front Immunol,* 7**,** 461.

KORFHAGEN, T. R., SHEFTELYEVICH, V., BURHANS, M. S., BRUNO, M. D., ROSS, G. F., WERT, S. E., STAHLMAN, M. T., JOBE, A. H., IKEGAMI, M., WHITSETT, J. A. & FISHER, J. H. 1998. Surfactant protein-D regulates surfactant phospholipid homeostasis in vivo. *J Biol Chem,* 273**,** 28438-43.

KUAN, S. F., RUST, K. & CROUCH, E. 1992. Interactions of surfactant protein D with bacterial lipopolysaccharides. Surfactant protein D is an Escherichia coli-binding protein in bronchoalveolar lavage. *J Clin Invest,* 90**,** 97-106.

KUROKI, Y., GASA, S., OGASAWARA, Y., SHIRATORI, M., MAKITA, A. & AKINO, T. 1992. Binding specificity of lung surfactant protein SP-D for glucosylceramide. *Biochem Biophys Res Commun,* 187**,** 963-9.

LAHTI, M., LOFGREN, J., MARTTILA, R., RENKO, M., KLAAVUNIEMI, T., HAATAJA, R., RAMET, M. & HALLMAN, M. 2002. Surfactant protein D gene polymorphism associated with severe respiratory syncytial virus infection. *Pediatr Res,* 51**,** 696-9.

LEITNER, A., WALZTHOENI, T., KAHRAMAN, A., HERZOG, F., RINNER, O., BECK, M. & AEBERSOLD, R. 2010. Probing native protein structures by chemical cross-linking, mass spectrometry, and bioinformatics. *Mol Cell Proteomics,* 9**,** 1634-49.

LEMKE, A., CASTILLO-SANCHEZ, J. C., PRODINGER, F., CERANIC, A., HENNERBICHLER-LUGSCHEIDER, S., PEREZ-GIL, J., REDL, H. & WOLBANK, S. 2017. Human amniotic membrane as newly identified source of amniotic fluid pulmonary surfactant. *Sci Rep,* 7**,** 6406.

LETH-LARSEN, R., GARRED, P., JENSENIUS, H., MESCHI, J., HARTSHORN, K., MADSEN, J., TORNOE, I., MADSEN, H. O., SORENSEN, G., CROUCH, E. & HOLMSKOV, U. 2005. A common polymorphism in the SFTPD gene influences assembly, function, and concentration of surfactant protein D. *J Immunol,* 174**,** 1532-8.

LETH-LARSEN, R., HOLMSKOV, U. & HOJRUP, P. 1999. Structural characterization of human and bovine lung surfactant protein D. *Biochem J,* 343 Pt 3**,** 645-52.

LI, P., LI, M., LINDBERG, M. R., KENNETT, M. J., XIONG, N. & WANG, Y. 2010. PAD4 is essential for antibacterial innate immunity mediated by neutrophil extracellular traps. *J Exp Med,* 207**,** 1853-62.

LIM, B. L., WANG, J. Y., HOLMSKOV, U., HOPPE, H. J. & REID, K. B. 1994. Expression of the carbohydrate recognition domain of lung surfactant protein D and demonstration of its binding to lipopolysaccharides of gram-negative bacteria. *Biochem Biophys Res Commun,* 202**,** 1674-80.

LIU, W., BENTLEY, C. M. & FLOROS, J. 2003. Study of human SP-A, SP-B and SP-D loci: allele frequencies, linkage disequilibrium and heterozygosity in different races and ethnic groups. *BMC Genet,* 4**,** 13.

LOPEZ-RODRIGUEZ, E., PASCUAL, A., ARROYO, R., FLOROS, J. & PEREZ-GIL, J. 2016. Human Pulmonary Surfactant Protein SP-A1 Provides Maximal Efficiency of Lung Interfacial Films. *Biophys J,* 111**,** 524-36.

LOPEZ-RODRIGUEZ, E. & PEREZ-GIL, J. 2014. Structure-function relationships in pulmonary surfactant membranes: from biophysics to therapy. *Biochim Biophys Acta,* 1838**,** 1568-85.

LU, J., WIEDEMANN, H., HOLMSKOV, U., THIEL, S., TIMPL, R. & REID, K. B. 1993. Structural similarity between lung surfactant protein D and conglutinin. Two distinct, C-type lectins containing collagen-like sequences. *Eur J Biochem,* 215**,** 793-9.

MAEDA, Y., DAVE, V. & WHITSETT, J. A. 2007. Transcriptional control of lung morphogenesis. *Physiol Rev,* 87**,** 219-44.

MARKART, P., RUPPERT, C., WYGRECKA, M., COLARIS, T., DAHAL, B., WALMRATH, D., HARBACH, H., WILHELM, J., SEEGER, W., SCHMIDT, R. & GUENTHER, A. 2007. Patients with ARDS show improvement but not normalisation of alveolar surface activity with surfactant treatment: putative role of neutral lipids. *Thorax,* 62**,** 588-94.

MARTIN, Y., WILLIAMS, C. C., WICKRAMASINGHE, H. K. 1987. Atomic force microscope-force mapping profiling on a sub 100-Å scale. *J Appl. Phys.* 61, 4793.

MASON, R. J., NIELSEN, L. D., KUROKI, Y., MATSUURA, E., FREED, J. H. & SHANNON, J. M. 1998. A 50-kDa variant form of human surfactant protein D. *Eur Respir J,* 12**,** 1147-55.

MCCORMACK, F. X. & WHITSETT, J. A. 2002. The pulmonary collectins, SP-A and SP-D, orchestrate innate immunity in the lung. *J Clin Invest,* 109**,** 707-12.

MIYAMURA, K., MALHOTRA, R., HOPPE, H. J., REID, K. B., PHIZACKERLEY, P. J., MACPHERSON, P. & LOPEZ BERNAL, A. 1994. Surfactant proteins A (SP-A) and D (SP-D): levels in human amniotic fluid and localization in the fetal membranes. *Biochim Biophys Acta,* 1210**,** 303-7.

MULLASSERY, D. & SMITH, N. P. 2015. Lung development. *Semin Pediatr Surg,* 24**,** 152-5.

NADESALINGAM, J., BERNAL, A. L., DODDS, A. W., WILLIS, A. C., MAHONEY, D. J., DAY, A. J., REID, K. B. & PALANIYAR, N. 2003. Identification and characterization of a novel interaction between pulmonary surfactant protein D and decorin. *J Biol Chem,* 278**,** 25678-87.

NAFFAH DE SOUZA, C., BREDA, L. C. D., KHAN, M. A., DE ALMEIDA, S. R., CAMARA, N. O. S., SWEEZEY, N. & PALANIYAR, N. 2017. Alkaline pH Promotes NADPH Oxidase-Independent Neutrophil Extracellular Trap Formation: A Matter of Mitochondrial Reactive Oxygen Species Generation and Citrullination and Cleavage of Histone. *Front Immunol,* 8**,** 1849.

NG, A. W., BIDANI, A. & HEMING, T. A. 2004. Innate host defense of the lung: effects of lung-lining fluid pH. *Lung,* 182**,** 297-317.

NISHIKIORI, H., CHIBA, H., ARIKI, S., KURONUMA, K., OTSUKA, M., SHIRATORI, M., IKEDA, K., WATANABE, A., KUROKI, Y. & TAKAHASHI, H. 2014. Distinct compartmentalization of SP-A and SP-D in the vasculature and lungs of patients with idiopathic pulmonary fibrosis. *BMC Pulm Med,* 14**,** 196.

NOGEE, L. M. 2004. Alterations in SP-B and SP-C expression in neonatal lung disease. *Annu Rev Physiol,* 66**,** 601-23.

OGASAWARA, Y., KUROKI, Y. & AKINO, T. 1992. Pulmonary surfactant protein D specifically binds to phosphatidylinositol. *J Biol Chem,* 267**,** 21244-9.

OGASAWARA, Y. & VOELKER, D. R. 1995. The role of the amino-terminal domain and the collagenous region in the structure and the function of rat surfactant protein D. *J Biol Chem,* 270**,** 19052-8.

OHYA, M., NISHITANI, C., SANO, H., YAMADA, C., MITSUZAWA, H., SHIMIZU, T., SAITO, T., SMITH, K., CROUCH, E. & KUROKI, Y. 2006. Human pulmonary surfactant protein D binds the extracellular domains of Toll-like receptors 2 and 4 through the carbohydrate recognition domain by a mechanism different from its binding to phosphatidylinositol and lipopolysaccharide. *Biochemistry,* 45**,** 8657-64.

OKUYAMA, K. 2008. Revisiting the molecular structure of collagen. *Connect Tissue Res,* 49**,** 299-310.

OLMEDA, B., GARCIA-ALVAREZ, B., GOMEZ, M. J., MARTINEZ-CALLE, M., CRUZ, A. & PEREZ-GIL, J. 2015. A model for the structure and mechanism of action of pulmonary surfactant protein B. *FASEB J,* 29**,** 4236-47.

OLMEDA, B., GARCIA-ALVAREZ, B. & PEREZ-GIL, J. 2013. Structure-function correlations of pulmonary surfactant protein SP-B and the saposin-like family of proteins. *Eur Biophys J,* 42**,** 209-22.

OLMEDA, B., MARTINEZ-CALLE, M. & PEREZ-GIL, J. 2017. Pulmonary surfactant metabolism in the alveolar airspace: Biogenesis, extracellular conversions, recycling. *Ann Anat,* 209**,** 78-92.

ORGEIG, S., BERNHARD, W., BISWAS, S. C., DANIELS, C. B., HALL, S. B., HETZ, S. K., LANG, C. J., MAINA, J. N., PANDA, A. K., PEREZ-GIL, J., POSSMAYER, F., VELDHUIZEN, R. A. & YAN, W. 2007. The anatomy, physics, and physiology of gas exchange surfaces: is there a universal function for pulmonary surfactant in animal respiratory structures? *Integr Comp Biol,* 47**,** 610-27.

PALANIYAR, N., CLARK, H., NADESALINGAM, J., SHIH, M. J., HAWGOOD, S. & REID, K. B. 2005. Innate immune collectin surfactant protein D enhances the clearance of DNA by macrophages and minimizes anti-DNA antibody generation. *J Immunol,* 174**,** 7352-8.

PALANIYAR, N., IKEGAMI, M., KORFHAGEN, T., WHITSETT, J. & MCCORMACK, F. X. 2001. Domains of surfactant protein A that affect protein oligomerization, lipid structure and surface tension. *Comp Biochem Physiol A Mol Integr Physiol,* 129**,** 109-27.

PALANIYAR, N., NADESALINGAM, J., CLARK, H., SHIH, M. J., DODDS, A. W. & REID, K. B. 2004. Nucleic acid is a novel ligand for innate, immune pattern recognition collectins surfactant proteins A and D and mannose-binding lectin. *J Biol Chem,* 279**,** 32728-36.

PALANIYAR, N., ZHANG, L., KUZMENKO, A., IKEGAMI, M., WAN, S., WU, H., KORFHAGEN, T. R., WHITSETT, J. A. & MCCORMACK, F. X. 2002. The role of pulmonary collectin N-terminal domains in surfactant structure, function, and homeostasis in vivo. *J Biol Chem,* 277**,** 26971-9.

PAPAYANNOPOULOS, V., METZLER, K. D., HAKKIM, A. & ZYCHLINSKY, A. 2010. Neutrophil elastase and myeloperoxidase regulate the formation of neutrophil extracellular traps. *J Cell Biol,* 191**,** 677-91.

PARMIGIANI, S. & SOLARI, E. 2003. The era of pulmonary surfactant from Laplace to nowadays. *Acta Biomed,* 74**,** 69-75.

PARRA, E. & PEREZ-GIL, J. 2015. Composition, structure and mechanical properties define performance of pulmonary surfactant membranes and films. *Chem Phys Lipids,* 185**,** 153-75.

PATTLE, R. E. 1955. Properties, function and origin of the alveolar lining layer. *Nature,* 175**,** 1125-6.

PEREZ-GIL, J. 2008. Structure of pulmonary surfactant membranes and films: the role of proteins and lipid-protein interactions. *Biochim Biophys Acta,* 1778**,** 1676-95.

PEREZ-GIL, J. & KEOUGH, K. M. 1998. Interfacial properties of surfactant proteins. *Biochim Biophys Acta,* 1408**,** 203-17.

PEREZ-GIL, J. & WEAVER, T. E. 2010. Pulmonary surfactant pathophysiology: current models and open questions. *Physiology (Bethesda),* 25**,** 132-41.

PERSIKOV, A. V., RAMSHAW, J. A. & BRODSKY, B. 2005a. Prediction of collagen stability from amino acid sequence. *J Biol Chem,* 280**,** 19343-9.
PERSIKOV, A. V., RAMSHAW, J. A., KIRKPATRICK, A. & BRODSKY, B. 2005b. Electrostatic interactions involving lysine make major contributions to collagen triple-helix stability. *Biochemistry,* 44**,** 1414-22.
PERSSON, A., CHANG, D., RUST, K., MOXLEY, M., LONGMORE, W. & CROUCH, E. 1989. Purification and biochemical characterization of CP4 (SP-D), a collagenous surfactant-associated protein. *Biochemistry,* 28**,** 6361-7.
PERSSON, A., RUST, K., CHANG, D., MOXLEY, M., LONGMORE, W. & CROUCH, E. 1988. CP4: a pneumocyte-derived collagenous surfactant-associated protein. Evidence for heterogeneity of collagenous surfactant proteins. *Biochemistry,* 27**,** 8576-84.
PETTENAZZO, A., JOBE, A., HUMME, J., SEIDNER, S. & IKEGAMI, M. 1988. Clearance of surfactant phosphatidylcholine via the upper airways in rabbits. *J Appl Physiol (1985),* 65**,** 2151-5.
PHELPS, D. S. & TAEUSCH, H. W., JR. 1985. A comparison of the major surfactant-associated proteins in different species. *Comp Biochem Physiol B,* 82**,** 441-6.
PIKAAR, J. C., VOORHOUT, W. F., VAN GOLDE, L. M., VERHOEF, J., VAN STRIJP, J. A. & VAN IWAARDEN, J. F. 1995. Opsonic activities of surfactant proteins A and D in phagocytosis of gram-negative bacteria by alveolar macrophages. *J Infect Dis,* 172**,** 481-9.
POSSMAYER, F. 1988. A proposed nomenclature for pulmonary surfactant-associated proteins. *Am Rev Respir Dis,* 138**,** 990-8.
POULAIN, F. R., AKIYAMA, J., ALLEN, L., BROWN, C., CHANG, R., GOERKE, J., DOBBS, L. & HAWGOOD, S. 1999. Ultrastructure of phospholipid mixtures reconstituted with surfactant proteins B and D. *Am J Respir Cell Mol Biol,* 20**,** 1049-58.
RIDER, E. D., IKEGAMI, M. & JOBE, A. H. 1992. Localization of alveolar surfactant clearance in rabbit lung cells. *Am J Physiol,* 263**,** L201-9.
RIDSDALE, R. A., PALANIYAR, N., HOLTERMAN, C. E., INCHLEY, K., POSSMAYER, F. & HARAUZ, G. 1999. Cation-mediated conformational variants of surfactant protein A. *Biochim Biophys Acta,* 1453**,** 23-34.
RODRIGUEZ-CAPOTE, K., MANZANARES, D., HAINES, T. & POSSMAYER, F. 2006. Reactive oxygen species inactivation of surfactant involves structural and functional alterations to surfactant proteins SP-B and SP-C. *Biophys J,* 90**,** 2808-21.
ROLDAN, N., GOORMAGHTIGH, E., PEREZ-GIL, J. & GARCIA-ALVAREZ, B. 2015. Palmitoylation as a key factor to modulate SP-C-lipid interactions in lung surfactant membrane multilayers. *Biochim Biophys Acta,* 1848**,** 184-91.
ROLDAN, N., NYHOLM, T. K. M., SLOTTE, J. P., PEREZ-GIL, J. & GARCIA-ALVAREZ, B. 2016. Effect of Lung Surfactant Protein SP-C and SP-C-Promoted Membrane Fragmentation on Cholesterol Dynamics. *Biophys J,* 111**,** 1703-1713.

ROUSER, G., SIAKOTOS, A. N. & FLEISCHER, S. 1966. Quantitative analysis of phospholipids by thin-layer chromatography and phosphorus analysis of spots. *Lipids,* 1**,** 85-6.

RUANO, M. L., NAG, K., CASALS, C., PEREZ-GIL, J. & KEOUGH, K. M. 1999. Interactions of pulmonary surfactant protein A with phospholipid monolayers change with pH. *Biophys J,* 77**,** 1469-76.

RUANO, M. L., PEREZ-GIL, J. & CASALS, C. 1998. Effect of acidic pH on the structure and lipid binding properties of porcine surfactant protein A. Potential role of acidification along its exocytic pathway. *J Biol Chem,* 273**,** 15183-91.

SAFFARZADEH, M., JUENEMANN, C., QUEISSER, M. A., LOCHNIT, G., BARRETO, G., GALUSKA, S. P., LOHMEYER, J. & PREISSNER, K. T. 2012. Neutrophil extracellular traps directly induce epithelial and endothelial cell death: a predominant role of histones. *PLoS One,* 7**,** e32366.

SALGADO, D., FISCHER, R., SCHILLBERG, S., TWYMAN, R. M. & RASCHE, S. 2014. Comparative evaluation of heterologous production systems for recombinant pulmonary surfactant protein D. *Front Immunol,* 5**,** 623.

SANCHEZ-BARBERO, F., RIVAS, G., STEINHILBER, W. & CASALS, C. 2007. Structural and functional differences among human surfactant proteins SP-A1, SP-A2 and co-expressed SP-A1/SP-A2: role of supratrimeric oligomerization. *Biochem J,* 406**,** 479-89.

SANO, H. & KUROKI, Y. 2005. The lung collectins, SP-A and SP-D, modulate pulmonary innate immunity. *Mol Immunol,* 42**,** 279-87.

SATO, A., WHITSETT, J. A., SCHEULE, R. K. & IKEGAMI, M. 2010. Surfactant protein-d inhibits lung inflammation caused by ventilation in premature newborn lambs. *Am J Respir Crit Care Med,* 181**,** 1098-105.

SCHAGGER, H. 2001. Blue-native gels to isolate protein complexes from mitochondria. *Methods Cell Biol,* 65**,** 231-44.

SCHOEL, W. M., SCHURCH, S. & GOERKE, J. 1994. The captive bubble method for the evaluation of pulmonary surfactant: surface tension, area, and volume calculations. *Biochim Biophys Acta,* 1200**,** 281-90.

SCHURCH, D., OSPINA, O. L., CRUZ, A. & PEREZ-GIL, J. 2010. Combined and independent action of proteins SP-B and SP-C in the surface behavior and mechanical stability of pulmonary surfactant films. *Biophys J,* 99**,** 3290-9.

SCHURCH, S., BACHOFEN, H., GOERKE, J. & POSSMAYER, F. 1989. A captive bubble method reproduces the in situ behavior of lung surfactant monolayers. *J Appl Physiol (1985),* 67**,** 2389-96.

SCHURCH, S., GREEN, F. H. & BACHOFEN, H. 1998. Formation and structure of surface films: captive bubble surfactometry. *Biochim Biophys Acta,* 1408**,** 180-202.

SEATON, B. A., CROUCH, E. C., MCCORMACK, F. X., HEAD, J. F., HARTSHORN, K. L. & MENDELSOHN, R. 2010. Review: Structural determinants of pattern recognition by lung collectins. *Innate Immun,* 16**,** 143-50.

SHRIVE, A. K., THARIA, H. A., STRONG, P., KISHORE, U., BURNS, I., RIZKALLAH, P. J., REID, K. B. & GREENHOUGH, T. J. 2003. High-resolution structural insights into ligand binding and immune cell recognition by human lung surfactant protein D. *J Mol Biol,* 331**,** 509-23.

SMITH, P. K., KROHN, R. I., HERMANSON, G. T., MALLIA, A. K., GARTNER, F. H., PROVENZANO, M. D., FUJIMOTO, E. K., GOEKE, N. M., OLSON, B. J. & KLENK, D. C. 1985. Measurement of protein using bicinchoninic acid. *Anal Biochem,* 150**,** 76-85.

SORENSEN, G. L. 2018. Surfactant Protein D in Respiratory and Non-Respiratory Diseases. *Front Med (Lausanne),* 5**,** 18.

SORENSEN, G. L., HOEGH, S. V., LETH-LARSEN, R., THOMSEN, T. H., FLORIDON, C., SMITH, K., KEJLING, K., TORNOE, I., CROUCH, E. C. & HOLMSKOV, U. 2009. Multimeric and trimeric subunit SP-D are interconvertible structures with distinct ligand interaction. *Mol Immunol,* 46**,** 3060-9.

SORENSEN, G. L., HUSBY, S. & HOLMSKOV, U. 2007. Surfactant protein A and surfactant protein D variation in pulmonary disease. *Immunobiology,* 212**,** 381-416.

STAHLMAN, M. T., GRAY, M. E., HULL, W. M. & WHITSETT, J. A. 2002. Immunolocalization of surfactant protein-D (SP-D) in human fetal, newborn, and adult tissues. *J Histochem Cytochem,* 50**,** 651-60.

STARK, H. & CHARI, A. 2016. Sample preparation of biological macromolecular assemblies for the determination of high-resolution structures by cryo-electron microscopy. *Microscopy (Oxf),* 65**,** 23-34.

STRANG, C. J., SLAYTER, H. S., LACHMANN, P. J. & DAVIS, A. E., 3RD 1986. Ultrastructure and composition of bovine conglutinin. *Biochem J,* 234**,** 381-9.

STRONG, P., KISHORE, U., MORGAN, C., LOPEZ BERNAL, A., SINGH, M. & REID, K. B. 1998. A novel method of purifying lung surfactant proteins A and D from the lung lavage of alveolar proteinosis patients and from pooled amniotic fluid. *J Immunol Methods,* 220**,** 139-49.

SUZUKI, T. & TRAPNELL, B. C. 2016. Pulmonary Alveolar Proteinosis Syndrome. *Clin Chest Med,* 37**,** 431-40.

TAEUSCH, H. W., BERNARDINO DE LA SERNA, J., PEREZ-GIL, J., ALONSO, C. & ZASADZINSKI, J. A. 2005. Inactivation of pulmonary surfactant due to serum-inhibited adsorption and reversal by hydrophilic polymers: experimental. *Biophys J,* 89**,** 1769-79.

TECLE, T., WHITE, M. R., SORENSEN, G., GANTZ, D., KACAK, N., HOLMSKOV, U., SMITH, K., CROUCH, E. C. & HARTSHORN, K. L. 2008. Critical role for cross-linking of trimeric lectin domains of surfactant protein D in antiviral activity against influenza A virus. *Biochem J,* 412**,** 323-9.

TRAPNELL, B. C. & WHITSETT, J. A. 2002. Gm-CSF regulates pulmonary surfactant homeostasis and alveolar macrophage-mediated innate host defense. *Annu Rev Physiol,* 64**,** 775-802.

UNDERWOOD, M. A., GILBERT, W. M. & SHERMAN, M. P. 2005. Amniotic fluid: not just fetal urine anymore. *J Perinatol,* 25**,** 341-8.

VAN DE WETERING, J. K., VAN GOLDE, L. M. & BATENBURG, J. J. 2004. Collectins: players of the innate immune system. *Eur J Biochem,* 271**,** 1229-49.

VAN EIJK, M., VAN DE LEST, C. H., BATENBURG, J. J., VAANDRAGER, A. B., MESCHI, J., HARTSHORN, K. L., VAN GOLDE, L. M. & HAAGSMAN, H. P. 2002. Porcine surfactant protein D is N-glycosylated in its carbohydrate

recognition domain and is assembled into differently charged oligomers. *Am J Respir Cell Mol Biol,* 26**,** 739-47.

VANDENBUSSCHE, G., CLERCX, A., CLERCX, M., CURSTEDT, T., JOHANSSON, J., JORNVALL, H. & RUYSSCHAERT, J. M. 1992. Secondary structure and orientation of the surfactant protein SP-B in a lipid environment. A Fourier transform infrared spectroscopy study. *Biochemistry,* 31**,** 9169-76.

VARKI, A., CUMMINGS, R. D., AEBI, M., PACKER, N. H., SEEBERGER, P. H., ESKO, J. D., STANLEY, P., HART, G., DARVILL, A., KINOSHITA, T., PRESTEGARD, J. J., SCHNAAR, R. L., FREEZE, H. H., MARTH, J. D., BERTOZZI, C. R., ETZLER, M. E., FRANK, M., VLIEGENTHART, J. F., LUTTEKE, T., PEREZ, S., BOLTON, E., RUDD, P., PAULSON, J., KANEHISA, M., TOUKACH, P., AOKI-KINOSHITA, K. F., DELL, A., NARIMATSU, H., YORK, W., TANIGUCHI, N. & KORNFELD, S. 2015. Symbol Nomenclature for Graphical Representations of Glycans. *Glycobiology,* 25**,** 1323-4.

VELDHUIZEN, R., NAG, K., ORGEIG, S. & POSSMAYER, F. 1998. The role of lipids in pulmonary surfactant. *Biochim Biophys Acta,* 1408**,** 90-108.

VIEIRA, F., KUNG, J. W. & BHATTI, F. 2017. Structure, genetics and function of the pulmonary associated surfactant proteins A and D: The extra-pulmonary role of these C type lectins. *Ann Anat,* 211**,** 184-201.

VOSS, T., MELCHERS, K., SCHEIRLE, G. & SCHAFER, K. P. 1991. Structural comparison of recombinant pulmonary surfactant protein SP-A derived from two human coding sequences: implications for the chain composition of natural human SP-A. *Am J Respir Cell Mol Biol,* 4**,** 88-94.

WALTERS, R. W., JENQ, R. R. & HALL, S. B. 2000. Distinct steps in the adsorption of pulmonary surfactant to an air-liquid interface. *Biophys J,* 78**,** 257-66.

WANG, G., BATES-KENNEY, S. R., TAO, J. Q., PHELPS, D. S. & FLOROS, J. 2004. Differences in biochemical properties and in biological function between human SP-A1 and SP-A2 variants, and the impact of ozone-induced oxidation. *Biochemistry,* 43**,** 4227-39.

WANG, G., MYERS, C., MIKEROV, A. & FLOROS, J. 2007. Effect of cysteine 85 on biochemical properties and biological function of human surfactant protein A variants. *Biochemistry,* 46**,** 8425-35.

WANG, J. Y., SHIEH, C. C., YOU, P. F., LEI, H. Y. & REID, K. B. 1998. Inhibitory effect of pulmonary surfactant proteins A and D on allergen-induced lymphocyte proliferation and histamine release in children with asthma. *Am J Respir Crit Care Med,* 158**,** 510-8.

WANG, Y., LI, M., STADLER, S., CORRELL, S., LI, P., WANG, D., HAYAMA, R., LEONELLI, L., HAN, H., GRIGORYEV, S. A., ALLIS, C. D. & COONROD, S. A. 2009. Histone hypercitrullination mediates chromatin decondensation and neutrophil extracellular trap formation. *J Cell Biol,* 184**,** 205-13.

WEAVER, T. E. & WHITSETT, J. A. 1991. Function and regulation of expression of pulmonary surfactant-associated proteins. *Biochem J,* 273(Pt 2)**,** 249-64.

WRIGHT, J. R. 2005. Immunoregulatory functions of surfactant proteins. *Nat Rev Immunol,* 5**,** 58-68.

YAMAZOE, M., NISHITANI, C., TAKAHASHI, M., KATOH, T., ARIKI, S., SHIMIZU, T., MITSUZAWA, H., SAWADA, K., VOELKER, D. R., TAKAHASHI, H. & KUROKI, Y. 2008. Pulmonary surfactant protein D inhibits lipopolysaccharide (LPS)-induced inflammatory cell responses by altering LPS binding to its receptors. *J Biol Chem,* 283**,** 35878-88.

YOUNG, N. S., LEVIN, J. & PRENDERGAST, R. A. 1972. An invertebrate coagulation system activated by endotoxin: evidence for enzymatic mediation. *J Clin Invest,* 51**,** 1790-7.

ZEHENDNER, C. M., LUHMANN, H. J. & YANG, J. W. 2013. A simple and novel method to monitor breathing and heart rate in awake and urethane-anesthetized newborn rodents. *PLoS One,* 8**,** e62628.

ZHANG, L., IKEGAMI, M., CROUCH, E. C., KORFHAGEN, T. R. & WHITSETT, J. A. 2001a. Activity of pulmonary surfactant protein-D (SP-D) in vivo is dependent on oligomeric structure. *J Biol Chem,* 276**,** 19214-9.

ZHANG, P., MCALINDEN, A., LI, S., SCHUMACHER, T., WANG, H., HU, S., SANDELL, L. & CROUCH, E. 2001b. The amino-terminal heptad repeats of the coiled-coil neck domain of pulmonary surfactant protein d are necessary for the assembly of trimeric subunits and dodecamers. *J Biol Chem,* 276**,** 19862-70.

ZUO, Y. Y., VELDHUIZEN, R. A., NEUMANN, A. W., PETERSEN, N. O. & POSSMAYER, F. 2008. Current perspectives in pulmonary surfactant--inhibition, enhancement and evaluation. *Biochim Biophys Acta,* 1778**,** 1947-77.

LIST OF PUBLICATIONS

Arroyo, R., Martin-González, A., Echaide, M., Jain, A., Brondyk, W.H., Rosenbaum, J., Moreno-Herrero, F., Perez-Gil, J. (2018) Supramolecular Assembly of Human Pulmonary Surfactant Protein SP-D. *Journal of Molecular Biology*, 430, 1495-150; DOI: 10.1016/j.jmb.2018.03.027

Echaide, M., Autilio, C., **Arroyo, R.**, Perez-Gil, J. (2017) Restoring pulmonary surfactant membranes and films at the respiratory surface. *Biochimica et Biophysica Acta* (BBA), 1859(9 Pt B):1725-1739; DOI: 10.1016/j.bbamem.201703.015

Lopez-Rodriguez, E., Pascual, A., **Arroyo, R.**, Floros, J., Perez-Gil, J. (2016) Human Pulmonary Surfactant Protein SP-A1 Provides Maximal Efficiency of Surfactant Films Under Breathing Dynamics. *Biophysical Journal*, Volume 111, Issue 3, 524-536; DOI: 10.1016/j.bpj.2016.06.025

Arroyo, R., Khan, M.A., Echaide, M., Perez-Gil, J., Palaniyar, N. (2018) An innate immune collectin SP-D suppresses LPS-induced NETosis and NET-induced pulmonary surfactant inactivation. *Nature Communications* (submitted)

Previous to this PhD Thesis:

Palacios, L., Rosado, H., Micol, V., Rosato, AE., Bernal, P., **Arroyo, R.**, Grounds, H., Anderson, JC., Stabler, RA., Taylor PW. (2014) Staphylococcal Phenotypes Induced by Naturally Occurring and Synthetic Membrane-Interactive Polyphenolic &[beta]-Lactam Resistance Modifiers. *PLOS ONE* 9(4):e93830; DOI: 10.1371/journal.pone.0093830